



Universiteit  
Leiden  
The Netherlands

## Structure and Mechanism of the Type-3 Copper Protein Tyrosinase

Tepper, Armand W.J.W.

### Citation

Tepper, A. W. J. W. (2005, March 3). *Structure and Mechanism of the Type-3 Copper Protein Tyrosinase*. Retrieved from <https://hdl.handle.net/1887/617>

Version: Corrected Publisher's Version

License: [Licence agreement concerning inclusion of doctoral thesis in the Institutional Repository of the University of Leiden](#)

Downloaded from: <https://hdl.handle.net/1887/617>

**Note:** To cite this publication please use the final published version (if applicable).

# Structure and Mechanism of the Type-3 Copper Protein Tyrosinase

PROEFSCHRIFT

Ter verkrijging van de graad van Doctor aan de Universiteit Leiden,

op gezag van de Rector Magnificus Dr. D.D. Breimer,

hoogleraar in de faculteit der Wiskunde en

Natuurwetenschappen en die der Geneeskunde,

volgens besluit van het College voor Promoties te verdedigen op

donderdag 3 maart 2005

te klokke 16:15 uur

door

**Armand Wilbrandt Jannes Wichert Tepper**

Geboren te Winschoten in 1971

## Promotiecommissie

Promotor: Prof. G.W. Canters  
Referent: Prof. F. Tuczek (Christian-Albrechts-Universität zu Kiel)  
Overige leden: Prof. J. Brouwer  
Prof. L. Casella (Università di Pavia)  
Prof. E.J.J. Groenen  
Prof. D.B. Janssen (Rijksuniversiteit Groningen)  
Prof. B. Krebs (Universität Münster)  
Prof. J. Reedijk

Penetrating so many secrets,  
we cease to believe in the unknowable.  
But there it sits nevertheless,  
calmly licking its chops.

*H. L. Mencken*

The aim of science is to seek the simplest explanation of complex facts. We are apt to fall into the error of thinking that the facts are simple because simplicity is the goal of our quest. The guiding motto in the life of every natural philosopher should be 'Seek simplicity and distrust it.'

*A. N. Whitehead*

The scientist does not study nature because it is useful;  
he studies it because he delights in it,  
and he delights in it because it is beautiful.  
If nature were not beautiful,  
it would not be worth knowing,  
and if nature were not worth knowing,  
life would not be worth living.

*J. H. Poincaré*

Voor mijn ouders

Cover front: The X-ray active site structure of the type-3 copper protein catechol oxidase, a protein closely related to tyrosinase

Cover back: The substrate L-tyrosine, L-DOPA and the orange colored reaction product DOPAchrome (Top). Paramagnetic NMR spectrum of oxidised tyrosinase with fluoride bound (Bottom)

Printed by: Optima Grafische Communicatie, Rotterdam

The investigations were supported by the Netherlands Research Council for Chemical Sciences (NWO/CW project number 700-28-047)

## Contents:

<b>Chapter 1</b>	General Introduction	7
<b>Chapter 2</b>	Tyrosinase: biology, structure and mechanism	15
<b>Chapter 3</b>	Structural basis and mechanism of the inhibition of tyrosinase by halide ions	47
<b>Chapter 4</b>	Stopped-flow fluorescence studies of inhibitor binding to tyrosinase	71
<b>Chapter 5</b>	Paramagnetic properties of the $Ty_{met}X$ species studied by $^1H$ NMR	103
<b>Chapter 6</b>	Paramagnetic NMR studies of p-nitrophenol binding to tyrosinase	121
<b>Chapter 7</b>	Summary, conclusion and future work	147
<b>Nederlandse samenvatting</b>		158
<b>List of publications</b>		164
<b>Curriculum Vitae</b>		165



# Chapter **1**

*General introduction*



## Metals in proteins

Proteins are the most important building blocks of a living cell. They are responsible for a wide variety of functions including cell motion, catalysis, structural stabilization, molecule transport, signal transduction and regulation. The entire collection of proteins of a living cell is also called the proteome. Although all genetic information (coding for the proteome) is stored in the form of DNA within the genome, it is the proteome that determines which (and at which levels) proteins should be expressed under given conditions in a given cell type.

It has been estimated that about one third of all proteins binds one or more metal ions as prosthetic groups. Many of these proteins contain metals like magnesium and calcium that often serve a role in structural stabilisation. A significant part of all metalloproteins contain transition metal ions such as iron, copper, nickel, zinc, molybdenum and vanadium (for an extensive review see <sup>1</sup> in references Chapter 2). Several of these transition metals, with iron and copper as the most significant examples, are redox active because they occur in various stable oxidation states. Proteins containing such metals are often involved in processes involving the exchange of electrons with the environment such as in catalysis and electron transfer reactions.

The metals are bound to the protein matrix through interactions with amino-acid residues such as His, Asp, Asn, Cys and Met. The coordination geometry of the bound metal ion is determined by the position and orientation of the coordinating residues within the protein matrix and the preference of the metal ion. Thus, the metal coordination sphere is pre-organised, which often leads to metal coordination geometries away from the energy minimum. Furthermore, the protein matrix plays an essential role in the intermolecular recognition between, for example, two proteins in electron transfer or an enzyme and a substrate in catalysis. The properties of the coordinated metal (e.g. redox potential) may be modulated by the protein matrix, for example upon a change in solution conditions (e.g. pH) or the binding or release of signalling molecules. For the reasons given above, protein bound metals are allowed to fulfill a large repertoire of functions, while each metalloprotein is adapted to fulfil its function in a highly specific and selective manner.

## Copper proteins

Metalloproteins containing Cu perform four basic functions: 1) metal ion storage, transport and uptake; 2) electron transfer; 3) dioxygen storage, transport and uptake; 4) catalysis. The presence of copper in proteins gives rise to characteristic spectroscopic properties. Based on these different spectroscopic signatures, the copper proteins have been historically classified into different classes. Initially, the subdivision consisted of 3

types (i.e. type 1, 2 and 3). Yet, the availability of more copper protein structures revealed an increasing repertoire of copper sites, requiring the definition of more types. The current classification is based on 7 different classes, as briefly summarized below.

**Type-1:** The type-1 copper sites are found in simple electron-transfer proteins such as plastocyanin, azurin, pseudoazurin and amicyanin. Due to their intense blue color in the oxidized Cu(II) form, these proteins also have been dubbed 'blue copper proteins'. The strong absorption at around 600 nm has been ascribed to a cysteine sulfur to copper LMCT transition but, more recently, has been labelled as a  $\pi$ - $\pi^*$  transition. The type-1 site is also found in redox enzymes such as nitrite reductase and in the multicopper oxidases (e.g. ascorbate oxidase, laccase, ceruloplasmin) that contain more than one copper site. In the latter proteins, the type 1 site is involved in shuttling electrons from and to the catalytically active center. The Cu coordination sphere is formed by two N (from His) and an S atom (from Cys) and a weakly axially coordinating S atom from methionine. Instead of methionine, a glutamine and a leucine have been found in a few cases.

**Type-2:** The copper centres in these proteins are ligated by four N or O ligands in a square planar or distorted tetrahedral geometry. The type-2 proteins are essentially colorless and their EPR spectra distinguish them from type-1 sites. Proteins containing a type-2 center are mostly involved in catalysis, where the presence of vacant coordination sites allows the catalytic oxidation of substrate molecules. The type-2 site is found in, for example, copper amine oxidases, galactose oxidase and Cu-Zn superoxide dismutase.

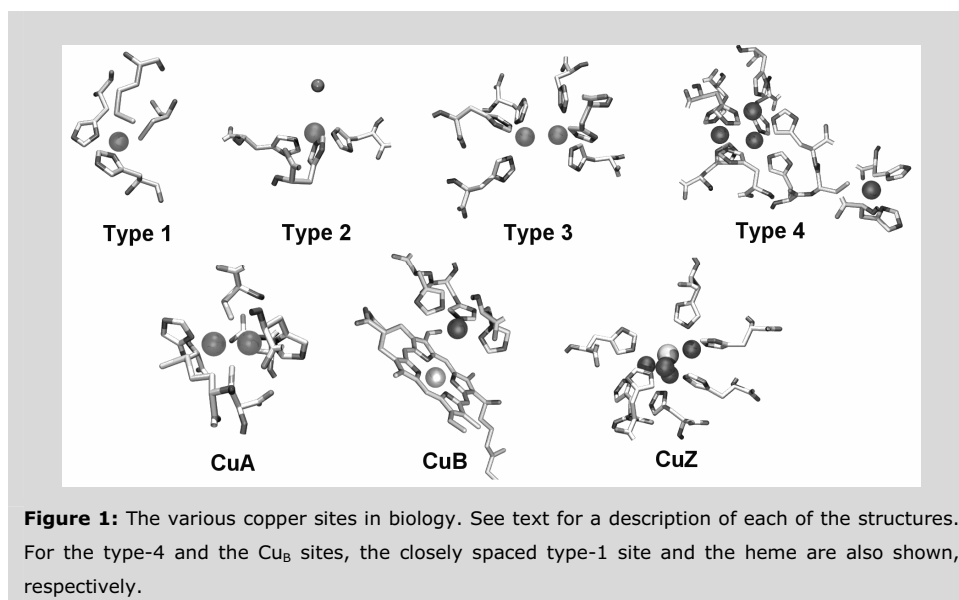
**Type-3:** The type-3 site consists of two closely spaced copper ions each coordinated by three His residues. The type-3 site in the oxidized form does not give rise to an EPR signal due to antiferromagnetic coupling between the two Cu(II) ions. Proteins containing a type-3 centre are involved in O<sub>2</sub> transport and activation. Examples of type-3 copper proteins are hemocyanin, catechol oxidase and tyrosinase. For a detailed description of the structure of the type-3 centre and its reactivity, the reader is referred to Chapter two.

**Type-4:** The type-4 copper site can be seen as being composed of a type-2 and a type-3 site, together forming a trinuclear cluster. The site occurs in proteins catalysing oxidation reactions such as laccase, ascorbate oxidase and ceruloplasmin. The three coppers are ligated by 8 His residues. Often, type-4 containing proteins also contain an additional type-1 center, in which case they are designated as multicopper oxidases or blue oxidases. The trinuclear cluster and the type-1 site are connected through a Cys-His electron transfer pathway.

**Cu<sub>A</sub>:** The Cu<sub>A</sub> site is dinuclear. The two coppers are bridged by two Cys derived S atoms. Each Cu is further ligated by a N atom from His. Its role is in long range electron transfer and the site can be found in, for example, cytochrome *c* oxidase and nitrous oxide reductase. The site shows a very characteristic EPR spectrum and has a purple color. In the oxidized form, each of the two copper occurs in a mixed-valence oxidation state, formally denoted as Cu(1.5)Cu(1.5). In contrast to most Cu systems, the Cu<sub>A</sub> site yields remarkably sharp paramagnetic NMR signals. This has led to a detailed description of the electronic structure of the site.

**Cu<sub>B</sub>:** The Cu<sub>B</sub> site occurs close to a Fe containing heme in the catalytic centre of cytochrome *c* oxidase (COX) that catalyses the 4-electron reduction of O<sub>2</sub> to water. The energy released by the oxidation is utilised to pump protons over the membrane in which the COX is embedded. The Cu<sub>B</sub> site is located *trans* to the axial His ligand of the heme *a*<sub>3</sub> center and is coordinated by three histidines in a trigonal pyramidal geometry with the open coordination position of the copper oriented towards the open coordination position on the heme iron.

**Cu<sub>Z</sub>:** The Cu<sub>Z</sub> cluster as occurring in nitrous oxide reductase is involved in the conversion of N<sub>2</sub>O into N<sub>2</sub>. The Cu<sub>Z</sub> center comprises four copper ions arranged in a distorted tetrahedron and seven histidine residues. Three coppers are ligated by two histidines, whereas the fourth is ligated by only one, thereby forming a putative substrate binding site. The copper ions in the cluster are bridged by an inorganic sulfur atom.



## Subject and scope of this thesis

This thesis deals with the type-3 copper protein tyrosinase (Ty). The enzyme catalyses the hydroxylation of monophenols to give *o*-diphenols and the oxidation of *o*-diphenols to the corresponding quinones. The formed quinones are the reactive precursors in the synthesis of melanin pigments that fulfil various roles in different organisms. Ty occurs widespread in nature and can be found throughout the phylogenetic tree. In man, defects in the enzyme are related to a number of pathologies such as oculocutaneous albinism. In fruits, vegetables and mushrooms, Ty is responsible for the economically important browning that occurs upon bruising or post-harvest storage. In other cases, the Ty activity is desired for the production of distinct organoleptic properties as in raisins and green tea. Furthermore, Ty catalyses the ‘mild’ oxidation of phenols, potentially applicable in industrial catalysis or bioremediation. Thus, Ty poses considerable interest from medical, agricultural and industrial points-of-view.

Research on Ty has got a long history; the first works date back to over a century ago. The kinetics of Ty substrate conversion was the subject of the PhD research of the science-fiction writer Isaac Asimov, and the thesis describing the work (1948) is the first publication on his impressive bibliography (see <sup>2</sup> in references Chapter 2). Research on Ty has been approached from a large number of disciplines, including biophysics, theoretical chemistry, genetics, biochemistry, spectroscopy, medicine and applied chemistry. A large part of the biological and chemical aspects of melanin synthesis and the Ty activity is published in the specialised journal ‘Pigment Cell Research’. Yet, despite the long-standing tradition of research on Ty, its structure and detailed mechanism of catalysis remain to be solved to date.

The work described in this thesis was aimed at obtaining insight into the Ty reaction mechanism on a structural and mechanistic level. Attention was particularly drawn to the question of how inhibitors and monophenolic and diphenolic substrates interact with the type-3 copper center. Understanding these interactions is of prime importance in understanding the Ty reaction mechanism. Such an understanding is in turn essential for predicting the enzyme’s behaviour (both *in vivo* and in industrial applications, for example), in the development of novel Ty inhibiting compounds (for example for medical applications such as skin treatment or for the prevention of the undesired browning of fruits, vegetables and mushrooms) and in the development of Cu<sub>2</sub> model compounds that mimic the Ty reaction chemistry.

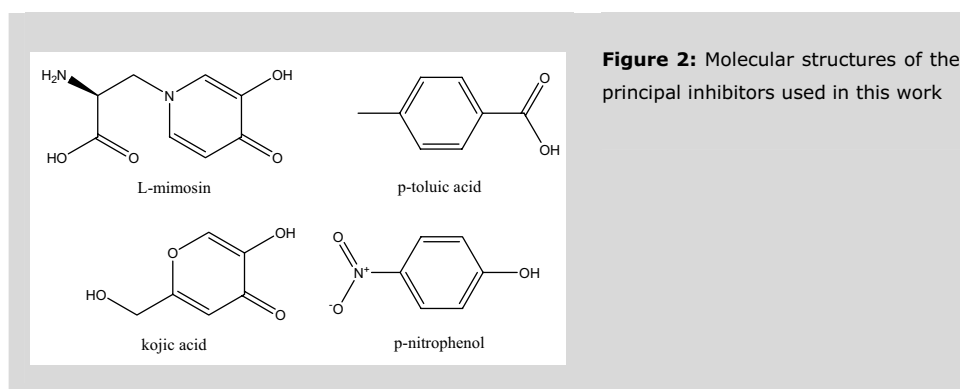
Although a large body information regarding the structure and reactivity of type-3 proteins is available (see Chapter 2), structural data on Ty and its complexes with substrates and/or inhibitors are rather scarce. Such data, however, are essential to understand the principles governing Ty function. The available knowledge mainly pertains to the structure of the Ty<sub>oxy</sub> site (oxygen bound Ty, [Cu<sup>2+</sup>-O<sub>2</sub><sup>2-</sup>-Cu<sup>2+</sup>], see Chapter 2) studied by, for example, EXAFS, Raman and UV/Vis) and the electronic structure of the Ty<sub>h-met</sub> site (half-oxidised Ty, [Cu<sup>2+</sup>-OH<sup>-</sup> Cu<sup>+</sup>], see Chapter 2) and the changes therein that occur upon ligand binding (studied by EPR and related techniques). The Ty<sub>h-met</sub> species is, however, not involved in the catalytic mechanism.

Thus, there has been limited insight into the structural factors that contribute to the Ty reactivity. One of the main reasons for this is the lack of a Ty crystal structure. Furthermore, spectroscopic studies of Ty have been few because of the limited applicability of available methods. For example, the resting oxidised [Cu<sup>2+</sup>-OH<sup>-</sup>-Cu<sup>2+</sup>] form (Ty<sub>met</sub>, see Chapter 2) of the enzyme shows no strong transitions in the UV/Vis and is EPR silent due to the antiferromagnetic coupling between the two Cu ions in the type-3 site, rendering the site diamagnetic in the ground-state. Additionally, spectroscopic studies usually require substantial amounts of purified, homogeneous and stable protein, while a convenient source of Ty has been lacking for long.

The latter problem has been overcome by the development of an over-expression system for *Streptomyces antibioticus* Ty that yields about 10 mg pure Ty per liter of cell culture. Furthermore, as the protein is excreted in the culture medium, the Ty is easily and efficiently purified to homogeneity by affinity chromatography. An additional advantage of the bacterial Tys is that they are the smallest Tys known (~ 30 kD) and that they are relatively stable, which is an advantage for NMR studies.

As far as the applicability of spectroscopic methods is concerned, the finding that paramagnetic NMR can be fruitfully applied to Ty has been an important step forward. Even though the type-3 site in the oxidised form is diamagnetic, the paramagnetic triplet excited state appears to be populated at room temperature, providing enough paramagnetism for the <sup>1</sup>H signals originating from the coordinated His residues to shift outside the diamagnetic envelope. Since only the signals of the coordinated residues (and Cu bound ligands) are affected, the paramagnetic NMR method provides a sensitive and selective probe of the electronic structure of the type-3 centre and the changes therein that occur upon inhibitor binding.

The paramagnetically shifted signals of  $Ty_{met}$  are remarkably sharp for a copper system and show good resolution, especially in the presence of chloride ion. Soon after the initial discovery, the paramagnetic NMR finally provided the proof that the type-3 site in Ty contains 6 His ligands as in Hcs and COs. A significant part of this thesis deals with the exploration of the paramagnetic NMR method in studying the interaction of Ty with exogenous ligands that act as inhibitors (Fig. 2), thereby providing information on the enzymatic mechanism on a structural level.



### Outline of this thesis

An overview of the literature regarding Ty and related subjects is presented in **Chapter 2**. In line with the content of this thesis, the focus is mainly on the structural and mechanistic aspects of type-3 copper proteins and small inorganic model complexes.

**Chapter 3** of this thesis concerns the structural and mechanistic aspects of the inhibition of Ty by halide ions and involved the application of paramagnetic  $^1H$  NMR and kinetic methods. This work was initiated after the observation that chloride profoundly influences the  $^1H$  paramagnetic NMR spectrum of  $Ty_{met}$ , while the reasons for this were unclear. The work was motivated by the ubiquitous presence of chloride ion in all living systems and in the environment. The studies included the characterisation of complexes of  $Ty_{met}$  with other halide ions ( $F^-$ ,  $Br^-$ ,  $I^-$ ) by paramagnetic NMR. Furthermore, the inhibition of Ty by halide ion, as well as its pH dependence, was characterised with kinetic methods. Paramagnetic NMR on complexes of  $Ty_{met}$  and various organic inhibitors provided insight into their binding mode with implications for the understanding of the diphenolase mechanism.

**Chapter 4** focuses on the fluorescence properties of Ty as a function of oxidation state and ligand binding. A primary goal of this work was to validate the use of fluorescence as

a probe in studying ligand binding to Ty, thereby providing another spectroscopic method to study the Ty mechanism. After initial characterisation of the Ty fluorescence, the binding of fluoride ion to  $Ty_{met}$  and its pH dependence have been studied by stopped-flow fluorescence spectroscopy. This was aimed at elucidating the kinetics and mechanism of fluoride binding, complementing the data presented in chapter 3. The obtained results were then checked against those obtained from  $^1H$  NMR. Furthermore, stopped-flow fluorescence was used to study the interaction of  $Ty_{met}$  with a range of (organic) inhibitors and transition state analogues to provide insight into the factors that determine the efficiency of inhibition, as well as to afford information on the binding mode of diphenolic substrates to the type-3 center.

**Chapter 5** describes a largely theoretical study that was initiated after an initial suggestion by Dr. Jesus Salgado who pointed out that it would be possible to calculate electronic relaxation times from the  $T_1$  data of the paramagnetic NMR His ligand proton signals in the different  $Ty_{met}$ -halide complexes. The motivation for pursuing this was twofold, namely 1) to provide insight into the mechanisms responsible for the sharpness of the paramagnetic NMR signals in the halide bound  $Ty_{met}$  species and 2) to establish the proton  $T_1$  relaxation mechanism stimulated by the possible prospect of determining distances of (inhibitor) protons to active site copper in order to elucidate the coordination geometry of  $Ty_{met}$  bound ligands. Furthermore, the magnitude of the antiferromagnetic coupling parameter  $-2J$  was estimated from the temperature dependence of the His  $^1H$  signal shifts for the different  $Ty_{met}$ -halide complexes, allowing for a limited magnetostructural correlation.

**Chapter 6** focuses on the interaction of p-nitrophenol (pnp) with  $Ty_{met}$  studied by paramagnetic NMR methods and is aimed at providing information on the binding mode of monophenolic substrates to the type-3 center. Although all proposed Ty mechanisms involve the coordination of phenolate to one of the coppers in  $Ty_{oxy}$ , this was never proven experimentally. The presented data involved titrations of native  $Ty_{met}$ ,  $Ty_{met}F$  and  $Ty_{met}Cl$  with pnp and following the changes that occur in the paramagnetic  $^1H$  NMR spectrum of the  $Ty_{met}$  complexes. Furthermore, the paramagnetic relaxation and shift parameters of pnp bound to  $Ty_{met}$  were estimated through  $^1H$  and  $^2H$  measurements of the pnp signals in the solution bulk. The obtained results were used to derive a structural model for monophenol binding to Ty. The latter provided an explanation for the absence of monophenolase activity in catechol oxidase.

# Chapter 2

*Tyrosinase: biology, structure and mechanism*



## Introduction

This chapter is aimed at providing a general overview of the current knowledge regarding tyrosinase and related subjects. The chapter is quite extensive on oxygen activation in model complexes, which is covered up to about 1998. In some cases, reference is given to relevant review articles, to which the reader is referred for the references to the original works.

## Melanins and melanogenesis: an overview

Tyrosinase (Ty) is the rate limiting enzyme in the biosynthesis of melanin pigments (melanogenesis) starting from tyrosine as the precursor substrate. Melanins are heterogeneous polyphenolic polymers with colours ranging from yellow to black. These compounds are widely distributed in nature, and can be found throughout the phylogenetic scale, from bacteria to man. Melanogenesis fulfils a number of physiological roles in different organisms (reviewed in <sup>3-5</sup>) as briefly discussed below.

*Fruits, fungi, vegetables.* Here, the melanins are responsible for the browning of wounded tissue when it is exposed to air and the browning occurring during post-harvest storage. In agriculture this poses a significant problem with huge economical impact, making the identification of compounds that inhibit melanin formation extremely important. In other cases (such as raisins, tea and cocoa), the Ty activity is needed for the production of distinct organoleptic properties. For fungi, it has been established that melanin is connected with the formation of the reproductive organs and spore formation, the virulence of pathogenic fungi and tissue protection after damage. The role of the browning in fruits and vegetables may serve a defensive role, although the exact reasons remain unclear at present.

*Invertebrates.* In invertebrates, apart from providing pigmentation, melanin is also involved in three physiologically important processes. These are defense reactions (immunity), wound healing and cuticular hardening (sclerotization). Insects and other arthropods use melanin production as a defence mechanism to encapsulate foreign organisms. Furthermore, deposition of melanin at a wound site prevents the loss of blood, while the cytotoxic melanogenic quinonoid precursors might kill invading microorganisms at the wound site. Finally, melanogenesis closely resembles the sclerotinogenic pathway. Sclerotization reactions employ catecholamines that are similar to melanogenic precursors, using a similar set of enzymes. During sclerotization, N-catecholamines are converted to quinones. These and other reactive metabolites are involved in cross-linking structural proteins, resulting in the formation of the hard cuticle.

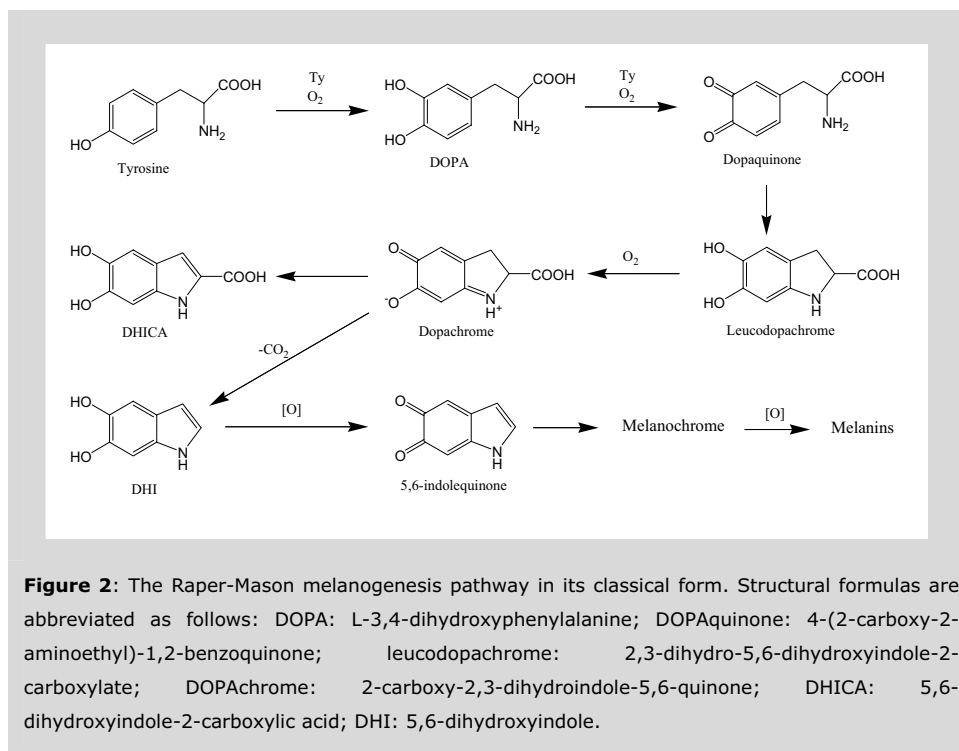
Arrest or even delay of this process has devastating consequences on insects. Knock-out of melanogenesis in *Drosophila* is lethal, for example.

*Mammals.* The colour of mammalian skin, hair and eyes is determined by a number of factors, the most important of which is the degree and distribution of melanin pigments. In mammals, the melanin is produced in specialised pigment-producing cells known as melanocytes, which originate in the neural crest during embryogenesis and are spatially distributed throughout the organism during development. This distribution is under strict genetic control and may lead to interesting skin patterns, like in the case of zebras and leopards. The pigments are synthesised in membranous organelles called melanosomes, which are located in the dendrites of melanocytes. In mammals, melanin pigments play several diverse and important roles, including thermoregulation, camouflage and sexual attraction.

In humans, the main role of the melanins is photoprotection of the skin by absorbing UV radiation that causes DNA damage and the formation of reactive oxygen species (ROS). Human deficiency in melanin causes serious disorders like oculocutaneous albinism and vitiligo. There has also been great interest in the involvement of melanins in malignant melanosomes, the carcinogenic tumours of the skin. The relationships between neuromelanins and damage of neurons and their selective vulnerability in Parkinson's disease have also been the subject of great attention. Abnormal melanin production causes a range of aesthetically relevant conditions such as freckles, melasma (large dark patches of skin) and lentigines (sun spots).

### **Melanin chemistry.**

In a period of about 100 years, much has been learned on the complex and heterogeneous structure of the melanins. There are two types of melanin, the eumelanins (brownish/black) and the phaeomelanins (yellow to reddish/brown). Both pigments are formed by a combination of enzymatic and chemical reactions. The biosynthesis of the eumelanins is described by the classic so-called Raper-Mason pathway depicted in Figure 2 that was already deduced in the 1920's. Much progress has been made since this ground breaking work, such as the discovery of the involvement of the reaction of cysteine with dopaquinone in the formation of the phaeomelanins. For an extensive review focussing on the historical background of research on melanin structure and chemistry, the reader is referred to <sup>6</sup>. Both *in vivo* and *in vitro*, the melanins contain free radicals that can react with a number of reactive species such as singlet oxygen and superoxide and can therefore serve as antioxidants.



### Enzymology, occurrence and role of Ty.

The copper containing enzyme tyrosinase (Ty), the subject of this thesis, is the key enzyme in the melanogenesis pathway. The enzyme is responsible for the conversion of tyrosine to L-DOPA and DOPAquinone (the first two reactions in Figure 2). The formed DOPAquinone is then converted further by a series of enzymatic and spontaneous conversions, ultimately yielding the different melanins. Single mutations in mammalian tyrosinase may lead to a complete halt of melanogenesis (e.g. <sup>7</sup>), leading to albinism mentioned above.

Not only the physiological substrates tyrosine and L-DOPA, but also various other phenols and diphenols are converted by Ty to the corresponding diphenols and quinones, respectively. Thus, in general, Ty catalyses both the *ortho* hydroxylation of monophenols (cresolase or monophenolase activity) and the two-electron oxidation of *o*-diphenols to *o*-quinones (catecholase or diphenolase activity). These reactions take place under concomitant reduction of dioxygen to water.

Early studies on Ty have demonstrated several key aspects of the reaction mechanism. Isotope labelling studies have shown that the incorporated oxygen derives from molecular oxygen. The two electrons which are required to reduce the remaining oxygen atom to water are supplied by the substrate. These findings demonstrated that Ty functions as a *monooxygenase*. The Ty activity has been classified under EC 1.14.18.1. Examples of other monooxygenating enzymes are, among others, the copper containing methane monooxygenase (pMMO, membrane bound form), quercetinase and ammonia monooxygenase.

About 20 tyrosinase sequences have been established (reviewed in <sup>3</sup>), the genes originating from prokaryotic organisms to humans. Within different taxa, the sequence homology is high, and several conserved domains can be identified. Some of these regions are found in all tyrosinases, while others are only present in one group. For example, the plant tyrosinases possess transit peptides that post-translationally direct the protein to the chloroplast envelope for subsequent processing and transport. In human and mouse tyrosinases, putative signal peptides are present, which were proposed to be involved in the transfer of the enzyme to melanosomes. In the known sequences of fungal and insect tyrosinases, no evidence for the presence of signal peptides was obtained.

In higher plants, the enzyme is mostly membrane bound in non-senescent tissues. In fruits, more enzyme becomes soluble as the fruit ages, and both soluble and membrane-bound tyrosinases have been described. Mammalian tyrosinases are melanosomal membrane proteins with a single membrane spanning helix located in the C-terminal part of the enzymes. The *Agaricus bisporus* as well as the *Neurospora crassa* tyrosinase are cytosolic, while those of the *Streptomyces* species are secreted out of the cell.

Many tyrosinases from plant, fungal and invertebrate origin exist as latent enzymes which have to be activated. In this latent form, the pro-enzyme appears to be very stable which is not the case for the mature protein. The *in vivo* mechanism of activation is still largely unknown, but it has been suggested that an endogenous protease might be involved in the activation, cleaving off a protecting peptide. Yet, the proenzyme can be activated *in vitro* by a broad spectrum of substances, like detergents as SDS. Also activation by acidification and lipids has been described.

The *Streptomyces* tyrosinases are monomeric proteins characterised by a low molecular weight of ~30 kDa. As mentioned above, the tyrosinases that are found in *Streptomyces* species are secreted out of the cell, where they are involved in extracellular melanin production <sup>8</sup>. The reasons for this are still unclear but it has been proposed that the extracellular melanin is synthesised for its bacteriostatic properties <sup>3</sup>. Yet, the tyrosinase

activity is non-essential for the organism, as *Streptomyces lividans* does not produce and secrete active tyrosinase.

In the species of *Streptomyces*, the tyrosinase gene is part of the so-called *melC* operon. Next to the tyrosinase gene (*melC2*), this operon contains an additional ORF called *melC1* which is essential for the correct expression of the tyrosinase. Both genes are transcribed from the same promoter<sup>9</sup>. The *melC1* gene contains a putative signal-sequence which might indicate that the *melC1* protein is involved in the tyrosinase transport process<sup>9</sup>. Furthermore, it was hypothesised that *melC1* could be involved in the copper uptake by the apotyrosinase<sup>9</sup>. In the absence of copper, the *melC1* and the apotyrosinase form a stable complex which can be detected in both the intra- and extracellular fractions<sup>8</sup>. After the addition of copper, this complex dissociates in the *melC1* and the holotyrosinase<sup>8</sup>. During the incorporation of copper, the tyrosinase presumably undergoes a conformational transition, the activation energy of which may be lowered by binding to the *melC1* chaperone<sup>8</sup>. The best characterised *Streptomyces* tyrosinase is that from *Streptomyces glaucescens*<sup>10</sup>.

### Ty as a member of the type-3 copper protein family.

It was already shown early on that Ty contains two copper ions that are closely spaced within the protein matrix. The two copper binding regions, called CuA and CuB, are found in all tyrosinases (these Ty CuA and CuB sites are not to be confused with the CuA and CuB Cu sites described in chapter 1). These regions each contain three conserved histidine residues, which coordinate to a pair of copper ions in the active site of the enzyme. This copper pair is the site of interaction of tyrosinase with both molecular oxygen and its substrates. The CuA and CuB regions share strong homology with the corresponding regions of hemocyanins (Hcs), which are oxygen carriers found in many molluscs and arthropods<sup>11</sup> and the catechol oxidases (COs) that oxidise diphenols but do not show the Ty hydroxylation activity<sup>12</sup>. These proteins also contain a dinuclear copper site and share strong functional, mechanistic and structural similarities with the tyrosinases. Together the Tys, Hcs and COs are classified as 'type-3' copper proteins, following the early nomenclature of copper containing proteins (see Chapter 1).

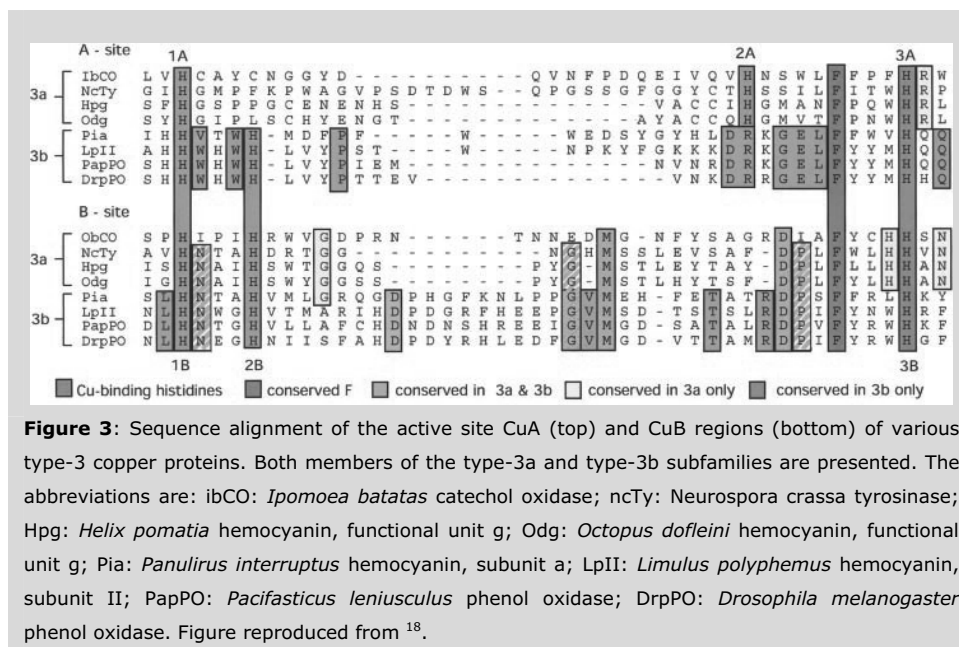
Several spectroscopic, structural and chemical studies on derivatives of Hcs, COs and Tys have shown that these enzymes share remarkably similar active sites. Like in the Tys, the type-3 center of the Hcs and the COs bind dioxygen reversibly as the peroxide<sup>10</sup>. The main difference between the two enzymes is that the bound oxygen is not activated for cleavage in hemocyanin, while this is the case with Tys and COs. Furthermore, while Ty is able to hydroxylate phenolic substrates, this activity is lacking in the COs.

With the notable exception of Ty, X-ray structures are available for various members of the other classes of type-3 proteins. Specifically, structures have been reported for the Hc from the spiny lobster *Panulirus interuptus*<sup>13</sup>, the horseshoe crab *Limulus polyphemus*<sup>14</sup>, the gastropod *Rapana thomasi*<sup>15</sup> and the octopus *Octopus dofleini*<sup>16</sup>, as well as for the CO from the sweet potato *Ipomoea batatas*<sup>17</sup>. An examination of these structures shows that, although they contain almost identical type-3 copper centers, the primary, secondary and tertiary structures appear markedly different between these proteins. For example, the Ty from *Streptomyces* exists as a monomeric protein of about 30 kDa, while the Hcs from molluscs exist as truly immense aggregates consisting of 350-450 kDa subunits with a total mass approaching 9 MDa.

### Sequence and structural homology within the type-3 protein family.

The homology in the primary sequences of the type-3 copper proteins is mainly restricted to the CuA and CuB regions. Each of the CuA and CuB regions supplies 3 histidines that coordinate to a Cu ion of the type-3 center. A sequence alignment of several Tys, Hcs and a CO shows that these His residues in the CuA and CuB regions are nearly fully conserved in all sequences. The main difference between the primary sequences lies within the relative position of the 'second' coordinating His in the CuA site (Figure 3). According to this difference, the type-3 family has been subdivided into two subfamilies dubbed 'type-3a' and 'type-3b'<sup>18</sup>. Both the CuA and CuB sites contain 2 alpha helices interconnected by loops that together provide the coordinating His residues. This 4  $\alpha$ -helix motif is structurally conserved in all type-3 proteins for which a structure is available. The second His in the CuA site of the type-3a subfamily is located on a loop connecting the 2 helices that each provide one His to the CuA atom. In the type-3b family, instead, the second coordinating His is part of the helix that also provides the first CuA coordinating His. The latter arrangement is similar to that of the CuB site, from which it has been suggested that the dinuclear type-3b copper site arose from a gene duplication of a mononuclear Cu protein early in evolution<sup>18</sup>.

It has been proposed that the type-3 proteins have diverged from a common ancient Ty ancestor that may have been involved in scavenging of the then toxic oxygen from a largely anaerobic atmosphere<sup>18</sup>. If this is the case, the type-3 proteins are ancient indeed as these conditions existed more than a billion years ago.



### Differences within the type-3 copper family

From the above it is clear that the type-3 proteins all share very similar active sites, whereas their physiological functions differ: Hcs serve as oxygen carrier proteins, COs catalyse the oxidation of diphenols and Tys *ortho* hydroxylate monophenols and oxidize diphenols to *o*-quinones. It is of great importance to establish the structural features responsible for these functional differences.

It is generally accepted that one of the main reasons for the absence of catalytic activity in Hcs is related to the inaccessibility of the type-3 center to potential substrates. It has been early recognised that the type-3 site of Ty is more accessible to exogenous ligands than the type-3 site of Hc. This is illustrated by the large difference in the rate of displacement of the E<sub>oxy</sub> peroxide by exogenous ligands in Ty and Hc <sup>25</sup>. This was later confirmed by the X-ray structures of several Hcs and the CO from sweet potato. For example, in octopus Hc, an extra domain is present that shields the type-3 site from the solvent, while this domain is not present in the mature CO. In fact, sweet potato CO also exists in a latent form where cleavage of a capping domain is required for activity. Interestingly, this capping domain shows strong sequence homology with that of octopus Hc <sup>42</sup>. The capping domain was further suggested to be involved in copper uptake <sup>42</sup>.

There is an X-ray structure of CO with the inhibitor phenylthiourea (PTU) bound. In arthropodan Hcs, a Phe residue is present that shields access to the type-3 site. The phenyl ring of this HC Phe residue aligns perfectly with the aromatic ring of PTU bound to the CO active site when the structures are superimposed. In tarantula Hc, the removal of this Phe residue by limited proteolysis induces a significant level of monophenolase and diphenolase activities, whereas this is not observed for the native form<sup>43</sup>. Diphenolase activity can be induced further in octopus Hc and several arthropodan Hcs upon artificial activation<sup>44</sup>, strongly suggesting that the absence of CO activity in native Hcs is due to efficient shielding of the type-3 center.

To explain the absence of monophenolase activity in COs, it has been suggested that phenolic substrates interact with CuA in Ty, whereas this is not possible in CO where a Phe residue (Phe261) blocks access to this copper. This is supported by the detection of monophenolase activity in tarantula Hc that has an Ile residue in the position homologous to Phe261 in sweet potato CO. Binding of monophenols to CuA in Tys is further supported by molecular modeling; if the Phe residue of PTU in CO is replaced by a tyrosine at a similar position in the structures of Octopus and Limulus Hc, the phenolic oxygen points to CuA. Such reasoning assumes, however, that the position of the amino acid function of the substrate L-tyrosine bound to the Ty active-site corresponds to the position of the backbone amino acid function of the shielding Phe in Hc. The hypothesis that monophenolic substrate docks at CuA in Tys remains to be proven experimentally.

### The type-3 site in detail

The type-3 copper site can exist in various forms depending on the oxidation state of the Cu ions. These derivatives are the oxygenated ( $E_{oxy}$ ), the deoxy or reduced ( $E_{red}$ ), the oxidised met ( $E_{met}$ ) and the half-met ( $E_{h-met}$ ) forms. In all of these forms, each of the two Cu ions in the type-3 site are coordinated by 3 His residues, while the forms differ in the coordination geometry, the Cu-Cu distance, Cu oxidation state and the presence exogenous ligands. Some important characteristics of the different forms are presented in Table 1 and will be discussed in more detail in the following section.



**Table 1:** The various derivatives of tyrosinase and some important characteristics. The absorption maxima and  $\epsilon$  values are somewhat dependent on the source of the enzyme<sup>10</sup>, values are given for *Streptomyces glaucescens* tyrosinase<sup>10</sup>.

Derivative	Symbolic representation	EPR Detectable	Abs. max. (nm)	$\epsilon$ ( $M^{-1}cm^{-1}$ )	Cu-Cu distance (Å)
Met	[Cu(II)-OH-Cu(II)]	No	-	-	2.9
Oxy	[Cu(II)O <sub>2</sub> <sup>2-</sup> -Cu(II)]	No	345 640	17500 1000	3.6
Red	[Cu(I) Cu(I)]	No	-	-	4.4
Half-met	[Cu(II) Cu(I)]	Yes	-	-	Nd

### The met derivative E<sub>met</sub>

The met derivative of tyrosinase is the main component of the 'resting form' of the enzyme. As isolated and at atmospheric pressure, room temperature, neutral pH and in the absence of substrate, about 85% to 90% of the enzyme is in the Ty<sub>met</sub> form, depending on the source of the enzyme<sup>19</sup>.

X-ray structures where both Cu ions occur in the cupric form have been solved for sweet potato CO and *Limulus* Hc. In both structures, the Cu ions are spaced at a distance of about 2.9 Å. In the structure of oxidised CO, an atom bridging the two Cu ions was refined in the electron density map, probably representing a hydroxide or chloride ion originating from the solvent. The presence of a bridging atom was already inferred from early spectroscopic studies<sup>20</sup>, which showed that type-3 proteins in the met form are devoid of an EPR signal. This is due to strong antiferromagnetic coupling between the two  $S = \frac{1}{2}$  copper centres, which leads to an EPR silent  $S = 0$  ground state. This magnetic coupling requires the presence of a superexchange pathway associated with an exogenous bridging ligand or an endogenous bridging amino acid residue<sup>10</sup>. In the met form, each of the Cu(II) ions is coordinated by 3 His residues and the Cu<sub>2</sub> bridging atom<sup>21</sup>. The coordination can best be described as trigonal pyramidal for both Cu ions with one His residue in the apical position<sup>10</sup>.

The met derivative does not possess clearly distinguishable features in its UV/VIS spectrum. This, together with its EPR silence, made this derivative difficult to study through standard spectroscopic methods and structural studies on E<sub>met</sub> are therefore scarce. In contrast to diphenolic substrates, monophenolic substrates do not react with Ty<sub>met</sub>.

**The half-met derivative  $E_{h\text{-met}}$** 

The  $E_{h\text{-met}}$  derivatives have an  $S = 1/2$  ground state, and are thus EPR active<sup>22</sup>. Even though the  $E_{h\text{-met}}$  derivative does not seem to occur under physiological conditions or during substrate turnover, it has proved to be a particularly useful probe of the active site. The half-met derivative can be prepared in a number of ways, including incubating the deoxy protein with nitric oxide<sup>23</sup>, nitrite<sup>23</sup>, nitrite + ascorbate or nitrogen dioxide<sup>23</sup>. Since these compounds all are nitrogen oxides, it has been postulated that the same oxidant is formed from different precursors<sup>24</sup>. The nature of the true active oxidant has been a matter of debate. Salvato and co-workers<sup>24</sup> have suggested that the active oxidant is  $\text{NO}_2$ , whereas others propose that the active oxidant is  $\text{NO}_2^-$ <sup>25</sup> or  $\text{NO}$ <sup>26</sup>. In this context it is important to note that all three species ( $\text{NO}_2$ ,  $\text{NO}$  and nitrite) are always present in solutions containing nitrogen oxides<sup>24</sup>, which may lead to misleading conclusions. More recent work<sup>27</sup> has indicated that it is  $\text{NO}^{2-}$  that is bound to one of the coppers, as opposed to earlier suggestions<sup>28</sup> which stated that the nitrite might be bound to both coppers as a bridging ligand.

The paramagnetic nature makes this derivative amenable to EPR and related techniques such as ESEEM, ENDOR and HYSCORE. These techniques have been applied to Hcs (e.g. <sup>27:29-31</sup>) and Tys (e.g. <sup>25:32-34</sup>). From these studies it appears that the electronic structures of the  $E_{h\text{-met}}$  centers are remarkably similar between the Hcs and Tys. Early studies (<sup>34</sup> and references therein) indicated that the ligand field around the Cu(II) ion is best described as 4-coordinate tetragonal. Addition of aromatic carboxylic acid inhibitors, which bind directly to at least one copper centre, induce a distortion of the tetragonal pyramidal geometry towards a trigonal bipyramidal arrangement<sup>34</sup>. When a similar rearrangement also takes place upon binding of monophenolic substrates to  $\text{Ty}_{\text{oxy}}$ , the bound peroxide should be displaced. This event may be the key step in the initiation of oxygen transfer to the substrate<sup>10</sup>. However, the possible involvement of such a rearrangement in the catalytic process was not proven to date and it may even be that these changes in coordination geometry only occur in  $\text{Ty}_{h\text{-met}}$  and does not play a role in the catalytic turnover of mono and diphenolic substrates.

Recently, two papers regarding EPR related work (cwEPR, HYSCORE, ESEEM) on the half-met derivative of *Streptomyces antibioticus* have been published<sup>32,33</sup>. This work confirmed that the cupric Cu is 4-coordinated in the absence of exogenously added ligands in a distorted tetragonal geometry. Three of the ligands are the conserved histidines, whereas the fourth ligand represents an equatorially coordinated solvent exchangeable hydroxide or water group. The binding of p-nitrophenol to  $\text{Ty}_{h\text{-met}}$  causes the latter signal to vanish in the HYSCORE spectrum, while the Cu(II) remains 4-coordinate

without large changes in the coordination geometry. This is most easily interpreted as an exchange of the equatorial hydroxide/water upon monophenol binding. On the other hand, the paramagnetic Cu ion becomes 5-coordinate upon the binding of bidentate inhibitors and transition state analogues such as toluic acid and mimosin. From this it has been concluded that mono- and diphenolic substrates dock in the same region in the active site. Furthermore, simulation of the ESEEM data was only possible assuming that CuB is the paramagnetic Cu (using the X-ray structure of *Limulus polyphemus* Hc as a template), suggesting that it is CuB rather than CuA that interacts with both monophenolic and diphenolic substrates.

### The reduced derivative $E_{\text{red}}$

The reduced Cu ions in  $E_{\text{red}}$  occur in a  $3d^{10}$  electronic configuration and are consequently diamagnetic and EPR silent. The  $E_{\text{red}}$  derivative is further devoid of characteristic features in the UV/Vis spectrum. The Cu-Cu distance amounts to  $\sim 4.5$  Å in the sweet potato CO, which is considerably longer than the Cu-Cu distances found in the  $E_{\text{met}}$  and  $E_{\text{oxy}}$  forms (table 1). Yet, upon the conversion from  $E_{\text{oxy}}$  to  $E_{\text{red}}$ , the His ligands do not move by a large amount. Each of the coppers is 3 His coordinate in an approximately trigonal planar geometry.

### The oxygen bound derivative $E_{\text{oxy}}$

The  $E_{\text{oxy}}$  derivative is the best studied derivative for all members of the type-3 protein family. Furthermore, the synthesis and characterisation of several dinuclear copper model complexes, which bind oxygen similar to tyrosinase and hemocyanin, have contributed greatly to the understanding of the  $E_{\text{oxy}}$  derivatives of Hcs, Tys and COs. The design of these compounds has been driven by the desire to understand the mechanism of oxygen binding and activation in natural systems, as well as by the prospect of using these compounds as industrial oxygenation catalysts (e.g. <sup>35</sup>). Consequently, a wealth of papers concerning the synthesis, characterisation and theory of these oxygen binding dinuclear copper model compounds has appeared over the last two decades or so (see below).

The oxygenated derivative of tyrosinase ( $Ty_{\text{oxy}}$ ) can be prepared from  $Ty_{\text{met}}$  by the addition of peroxide or by the two-electron reduction of  $Ty_{\text{met}}$  to the [Cu(I) Cu(I)] deoxy form followed by the reversible binding of  $O_2$  <sup>36</sup>. The  $O_2$  binds as peroxide, giving a formal charge of +2 to each of the coppers. The  $Ty_{\text{oxy}}$  derivative reacts with monophenolic as well as diphenolic substrates <sup>34</sup>. Therefore, the understanding of the  $Ty_{\text{oxy}}$  site is a key aspect to understand the chemistry of tyrosinase. EXAFS on tyrosinase ( $Ty_{\text{oxy}}$ ) has shown that the distance between the two copper atoms is about 3.6 Å (<sup>37</sup> and references therein). The UV/VIS absorption spectra of  $Hc_{\text{oxy}}$  and  $Ty_{\text{oxy}}$  are shown in Figure 4.

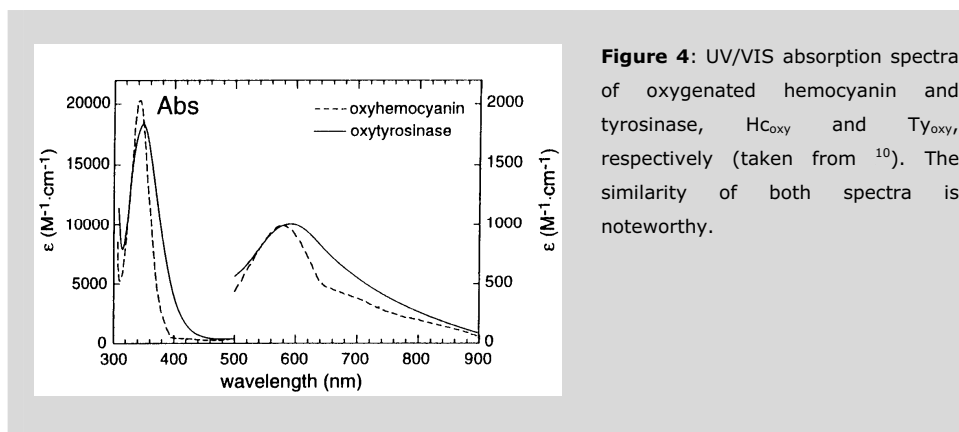


**Figure 4:** UV/VIS absorption spectra of oxygenated hemocyanin and tyrosinase,  $Hc_{oxy}$  and  $Ty_{oxy}$ , respectively (taken from <sup>10</sup>). The similarity of both spectra is noteworthy.

The spectra are very similar and share some unique features. They both exhibit a weak and broad band at about 570 nm with  $\epsilon \approx 1000 \text{ M}^{-1}\text{cm}^{-1}$  and an intense absorption band around 350 nm with  $\epsilon \approx 20,000 \text{ M}^{-1}\text{cm}^{-1}$ , which overshadows any UV/VIS spectral features of other derivatives when only minute amounts of  $Ty_{oxy}$  are present in the sample. Resonance Raman studies on both  $Ty_{oxy}$  and  $Hc_{oxy}$  show a very low O-O stretching frequency of  $\sim 750 \text{ cm}^{-1}$ , indicating a low O-O bonding energy (<sup>10</sup> and references therein). These studies also showed that the dioxygen is bound symmetrically as the peroxide. Like the  $Ty_{met}$  derivative, the  $Ty_{oxy}$  form is EPR silent, which is again due to strong antiferromagnetic coupling between the two copper atoms via the bridging peroxide superexchange pathway ( $-2J > 1000 \text{ cm}^{-1}$  <sup>10</sup>).

To explain the spectroscopic data in terms of the peroxide binding mode, a *cis- $\mu$ -1,2* peroxide ‘end-on’ bridging mode (Figure 5) was proposed in early literature, since this was the only geometry known at the time which was reasonably consistent with the experimental data (e.g. <sup>31</sup>). This structure is common for peroxide-bridged cobalt dimers <sup>38</sup>. Yet, no analogue copper-peroxide complex had been prepared at that time.

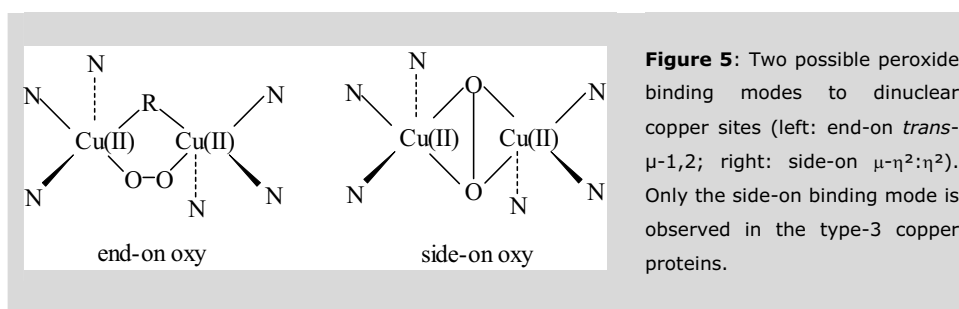
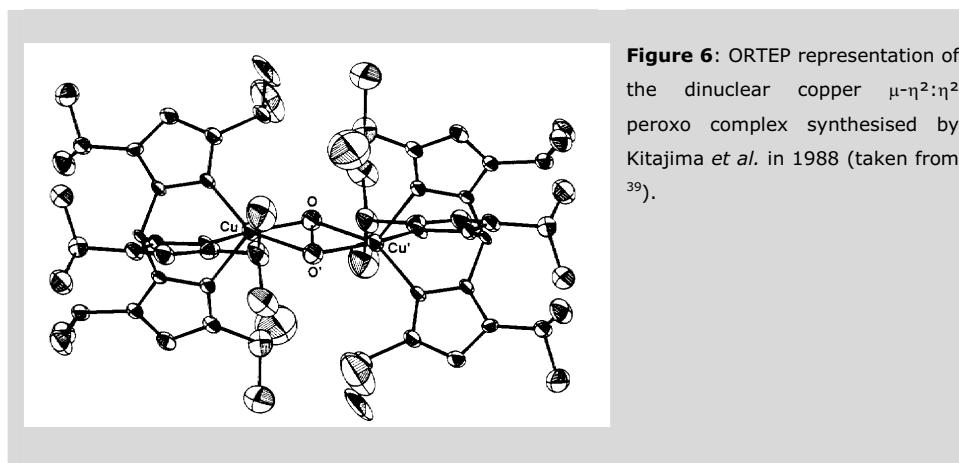


**Figure 5:** Two possible peroxide binding modes to dinuclear copper sites (left: end-on *trans- $\mu$ -1,2*; right: side-on  $\mu$ - $\eta^2$ : $\eta^2$ ). Only the side-on binding mode is observed in the type-3 copper proteins.

In 1984, Karlin *et al.* succeeded in preparing a dinuclear copper-complex that could bind dioxygen reversibly at low temperatures ( $-80\text{ }^{\circ}\text{C}$ ; <sup>39</sup> and references therein). Spectroscopic and chemical studies on this complex showed that the peroxide bridged the two copper atoms in a *trans*- $\mu$ -1,2 manner (Figure 5). The *trans*- $\mu$ -1,2 copper complex was also structurally characterised by X-ray crystallography. Several analogues were also synthesised (<sup>40</sup> and references therein). Although the complexes appeared very promising model-systems for the copper monooxygenases, spectroscopic studies on these complexes showed that the spectroscopic features of  $\text{Hc}_{\text{oxy}}$  and  $\text{Ty}_{\text{oxy}}$  were different from those of the model complexes, especially concerning the low O-O stretching frequency and the intense 350 nm LMCT absorption band.

A major breakthrough was achieved in 1988 when Kitajima *et al.* succeeded in synthesising a dinuclear copper complex which showed a novel copper/oxygen coordination mode (Figure 6; <sup>41</sup>). This complex contains sterically hindered facial  $\text{N}_3$  tris(pyrazolyl)borate ligands, which provide a coordination environment similar to that of  $\text{Hc}_{\text{oxy}}$ . The spectroscopic properties of the oxygen bound complex show remarkable resemblance to those of  $\text{Hc}_{\text{oxy}}$  and  $\text{Ty}_{\text{oxy}}$ . X-ray analysis of an analogous complex showed that the peroxide is bound in a  $\mu$ - $\eta^2$ : $\eta^2$  fashion. The coordination mode was designated  $\mu$ - $\eta^2$ : $\eta^2$  because the Cu-O and Cu-O' distances are nearly identical in the crystal structure of the complex, and because the two copper atoms and the peroxide reside in the same plane <sup>39</sup>.



In the Kitajima complexes, four of the Cu-N distances are relatively short ( $\sim 2.00\text{ \AA}$ ) and almost identical to the Cu-O distances, whereas the remaining two Cu-N bonds are elongated ( $\sim 2.26\text{ \AA}$ ). The coordination geometry around each Cu can therefore be described as square-pyramidal with the basal plane consisting of the two oxygen and two

nitrogen atoms, although the structure is somewhat distorted from this ideal geometry<sup>37</sup>, especially in the equatorial plane. The square-pyramidal geometry is preferred since the cupric ion (II) favours a five coordination mode over a tetrahedral four-coordinate mode. The Cu-Cu distance in the  $\mu\text{-}\eta^2\text{:}\eta^2$  complex is remarkably close to those found for Hc<sub>oxy</sub> and Ty<sub>oxy</sub> (3.56 Å; Table 2).

**Table 2:** Physicochemical properties of Hc<sub>oxy</sub>, Ty<sub>oxy</sub> and the Kitajima model complex depicted in Figure 6 (taken from<sup>37</sup>).

Compound	magnetic property	absorption bands (nm)	$\epsilon$ (M <sup>-1</sup> cm <sup>-1</sup> )	$\nu(\text{O-O})$ (cm <sup>-1</sup> )	Cu-Cu distance (Å)
Model complex Figure 6	diamagnetic	349	21000	741	~3.6
		551	790		
Hc <sub>oxy</sub>	diamagnetic	340	20000	744-752	3.5-3.7
		580	1000		
Ty <sub>oxy</sub>	diamagnetic	345	18000	755	~3.6
		600	1200		

Magnetic susceptibility measurements on a model complex analogous to that in Figure 6 showed a large antiferromagnetic coupling between the two copper centres of  $-2J > 1000$  cm<sup>-1</sup>, again similar to the corresponding values of both Hc<sub>oxy</sub> and Ty<sub>oxy</sub> (<sup>41</sup> and references therein). Based on the similarities between the model complexes synthesised by Kitajima and the oxygenated forms of Ty and Hc, it has now been generally accepted that the peroxide binds in a  $\mu\text{-}\eta^2\text{:}\eta^2$  fashion to the dinuclear copper sites in these proteins<sup>37</sup>. The  $\mu\text{-}\eta^2\text{:}\eta^2$  binding mode has already been confirmed experimentally for Hc<sub>oxy</sub> from a XRD study of the oxygenated derivative of this protein<sup>13</sup>.

The interpretation of the UV/VIS absorption bands of Hc<sub>oxy</sub> and Ty<sub>oxy</sub> has been subject of extensive experimental and theoretical studies. These have led to a general description of the absorption characteristics of dinuclear copper  $\mu\text{-}\eta^2\text{:}\eta^2$  peroxo structures. The intense 350 nm and less intense 570 nm band arise from two peroxide-to-copper LMCT transitions, one from each of the  $\pi^*$  orbitals, which are the highest occupied MO's (HOMO's) of the peroxide<sup>38</sup>. The intense band at 350 nm has been assigned to the  $\pi^*\sigma \rightarrow \text{Cu}$  CT transition whereas the 570 nm band is assigned to the  $\pi^*\nu \rightarrow \text{Cu}$  CT transition<sup>38</sup>. The greater intensity of the 350 nm band arises from the greater overlap of the half-occupied copper dx<sup>2</sup>-y<sup>2</sup> HOMOs compared to the orbital overlap of the  $\pi^*\nu \rightarrow \text{Cu}$  CT transition<sup>38</sup>.

### The Ty reaction mechanism

Numerous reports on the action of Ty have appeared in the past to explain the monophenolase and diphenolase activities of the enzyme on a structural level. Several structural mechanisms have been proposed by different investigators, although none of them was proven experimentally. Thus, after decades of research on the enzyme, the mechanism is still not known. Some of the most recently proposed mechanisms, based on the now generally accepted  $\mu\text{-}\eta^2\text{:}\eta^2$  peroxide binding mode, are discussed below.

The activation and cleavage of the peroxide bond is perhaps the most intriguing step in the mechanism. The dioxygen activation mechanism is not only relevant to Ty, but also for other metalloenzymes and synthetic catalysts that bind, utilise or activate dioxygen (e.g. hemocyanin, dopamine  $\beta$ -monooxygenase, methane monooxygenase and so on). The binding and activation of dioxygen by metallic complexes (and proteins) also has an economical and industrial relevance, namely in the design and applications of oxygenating catalysts and oxygen scavenging/storing compounds. The mechanism of oxygen-binding and activation in model complexes will be discussed separately below.

### The kinetic mechanism of Ty catalysis.

The elucidation of the kinetic mechanism supplies the basic information needed to propose a minimal reaction scheme of the catalytic cycle in which all relevant reaction intermediates are present. The Ty kinetic scheme is rather complex since it must explain both the monophenolase and diphenolase activities, as well as the lag phase observed in the conversion of monophenolic compounds. Consequently, in the literature, 5 different kinetic schemes were proposed by different authors over a time-span of over 40 years. For a detailed and historical description of these reaction cycles the reader is referred to <sup>4</sup>. A general consensus regarding the kinetic mechanism has now been reached, which is symbolically presented in Figure 7.

The data in Table 3 show that the critical and rate-limiting step in the conversion of tyrosine is the conversion of  $\text{Ty}_{\text{oxy}}$ -Tyrosine to  $\text{Ty}_{\text{met}}$ -DOPA ( $10^3 \text{ s}^{-1}$ ), the reaction step which also includes the cleavage of the peroxide bond. This step is followed by the rapid conversion ( $10^7 \text{ s}^{-1}$ ) of the  $\text{Ty}_{\text{met}}$ -diphenol back to  $\text{Ty}_{\text{red}}$ . The 'suicide-inactivation' of Ty by diphenols also can be distinguished in the cycle. Addition of diphenol to an enzyme solution containing  $\text{Ty}_{\text{oxy}}$  results in the formation of  $\text{Ty}_{\text{met}}$ , which is incapable of reacting further with tyrosine. The dead-end derivative  $\text{Ty}_{\text{met}}$  can only be efficiently converted back to  $\text{Ty}_{\text{red}}$  at relatively high diphenol concentrations ( $K_{\text{DOPA-Ty}_{\text{met}}} = 0.14 \text{ mM}$ ).

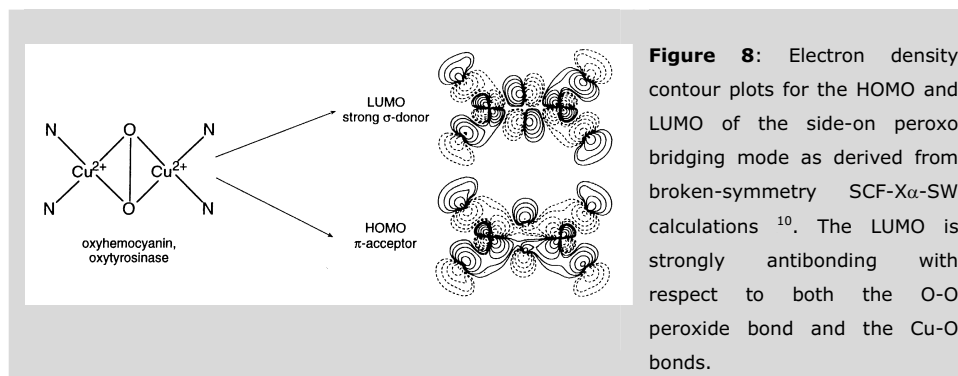




evidence that the latter hypothesis is correct<sup>46;47</sup>. In this mechanism, the observed behaviour arises from the fact that monophenolic compounds only can react with  $Ty_{oxy}$ , while diphenolic substrates can react with both  $Ty_{oxy}$  and  $Ty_{met}$ . Since the enzyme is present in 10-15%  $Ty_{oxy}$  and 85-90%  $Ty_{met}$  at STP, and  $Ty_{met}$  cannot bind dioxygen, only a small percentage of the enzyme is able to react with monophenolic compounds in the initial phase, resulting in a low observed rate of conversion. The presence of diphenolic compounds in the reaction medium ultimately results in the conversion of  $Ty_{met}$  into  $Ty_{red}$ , which binds dioxygen and puts this enzyme in the monophenolase pathway, thus raising the observed catalytic rate. A further factor in the lag phase kinetics is due to substrate inhibition that arises from the binding of monophenol to  $Ty_{met}$ , forming a dead end complex. In the oxidation of tyrosine, the diphenolic activator is formed indirectly by the disproportionation of *ortho*-quinone into DOPACHrome and DOPA<sup>46</sup>, as products in the melanogenesis pathway (Figure 1), as well as by the release of diphenolic product formed by the hydroxylation of the monophenolic substrate<sup>47</sup>.

### Proposed structural mechanisms of Ty and their main characteristics.

Solomon's group has published several papers directly or indirectly related to the action of Ty and other dinuclear copper-proteins (reviewed in<sup>10;48</sup>). The complete catalytic cycle of the Ty mono- and diphenolase activities proposed by Solomon is depicted in Figure 9. The mechanism follows the kinetic scheme depicted in Figure 7, with the exception that the binding of monophenol to the  $Ty_{met}$  form is not included in the Solomon mechanism.



The elementary features concerning the monophenolase cycle are interpreted as follows. The monophenol binds to an axial position of one of the coppers in  $Ty_{oxy}$ , resulting in the donation of spin density into the peroxide antibonding orbital. This weakens the O-O bond and activates it for cleavage. The site then undergoes a trigonal bipyramidal rearrangement towards the equatorial plane, which orients the substrate to an arrangement

facilitating hydroxylation. This event generates a coordinated diphenolate which is oxidised to the *o*-quinone through the transfer of two electrons to the coppers, leaving the reduced derivative of the enzyme, which is then available for further turnover, and the quinone reaction product.

In the diphenolase cycle, both  $Ty_{met}$  and  $Ty_{oxy}$  derivatives react with the diphenol, oxidising it to the quinone. From inhibitor-binding studies it was shown that bulky substituents on the phenyl ring strongly reduce the monophenolase activity, but not the diphenolase activity<sup>34</sup>. It was suggested that rearrangement of the coordinated substrate from an axial to an equatorial position is not necessary for the simple two-electron transfer associated with the diphenolase activity<sup>10</sup>.

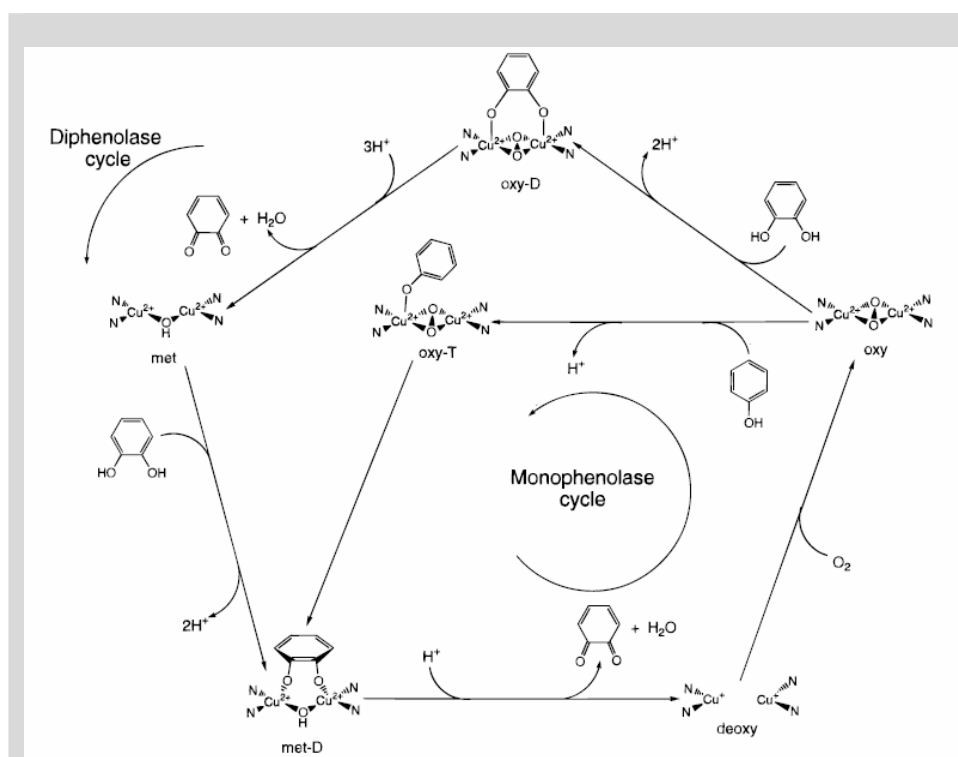
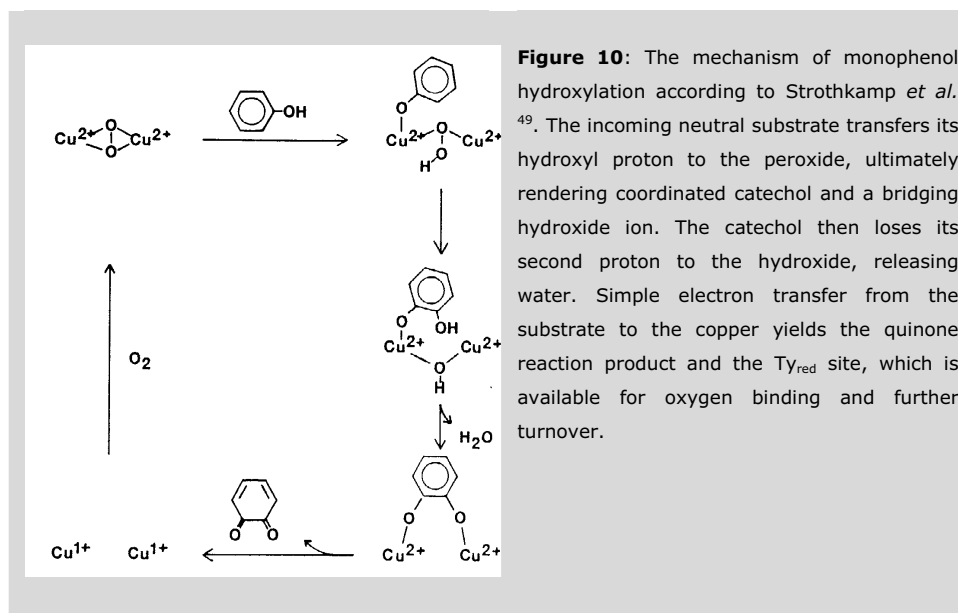


**Figure 9:** The catalytic mechanism of Ty proposed by Wilcox & Solomon<sup>34</sup>. The direct coordination of monophenolic compounds to at least one of the square-pyramidal coordinated copper centres induces a rearrangement towards a trigonal bipyramidal geometry, displacing the bound peroxide and thereby facilitating hydroxylation. The quinone is formed through simple electron transfer from the coordinated diphenolic substrate to the copper, after which the product is released from the enzyme. The diphenolic substrate is proposed to coordinate in a  $Cu_2$  bridging fashion.

The role of the protons that are subtracted from the substrate and the ones involved in the reduction to water was addressed by Strothkamp and co-workers<sup>49</sup> by evaluating the pH dependence and the solvent deuterium isotope effects of the inhibition process. Considering the fact that inhibitor binding is thought to involve coordination to copper, and that both carboxylic acids and phenols must lose a proton upon binding, transfer of a proton to some other group in the enzyme is likely to occur. One possibility is that one weak ligand in the free enzyme is protonated and displaced from the copper atom(s) on binding of a protonated inhibitor/substrate molecule, keeping the copper coordination number the same. The latter hypothesis was supported by the deuterium isotope effect. The linear relationship between the enzyme-inhibitor formation constant and the fraction  $D_2O$  in solution indicated that only one proton is responsible for the observed isotope effect.

When proton-exchange with a group already carrying an exchangeable proton would occur, a non-linear relationship would have been expected. Thus, exchange of a proton with active-site water, hydroxide-ion, amino-acid side chains or other protein functional groups seemed unlikely, since these possibilities would most likely lead to a non-linear proton inventory plot. This conclusion formed the basis for a mechanism as depicted in Figure 10.



The key element in the scheme presented in Figure 10 is that the bound peroxide is the proton acceptor in the binding process. The actual substrate is the acidic form of the phenol. Electrophilic attack of the coordinated peroxide on the ring and cleavage of the O-O bond produces coordinated catechol and a bridging hydroxide ion. The catechol then (possibly) rearranges to a bidentate coordination mode over both coppers, in which the second proton is transferred to the hydroxide, releasing water. Electron transfer from the catechol to the coppers leaves the quinone and the reduced coppers, which are then available for dioxygen binding and further turnover. Based on model-compound studies, Karlin also suggested a role for protonation of bound oxygen to generate a reactive hydroperoxide species (<sup>39</sup>; see below). The products released in this scheme are electrically neutral (water and quinone), which would be consistent with the proposed hydrophobic active site structure of the enzyme.

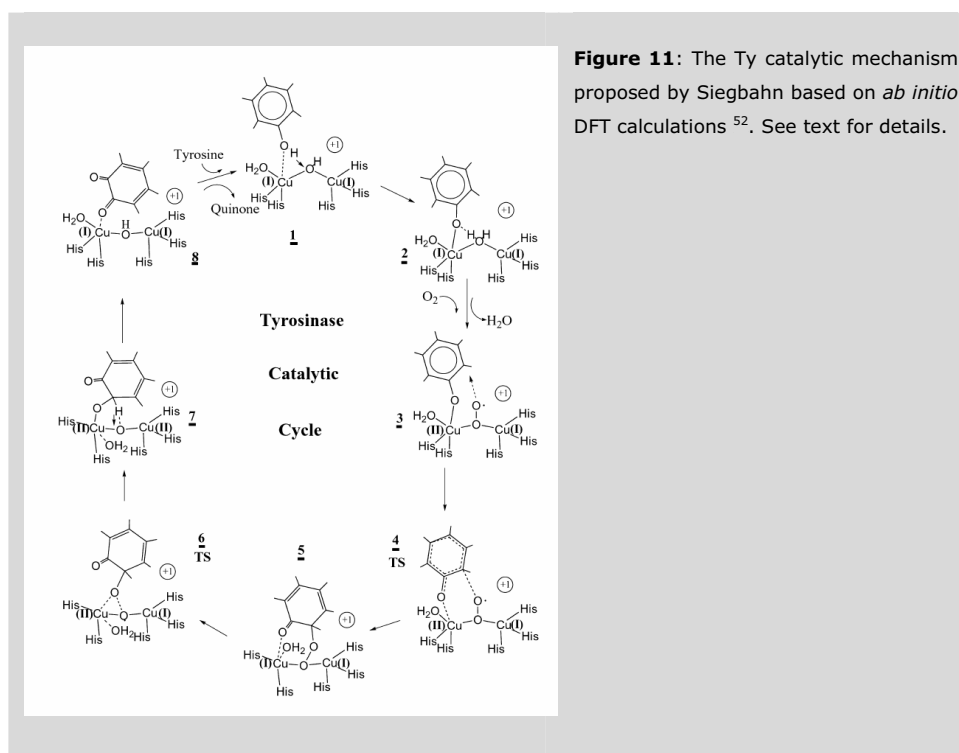
#### **A monophenolase mechanism from ab-initio calculations.**

Only in recent years the methodologies and computational power have become available to study enzyme catalysis (involving a considerable number of atoms) on a quantum mechanical level. A series of theoretical studies related to the Ty reaction chemistry performed by Siegbahn and co-workers have appeared in the literature that together resulted in a proposal for the Ty reaction mechanism <sup>50-52</sup>. Since no X-ray structure is available for any Ty, the active site structures of Hcs and CO have been used as a model to guide the calculations. One important result of the calculations (all performed using the DFT method B3LYP) was that the bis( $\mu$ -oxo) Cu(III)<sub>2</sub>O<sub>2</sub> core as occurring in the Tolman complexes (described below) is an unlikely intermediate in the Ty reaction mechanism, even as a short-lived transient species.

Several possible pathways for the monophenolase reaction have been evaluated, mainly based on previously proposed mechanisms (see above). Only one investigated pathway gave results consistent with the experimentally observed rate constants, which is schematically presented in Figure 11. In this mechanism, the phenol binds to the reduced enzyme (structures 1 & 2), which is then followed by the binding of the oxygen co-substrate. This results in the formation of a Cu<sub>2</sub> bridging peroxide radical that attacks the phenolic ring (structures 3, 4 & 5), followed by cleavage of the O-O bond (structure 6). The hydrogen at the sp<sup>3</sup> hybridized carbon of the quinone ring is then transferred to the  $\mu$ -oxide (structure 7), completing the formation of the ortho-quinone (structure 8) and closing the catalytic cycle.

An important feature in this mechanism is that one copper in the Cu<sub>2</sub> site contains only 2 His ligands during the reaction. The possibility that the Ty type-3 site contains a total of 5

instead of 6 His ligands can be excluded *a priori* based on sequence homologies and experimental evidence from  $^1\text{H}$  paramagnetic NMR studies on  $\text{Ty}_{\text{met}}$ <sup>21</sup>. Thus, if the Siegbahn mechanism is correct, it has to be assumed that one Cu coordinated His ligand moves away from Cu to the second coordination sphere. Furthermore, the oxygen is proposed to bind *after* binding of the phenol substrate while it is generally believed that the contrary is the case. In fact, under standard conditions, > 95 % of Ty occurs in the oxygen bound  $\text{Ty}_{\text{oxy}}$  form in preparations of  $\text{Ty}_{\text{red}}$  resulting from the highly efficient binding of  $\text{O}_2$  to  $\text{Ty}_{\text{red}}$  in the absence of substrate (the oxygen /  $\text{Ty}_{\text{red}}$  binding constant is  $\sim 10^6 \text{ M}^{-1}$ <sup>4</sup>).

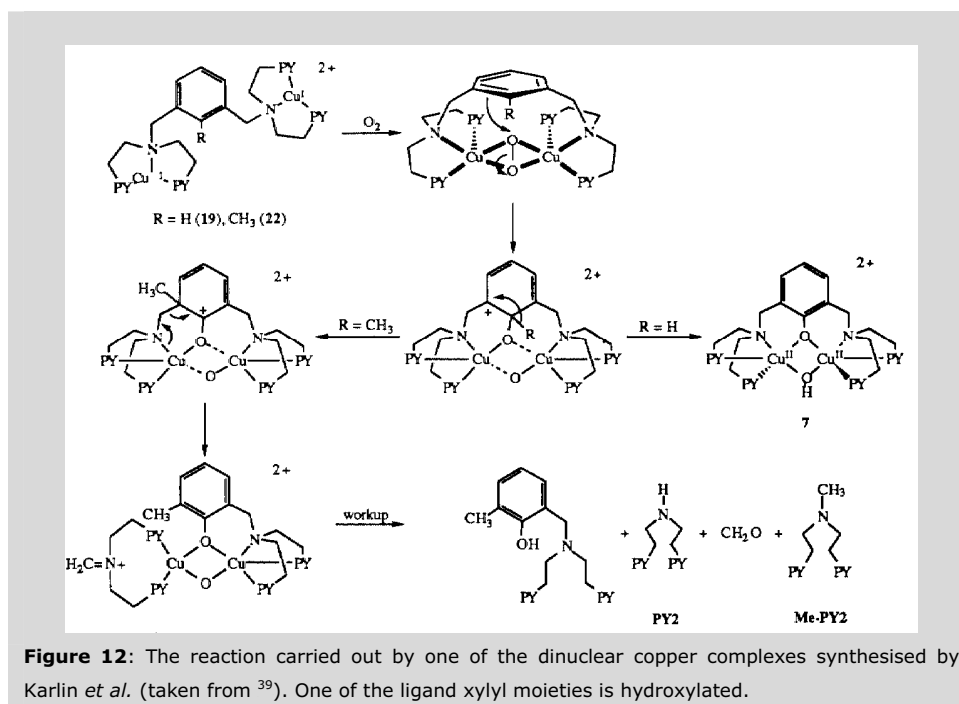


### The mechanism of oxygen-activation.

The mechanism of binding and activation of dioxygen by (dinuclear) metalloproteins like tyrosinase is a heavily researched topic in modern bioinorganic chemistry. Detailed investigations of synthetic model complexes have contributed greatly to the understanding of dioxygen binding and activation by metal ions in biological and other catalytic systems. The most relevant information concerning the binding and activation of dioxygen by dinuclear copper complexes will be summarised in the next sections.

### Reactions of the Karlin complexes.

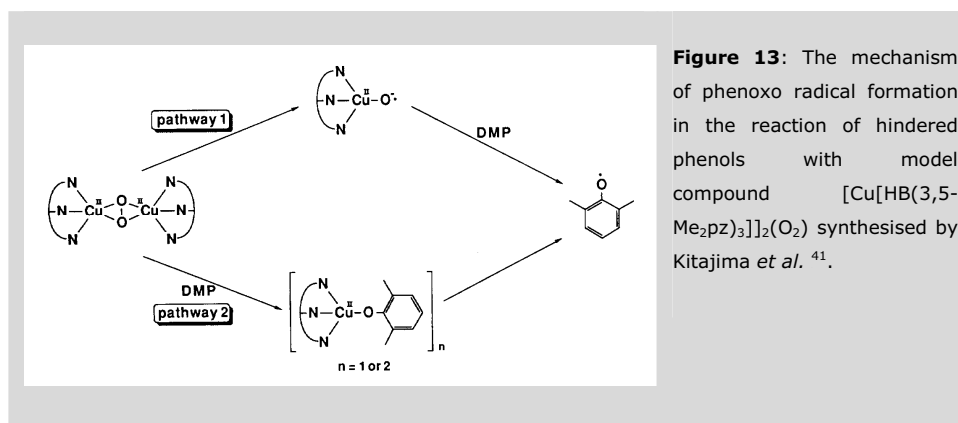
The intramolecular hydroxylation of a xylyl group connecting two tridentate chelates is schematically shown in Figure 12.



Kinetic and chemical studies on the hydroxylation reaction have shown that the reaction is carried out via electrophilic attack of the peroxide on the aromatic CH group. Another important observation was made when a methyl group was incorporated into the 2-position of the ligand. With this compound, 2-hydroxylation still occurs and the methyl group undergoes 1,2-migration. This process is reminiscent of a so-called 'NIH-shift' mechanism. These results have led to the proposal of a reaction scheme consistent with all experimental data, which is shown in Figure 14. Karlin *et al.* suggested that a similar reaction could occur in Ty<sup>37</sup>. It must be noted, however, that the μ-peroxo intermediate was not directly observed and that the substrate was not directly coordinated to one of the copper atoms, as probably occurs in Ty. Also, the hydroxylation reaction is not carried out on externally added substrates as is the case with Ty.

### Reactions of the Kitajima complexes.

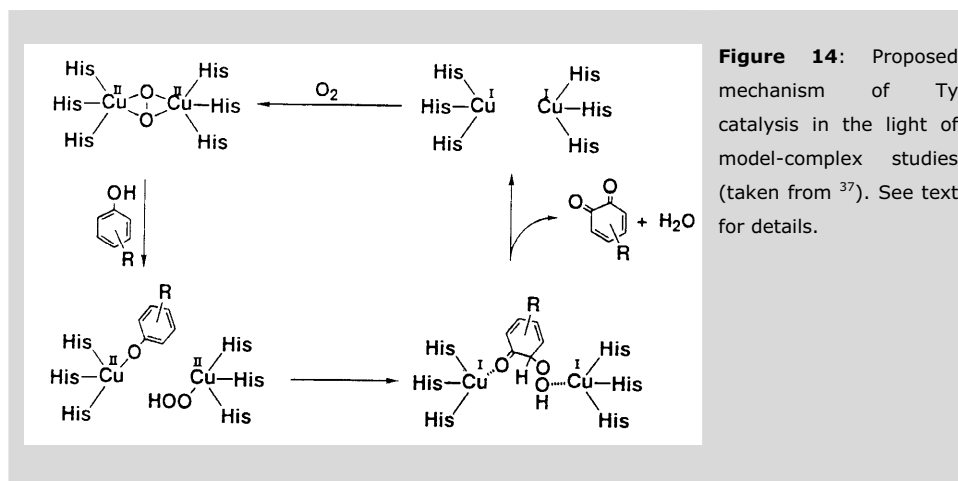
Of the several dinuclear copper  $\mu$ - $\eta^2$ : $\eta^2$ -peroxo model complexes synthesised by Kitajima *et al.* (reviewed in <sup>37</sup>), the compound  $[\text{Cu}[\text{HB}(3,5\text{-Me}_2\text{pz})_3]]_2(\text{O}_2)$  appears to catalyse the conversion of sterically hindered phenols into diphenoquinones. Although Ty primarily reacts with phenols to render benzoquinones, diphenoquinones appear to be generated by the enzyme when hindered phenols are used as the substrate. Thus, the model compound resembles the reaction chemistry of Ty with these sterically hindered substrates, and can be used as a model for the Ty monophenolase activity.



The reactions of hindered phenols with the model compound are thought to proceed through a phenoxo radical which is generated via two distinct pathways (Figure 13). One pathway involves the spontaneous cleavage of the peroxide bond to afford a Cu(II)-O• species which abstracts H• from phenol. The other pathway is characterised by a replacement between the phenol and the peroxide to render a phenoxo intermediate which undergoes a reductive Cu-O bond cleavage resulting in the formation of a phenoxo radical. The O-O bond cleavage (pathway 1) probably does not occur in Ty, since the copper ions are held in place by the protein matrix, so as to reverse the cleavage. In contrast, pathway 2 is a possible mechanism for the Ty hydroxylation reaction.

In another alkylperoxo model complex, it is observed that the hydroperoxo intermediate undergoes Cu-O bond homolysis, releasing  $\text{HOO}\cdot$  <sup>37</sup>. Kitajima suggests that this also occurs with the  $[\text{Cu}[\text{HB}(3,5\text{-Me}_2\text{pz})_3]]_2(\text{O}_2)$  complex. The formed phenoxo radical and the  $\text{HOO}\cdot$  radical instantaneously couple to each other to give a hydroperoxyquinone which is converted to benzoquinone, completing the reaction-cycle. The fact that diphenoquinone, and not benzoquinone, is generated is explained by the fact that hindered phenols are used. In this case, the inner-sphere coupling between the phenoxide and the hydroperoxide may

not occur effectively, so that the phenoxo radical is released from the complex to give a diphenoquinone via a free-radical mechanism.

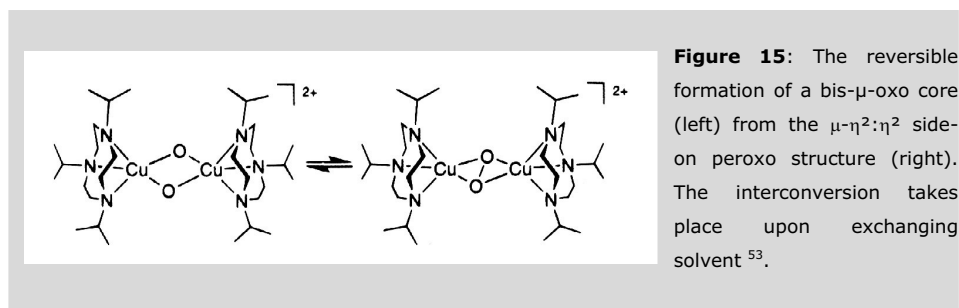


The mechanism in Figure 14 bears some similarities with the reaction scheme proposed by Conrad *et al.*<sup>49</sup> (Figure 10) in the sense that the acidic proton of the phenol hydroxyl is directly transferred to the bridged peroxo group. Still, the two schemes are fundamentally different since the reaction proceeds via an electrophilic attack in the scheme of Conrad *et al.*<sup>49</sup>, while it proceeds via a free-radical mechanism in the scheme of Kitajima *et al.* One argument that contradicts a free radical mechanism is that the reaction-rate of Ty is significantly altered when electron-withdrawing groups are present in the *para* position with respect to the hydroxyl moiety of the substrates<sup>49</sup>, suggesting a mechanism via electrophilic attack. Moreover, the side-on coordination mode of the peroxide seems to favour an electrophilic mechanism relative to other oxygen binding modes<sup>10</sup>.

#### The reversible cleavage and formation of the peroxo O-O bond in Tolman's $\mu\text{-}\eta^2\text{:}\eta^2\text{-peroxo}$ model complexes and its reaction with aliphatic molecules.

The reversible scission and formation of the O-O bond (Figure 15) in a synthetic dinuclear copper model complex in which peroxide bridges the two Cu ions in the  $\mu\text{-}\eta^2\text{:}\eta^2$  side-on bridging mode was first demonstrated by Tolman and co-workers (<sup>53</sup>, reviewed in <sup>35;54</sup>). Further investigations of this model complex showed that the derivative efficiently cleaved a ligand appendage by a dealkylation reaction that models the action of Ty.





The two interconvertible derivatives of the model complex are schematically depicted in Figure 15. The complex consists of two copper ions each coordinated by a tridentate 1,4,7-tribenzyl-1,4,7-triazacyclononane ligand, which is similar to the coordination mode in the Kitajima and the Karlin complexes mentioned above. At low temperatures ( $-80\text{ }^\circ\text{C}$ ), oxygen binds reversibly to this complex in the side-on  $\mu$ - $\eta^2$ : $\eta^2$  bridging mode. The  $\mu$ - $\eta^2$ : $\eta^2$ -peroxo structure can be reversibly and quantitatively converted to a complex wherein the peroxide O-O bond is broken (rendering a bis( $\mu$ -oxo) $\text{Cu(III)}_2$  core) by changing the solvent (dichloromethane  $\leftrightarrow$  THF). The interconversion does not involve mononuclear species or molecular oxygen. The preferred oxygen binding mode is dependent on several factors. First, it was found that the Cu...Cu distance in the bis( $\mu$ -oxo) structure is considerably shorter than that in the peroxo structure (2.9 Å and  $\sim$ 3.6 Å, respectively). Hence, it seems that the bis( $\mu$ -oxo) structure is favoured by shorter Cu...Cu distances.

The spectroscopic characteristics of the bis( $\mu$ -oxo) derivative of the model compound are different from those of the corresponding peroxo structure, the latter being almost identical to the spectroscopic characteristics of  $\text{Ty}_{\text{oxy}}$ ,  $\text{Hc}_{\text{oxy}}$  and the several other  $\mu$ - $\eta^2$ : $\eta^2$  peroxo model complexes described above (UV/VIS, Raman, EPR). Although both derivatives share the feature of a  $S = 0$  ground state and thus lack an EPR signal, the optical spectra of both compounds are different from each other (Figure 16). The bis( $\mu$ -oxo) structure shows an intense LMCT transition at  $\sim$ 430 nm with  $\epsilon = 14.5 \cdot 10^3\text{ M}^{-1}\text{cm}^{-1}$ . This makes the compound readily distinguishable from the peroxo structure, which has the strongest absorption maximum at a lower wavelength of about 370 nm and  $\epsilon = 23 \cdot 10^3\text{ M}^{-1}\text{cm}^{-1}$ .

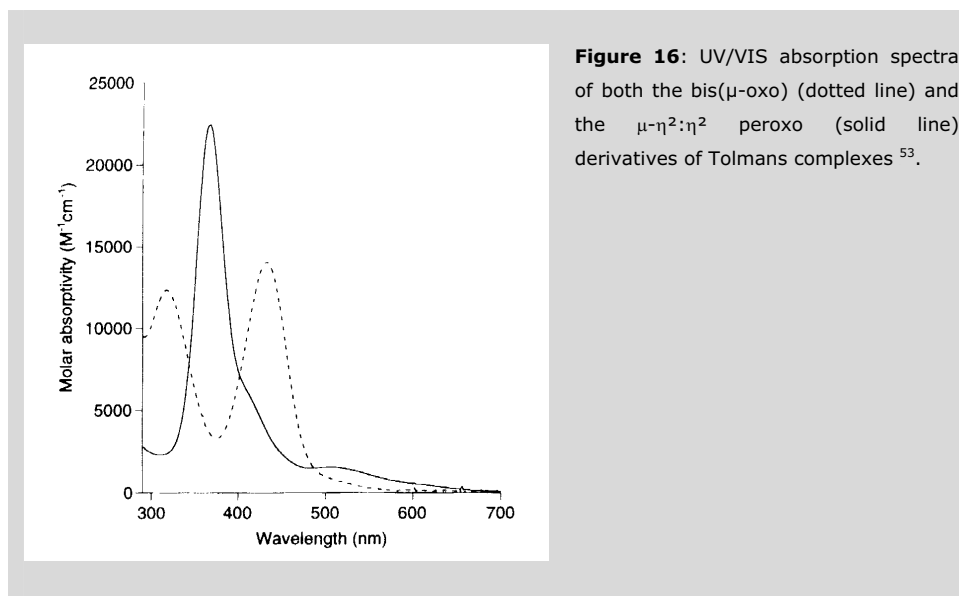
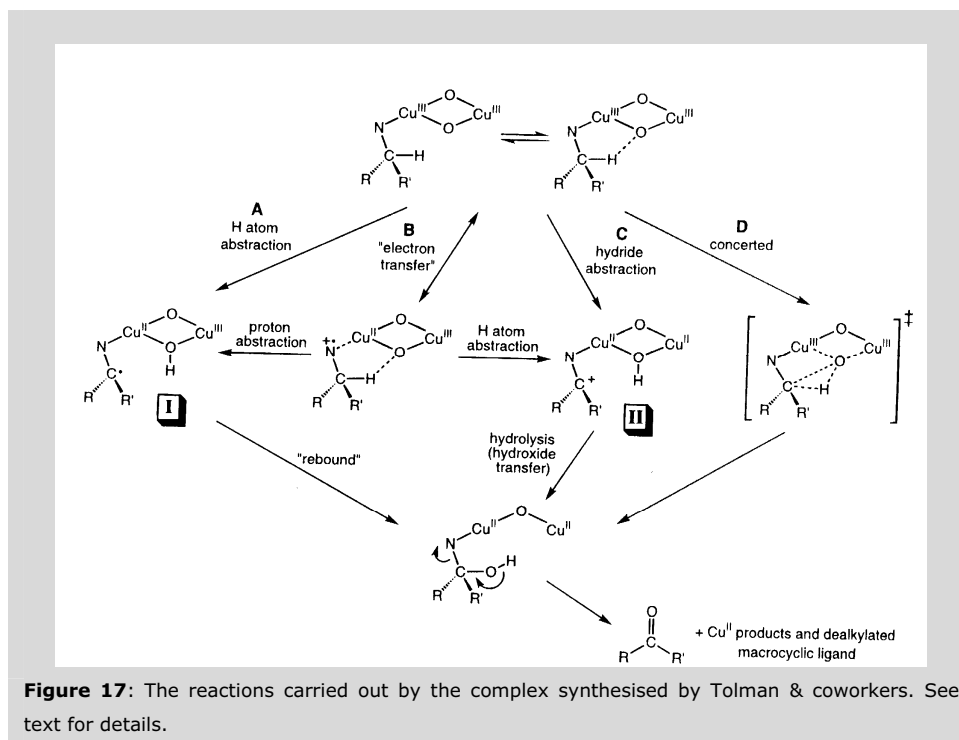


**Figure 16:** UV/VIS absorption spectra of both the bis( $\mu$ -oxo) (dotted line) and the  $\mu$ - $\eta^2$ : $\eta^2$  peroxo (solid line) derivatives of Tolmans complexes<sup>53</sup>.

Both the peroxo and bis( $\mu$ -oxo) structures are thermally unstable. The decomposition is accompanied by a dealkylation reaction in which a phenyl group is cleaved from the ligands, yielding the free modified ligands and a benzaldehyde molecule (Figure 17). Based on isotope labelling studies, the decomposition is identified as a monooxygenase reaction. The rate-determining step in the reaction is the  $\alpha$ -C-H bond scission and the thermodynamics for the process are consistent with the bis( $\mu$ -oxo) core behaving as an electrophilic radical. It was also shown that the dealkylation is an intramolecular reaction that does not involve diffusible monomeric species. The dealkylation reaction may proceed via two distinct pathways as indicated in Figure 17. The first pathway (a) involves hydrogen abstraction from the C-H bond by the bridging oxygen atom. This generates a carbon-centered radical that is trapped by the resulting Cu-hydroxyl species. Alternatively (b), C-H bond scission and oxygen transfer may proceed in a concerted manner.

The bis( $\mu$ -oxo) structure was never observed in any protein to date. However, considering the high reactivity of such a structure, it may be possible that the intermediate does indeed exist in biological oxygenation reactions (e.g. with the monophenolase reactivity of Ty) but that it is short lived and consequently escaped detection in previous investigations. As mentioned above, *ab initio* calculations argue against a role for the bis( $\mu$ -oxo) core in the Ty monophenolase reaction<sup>50-52</sup>.



## References

- (1) Holm, R. H.; Kennepohl, P.; Solomon, E. I. *Chemical Reviews* **1996**, *96*, 2239-2314.
- (2) Asimov, I.; Dawson, C. R. *J. Am. Chem. Soc.* **1950**, *72*, 820-828.
- (3) van Gelder, C. W.; Flurkey, W. H.; Wichers, H. J. *Phytochem.* **1997**, *45*, 1309-1323.
- (4) Sanchez-Ferrer, A.; Rodriguez-Lopez, J. N.; Garcia-Canovas, F.; Garcia-Carmona, F. *Biochim. Biophys. Acta* **1995**, *1247*, 1-11.
- (5) Seo, S. Y.; Sharma, V. K.; Sharma, N. *J. Agric. Food Chem.* **2003**, *51*, 2837-2853.
- (6) Prota, G. *Pigment Cell Res.* **2000**, *13*, 283-293.
- (7) Camand, O.; Marchant, D.; Boutboul, S.; Pequignot, M.; Odent, S.; Dollfus, H.; Sutherland, J.; Levin, A.; Menasche, M.; Marsac, C.; Dufier, J. L.; Heon, E.; Abitbol, M. *Human Mutat.* **2001**, *17*, 352.
- (8) Leu, W. M.; Chen, L. Y.; Liaw, L. L.; Lee, Y. H. *J. Biol. Chem.* **1992**, *267*, 20108-20113.

## Chapter 2

### Tyrosinase: biology, structure and mechanism

- (9) Bernan, V.; Filpula, D.; Herber, W.; Bibb, M.; Katz, E. *Gene* **1985**, *37*, 101-110.
- (10) Solomon, E. I.; Sundaram, U. M.; Machonkin, T. E. *Chem. Rev.* **1996**, *96*, 2563-2605.
- (11) Lang, W. H.; van Holde, K. E. *Proc. Natl. Acad. Sci. U.S.A* **1991**, *88*, 244-248.
- (12) Eicken, C.; Krebs, B.; Sacchettini, J. C. *Curr. Opin. Struct. Biol.* **1999**, *9*, 677-683.
- (13) Volbeda, A.; Hol, W. G. *J. Mol. Biol.* **1989**, *209*, 249-279.
- (14) Hazes, B.; Magnus, K. A.; Bonaventura, C.; Bonaventura, J.; Dauter, Z.; Kalk, K. H.; Hol, W. G. *J. Protein Sci.* **1993**, *2*, 597-619.
- (15) Perbandt, M.; Guthohrlein, E. W.; Rypniewski, W.; Idakieva, K.; Stoeva, S.; Voelter, W.; Genov, N.; Betzel, C. *Biochemistry* **2003**, *42*, 6341-6346.
- (16) Cuff, M. E.; Miller, K. I.; van Holde, K. E.; Hendrickson, W. A. *J. Mol. Biol.* **1998**, *278*, 855-870.
- (17) Klabunde, T.; Eicken, C.; Sacchettini, J. C.; Krebs, B. *Nat. Struct. Biol.* **1998**, *5*, 1084-1090.
- (18) van Holde, K. E.; Miller, K. I.; Decker, H. *J. Biol. Chem.* **2001**, *276*, 15563-15566.
- (19) Jolley, R. L.; Evans, L. H.; Mason, H. S. *Biochem. Biophys. Res. Commun.* **1972**, *46*, 878-884.
- (20) Himmelwright, R. S.; Eickman, N. C.; Solomon, E. I. *Biochem. Biophys. Res. Commun.* **1979**, *86*, 628-634.
- (21) Bubacco, L.; Salgado, J.; Tepper, A. W.; Vijgenboom, E.; Canters, G. W. *FEBS Lett.* **1999**, *442*, 215-220.
- (22) Himmelwright, R. S.; Eickman, N. C.; Solomon, E. I. *Biochem. Biophys. Res. Commun.* **1978**, *84*, 300-305.
- (23) Uiterkamp, A. J.; Mason, H. S. *Proc. Natl. Acad. Sci. U.S.A* **1973**, *70*, 993-996.
- (24) Salvato, B.; Giacometti, G. M.; Beltramini, M.; Zilio, F.; Giacometti, G.; Magliozzo, R. S.; Peisach, J. *Biochemistry* **1989**, *28*, 680-684.
- (25) Himmelwright, R. S.; Eickman, N. C.; LuBien, C. D.; Lerch, K.; Solomon, E. I. *J. Am. Chem. Soc.* **1980**, *102*, 7339-7344.
- (26) Verplaetse, J.; Van Tornout, P.; Defreyne, G.; Witters, R.; Lontie, R. *Eur. J. Biochem.* **1979**, *95*, 327-331.

## Chapter 2

### Tyrosinase: biology, structure and mechanism

- (27) Bubacco, L.; Magliozzo, R. S.; Wirt, M. D.; Beltramini, M.; Salvato, B.; Peisach, J. *Biochemistry* **1995**, *34*, 1524-1533.
- (28) Westmoreland, T. D., Wilcox, D. E., Baldwin, M. J., Mims, W. B., and Solomon, E. I. *J. Am. Chem. Soc.* **1989**, *111*(16), 6106-6123.
- (29) Alzuet, G.; Bubacco, L.; Casella, L.; Rocco, G. P.; Salvato, B.; Beltramini, M. *Eur. J. Biochem.* **1997**, *247*, 688-694.
- (30) Magliozzo, R. S.; Bubacco, L.; Mccracken, J.; Jiang, F.; Beltramini, M.; Salvato, B.; Peisach, J. *Biochemistry* **1995**, *34*, 1513-1523.
- (31) Winkler, M. E.; Lerch, K.; Solomon, E. I. *Abstr. Pap. Am. Chem. Soc.* **1981**, *182*, 203.
- (32) Bubacco, L.; van Gastel, M.; Groenen, E. J.; Vijgenboom, E.; Canters, G. W. *J. Biol. Chem.* **2003**, *278*, 7381-7389.
- (33) van Gastel, M.; Bubacco, L.; Groenen, E. J.; Vijgenboom, E.; Canters, G. W. *FEBS Lett.* **2000**, *474*, 228-232.
- (34) Wilcox, D. E., Porras, A. G., Lerch, K., Lerch, K., Winkler, M. E., and Solomon, E. I. *J. Am. Chem. Soc.* *107*(13), 4015-4027. 1985.
- (35) Que, L.; Tolman, W. B. *Angew. Chem. Int. Ed Engl.* **2002**, *41*, 1114-1137.
- (36) Jolley, R. L.; Mason, H. S.; Evans, L. H. *Biochem. Biophys. Res. Comm.* **1972**, *46*, 878.
- (37) Kitajima, N.; Morooka, Y. *Chem. Rev.* **1994**, *94*, 737-757.
- (38) Baldwin, M. J.; Root, D. E.; Pate, J. E.; Fujisawa, K.; Kitajima, N.; Solomon, E. I. *J. Am. Chem. Soc.* **1992**, *114*, 10421-10431.
- (39) Karlin, K. D. and Tyeklár, Z. *Bioinorganic Chemistry of Copper*. Chapman & Hall . 1993.
- (40) Karlin, K. D., Hayes, J. C., Hutchinson, J. P., and Zubieta, J. *J. Chem. Soc. Chem. Commun.* *7*, 376-378. 1983.
- (41) Kitajima, N.; Fujisawa, K.; Morooka, Y.; Toriumi, K. *J. Am. Chem. Soc.* **1989**, *111*, 8975-8976.
- (42) Gerdemann, C.; Eicken, C.; Galla, H. J.; Krebs, B. *J. Inorg. Biochem.* **2002**, *89*, 155-158.
- (43) Decker, H.; Rimke, T. *J. Biol. Chem.* **1998**, *273*, 25889-25892.
- (44) Decker, H.; Dillinger, R.; Tuczec, F. *Angew. Chem. Int. Ed Engl.* **2000**, *39*, 1591-1595.
- (45) Rodriguez-Lopez, J. N.; Tudela, J.; Varon, R.; Garcia-Carmona, F.; Garcia-Canovas, F. *J. Biol. Chem.* **1992**, *267*, 3801-3810.

## Chapter 2

### Tyrosinase: biology, structure and mechanism

- (46) Cooksey, C. J.; Garratt, P. J.; Land, E. J.; Pavel, S.; Ramsden, C. A.; Riley, P. A.; Smit, N. P. *J. Biol. Chem.* **1997**, *272*, 26226-26235.
- (47) Rodriguez-Lopez, J. N.; Fenoll, L. G.; Penalver, M. J.; Garcia-Ruiz, P. A.; Varon, R.; Martinez-Ortiz, F.; Garcia-Canovas, F.; Tudela, J. *Biochim. Biophys. Acta* **2001**, *1548*, 238-256.
- (48) Solomon, E. I.; Chen, P.; Metz, M.; Lee, S.-K.; Palmer, A. E. *Angew. Chem. Int. Ed Engl.* **2001**, *40*, 4570-4590.
- (49) Conrad, J. S.; Dawso, S. R.; Hubbard, E. R.; Meyers, T. E.; Strothkamp, K. G. *Biochemistry* **1994**, *33*, 5739-5744.
- (50) Siegbahn, P. E.; Wirstam, M. *J. Am. Chem. Soc.* **2001**, *123*, 11819-11820.
- (51) Siegbahn, P. E. *J. Biol. Inorg. Chem.* **2003**, *8*, 577-585.
- (52) Siegbahn, P. E. *J. Biol. Inorg. Chem.* **2003**, *8*, 567-576.
- (53) Halfen, J. A.; Mahapatra, S.; Wilkinson, E. C.; Kaderli, S.; Young, V. G., Jr.; Que, L., Jr.; Zuberbuhler, A. D.; Tolman, W. B. *Science* **1996**, *271*, 1397-1400.
- (54) Lewis, E. A.; Tolman, W. B. *Chem. Rev.* **2004**, *104*, 1047-1076.



# Chapter 3

## *Structural basis and mechanism of the inhibition of tyrosinase by halide ions.*

Published as: Tepper, A. W., Bubacco, L., and Canters, G. W. (2002) *J. Biol. Chem.* 277, 30436-30444.

### Summary

The inhibition of the type-3 copper enzyme tyrosinase by halide ions was studied on a mechanistic and a structural level by kinetic and paramagnetic  $^1\text{H}$  NMR methods. All halides are inhibitors in the conversion of diphenolic L-DOPA with apparent inhibition constants that follow the order  $\text{I}^- < \text{F}^- \ll \text{Cl}^- < \text{Br}^-$  at pH 6.80. The results show that the inhibition arises from the interaction of halide with both the oxidised (affinity  $\text{F}^- > \text{Cl}^- > \text{Br}^- \gg \text{I}^-$ ) and reduced (affinity  $\text{I}^- > \text{Br}^- > \text{Cl}^- \gg \text{F}^-$ ) enzyme. The paramagnetic  $^1\text{H}$  NMR of the oxidised enzyme complexed with the halides is consistent with a direct interaction of halide with the type-3 site and shows that the  $(\text{Cu-His}_3)_2$  coordination occurs in all halide bound species. It is surmised that halides bridge both copper ions in the active site. Fluoride and chloride are shown to only bind to the low pH form of oxidised tyrosinase, explaining the strong pH dependence of the inhibition by these ions. We further show that *p*-toluic acid and the bidentate transition-state analogue Kojic acid displace chloride from the oxidised active site while the monodentate substrate analogue *p*-nitrophenol forms a ternary complex with the enzyme and the chloride ion. On the basis of the experimental results a model is formulated for the inhibitor action and for the reaction of diphenols with the oxidised enzyme.



## Introduction

One of the unresolved questions in the enzymology of the type-3 copper containing tyrosinases (E.C. 1.14.18.1) is the detailed molecular mechanism of both inhibitor action and substrate conversion. This report focuses on the mechanism of their inhibition by halides. Tyrosinases are monooxygenating enzymes catalyzing the *ortho*-hydroxylation of monophenols and the subsequent oxidation of the diphenolic products to the corresponding quinones. The reactions take place under concomitant reduction of molecular oxygen to water. The formed quinones are reactive precursors in the synthesis of melanin pigments. In fruits, vegetables and mushrooms, Ty is a key enzyme in the browning that occurs upon bruising or long-term storage. In mammals, Ty is responsible for skin pigmentation. Defects in the enzyme may lead to some forms of oculocutaneous albinism or vitiligo (1). Furthermore, the enzyme has been linked to Parkinson's and other neurodegenerative diseases (2-6). Consequently, the enzyme poses considerable interest from medical, agricultural and industrial points-of-view.

The current knowledge of Ty at the biological, mechanistic and structural level has recently been reviewed (7-10). Ty harbours a dinuclear so-called type-3 copper centre, the occurrence of which has also been established in Hemocyanins (Hcs), which act as oxygen carriers in arthropods and molluscs, and the catechol oxidases (COs), which oxidise *o*-diphenols to the corresponding quinones. The two closely spaced copper ions in the type-3 active site are coordinated each by 3 histidine residues through the N<sup>ε</sup> atoms (9). Although the known type-3 centres are found to be similar both in structure and in their ability to bind molecular oxygen, they perform different functions. These differences are believed to result from variations in the substrate binding pocket or the accessibility of substrates to the active site, although the exact reasons remain to be defined (7).

The Ty type-3 site can exist in a variety of forms. The a), Ty<sub>red</sub>, [Cu(I) Cu(I)] reduced species binds oxygen to render b) the [Cu(II)-O<sub>2</sub><sup>2-</sup>-Cu(II)], Ty<sub>oxy</sub> derivative. In Ty<sub>oxy</sub>, molecular oxygen is bound as peroxide in a μ-η<sup>2</sup>:η<sup>2</sup> side-on bridging mode, which destabilises the O-O bond and activates it for reaction with mono- or diphenols (9). The Ty<sub>oxy</sub> species shows a strong LMCT (Ligand To Metal Charge transfer Transition) at ~345 nm (ε ≈ 18.5 mM<sup>-1</sup>cm<sup>-1</sup>) and is EPR silent. The latter property also holds for the resting-form of the enzyme, c) the oxidised [Cu(II)-Cu(II)], Ty<sub>met</sub> derivative, where antiferromagnetic coupling between the unpaired spins of the Cu<sup>2+</sup> ions occurs through spin superexchange mediated by a Cu<sub>2</sub> bridging ligand (11). Due to the diamagnetic nature of both Ty<sub>oxy</sub> and Ty<sub>met</sub> in the ground-state, magnetic resonance studies on Ty and its inhibitor bound species until now mainly dealt with d) the EPR active [Cu(I) Cu(II)], Ty<sub>half-met</sub> species, that can be prepared by partial reduction of Ty<sub>met</sub> (12). Albeit a non-



dependent on the source of the enzyme studied (16-18). The latter differences have been mainly explained in terms of the accessibility of the halide ion to the Ty active site (17). Furthermore, EPR studies on halide bound  $Hc_{\text{half-met}}$  derivatives have been reported (11, 19), showing that halides interact directly with copper in the type-3 hemocyanin active site.

Here we report on a detailed study of the inhibition of the 31 kDa Ty from *Streptomyces antibioticus* by halide ions, using paramagnetic  $^1\text{H}$  NMR as a complementary technique to the more conventional kinetic and optical spectroscopic methods. The pH dependencies of halide inhibition in the conversion of L-DOPA and of halide binding to  $Ty_{\text{met}}$  were studied, providing insight into the halide inhibition at a structural and at a mechanistic level and resulting in the proposal of a halide binding mode. Our results for the first time address the Ty halide inhibition by considering the interaction of halide with the physiologically relevant Ty species that participate in the enzymatic reaction pathway. The results show that the halide inhibition derives from the interaction of halide with the  $\text{Cu}_2$  center of both the oxidised and the reduced Ty species where the halide binding affinity is found to be dependent on the nature of the halide ion as well as on the Ty oxidation state. Furthermore, we show that halides can be used as probes in paramagnetic  $^1\text{H}$  NMR investigations of the coordination mode of exogenously added ligands such as substrate and transition-state analogues as well as aromatic carboxylic acid inhibitors. The relevance of the findings towards understanding the reaction of diphenolic substrates with  $Ty_{\text{met}}$  is discussed, forming the basis of a proposed structural scheme of Ty inhibition and of the reaction of  $Ty_{\text{met}}$  with diphenolic substrates.

## Experimental procedures

### Protein isolation and purification

The enzyme was obtained from the growth medium of liquid cultures of *Streptomyces antibioticus* harbouring the pIJ703 Ty expression plasmid (15). The protein was purified according to published procedures (15). Purity was checked by SDS-PAGE and exceeded 95% in all preparations. Protein concentrations in pure samples were routinely determined optically using a value of  $82 \text{ mM}^{-1}\text{cm}^{-1}$  for the extinction coefficient at 280 nm (20).

### Inhibition assays

Enzyme activity assays using L-DOPA as a substrate were performed at  $21 \text{ }^\circ\text{C}$  by optically following the formation of the DOPACHrome reaction product at 475 nm according to the method described in (21). Over the time-course of the experiment, linear product formation was observed in all cases. Inhibition constants were obtained by

measuring values of  $V_{\max}/K_m$ , corresponding to the slopes of the Michaelis-Menten plots, in the presence of at least 5 different concentrations of halide inhibitor, [I], and by using 5 different substrate concentrations at each [I]. The plots of  $V_{\max}/K_m$  vs. [I] appeared linear within the error of the experiment (estimated at  $\pm 10\%$ ) in all cases, allowing for an estimation of  $K_i^{\text{app}}$  from the slope and the intercept. The halide concentrations in the assay mixture were chosen both well below and above the value of the apparent inhibition constant for the halide under consideration. For the pH dependence of halide inhibition, a 75 mM phosphate / 25 mM borate instead of a 100 mM Pi buffer was used to ensure efficient buffering at all pH values used. The enzyme was stored in the form of a 5 mM Pi stock solution at pH 7.2 in order to prevent protein degradation during storage prior to the experiments. Enzyme was added to the assay medium directly from this stock. The reported pH values were measured on the final mixed solutions.

#### Preparation of $Ty_{\text{oxy}}/Ty_{\text{red}}$

All steps were performed in a cold chamber (4 °C) using air saturated buffers obtained by vigorous shaking under air for at least one hour. The pH of the buffers used was 6.80 (measured at 21 °C) throughout the procedure. A mixture containing  $Ty_{\text{oxy}}$  and  $Ty_{\text{red}}$  was prepared by the incubation of a 5 mM Pi solution containing the protein ( $\sim 5 \mu\text{M}$ ) with 0.5 mM hydroxylamine resulting in complete reduction of  $Ty_{\text{met}}$  to  $Ty_{\text{red}}$ . The binding of oxygen from the air saturated reaction buffer ( $\sim 0.27 \text{ mM O}_2$ ) to  $Ty_{\text{red}}$  results in the formation of a mixture of  $\sim 95\%$   $Ty_{\text{oxy}}$  and  $\sim 5\%$   $Ty_{\text{red}}$  ( $K_d = 17 \mu\text{M}$ ; Chapter 4). The reaction mixture was applied immediately to a small column containing  $\sim 0.5$  ml of CM Sepharose column material which was previously equilibrated with 5 mM Pi buffer. To remove excess hydroxylamine, the column was washed extensively with the equilibration buffer after which the protein was eluted with 100 mM Pi buffer in a volume varying between 2 and 5 ml. Since the  $Ty_{\text{oxy}}$  protein is unstable (unpublished data), the protein solution was made immediately prior to the experiments.

#### Halide titration of $Ty_{\text{oxy}}$

A solution of  $\sim 95\%$   $Ty_{\text{oxy}}$  and  $\sim 5\%$   $Ty_{\text{red}}$  (1 ml in a sealed cuvette; typically 3  $\mu\text{M}$  total concentration) in 100 mM air-saturated Pi buffer at pH 6.80 and 4 °C was allowed to equilibrate to 21 °C after which halide was added in 5-20  $\mu\text{l}$  volume steps from concentrated stock solutions of 2.00 M  $\text{F}^-$ , 5.00 M  $\text{Cl}^-$ , 1.00 M  $\text{Br}^-$  or 100 mM  $\text{I}^-$  made up in the assay buffer. Absorption changes were measured at 345 nm.

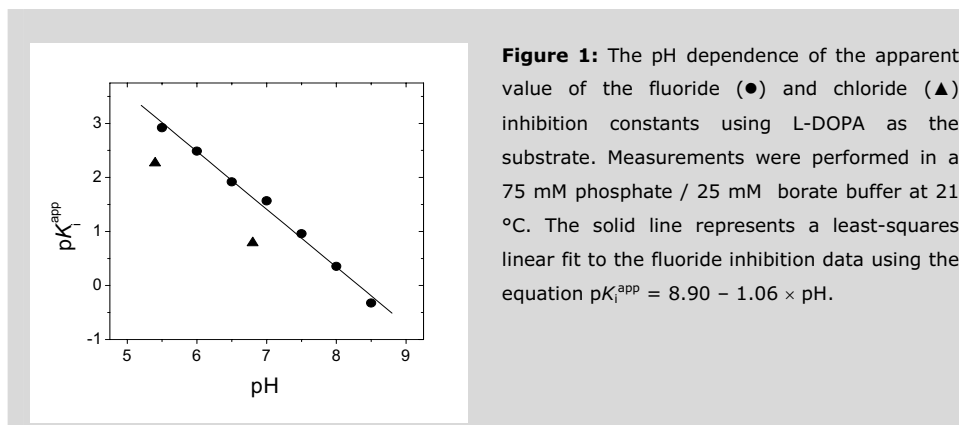
### NMR spectroscopy

NMR  $T_{y_{met}}$  samples (~0.6 mM in 100 mM NaPi at pH 6.80) were prepared as described before (14). Exogenous ligands were added to the samples from concentrated stock solutions prepared by using the same buffer as for the measurement. The pH of the NMR samples was varied by adding small aliquots of either dilute NaOH or 100 mM  $H_3PO_4$  under continuous mixing and monitoring of the pH.  $^1H$  spectra were recorded at 600 MHz using a Bruker DMX-600 spectrometer with the use of the super-WEFT pulse sequence (22). Depending on the required signal to noise ratio, 4,000 to 128,000 FIDs were recorded, Fourier transformed using a 60 Hz exponential window function (LB) and baseline corrected using the Bruker provided software. 1D NOEs on  $T_{y_{met}F}$  were measured as described before (14, 23).

## Results

### Halide inhibition

To characterise the effect of halides on the enzymatic activity, we performed steady-state kinetic measurements using diphenolic L-DOPA as the substrate at pH 6.80 and room temperature. In all cases, product formation linear in time was observed and the dependency of the reaction rate *vs.* [L-DOPA] obeyed Michaelis-Menten type kinetics. For all halides studied, the plots of  $K_m/V_{max}$  values obtained from the slope of the Michaelis-Menten plots *vs.* [X] showed linear dependencies (not shown), indicating that the binding of a single halide ion is responsible for the inhibition (24). The fluoride and chloride inhibition appear competitive, while iodide and bromide inhibit through an apparent noncompetitive mechanism (not shown). The order of strength of inhibition is  $I^- > F^- \gg Cl^- > Br^-$  with apparent inhibition constants of 3.8 mM, 11 mM, 0.16 M and 0.23 M, respectively.



We studied the pH dependence of fluoride inhibition. The fluoride inhibition appears very sensitive to the pH as depicted in Figure 1; in the plot of  $pK_{i,F}^{app}$  vs. pH, an approximately linear dependency is observed. A linear least-squares fit to the data yields the relationship  $pK_{i,F}^{app} = 8.9 - 1.06 \times \text{pH}$ . These data can be explained by adopting the following scheme:



where Ty\* denotes the acidic form of the enzyme, which is capable of binding fluoride. Assuming that  $\text{Ty}_{\text{met}}\text{F}$  is catalytically inactive, the equation relating the pH to the observed inhibition constant becomes:

$$K_{i,F^-}^{app} = K_{i,F^-} \left( \frac{K_a}{[\text{H}^+]} + 1 \right) \quad (\text{Equation 1})$$

In the region where  $[\text{H}^+] \ll K_a$ , Eq. 1 may be simplified to:

$$pK_{i,F^-}^{app} = -\log(K_a K_{i,F^-}) - \text{pH} = (pK_{i,F^-} + pK_a) - \text{pH} \quad (\text{Equation 2})$$

and  $pK_{i,F^-}^{app}$  becomes directly proportional to the pH. The data indicate a  $pK_a$  value  $< 5.5$  since little curvature as predicted by Eq. 1 in Figure 1 is apparent down to pH 5.5. Measurements at the lower pH values were prohibited due to complications arising from the less efficient chemical disproportionation of the enzymatic product DOPAquinone into L-DOPA and DOPochrome (25), the latter being the measured substance, as well as the intrinsic instability of the enzyme at pH values lower than  $\sim 5$ . We chose not to measure

above pH 8.5 because of the very high fluoride concentrations (hence ionic strengths) required to accurately measure  $pK_{i,F}^{app}$  values. The chloride inhibition constant was determined at both pH 6.80 and pH 5.40 (see Figure 1), showing that a similar pH dependency occurs for the inhibition by chloride ion. For comparison with  $^1H$  NMR data (*vide infra*), we also determined the apparent inhibition constant for fluoride at 4 °C and pH 6.80, which amounts to 3.4 mM ( $pK_{i,F}^{app} = 2.5$ ).

### Paramagnetic $^1H$ NMR

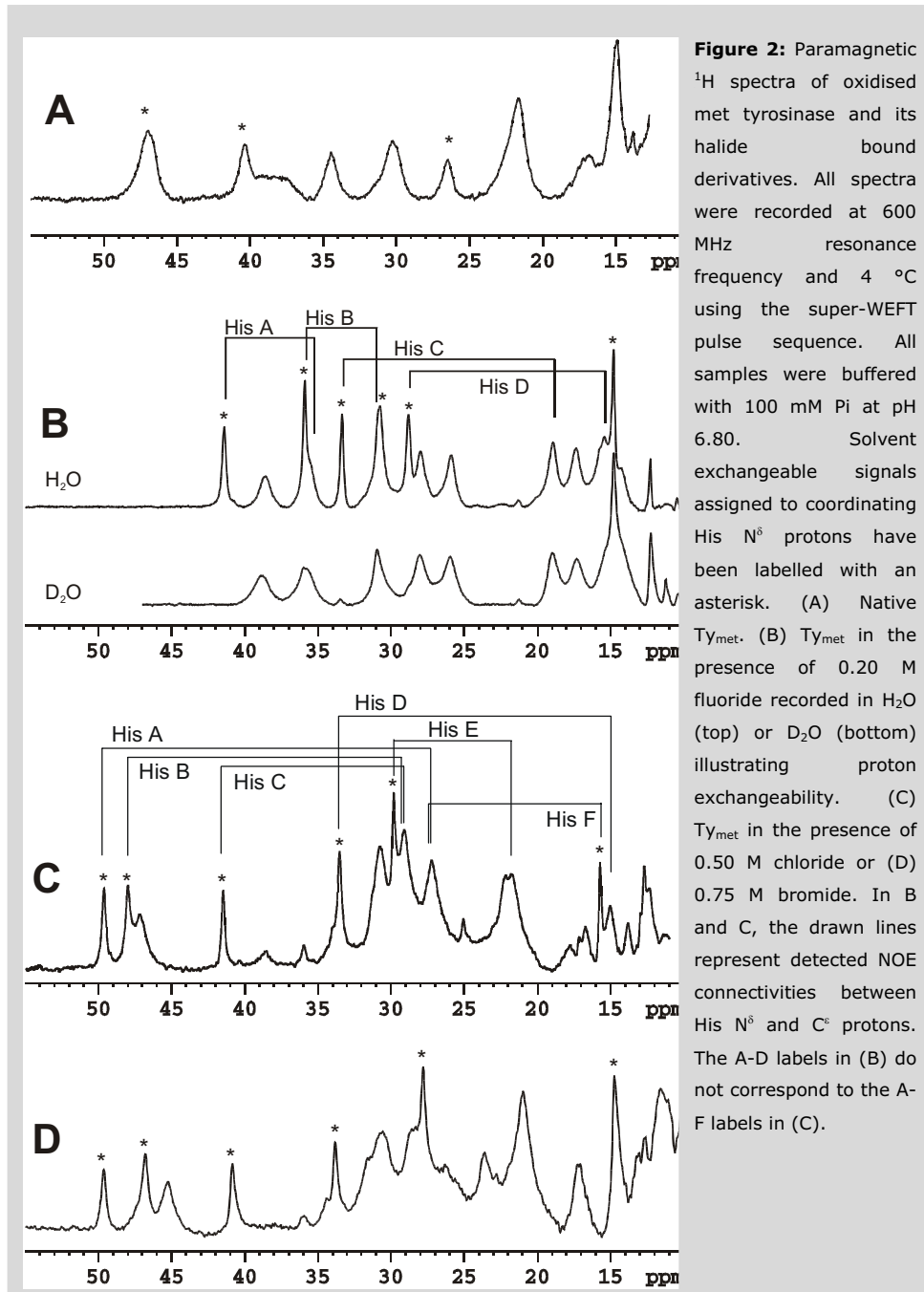
Figure 2 shows the 600 MHz  $^1H$  NMR spectra of native *Streptomyces antibioticus*  $Ty_{met}$  (A) and  $Ty_{met}$  in the presence of 0.2 M fluoride (B;  $Ty_{met}F$ ), 0.5 M chloride (C;  $Ty_{met}Cl$ ) and 0.5 M bromide (D;  $Ty_{met}Br$ ) between 55 and 10 ppm. All investigated species display well-resolved paramagnetically shifted NMR signals. No paramagnetically shifted signals could be detected in the upfield or in the  $> 55$  ppm downfield region in all cases. We did not attempt to detect paramagnetically affected signals under the diamagnetic envelope. Addition of iodide to a final concentration of 0.2 M to a sample of  $Ty_{met}$  did not lead to changes in the  $^1H$  NMR spectrum apart from a significant loss of signal intensity, possibly indicating that iodide ion reduces the copper ions under the conditions of the experiment or that it destabilises the  $Ty_{met}$  protein. The observed changes upon halide addition can not be assigned to the increase in ionic strength, as the addition of 0.25 M  $Na_2SO_4$  to a sample of native  $Ty_{met}$  in 100 mM  $P_i$  at pH 6.8 did not affect the paramagnetic part of the spectrum. The spectra of native  $Ty_{met}$  and  $Ty_{met}Cl$  have been discussed before (14).

The spectra of the three halide bound derivatives each display several well resolved paramagnetically shifted signals. The shift pattern is rather similar for the chloride and bromide bound species, while the signal distribution of the  $Ty_{met}F$  species appears to be quite different. Yet, in each halide bound derivative, 6 sharp signals together with several broader, partially overlapping, signals can be distinguished. The assignment of paramagnetically affected signals is not a trivial task due to the difficulty of predicting hyperfine shift magnitudes and the fast nuclear relaxation of nuclei in proximity of the paramagnetic centre (inducing line-broadening). The latter is especially true concerning systems characterised by slow electronic relaxation, such as mononuclear  $Cu^{2+}$ , where signals are often broadened beyond usefulness. Yet, in systems with favourable relaxation characteristics, assignments relying on customary assignment procedures and knowledge of the structure under study are sometimes possible. We were lucky in the case of  $Ty$ . The magnetic coupling of the two copper ions in the active site appears to reduce the unfavourable paramagnetic relaxation enhancement by yet to establish mechanisms (14), resulting in remarkably sharp  $^1H$  NMR signals for a  $Cu^{2+}$  system.

For  $\text{Ty}_{\text{met}}\text{Cl}$ , the hyperfine shifted resonances could be assigned (14) based on  $\text{H}_2\text{O}/\text{D}_2\text{O}$  exchange experiments, intra-residue NOE patterns and  $T_1$  relaxation data. The sharp solvent exchangeable signals, marked with an asterisk in Figure 2, were assigned to the histidine  $\text{N}\delta$  protons, while the broader signals could be assigned to the  $\text{His-C}^\epsilon$  and  $\text{His-C}^\delta$  protons of the coordinating histidines. The latter are closer to the copper and therefore experience stronger paramagnetic relaxation and hence more broadening compared to the  $\text{N}^\delta$  protons. Furthermore, the observed NOE patterns allowed us to couple each of the six sharp  $\text{N}^\delta$  proton signals with a broader  $\text{C}^\epsilon$  signal, thereby identifying each histidine residue in the six coordinate ligand sphere of the  $\text{Cu}_2$  site.

Since the observed signal shift pattern is quite different for the  $\text{Ty}_{\text{met}}\text{Cl}$  than for the  $\text{Ty}_{\text{met}}\text{F}$  species, we repeated the assignment procedure for  $\text{Ty}_{\text{met}}\text{F}$ . Figure 2B shows the spectrum recorded in  $\text{D}_2\text{O}$ . It can be observed that 5 of the 6 sharp signals are readily solvent exchangeable, similar to what is observed for the chloride bound species (14). The detection of NOE couplings between the paramagnetically shifted  $^1\text{H}$  signals in  $\text{Ty}_{\text{met}}\text{F}$  is complicated due to both the relatively fast  $\text{Ty}_{\text{met}}\text{F}$   $T_1$  proton relaxation (to be published) and the presence of considerable signal overlap, for example for the signal at 31 ppm that is composed of both a sharp and a broad signal. Yet, we were able to establish 4 NOE connectivities as indicated in the figure, leaving the expected NOE couplings from the sharp signals at 31.0 and 14.8 ppm to broader signals undetected as yet.





**pH titrations of  $Ty_{met}F$  and  $Ty_{met}Cl$**

The NMR spectra of samples of  $\sim 0.5$  mM  $Ty_{met}$  containing 0.2 M fluoride or 0.5 M chloride are clearly pH dependent as shown in Fig. 3 for fluoride ion. The observed effects are fully reversible. For both halide bound species similar titration behaviour is observed. The spectra of  $Ty_{met}$  recorded in the presence of fluoride or chloride at pH 9.6 superimpose well with the spectrum of native  $Ty_{met}$  at pH 6.8 (Figure 2A), showing that the protein reverts to native  $Ty_{met}$  when the pH is increased. No signal broadening effects or shifts are observed over the whole titration range for all observable signals for both species, showing that the halide exchange process is slow on the NMR timescale in both cases. As a consequence, the signals of native  $Ty_{met}$  and  $Ty_{met}F$  or  $Ty_{met}Cl$  can be followed independently. The midpoint of the titration occurs at a pH of  $\sim 8.2$  for  $Ty_{met}F$  ( $[F^-] = 0.2$  M) and at pH  $\sim 7.8$  for  $Ty_{met}Cl$  ( $[Cl^-] = 0.5$  M). We did not quantify signal intensities because partial protein degradation at the extremes of the pH values used prevented accurate comparison between individual spectra. A quantitative analysis of the pH dependence of fluoride binding is presented below. A pH titration of native  $Ty_{met}$  towards the lower pH values was unsuccessful due to irreversible protein degradation, leading to a rapid loss of signal intensity.

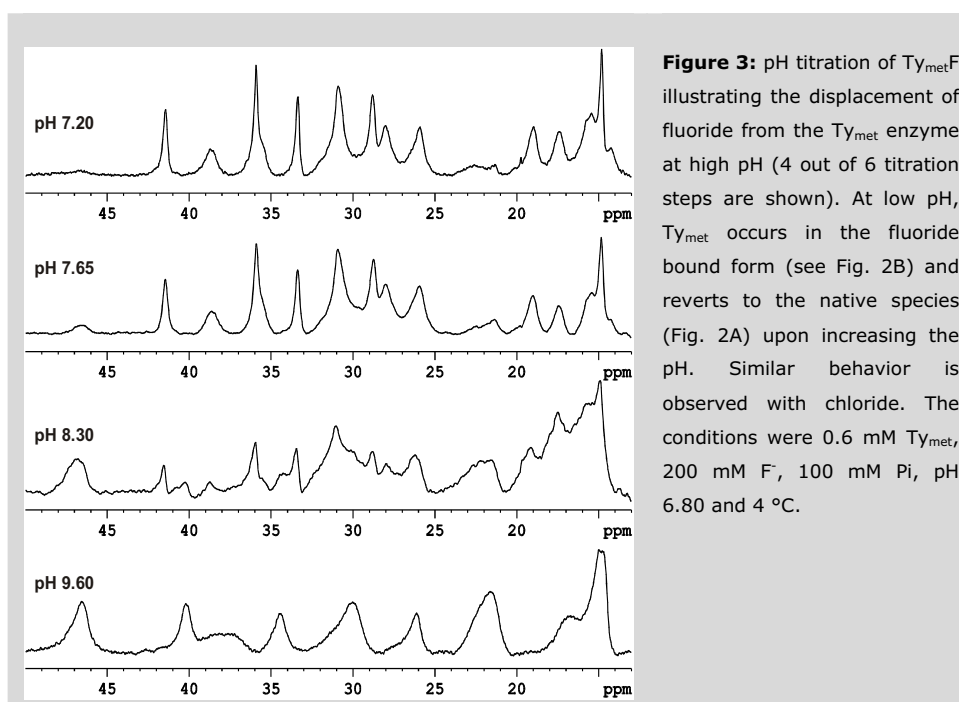


**Figure 3:** pH titration of  $Ty_{met}F$  illustrating the displacement of fluoride from the  $Ty_{met}$  enzyme at high pH (4 out of 6 titration steps are shown). At low pH,  $Ty_{met}$  occurs in the fluoride bound form (see Fig. 2B) and reverts to the native species (Fig. 2A) upon increasing the pH. Similar behavior is observed with chloride. The conditions were 0.6 mM  $Ty_{met}$ , 200 mM F<sup>-</sup>, 100 mM Pi, pH 6.80 and 4 °C.

### Fluoride titrations of native Ty<sub>met</sub> at two pH values

The observed pH dependency of fluoride binding and inhibition prompted us to investigate fluoride binding at fixed pH. More specifically, we performed a titration of native Ty<sub>met</sub> with fluoride at two pH values (pH 7.06, [F<sup>-</sup>] 0-38 mM and pH 8.03, [F<sup>-</sup>] 0-375 mM). These pH values were chosen in the region of maximal stability of the protein to prevent protein degradation during the experiment. The observed titration behaviour is the reverse of that observed in the pH titration above (Figure 3), in agreement with a two-state model where both species are in slow-exchange on the NMR timescale. There is no indication of the occurrence of intermediates during the titration, in agreement with the binding of a single fluoride ion. The relative amounts of native Ty<sub>met</sub> and Ty<sub>met</sub>F were determined by measuring peak heights. For native Ty<sub>met</sub>, this was carried out on the isolated signals at 47.2 ppm and 22.0 ppm where there is no overlap with signals originating from the fluoride bound species. The relative amount of Ty<sub>met</sub>F was determined by measuring the intensity of the sharp N<sup>δ</sup> proton signals 28.8, 33.3, 35.9 and 41.4 ppm. The intensities of the signals were normalised and then fitted to the general equation for two state binding under the conditions that the ligand is in large excess over the enzyme:

$$\frac{I_{\text{obs,A}}}{I_{\text{max,A}}} = 1 - \frac{[\text{F}^-]}{K_d^{\text{app}} + [\text{F}^-]} \quad (\text{Equation 3})$$

$$\frac{I_{\text{obs,F}}}{I_{\text{max,F}}} = \frac{[\text{F}^-]}{K_d^{\text{app}} + [\text{F}^-]} \quad (\text{Equation 4})$$

where  $I_{\text{obs,F}}$  and  $I_{\text{obs,A}}$  represent the observed signal intensities of Ty<sub>met</sub>F and native Ty<sub>met</sub>, respectively.  $K_d^{\text{app}}$  represents the apparent value for the dissociation constant of the fluoride bound complex,  $I_{\text{max,A}}$  the signal intensity of the native species at zero [F<sup>-</sup>] and  $I_{\text{max,F}}$  the Ty<sub>met</sub>F signal intensity at [F<sup>-</sup>]  $\gg K_d^{\text{app}}$ . For each of the two titration experiments,  $K_d^{\text{app}}$  was set as a shared parameter between the  $I_{\text{obs,F}}$  and  $I_{\text{obs,A}}$  vs. [F<sup>-</sup>] datasets, resulting in a single value for  $K_d^{\text{app}}$ ,  $I_{\text{max,A}}$  and  $I_{\text{max,F}}$  at each pH. At both pH values, good fits were obtained as depicted in Figure 4A (pH 7.06) and 4B (pH 8.03). The obtained values for  $K_d^{\text{app}}$  amounted to 5.8 mM and 51 mM at pH 7.06 and pH 8.03 with corresponding  $\text{p}K_d^{\text{app}}$  values of 2.24 and 1.29, respectively. The difference of the  $\text{p}K_d^{\text{app}}$  values is 0.94, comparing well to the difference in the pH values of the experiments (0.97). This shows that the fluoride dissociation constant, like the fluoride inhibition constant (Figure 1), is inversely proportional to the proton concentration in the pH range 7-8.

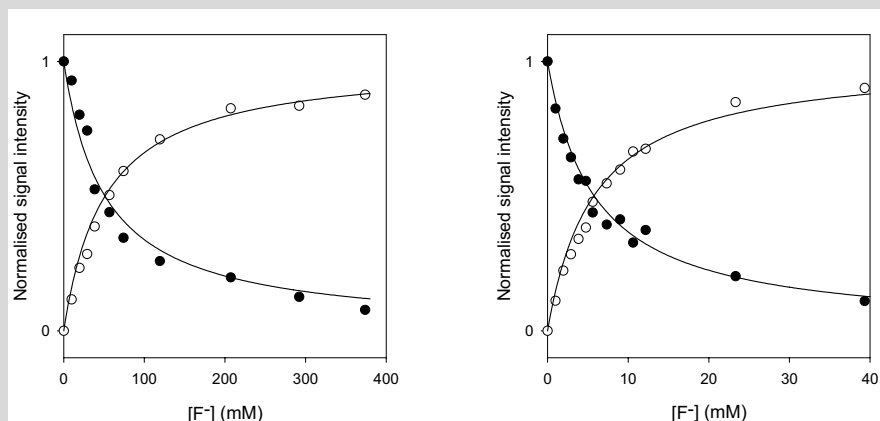


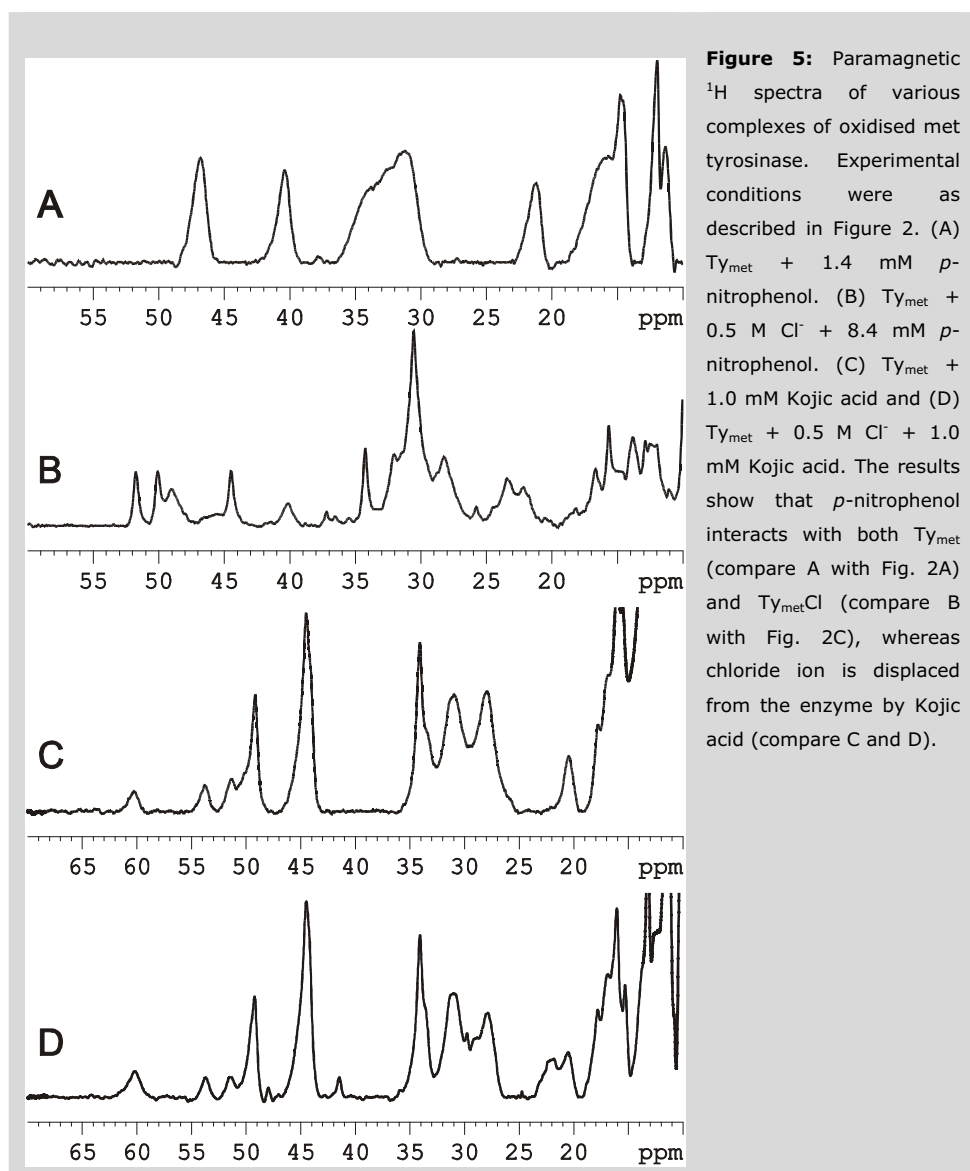
**Figure 4:** Normalised paramagnetic  $^1\text{H}$  signal intensities of native  $\text{Ty}_{\text{met}}$  ( $\bullet$ ) and  $\text{Ty}_{\text{met}}\text{F}$  ( $\circ$ ) as a function of  $[\text{F}^-]$  at pH 7.06 (left) and pH 8.03 (right). Solid lines represent best fits to Equations 3 and 4 yielding fluoride dissociation constants of 5.8 mM and 51 mM at pH 7.06 and 8.03, respectively. Measurements were made using 0.6 mM  $\text{Ty}_{\text{met}}$  in 100 mM Pi at 4  $^\circ\text{C}$  using the super-WEFT pulse sequence.

### Halide displacement studies

To obtain a better insight into the mode of halide and inhibitor binding in the met  $[\text{Cu}(\text{II})\text{Cu}(\text{II})]$  species, we recorded  $^1\text{H}$  NMR spectra of  $\sim 0.5$  mM native  $\text{Ty}_{\text{met}}$  and  $\text{Ty}_{\text{met}}\text{Cl}$  ( $[\text{Cl}^-] = 0.5$  M) in the presence of the bidentate inhibitor Kojic acid or the monodentate ligand *p*-nitrophenol. The resulting spectra are presented in Figure 5. It appears that the spectra of  $\text{Ty}_{\text{met}} + \text{Kojic acid}$  recorded in the absence and in the presence of chloride are nearly identical (Figure 5C and 5D), indicating that Kojic acid displaces chloride from the active site. The small differences between the spectra can be explained by assuming that there is still a small fraction of  $\text{Ty}_{\text{met}}\text{Cl}$  present in solution (compare Figure 2C with Figure 5D). Analogous behaviour is observed with the bidentate carboxylic acid inhibitor *p*-toluic acid (not shown). The situation is different with the monodentate phenolic substrate analogue *p*-nitrophenol where the spectrum is clearly dependent on the presence of chloride (Figure 5A and 5B). Interestingly, in the absence of chloride, the spectrum of  $\text{Ty}_{\text{met}}$  containing *p*-nitrophenol shows some similarities with that of the native enzyme (compare Figure 2A with 5A): large changes only occur for the signals at 34.5, 30.2 and 26.5 ppm in the native species.

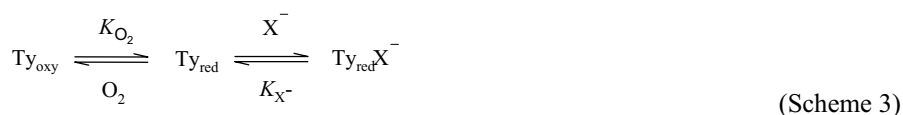
When chloride is added to a sample containing the  $\text{Ty}_{\text{met}}$  enzyme and *p*-nitrophenol, the spectrum changes significantly as shown in Figure 5B and is clearly different from the spectrum of  $\text{Ty}_{\text{met}}\text{Cl}$  (compare peak positions with Figure 2C). Significantly more *p*-

nitrophenol is required to observe changes in the spectrum when chloride is present than in the absence of chloride. The obtained spectra were not dependent on the order in which *p*-nitrophenol and chloride were added to the  $Ty_{met}$  sample. These data firmly demonstrate that both *p*-nitrophenol and chloride can bind simultaneously to the  $Ty_{met}$  protein, thereby forming a ternary complex.



### Displacement of Ty bound oxygen by halide

The effects of halide on the  $\text{Ty}_{\text{oxy}} \leftrightarrow \text{Ty}_{\text{red}} + \text{O}_2$  equilibrium have been studied by halide titration of a mixture of ~95 %  $\text{Ty}_{\text{oxy}}$  and ~5 %  $\text{Ty}_{\text{red}}$  in an air saturated buffer at 21 °C ( $[\text{O}_2] = 0.27 \text{ mM}$ ) and pH 6.80 by following the LMCT transition at 345 nm associated with  $\text{Ty}_{\text{oxy}}$ . The addition of fluoride up to 200 mM did not lead to significant changes in the  $\text{Ty}_{\text{oxy}}$  spectrum, indicating that this ion does not interact with either  $\text{Ty}_{\text{oxy}}$  or  $\text{Ty}_{\text{red}}$ . This was different for  $\text{Cl}^-$ ,  $\text{Br}^-$ , and  $\text{I}^-$  where a decrease in the  $\text{Ty}_{\text{oxy}}$  LMCT intensity was observed as shown in Figure 6 for iodide ion. The observed changes are reversible. The titration data obtained for  $\text{Br}^-$  and  $\text{I}^-$  could be fitted accurately to a function of the type of Equation 4, yielding apparent dissociation constants of 50 mM and 3.0 mM respectively. The  $\text{Cl}^-$  titration data showed little saturation up to 1 M of chloride and only allowed estimation of a lower limit for  $K_{\text{d}}^{\text{app}}$  of ~0.5 M. All titration data are easily explained by assuming that halide is in competition with molecular oxygen for binding to  $\text{Ty}_{\text{red}}$  according to Scheme 3.



where the apparent dissociation constant for halide  $K_{\text{X}^-}^{\text{app}}$  is dependent on the oxygen concentration in the sample, according to:

$$K_{\text{X}^-}^{\text{app}} = K_{\text{X}^-} \cdot \frac{(K_{\text{O}_2} + [\text{O}_2])}{K_{\text{O}_2}} \quad (\text{Equation 5})$$

Where  $K_{\text{X}^-}$  denotes the dissociation constant for the halide-Tyred complex and  $K_{\text{O}_2}$  denotes the oxygen dissociation constant of  $\text{Ty}_{\text{oxy}}$ . By using a value for the oxygen equilibrium dissociation constant of 17  $\mu\text{M}$  (Chapter 4), the true binding constants for bromide and iodide can be calculated, amounting to 3.4 and 0.20 mM respectively.

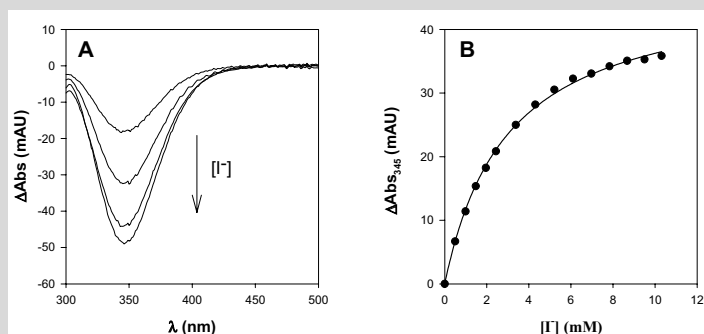


**Figure 6:** Displacement of molecular oxygen from  $Ty_{oxy}$  by iodide. A) Difference absorption spectra obtained by adding an increasing amount of  $I^-$  to a sample containing  $\sim 95\%$   $Ty_{oxy}$  and  $\sim 5\%$   $Ty_{red}$  ( $\sim 3\ \mu M$  total concentration) in 100 mM Pi buffer at pH 6.80 and 21 °C. B)  $\Delta Abs_{345}$  vs.  $[I^-]$ . The solid line represents the best fit to the data ( $K_d^{app} = 3.0\ mM$ ). Bromide ( $K_d^{app} = 50\ mM$ ) and chloride ( $K_d^{app} > 0.5\ M$ ) exert similar behavior while no significant changes in the  $Ty_{oxy}$  spectrum are observed when fluoride is used as the titrant (not shown).

## Discussion

We have studied the mechanism of halide inhibition in detail through complementary kinetic, optical equilibrium titration and paramagnetic  $^1H$  NMR studies. It appears that all halides act as inhibitors in the conversion of diphenolic L-DOPA, as was found before with Tys from other organisms (16-18). The determined inhibition constants follow the order  $I^- < F^- \ll Cl^- < Br^-$  while different orders have been found for other Tys (16, 17) (*vide infra*). With respect to the L-DOPA conversion, the inhibition mechanism is purely competitive for fluoride and chloride, whereas iodide and bromide apparently inhibit non-competitively. Our results show that this can be explained by invoking a different interaction of different halides with the oxidised  $Ty_{met}$  and reduced  $Ty_{red}$  enzyme species. These interactions will be discussed separately. We will first consider the interaction of halides with the  $Ty_{met}$  species, which is EPR silent, shows no strong UV/VIS absorption bands and is therefore not easily studied by spectroscopic techniques other than paramagnetic NMR.

### The interaction of halide ion with $Ty_{met}$

All collected data are in agreement with halides directly interacting with the dinuclear type-3 copper active centre, as previously proposed for other tyrosinases (16-18) and hemocyanins (11, 26, 27). This is exemplified by the large changes in the paramagnetic  $^1H$  NMR that occur when halide ( $X^- = F^-, Cl^-, Br^-$ ) is added to native  $Ty_{met}$  (Figure 2), showing that the electronic structure of the dinuclear site is strongly perturbed upon halide

binding. Changes occur over the whole spectrum when halide is added to native  $Ty_{met}$ , both in terms of signal distribution and linewidths, indicating alterations in the spin distribution over the ligands and in the relaxation properties of the coupled system. Through a detailed assignment procedure it was shown before that the two copper ions in  $Ty_{met}Cl$  are coordinated by six His residues through their  $N^\epsilon$  atoms (14), similar to the coordination mode found in other type-3 copper proteins for which a structure has been reported (28-31). The clear similarities between the  $Ty_{met}Cl$  (Figure 2C) and  $Ty_{met}Br$  (Figure 2D) spectra indicate that the typical type-3 coordination mode also occurs in  $Ty_{met}Br$ . Since the signal distribution appeared quite different in  $Ty_{met}F$  (Figure 2B), the assignment procedure was repeated for this species, leading us to conclude that the typical type-3 coordination is maintained in  $Ty_{met}F$  as well. If the halide ion coordinates to copper in the active site, it must therefore bind to a position that is not occupied by a histidine. We propose that halides ( $F^-$ ,  $Cl^-$ ,  $Br^-$ ) bridge the two copper ions in the active-site. Indeed, halide bridging is commonly found in dinuclear copper model complexes e.g. (32-39) and it has also been proposed for both met and half-met hemocyanin (11, 26, 27). We note that exchange of the  $Cu_2$  bridging ligand would affect the magnitude of the antiferromagnetic coupling (i.e.  $-2J$ ) between both copper ions (33, 38, 39) and the electron spin distribution over the ligands of both copper ions, thereby affecting the contact coupling constant  $A$  for each signal. Since the hyperfine shifts are a function of both  $-2J$  and  $A$  (14), it is expected that the shifts for the paramagnetically affected  $^1H$  NMR signals are all affected upon exchange of the  $Cu_2$  bridging ligand. These considerations would indeed be consistent with the observed differences in the paramagnetic  $^1H$  spectra of the different halide bound  $Ty_{met}$  species. The variations in the nuclear relaxation rates, coupling constants and the magnitude of  $-2J$  between the three  $Ty_{met}X$  species will be described in Chapter 5.

It appears that the apparent fluoride and chloride inhibition constants (Figure 1), as well as the dissociation constants for fluoride and chloride binding to native  $Ty_{met}$  (Figures 3 and 4), are pH dependent. The simplest way to explain these data is by using Scheme 2, where the halide binding is under control of a single protein derived acid/base equilibrium and where halide only binds to the acidic form of the enzyme, rendering a kinetically inactive complex. The presented data only allow us to conclude that the  $pK_a$  value of this acid/base is less than 5.5. A pH dependent anion binding has also been observed for met hemocyanin (40) and several dinuclear copper model complexes (41, 42).

To explain the pH dependence of the inhibition of Ty by halides it was previously suggested that a coordinating His residue dissociates from one copper at low pH, thereby providing a binding site for halide ion (16-18). Our results clearly demonstrate that this is not the case for bacterial  $Ty_{met}$ . The observed pH dependence of halide binding might originate from the protonation or direct dissociation of the hydroxide molecule that



bridges the two copper ions in the native  $Ty_{met}$  active site at low pH, leaving the bridging position vacant and accessible for halides to bind. A pH dependent dissociation of  $Cu_2$  bridging hydroxide (42-45), as well as the replacement of bridging hydroxide by anions (42, 45, 46), has been observed for a number of  $Cu_2$  model complexes. The presence of a hydroxide or water molecule at an equatorial  $Cu^{2+}$  coordination position and its displacement by exogenous ligands has been unequivocally demonstrated for *Streptomyces antibioticus*  $Ty_{half-met}$  by means of pulsed EPR spectroscopies (13). The kinetics of fluoride binding, and its pH dependence, are described in detail in chapter 4.

### The interaction of halide with the reduced [Cu(I) Cu(I)] enzyme $Ty_{red}$

The  $Ty_{oxy}$  titration data (Figure 6) show that addition of halide ( $Cl^-$ ,  $Br^-$ ,  $I^-$ ) causes a decrease in the optical absorption at 345 nm associated with  $Ty_{oxy}$ , while this effect is not seen when fluoride is used as the titrant, not even when fluoride concentrations (200 mM) much higher than the apparent inhibition constant at pH 6.80 (11.8 mM) are used. The apparent dissociation constants determined at pH 6.80 decrease as we go down the halide group ( $K_d$ :  $I^- < Br^- < Cl^- \ll F^-$ ). Although an allosteric effect of halide binding on the oxygen binding affinity cannot be excluded, the data can be more easily interpreted by assuming that halide is in competition with molecular oxygen for binding to  $Ty_{red}$  according to Scheme 3. This is in line with the non-competitive inhibition with respect to [L-DOPA] as observed for iodide in the conversion of diphenols. Non-competitive inhibition means that inhibitor and substrate do not combine with the same enzyme form, which is the case when iodide only binds to  $Ty_{red}$  (Scheme 1).

### Correlations between the inhibition and the nature of the halide ion

At pH 6.80, the inhibition strengths follow the order  $I^- > F^- \gg Cl^- > Br^-$ . In an earlier study on Ty halide inhibition (17), different orders in halide inhibition strength were found for different tyrosinases (frog epidermis Ty:  $I^- > Br^- > Cl^- \gg F^-$ ; mushroom Ty:  $F^- > I^- > Cl^- > Br^-$ ; mouse melanoma Ty:  $F^- > Cl^- \gg Br^- > I^-$ ). These differences in inhibition strength have been mainly explained by relating the anion size to the accessibility to the active site. Our results show that such an explanation may be too simple.

It appears that the halide inhibition is a combination of the interaction with the oxidised protein, giving rise to competitive inhibition in the conversion of L-DOPA, and of the interaction with the reduced protein  $Ty_{red}$ , giving rise to non-competitive inhibition. The results show that iodide solely interacts with the reduced protein as apparent from the lack of changes in the paramagnetic  $^1H$  spectra of  $Ty_{met}$  upon addition of 0.2 M iodide ( $> 50 \times K_{i,I}^{app}$ ) and the good agreement between the inhibition constant of iodide (3.5 mM) and

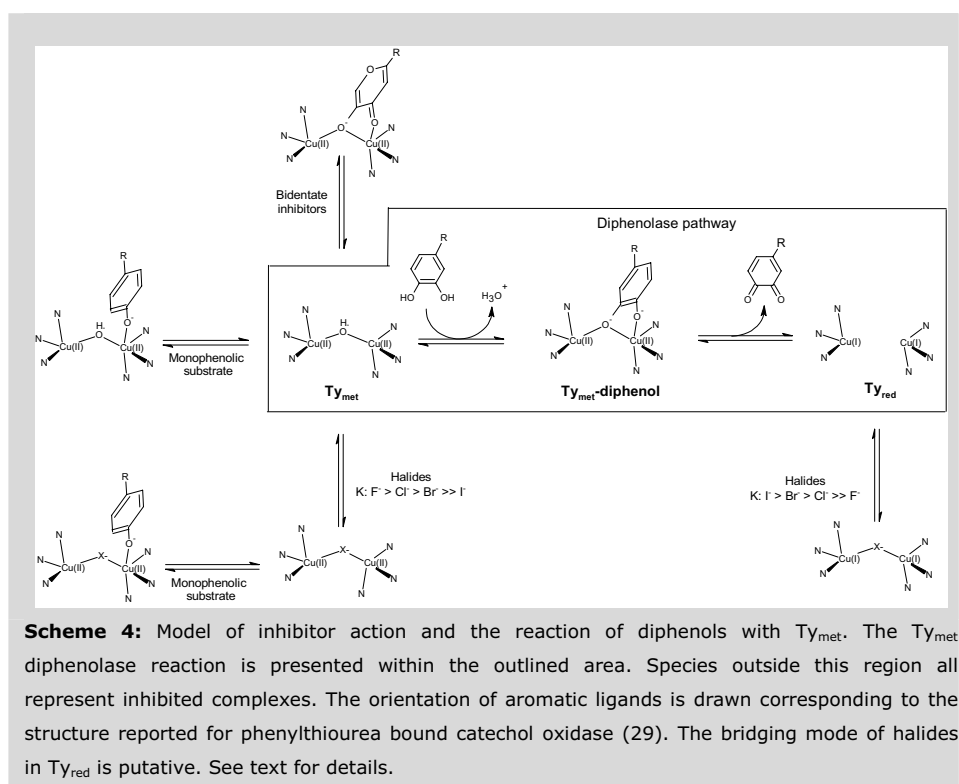
the apparent dissociation constant for binding to  $Ty_{red}$  (3.0 mM). In contrast, the oxidised  $Ty_{met}$  species seems the primary site of interaction with the small  $F^-$  ion since no evidence of binding to either  $Ty_{oxy}$  or  $Ty_{red}$  was obtained while the apparent fluoride inhibition constant determined at 4 °C and pH 6.80 (3.4 mM; extrapolating to 6.2 mM at pH 7.06 based on Equation 1) is in good agreement with the fluoride dissociation constant for  $Ty_{met}$  determined using  $^1H$  paramagnetic NMR at pH 7.06 and 4 °C (5.8 mM, Figure 4). Chloride and bromide are intermediate cases that interact with both  $Ty_{met}$  and  $Ty_{red}$ . Although the mechanism of inhibition is thus different for iodide and fluoride, their  $K_i$  values are incidentally close.

Overall, the binding affinities to  $Ty_{met}$  follow the order  $F^- > Cl^- > Br^- \gg I^-$  while the binding to  $Ty_{red}$  is the exact reverse  $I^- > Br^- > Cl^- \gg F^-$ . Indeed, this is the behaviour expected from simple hard/soft ligand binding rules, the softer ligands favouring the lower oxidation state of the Cu ions. The observations are also in-line with the finding that the Cu-Cu distance in reduced sweet potato catechol oxidase is larger than the distance found for the oxidised analogue (4.4 Å vs. 2.9 Å) (29). This corresponds with our observation that the  $Ty_{met}$  protein seems to favour smaller anions while a larger Cu-Cu distance in the  $Ty_{red}$  reduced protein would facilitate a stable binding of the larger anions like iodide. Indeed, the Cu-Cu distance has previously been shown to be the critical factor in controlling the selectivity of anion bridging in small dinuclear copper model complexes (42) where it was found that the strongest anion binding occurs for ligands that best fit between the two Cu atoms.

#### Halide / inhibitor displacement studies

The data presented in Figure 5 clearly show that the monophenolic substrate analogue *p*-nitrophenol binds to the oxidised  $Ty_{met}$  protein. The formed complex is kinetically dead-end according to Scheme 1, which means that this is a wasteful event from a mechanistic point-of-view. This interaction of  $Ty_{met}$  with monophenols was proposed earlier on the basis of kinetic data (47-49) but has never been shown directly. The data further show that *p*-nitrophenol also binds to  $Ty_{met}Cl$ , yielding a ternary  $Ty_{met}Cl$ -*p*-nitrophenol complex. Apparently, the binding of the monophenolic ligand does not displace the halide ion, meaning that the monophenol probably coordinates to an axial position on one of the coppers if it is assumed that halides block the bridging position. This is in agreement with the diphenol coordination proposed for the closely related enzyme sweet potato catechol oxidase on the basis of X-ray structure data of the oxidised protein with the inhibitor phenylthiourea bound (29). Different *p*-nitrophenol- $Ty_{met}$  complexes are presently under NMR investigation.

In contrast to the monophenolic *p*-nitrophenol, inhibitors containing a hydroxy-ketone or carboxylate functional group clearly displace the chloride ion from the active-site (Figures 5C and 5D). We interpret these results in the light of EPR studies on  $Ty_{\text{half-met}}$  (13). There we showed that bidentate ligands coordinate in a bidentate fashion to one copper in the active site, displacing the equatorially bound water or hydroxide that is present in absence of exogenous ligands. The results presented here corroborate these findings and further allow us to extend the model to the diphenolase pathway as shown schematically in Scheme 4 where we propose that the diphenolic substrate adopts a similar coordination geometry as bidentate transition state analogues.



### Concluding remarks

Since both the pH and chloride concentration may vary strongly in biological materials, the presented findings have relevance towards biotechnological applications of Ty, such as Ty based biosensors (e.g. (50-52)). Yet, the current work may also have physiological implications. It has been found that the activity of Ty is higher in Black than in Caucasian melanocytes (53, 54). This variation is not due to differences in the number of

melanocytes, the Ty abundance, the Ty gene activity or the Ty gene sequence, suggesting that the Ty activity is regulated at the molecular level (54-57). In a recent study (55), it has been suggested that this difference originates from a lower pH in Caucasian melanosomes with respect to the pH in the Black organelles, causing the Ty activity, and hence the extent of pigmentation, to be lower in Caucasians. The present results may provide the structural basis for this effect. For the bacterial Ty, we found that the apparent chloride inhibition constant (0.16 M at pH 6.80) is in the order of physiological chloride concentrations (5-200 mM). Similar values for the apparent chloride inhibition constant have been found for other Tys (17). A decrease in pH of one unit leads to a ten-fold increase in the fraction of Ty that is in the inactive chloride bound form. Depending on the  $[Cl^-]/K_i^{app}$  ratio, this would correspond to a maximal ten-fold decrease in total activity, thereby providing a possible explanation of the sensitivity of Ty activity to melanosomal pH. As a final remark, we note that also the multicopper laccases are inhibited by halide ions in a complex manner (58). Here, differences in halide inhibition strength among various laccases have been proposed to originate from variations in the accessibility in the channel leading to the T2/T3 site. It may well be that these variations, and the apparent complexity of the halide inhibition, arise from similar phenomena as described for the current system.

## References

1. Oetting, W. S. (2000) *Pigment Cell Res.* **13**, 320-325
2. Tief, K., Schmidt, A., and Beermann, F. (1998) *Brain Res. Mol. Brain Res.* **53**, 307-310
3. Xu, Y., Stokes, A. H., Freeman, W. M., Kumer, S. C., Vogt, B. A., and Vrana, K. E. (1997) *Brain Res. Mol. Brain Res.* **45**, 159-162
4. Berman, S. B. and Hastings, T. G. (1997) *J. Neurochem.* **69**, 1185-1195
5. Berman, S. B. and Hastings, T. G. (1999) *J. Neurochem.* **73**, 1127-1137
6. Higashi, Y., Asanuma, M., Miyazaki, I., and Ogawa, N. (2000) *J. Neurochem.* **75**, 1771-1774
7. Decker, H. and Tuczek, F. (2000) *Trends Biochem. Sci.* **25**, 392-397
8. Sánchez-Ferrer, A., Rodríguez-López, J. N., García-Cánovas, F., and García-Cánovas, F. (1995) *Biochim. Biophys. Acta* **1247**, 1-1
9. Solomon, E. I., Sundaram, U. M., and Machonkin, T. E. (1996) *Chem. Rev.* **96**, 2563-2605
10. van Gelder, C. W., Flurkey, W. H., and Wichers, H. J. (1997) *Phytochem.* **45**, 1309-1323

## Chapter 3

### Structural basis of halide inhibition

11. Himmelwright, R. S., Eickman, N. C., and Solomon, E. I. (1979) *Biochem. Biophys. Res. Commun.* **86**, 628-634
12. Wilcox, D. E., Porras, A. G., Hwang, Y. T., Lerch, K., Winkler, M. E., and Solomon, E. I. (1985) *J. Am. Chem. Soc.* **107**, 4015
13. van Gastel, M., Bubacco, L., Groenen, E. J., Vijgenboom, E., and Canters, G. W. (2000) *FEBS Lett.* **474**, 228-232
14. Bubacco, L., Salgado, J., Tepper, A. W., Vijgenboom, E., and Canters, G. W. (1999) *FEBS Lett.* **442**, 215-220
15. Bubacco, L., Vijgenboom, E., Gobin, C., Tepper, A. W. J. W., Salgado, J., and Canters, G. W. (2000) *J. Mol. Cat. B* **8**, 27-35
16. Martínez, J. H., Solano, F., García-Borrón, J. C., Iborra, J. L., and Lozano, J. A. (1985) *Biochem. Int.* **11**, 729-738
17. Martínez, J. H., Solano, F., Peñafiel, R., Galindo, J. D., Iborra, J. L., and Lozano, J. A. (1986) *Comp. Biochem. Physiol B* **83**, 633-636
18. Peñafiel, R., Galindo, J. D., Solano, F., Pedreño, E., Iborra, J. L., and Lozano, J. A. (1984) *Biochim. Biophys. Acta* **788**, 327-332
19. Himmelwright, R. S., Eickman, N. C., and Solomon, E. I. (1978) *Biochem. Biophys. Res. Commun.* **84**, 300-305
20. Jackman, M. P., Hajnal, A., and Lerch, K. (1991) *Biochem. J.* **274 ( Pt 3)**, 707-713
21. Lerch, K. and Ettlinger, L. (1972) *Pathol. Microbiol. (Basel)* **38**, 23-25
22. Inubushi, T. and Becker, E. D. (1983) *J. Magn. Reson.* **51**, 128-133
23. Calzolari, L., Gorst, C. M., Bren, K. L., Zhou, Z. H., Adams, M. W. W., and LaMar, G. N. (1997) *J. Am. Chem. Soc.* **119**, 9341-9350
24. Boyer, P. D. (1970) *The enzymes: Kinetics and Mechanism*, Third edition Ed., Academic Press, New York
25. Cánovas, F. G., García-Carmona, F., Sánchez, J. V., Pastor, J. L., and Teruel, J. A. (1982) *J. Biol. Chem.* **257**, 8738-8744
26. Eickman, N. C., Himmelwright, R. S., and Solomon, E. I. (1979) *Proc. Natl. Acad. Sci. USA* **76**, 2094-2098
27. Himmelwright, R. S., Eickman, N. C., LuBien, C. D., and Solomon, E. I. (1980) *J. Am. Chem. Soc.* **102**, 5378-5388
28. Cuff, M. E., Miller, K. I., van Holde, K. E., and Hendrickson, W. A. (1998) *J. Mol. Biol.* **278**, 855-870

### Chapter 3

#### Structural basis of halide inhibition

29. Klabunde, T., Eicken, C., Sacchettini, J. C., and Krebs, B. (1998) *Nat. Struct. Biol.* **5**, 1084-1090
30. Magnus, K. A., Hazes, B., Ton-That, H., Bonaventura, C., Bonaventura, J., and Hol, W. G. (1994) *Proteins* **19**, 302-309
31. Volbeda, A. and Hol, W. G. (1989) *J. Mol. Biol.* **209**, 249-279
32. Amudha, P., Kandaswamy, M., Govindasamy, L., and Velmurugan, D. (1998) *Inorg. Chem.* **37**, 4486-4492
33. Amudha, P., Akilan, P., and Kandaswamy, M. (1999) *Polyhedron* **18**, 1355-1362
34. Amudha, P., Thirumavalavan, M., and Kandaswamy, M. (1999) *Polyhedron* **18**, 1363-1369
35. Malachowski, M. R., Dorsey, B. T., Parker, M. J., Adams, M. E., and Kelly, R. S. (1998) *Polyhedron* **17**, 1289-1294
36. Oshio, H., Watanabe, T., Ohto, A., Ito, T., and Masuda, H. (1996) *Inorg. Chem.* **35**, 472-479
37. Pons, J., Sanchez, F. J., Labarta, A., Casabo, J., Teixidor, F., and Caubet, A. (1993) *Inorg. Chim. Acta* **208**, 167-171
38. Rodríguez, M., Llobet, A., Corbella, M., Martell, A. E., and Reibenspies, J. (1999) *Inorg. Chem.* **38**, 2328-2334
39. Thompson, L. K., Tandon, S. S., and Manuel, M. E. (1995) *Inorg. Chem.* **34**, 2356-2366
40. Wilcox, D. E., Long, J. R., and Solomon, E. I. (1984) *J. Am. Chem. Soc.* **106**, 2186
41. Amendola, V., Bastianello, E., Fabbrizzi, L., Mangano, C., Pallavicini, P., Perotti, A., Lanfredi, A. M., and Ugozzoli, F. (2000) *Angew. Chem. Int. Ed.* **39**, 2917-2920
42. Amendola, V., Fabbrizzi, L., Mangano, C., Pallavicini, P., Poggi, A., and Taglietti, A. (2001) *Coord. Chem. Rev.* **219**, 821-837
43. Castro, I., Julve, M., Demunno, G., Bruno, G., Real, J. A., Lloret, F., and Faus, J. (1992) *J. Chem. Soc. Dalton Trans.*, 1739-1744
44. Monzani, E., Quinti, L., Perotti, A., Casella, L., Gullotti, M., Randaccio, L., Geremia, S., Nardin, G., Faleschini, P., and Tabbi, G. (1998) *Inorg. Chem.* **37**, 553-562
45. Monzani, E., Battaini, G., Perotti, A., Casella, L., Gullotti, M., Santagostini, L., Nardin, G., Randaccio, L., Geremia, S., Zanello, P., and Opromolla, G. (1999) *Inorg. Chem.* **38**, 5359-5369
46. Fabbrizzi, L., Pallavicini, P., Parodi, L., and Taglietti, A. (1995) *Inorg. Chim. Acta* **238**, 5-8

47. Rodríguez-López, J. N., Tudela, J., Varón, R., García-Carmona, F., and García-Cánovas, F. (1992) *J. Biol. Chem.* **267**, 3801-3810
48. Fenoll, L. G., Rodríguez-López, J. N., García-Sevilla, F., Tudela, J., García-Ruiz, P. A., Varón, R., and García-Cánovas, F. (2000) *Eur. J. Biochem.* **267**, 5865-5878
49. Fenoll, L. G., Rodríguez-López, J. N., García-Sevilla, F., García-Ruiz, P. A., Varón, R., García-Cánovas, F., and Tudela, J. (2001) *Biochim. Biophys. Acta* **1548**, 1-22
50. Peña, N., Reviejo, A. J., and Pingarrón, J. M. (2001) *Talanta* **55**, 179-187
51. Streffer, K., Vijgenboom, E., Tepper, A. W. J. W., Makower, A., Scheller, F. W., Canters, G. W., and Wollenberger, U. (2001) *Anal. Chim. Acta* **427**, 201-210
52. Wang, B., Zhang, J., and Dong, S. (2000) *Biosens. Bioelec.* **15**, 397-402
53. Abdel-Malek, Z., Swope, V., Collins, C., Boissy, R., Zhao, H. Q., and Nordlund, J. (1993) *J. Cell Sci.* **106**, 1323-1331
54. Iwata, M., Corn, T., Iwata, S., Everett, M. A., and Fuller, B. B. (1990) *J. Invest. Dermatol.* **95**, 9-15
55. Fuller, B. B., Spaulding, D. T., and Smith, D. R. (2001) *Exper. Cell Res.* **262**, 197-208
56. Naeyaert, J. M., Eller, M., Gordon, P. R., Park, H. Y., and Gilchrist, B. A. (1991) *Brit. J. Dermatol.* **125**, 297-303
57. Iozumi, K., Hoganson, G. E., Penella, R., Everett, M. A., and Fuller, B. B. (1993) *J. Invest. Dermatol.* **100**, 806-811
58. Xu, F. (1996) *Biochemistry* **35**, 7608-7614

# Chapter 4

## *Stopped-flow fluorescence studies of inhibitor binding to tyrosinase*

Partially published as: Tepper, A. W.; Bubacco, L.; Canters, G. W. *J. Biol. Chem.* 2004, 279, 13425-13435.

### Summary

Tyrosinase is a type-3 copper protein involved in the rate-limiting step of melanin synthesis. It is shown that the endogenous Trp fluorescence of tyrosinase from *Streptomyces antibioticus* is remarkably sensitive to the redox state. The fluorescence emission intensity of the [(Cu(I) Cu(I)] reduced species is more than twice that of the oxygen bound [Cu(II)-O<sub>2</sub><sup>2-</sup>-Cu(II)] form. The emission intensity of the oxidised [Cu(II)-OH<sup>-</sup>-Cu(II)] protein (Ty<sub>met</sub>) appears to be dependent on an ionisation process with a pK<sub>a</sub> value of 4.50. The binding of several transition-state analogues and inhibitors was studied under pseudo first-order conditions using stopped-flow fluorescence spectroscopy. The kinetic parameters  $k_{on}$ ,  $K_d$  and the fraction of fluorescence emission quenched upon fluoride binding depend on an ionisation process with a pK<sub>a</sub> value of 4.61, which is ascribed to the dissociation of Cu<sub>2</sub> bridging hydroxide at low pH. It is further shown that Ty is rapidly inactivated at low pH and that halide protects the enzyme from this inactivation. All results support the hypothesis that halide displaces hydroxide as the Cu<sub>2</sub> bridging ligand in Ty<sub>met</sub>. The relevance of the presented findings to the catalytic cycle is discussed. The data are consistent with the data obtained by using other techniques, validating the use of fluorescence quenching as a sensitive and useful tool in studying ligand binding and substrate conversion.



## Introduction

The details of the interaction of inhibitors with the dinuclear copper enzyme tyrosinase (Ty; E.C. 1.14.18.1) are still far from a complete understanding. They are the subject of this report. Tyrosinases are involved in the rate-limiting step in the synthesis of melanin pigments, which fulfill various roles in living organisms. In mammals, melanins are responsible for skin, eye, inner-ear and hair pigmentation and defects in Ty are related to a range of medical conditions like type I human oculocutaneous albinism (1;2). In fruits and mushrooms, melanin formation is responsible for the browning of tissue occurring after bruising or long time storage (3), while in insects it is thought that melanins assist in wound healing and sclerotization of the cuticle (4). In eukaryotes, the melanogenic pathway is complex and involves several enzymatic and non-enzymatic steps (5). The pathway starts with the Ty catalysed hydroxylation and subsequent oxidation of L-tyrosine to L-DOPAquinone, which is then converted to DOPACHROME. DOPACHROME, in turn, is a precursor in the synthesis of polyphenolic melanin pigments. Although the Ty activity has been studied for over a century (see refs. (3-7) for recent overviews), both the enzyme structure and its detailed mechanism of action remain to be solved.

Tyrosinase contains a so-called type-3 copper site that is composed of two closely spaced copper ions, which are each coordinated by 3 histidine residues (4;8). The type-3 site also occurs in the hemocyanins (Hcs), that function as oxygen carriers and storage proteins in arthropods and molluscs, and in the plant catechol oxidases (COs), that oxidise diphenols to the corresponding quinones but lack the Ty hydroxylation activity. Although the type-3 proteins fulfill different functions, the dinuclear active site seems to be highly conserved as witnessed by its characteristic spectroscopic signatures and the available crystal structures for several Hcs (9-11) and a CO (12). The differences in functionality are therefore thought to derive from variations in the accessibility of substrates to the active site or the ability of substrates to appropriately dock into the active centre (7;13;14).

The Ty type-3 site can exist in various forms, including a) the  $[\text{Cu(I) Cu(I)}]$  reduced  $\text{Ty}_{\text{red}}$  species, that binds molecular oxygen in a side-on bridging mode to render b) the  $[\text{Cu(II)-O}_2^{2-}\text{-Cu(II)}]$   $\text{Ty}_{\text{oxy}}$  species. The  $\text{Ty}_{\text{oxy}}$  form is competent to react with both monophenols and diphenols and is characterised by a strong Ligand to Metal Charge Transfer (LMCT) band centred around 345 nm and a low O-O stretching vibration frequency of approximately  $750 \text{ cm}^{-1}$  (4). The oxidation of diphenol by  $\text{Ty}_{\text{oxy}}$  yields the quinone product and leaves the enzyme in c) the  $[\text{Cu(II)-OH-Cu(II)}]$  oxidised met-form ( $\text{Ty}_{\text{met}}$ ), which is competent to react with diphenols only.

Detailed knowledge of the interaction of Ty with its inhibitors is of paramount importance for understanding the Ty enzyme mechanism, as well as for the development of novel Ty inhibitors relevant to, for example, skin treatment and the economically important prevention of the browning of fruits, vegetables and mushrooms. Consequently, steady-state kinetic studies of Ty inhibition are abundant and many inhibitors have been identified (e.g. (15-24)). Yet, direct spectroscopic investigations of inhibitor bound tyrosinases have long been few due to the scarcity of suitable spectroscopic probes. For example,  $Ty_{met}$  shows no strong UV/Vis absorption bands and is EPR silent due to the antiferromagnetic coupling between the two unpaired spins on the copper ions (4). Spectroscopic studies on the enzyme mainly pertained to the half-oxidised species, in which one of the copper ions in the active site occurs in the Cu(II) and the other in the Cu(I) oxidation state, rendering the site suitable for study by EPR techniques. While EPR studies on  $Ty_{half-met}$  have yielded much information regarding the coordination geometry of the oxidised copper and the changes that occur when ligands bind to the active site, the half-met form does not occur naturally and the technique allows for the investigation of only one of the copper ions in the type-3 site.

It was a step forward when, recently, the oxidised  $Ty_{met}$  derivative appeared amenable to paramagnetic NMR (8;25;26); the  $S = 1$  spin state of  $Ty_{met}$  was found to be thermally accessible at room temperature, providing sufficient paramagnetism for the signals of the coordinating histidine protons to shift outside the diamagnetic envelope. The NMR studies demonstrated that Ty contains a classical type-3 site in which the two copper ions are coordinated by six histidine residues through their  $N^{\epsilon}$  atoms (8). Furthermore, large changes in the  $Ty_{met}$  paramagnetic  $^1H$  NMR spectrum are observed when inhibitors bind to the active-site (25;26), allowing to follow ligand binding and to obtain structural information on the complexes. For instance, it was shown that halides interact with both the oxidised and reduced Ty, where the affinity for halide ion and the mechanism of inhibition depend both on the nature of the halide ion and the oxidation state of the type-3 site (26) ( $K_d^{red}$ :  $I^- < Br^- < Cl^- \ll F^-$ ;  $K_d^{met}$ :  $F^- < Cl^- < Br^- \ll I^-$ ). The binding of halide to  $Ty_{met}$  is strongly pH dependent where halide only binds to the acidic form of the enzyme, resulting in stronger inhibition with decreasing pH. As a consequence of the instability of the enzyme at low pH and of the relatively long experimental times required, we were able to determine only an upper limit of 5.5 for the  $pK_a$  of the process modulating the halide binding. In the same study it was also proposed that halides bridge the two copper ions in the active site.

Fluorescence studies on proteins in which use is made of the emission of endogenous Tyr and Trp residues have been widely performed to study protein structure and its dynamics. Several Hcs (e.g. (27-39)) and one Ty (40) have been subject of such investigations. This

report focuses on the fluorescence properties of the Ty from *Streptomyces antibioticus* as a function of pH and inhibitor binding. Significant changes in protein emission quantum yield occur when inhibitors bind to the oxidised Ty<sub>met</sub> type-3 centre, allowing the use of protein fluorescence as a sensitive technique to study ligand binding.

Based on experience (26), fluoride was chosen as a model compound to study the transient-state kinetics of its binding to the Ty<sub>met</sub> enzyme, as well as its pH dependence. Stopped-flow fluorescence spectroscopy studies was used to obtain insight into the interaction of fluoride with Ty, as well as to validate the use of fluorescence quenching in studying ligand binding kinetics. We further evaluated the kinetics of the binding of several organic inhibitors to Ty<sub>met</sub> to obtain insight into the factors that contribute to the affinity to the Ty<sub>met</sub> site. Finally, the inactivation of Ty was studied at various pH values and under different conditions. To our knowledge, this is the first report on the kinetics of inhibitor binding to oxidised tyrosinase.

## Experimental procedures

### Protein isolation and purification.

Tyrosinase was obtained from liquid cultures of *Streptomyces antibioticus* carrying the Ty pIJ703 overexpression plasmid (25). The enzyme was purified from the growth medium according to published procedures (25). The pure enzyme was obtained as a mixture of Ty<sub>met</sub>, Ty<sub>red</sub> and Ty<sub>oxy</sub> and the purity exceeded 95% in all cases as estimated by SDS-PAGE. Protein concentrations were routinely determined optically using a value of 82 mM<sup>-1</sup>cm<sup>-1</sup> for the extinction coefficient at 280 nm (41). The protein was stored at -80 °C at a concentration of 1 mg/ml in 100 mM Pi buffer at pH 6.8 containing 20 % glycerol as a cryoprotectant. Prior to further experiments, glycerol was removed from the storage buffer by dialysis at 4 °C against 100 mM Pi at pH 6.80. The reduced enzyme was prepared by reduction with hydroxylamine as previously described (26) and used immediately.

### Optical spectroscopy.

Optical measurements were performed on a Perkin-Elmer Lambda 800 spectrometer. Steady-state fluorescence measurements were performed on a Perkin Elmer LS 50B fluorimeter. For recording the emission spectra, the freshly prepared enzyme was diluted in the measurement buffer immediately prior to the measurement. Anaerobic, air-saturated or oxygen-saturated buffers were prepared by extensive bubbling with pure argon, air or oxygen, respectively. The concentration of oxygen was 0.27 mM for the air-saturated solutions at 20° and 1.32 mM for the oxygen saturated solutions (42). For the oxygen titration experiments, small aliquots of oxygen saturated buffer were introduced into the

cuvette through an air-tight septum using a 10  $\mu$ L Hamilton syringe.

## Kinetics

Stopped-flow experiments were performed using a computer-controlled Applied-Photophysics SX18MV stopped-flow system equipped with a PBP 05-109 Spectrakinet monochromator. The system was temperature controlled at 21 °C using a Neslab RTE-111 circulation cryostat. Ty fluorescence was detected using a photomultiplier tube equipped with an optical cut-off filter of 320 nm supplied with the stopped-flow system, thus resulting in the detection of all emitted light above 320 nm. The enzyme was introduced into the reaction chamber from a stock solution kept at 4 °C. For the study of ligand binding kinetics, the time dependence of the binding process was recorded using at least 10 different ligand concentrations in the range of the dissociation constant for the ligand. The ligand solutions were prepared by dilution from concentrated stock-solutions, made up in the reaction buffer, using 100 mM Pi at pH 6.8.

Ligand binding traces were fitted to a single-exponential decay function of the form  $F_t = F_\infty + A \cdot \exp(-k_{\text{obs}} \cdot t)$ , where  $F_t$  denotes the fluorescence at time  $t$ ,  $F_\infty$  is the fluorescence level at completion of the binding reaction,  $A$  is the signal amplitude and  $k_{\text{obs}}$  is the observed rate constant. The fitting was performed using the least-squares fitting algorithm implemented in the stopped-flow software. The reported kinetic parameters  $k_{\text{obs}}$  and  $A$  represent the average of at least 4 measurements. The standard errors were less than 10 % in all cases. Since some ligands significantly absorbed at the excitation wavelength resulting in the quenching of fluorescence due to the inner-filter effect, manifested as an apparent decrease in the emission level at  $t = 0$  at given  $[L]$ , values for  $F_0$  (i.e. the fluorescence level at  $t = 0$ ) were calculated from  $F_\infty + A$ . Since fluoride ion protonates at low pH forming HF, effective free fluoride concentrations were calculated using a value of 3.14 for the  $pK_a$  for the  $\text{HF} \leftrightarrow \text{F}^- + \text{H}^+$  equilibrium (42).

## Results

### pH dependent inactivation of Ty

From previous studies (43), it is known that the Ty from *Streptomyces antibioticus* is unstable at low pH. The closely related Ty from *Streptomyces glaucescens* (93% sequence identity with *Streptomyces antibioticus* Ty), is more stable in Tris-HCl buffer than in phosphate buffer, especially at the lower pH values (44). To investigate the pH stability of *Streptomyces antibioticus* Ty, and its dependence on the presence of halide ion, we performed experiments at 21 °C where the protein in 5 mM Pi at pH 7.20 was pH-jumped

by rapidly mixing with 200 mM phosphate buffer at the pH of interest in 1:1 volume ratio (end buffer concentration 102.5 mM Pi) using stopped-flow. The reported pH values were measured on the final mixed solutions. The mixture was allowed to incubate for a defined amount of time after which the solution was rapidly mixed with 5 mM solution of *t*-butylcatechol in 5 mM Pi at the pH of the experiment. The steady-state velocity of formation of the stable reaction product *t*-butylquinone was optically measured at 410 nm for 1 sec. After reaching the steady-state ( $t < \sim 50$  msec), linear product formation was observed.

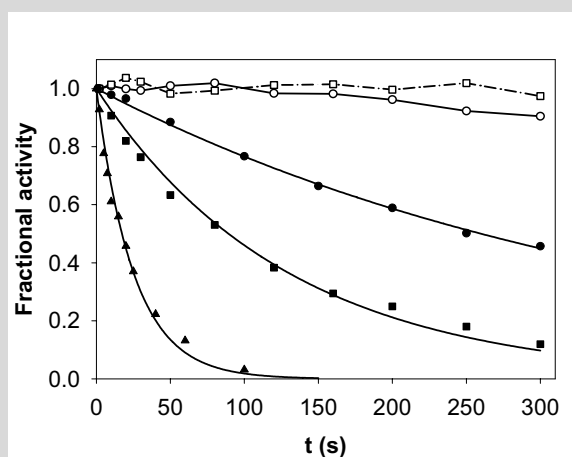


**Figure 1:** The pH dependent inactivation of *Streptomyces antibioticus* Ty and the stabilisation by halide ion. Measurements were made at 21 °C by pH-jump sequential stopped-flow where the protein was incubated at pH 3.63 (▲), pH 4.40 (■) and pH 4.85 (●) for a fixed time-period and then assayed for remaining activity using 5 mM *t*-butylcatechol (see materials and methods for experimental details). Solid lines represent least-squares fits to a mono-exponential decay function. Little inactivation could be detected when either 6 mM of chloride (○) or 6 mM of fluoride (□) was present in the incubation mixture at pH 4.40.

Figure 1 shows the normalised reaction rates vs. incubation time under various conditions. The inactivation profiles obtained in the absence of halide (solid data-points in Fig. 1) clearly show a pH dependent inactivation of the protein. The data were fitted to a single-exponential decay function yielding inactivation rate constants of 2.09, 0.43 and 0.16 min<sup>-1</sup> at pH 3.63, pH 4.40 and pH 4.85, respectively. Curiously, little inactivation of the enzyme could be detected when 6 mM of either fluoride or chloride was present in the incubation and reaction mixtures at pH 4.40 (open symbols in Fig. 1). Here, product formation was measured for 5 sec to compensate for the inhibitory effect of halide. Apparently, the presence of halide significantly stabilises the protein at low pH.

### Fluorescence emission of Ty in its three different oxidation states.

Fluorescence emission spectra of  $Ty_{red}$  under anaerobic (A) and air-saturated (D) conditions at pH 6.80 and 21 °C are presented in Fig. 2. While under anaerobic conditions only  $Ty_{red}$  is present, under air-saturated conditions the protein exists as a mixture of 94%  $Ty_{oxy}$  and 6%  $Ty_{red}$  as calculated from  $K_{O_2}$  and  $[O_2]$  (see below and Fig. 3). Spectra of samples containing the resting form of the enzyme (predominantly  $Ty_{met}$ ) were recorded under anaerobic (Figure 2B) and aerobic (Figure 2C) conditions. All species display a similar lineshape for the emission band with a maximum centred at  $343 \pm 2$  nm and a half-width of  $60 \pm 2$  nm. Little fine structure can be distinguished and the absence of a shoulder at 300-310 nm with all species indicates that the emission is dominated by Trp fluorescence. It appears that the relative fluorescence emission intensities are highly dependent on the oxidation state of the protein, the emission intensities of  $Ty_{red}$  and  $Ty_{oxy}$  differing by a factor of more than 2. The optical absorption spectra in the 250-300 nm region were identical for all 3 preparations (resting Ty,  $Ty_{met}+Ty_{oxy}$  and  $Ty_{red}$ ; not shown).

The relative fluorescence intensity of the resting form of the enzyme (Figure 2B and 2C) depends on the presence of oxygen in the sample. This can be explained by considering that the resting form of the enzyme contains a percentage of  $Ty_{red}$  and  $Ty_{oxy}$  in addition to a predominant amount of  $Ty_{met}$  (4;5). Under anaerobic conditions only  $Ty_{met}$  and  $Ty_{red}$  are present and the total fluorescence is given by:

$$F_1 = x \cdot F_{met} + (1-x) \cdot F_{red} \quad (\text{Equation 1})$$

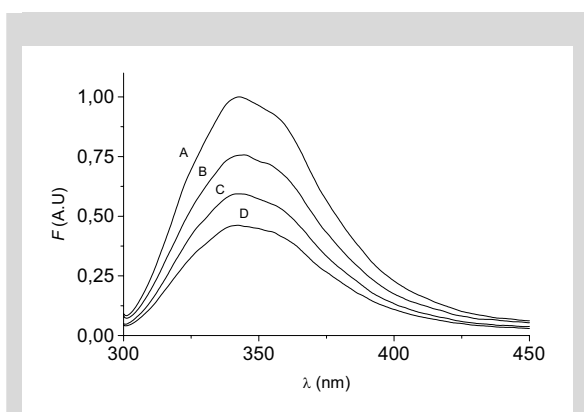


**Figure 2:** Normalised emission spectra of A)  $Ty_{red}$  recorded under anaerobic conditions, resting Ty (predominantly  $Ty_{met}$ , see text) under B) anaerobic and C) aerobic conditions and D) 94 %  $Ty_{oxy}$  + 6 %  $Ty_{red}$ . All measurements were made in 100 mM Pi buffer at pH 6.80 and at 21 °C using an excitation wavelength of 290 nm. In all cases the total  $[Ty]$  was  $\sim 0.3 \mu M$ .

where  $F_1$  is the observed emission intensity,  $x$  is the fraction  $Ty_{met}$  in the sample,  $F_{met}$  is the normalised fluorescence intensity of  $Ty_{met}$  and  $F_{red}$  is the normalised fluorescence intensity of  $Ty_{red}$ . When oxygen is present, an equilibrium between  $Ty_{red}$  and  $Ty_{oxy}$  is formed, the ratio of the two species depending on the oxygen dissociation constant  $K_{O_2}$  and  $[O_2]$ . The total emission is then given by

$$F_2 = x \cdot F_{met} + (1-x) \cdot \left(1 - \frac{K_{O_2}}{[O_2] + K_{O_2}}\right) \cdot F_{oxy} + (1-x) \cdot \left(\frac{K_{O_2}}{[O_2] + K_{O_2}}\right) \cdot F_{red} \quad (\text{Equation 2})$$

From the measured emission intensities at  $\lambda_{max}$  and Eqs. 1 and 2, the fraction of  $Ty_{met}$ , as well as the relative  $Ty_{met}$  emission intensity, can be calculated according to the following equations:

$$x = \frac{(F_1 - F_2 K_{O_2} + (F_1 - F_2 - F_{red} + F_{oxy})O_2]}{(F_{oxy} - F_{red})O_2} \quad (\text{Equation 3})$$

and

$$F_{met} = \frac{(F_{red}F_1 - F_{red}F_2 K_{O_2} + (F_{oxy}F_1 - F_{red}F_2)O_2]}{(F_1 - F_2 K_{O_2} + (F_1 - F_2 - F_{red} + F_{oxy})O_2)} \quad (\text{Equation 4})$$

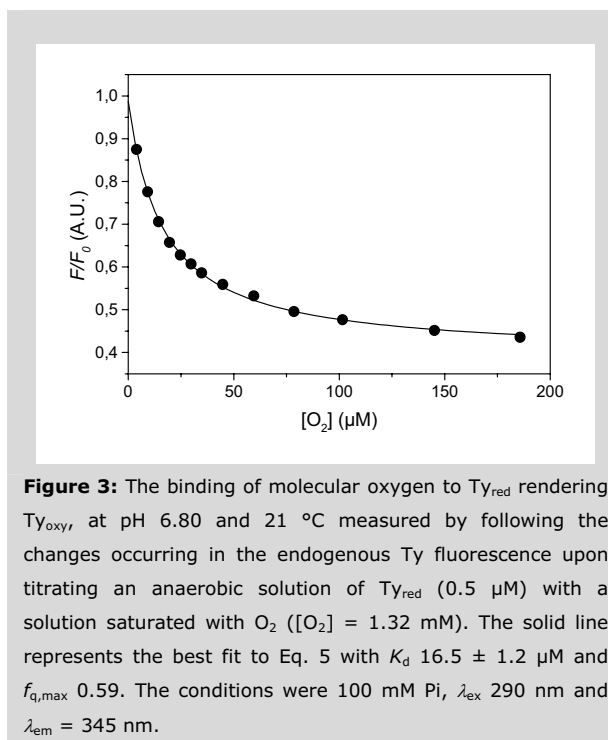
By using 0.27 mM for  $[O_2]$ , 16.5  $\mu$ M for  $K_{O_2}$  (see below and Fig. 3), 1 for  $F_{red}$ , 0.41 for  $F_{oxy}$  (see below) and the measured intensities  $F_1$  and  $F_2$ , amounting to 0.76 and 0.60 respectively, a value of 0.71 is obtained for the fraction  $Ty_{met}$  in the sample ( $x$ ) and a value of 0.66 for the fractional emission intensity  $F_{met}$  relative to that of  $Ty_{red}$ . In a resting  $Ty$  sample in air-saturated buffer at pH 6.80 and 21 °C, it is calculated that  $Ty_{oxy}$  and  $Ty_{red}$  contribute a fraction of 0.21 to the total fluorescence emission while 0.79 of the emission originates from the  $Ty_{met}$  species. We found the fraction of  $Ty_{met}$  in our fresh preparations to be constant under the used experimental conditions.

### Oxygen binding

We have studied the steady-state binding of molecular oxygen to Ty<sub>red</sub>, rendering Ty<sub>oxy</sub>, by following the changes occurring in the Ty Trp fluorescence as described above ( $\lambda_{\text{ex}}$  290 nm,  $\lambda_{\text{em}}$  345 nm). For this, 3.0 ml of a freshly prepared anaerobic solution of 0.1  $\mu\text{M}$  Ty<sub>red</sub> in 100 mM Pi at pH 6.80 was introduced in a sealed 3.5 ml quartz cuvette after which this solution was titrated with  $\mu\text{l}$  amounts of a 100 mM Pi buffer saturated with oxygen. The fluorescence emission intensity at 345 nm at given  $[\text{O}_2]$  was measured using a 5 sec instrument integration time. The resulting measured intensities, expressed as  $F/F_0$ , vs.  $[\text{O}_2]$  are presented in Fig. 3. The data could be accurately fitted assuming the binding of a single oxygen using the expression:

$$\frac{F}{F_0} = 1 - \frac{f_q \cdot [\text{L}]}{[\text{L}] + K_d} \quad (\text{Equation 5})$$

where  $F$  denotes the observed fluorescence intensity,  $F_0$  denotes the fluorescence intensity in the absence of ligand,  $[\text{L}]$  denotes the ligand concentration,  $K_d$  denotes the dissociation constant for ligand L and  $f_q$  denotes the fractional decrease in fluorescence upon complete saturation with the ligand, i.e. at  $[\text{L}] \gg K_d^{\text{app}}$ . Values of  $16.5 \pm 1.2 \mu\text{M}$  for the oxygen dissociation constant and of 0.59 for  $f_q$  were obtained. The latter value means that the fluorescence intensity of the Ty<sub>oxy</sub> species amounts to 0.41 of the Ty<sub>red</sub> fluorescence intensity.

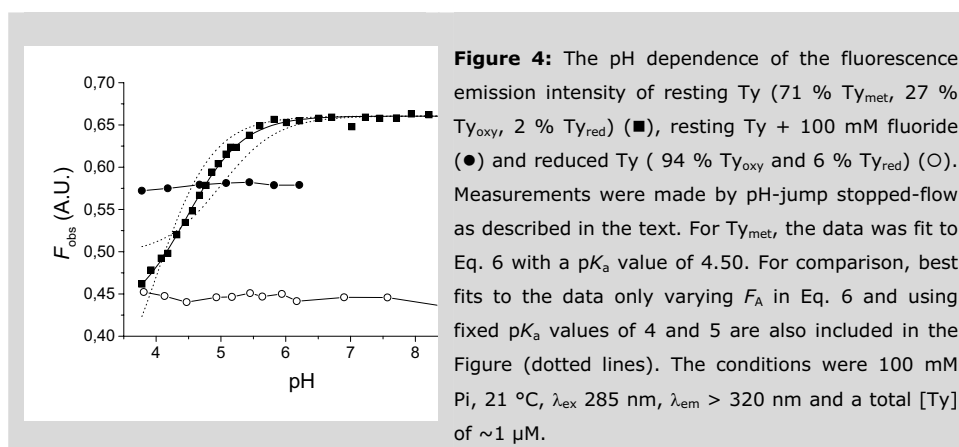




### The pH dependence of Ty fluorescence.

Since we found that Ty is unstable at low pH (see Fig. 1), we measured the pH dependence of Ty fluorescence by pH-jump stopped-flow at a timescale where the protein has not decayed to any measurable extent. For this, we rapidly mixed a  $\sim 2 \mu\text{M}$  Ty solution in 1 mM Pi at pH 7.20 with a 200 mM air-saturated Pi buffer at the pH of interest in a 1:1 volume ratio ( $[\text{Ty}] \sim 1 \mu\text{M}$ ;  $3.8 < \text{pH} < 9.0$ ). The fluorescence level was then measured for 0.25 sec. The measurements were performed with three Ty preparations: resting Ty (71 %  $\text{Ty}_{\text{met}}$ , 27 %  $\text{Ty}_{\text{oxy}}$ , 2 %  $\text{Ty}_{\text{red}}$ ), reduced Ty (94%  $\text{Ty}_{\text{oxy}}$ , 6 %  $\text{Ty}_{\text{red}}$ ) and resting Ty in the presence of 100 mM fluoride. In the time-period of the measurement the fluorescence was stable. The actual pH values were measured on the mixed solutions. The obtained emission intensity data, expressed as the fractions of emission intensity relative to that of  $\text{Ty}_{\text{red}}$ , are presented in Fig. 4. For the reduced sample containing  $\text{Ty}_{\text{oxy}}$  and  $\text{Ty}_{\text{red}}$ , there is no detectable pH dependence of the emission intensity. For the resting Ty sample the emission intensity decreases at low pH. Since the emission of the reduced sample was not sensitive to the pH, the observed variation in emission must be due to changes in the contribution of  $\text{Ty}_{\text{met}}$ . Accordingly, the experimental data were corrected for the contribution of  $\text{Ty}_{\text{oxy}}$  and  $\text{Ty}_{\text{red}}$  to the emission (0.21 of  $F_0$  at pH 6.80) and normalised using the calculated value of  $F_{\text{met}}$  of 0.66 at pH 6.80. The corrected data are plotted in Figure 4. The  $\text{Ty}_{\text{met}}$  emission data can be interpreted by assuming that the fluorescence level is under control of a single acid/base equilibrium according to:

$$F_{\text{obs}} = \frac{F_A \cdot [\text{H}^+] + F_B \cdot K_a}{[\text{H}^+] + K_a} \quad (\text{Equation 6})$$



where  $F_{obs}$  denotes the observed fluorescence level at given pH,  $F_A$  denotes the fluorescence level of the acidic form of the protein and  $F_B$  the fluorescence level of the basic form of the protein. Fitting the data to Eq. 6 yields a  $pK_a$  value of  $4.50 \pm 0.08$  and a value of 0.42 for  $F_A$ , i.e. the relative fluorescence level of the acidic form of the enzyme relative to the fluorescence level of  $Ty_{red}$ . Remarkably, the fluorescence level of resting Ty + fluoride is independent of the pH between pH 3.75 and pH 6.25. Here, a  $[F^-]$  of 100 mM was present in both the enzyme and the buffer solution. At this  $[F^-]$ , the  $Ty_{met}$  enzyme can be considered to be fully saturated with  $F^-$  at all pH values used in the experiment, while fluoride does not interact with  $Ty_{red}$  and  $Ty_{oxy}$  ((43); see below). Depending on the pH, the relative fluorescence intensities of  $Ty_{met}$  and  $Ty_{met}F$  differ significantly, showing that the protein fluorescence can be exploited as a probe to study the fluoride binding.

### Stopped-flow studies of fluoride binding

We studied the binding of fluoride to  $Ty_{met}$  and its pH dependence between pH 4.0 and pH 7.9 using stopped-flow fluorescence spectroscopy under pseudo first-order conditions ( $[F^-] \gg [Ty_{met}]$ ). Representative fluoride binding traces obtained by mixing  $\sim 2.5 \mu M$  resting Ty with various  $[F^-]$  (0-120 mM) at pH 6.80 in 1:1 volume ratio and 21 °C are presented in Fig. 5, where a decrease in fluorescence is observed upon binding of  $F^-$ . At all pH values and at all  $[F^-]$ , traces could be fitted with good accuracy to a mono-exponential decay function, yielding values for the apparent binding rate ( $k_{obs}$ ) and signal amplitude ( $A$ ) at each  $[F^-]$ . At pH 6.80, no change in protein fluorescence was observed when 50 mM fluoride was mixed with  $Ty_{oxy}$  and  $Ty_{red}$ , showing that the observed kinetics were solely due to the interaction of fluoride with  $Ty_{met}$ . This is in line with an earlier observation that the addition of fluoride to a solution of  $Ty_{oxy}$  does not influence the position or the intensity of the LMCT transition of  $Ty_{oxy}$  (43).

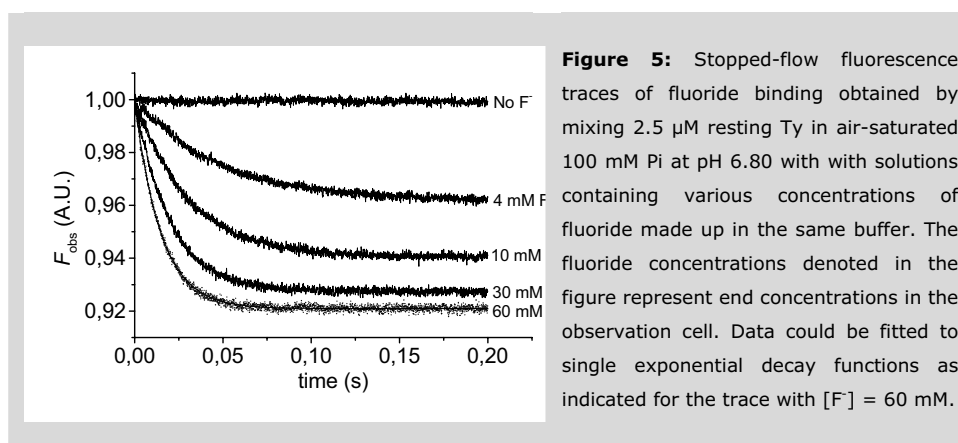
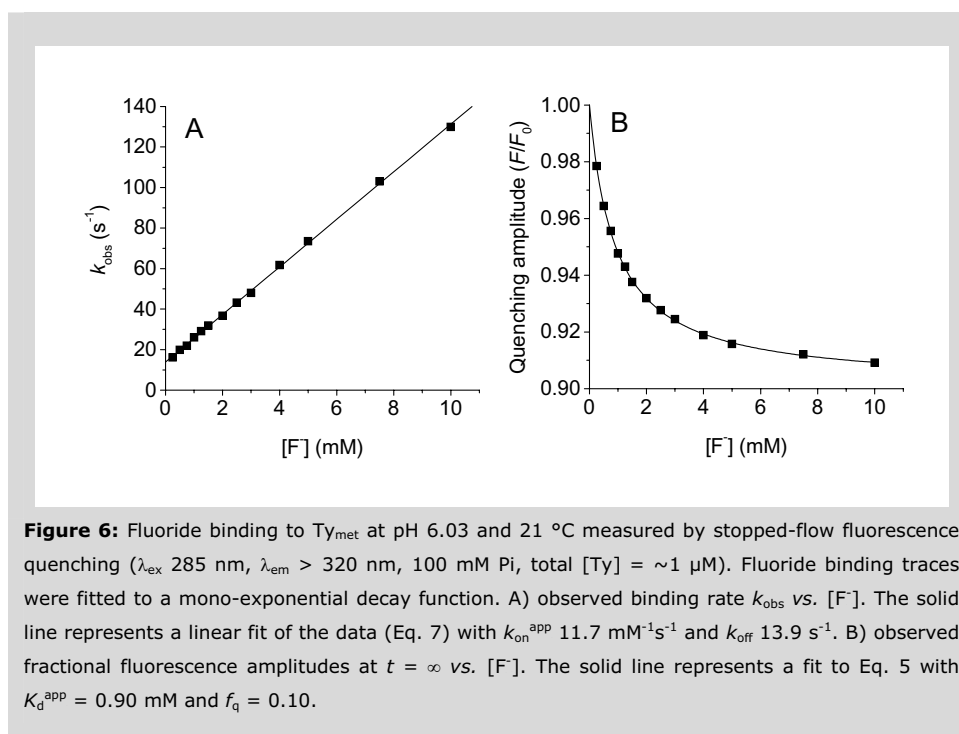


**Figure 5:** Stopped-flow fluorescence traces of fluoride binding obtained by mixing 2.5  $\mu M$  resting Ty in air-saturated 100 mM Pi at pH 6.80 with with solutions containing various concentrations of fluoride made up in the same buffer. The fluoride concentrations denoted in the figure represent end concentrations in the observation cell. Data could be fitted to single exponential decay functions as indicated for the trace with  $[F^-] = 60$  mM.

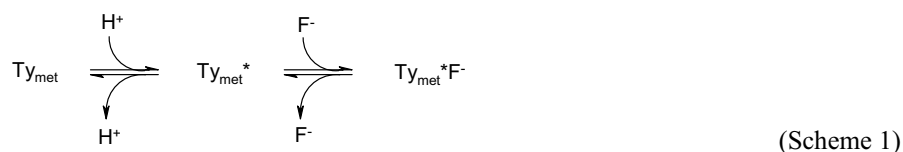
The plots of  $k_{\text{obs}}$  vs.  $[\text{F}^-]$  at given pH were linear in all cases, in agreement with a two-state binding scheme where a single fluoride ion binds to the enzyme. Representative data obtained at pH 6.03 are shown in Fig. 6A. The apparent first-order fluoride binding rate ( $k_{\text{on}}^{\text{app}}$ ) and the  $\text{Ty}_{\text{met}}\text{F}$  fluoride dissociation rate constant ( $k_{\text{off}}$ ) can be determined from the slope and intercept of  $k_{\text{obs}}$  vs.  $[\text{F}^-]$ , according to (45):

$$k_{\text{obs}} = k_{\text{on}}^{\text{app}} \cdot [\text{F}^-] + k_{\text{off}} \quad (\text{Equation 7})$$

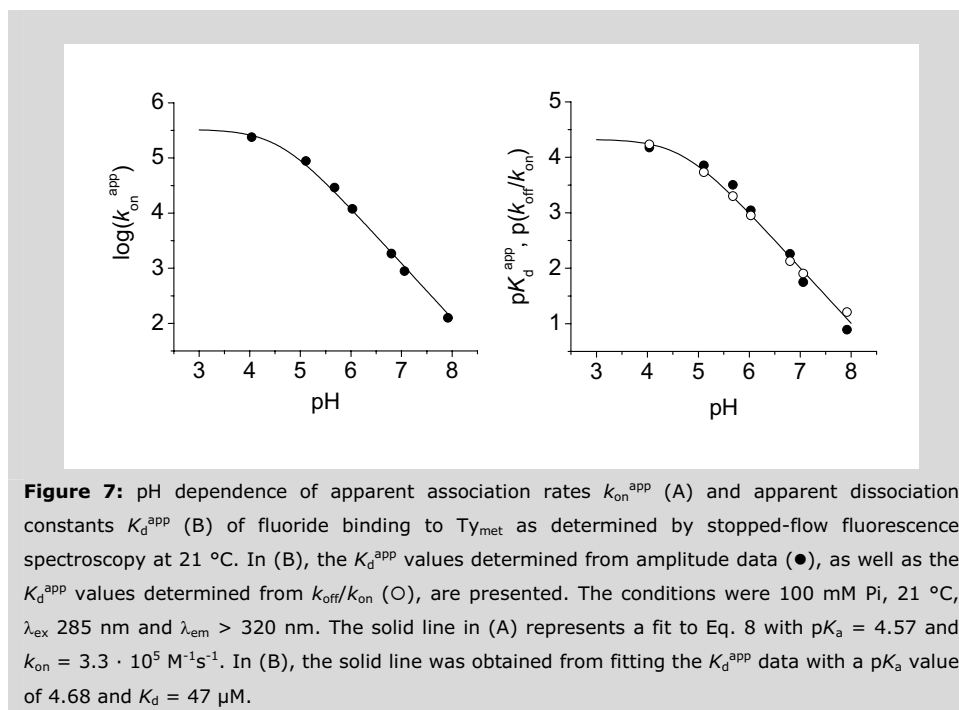
At pH 6.03 (Fig. 6A), values of  $11.7 \text{ mM}^{-1}\text{s}^{-1}$  and  $13.9 \text{ s}^{-1}$  for the  $k_{\text{on}}^{\text{app}}$  and  $k_{\text{off}}$  were obtained respectively. The signal amplitudes, expressed as  $F_{\infty}/F_0$ , are presented in Fig. 6B. As with the  $k_{\text{obs}}$  values, the data are in agreement with the binding of a single fluoride ion and were fitted to Eq. 5 with  $L = \text{F}^-$ . For the data at pH 6.03 in Fig. 6B, values of  $0.90 \text{ mM}$  and  $0.10$  were obtained for  $K_{\text{d}}^{\text{app}}$  and  $f_{\text{q}}$ , respectively.



Since the protein appeared unstable at the lower pH values (see Fig. 1), the fluoride binding at the two lowest pH values was studied using pH jump sequential stopped-flow where a  $\sim 5 \mu\text{M}$  protein solution in 1 mM Pi at pH 7.2 was mixed with 200 mM Pi buffer at the pH of interest after which the solution was allowed to equilibrate for 0.5 sec. The resulting solution was then mixed with a fluoride solution in 100 mM Pi at the pH of the experiment after which the fluorescence trace was recorded. The reported pH values were measured in the final mixed solutions. The sequential-flow method gave identical results to those obtained through single-mixing experiments at pH 6.0 as used for the higher pH values. At pH 4.04, an increase in fluorescence was observed, in agreement with the pH dependence of native  $\text{Ty}_{\text{met}}$  and  $\text{Ty}_{\text{met}}\text{F}$  fluorescence as depicted in Fig. 4 and indirectly illustrating the reversibility of the pH dependence of the native  $\text{Ty}_{\text{met}}$  emission. We did not measure the fluoride binding kinetics in the pH range of 4.2-5.0 since in this region the fluorescence levels of the native and the fluoride bound  $\text{Ty}_{\text{met}}$  do not differ by much (see Fig. 4). The log values of the obtained  $k_{\text{on}}^{\text{app}}$  values are presented in Fig. 7A. It appears that the  $\log(k_{\text{on}}^{\text{app}})$  is directly proportional to the pH in the pH range 6-8 while it levels off at  $\text{pH} < 5.5$ . This can be explained by assuming the following scheme:



where fluoride ion only binds to the acidic form of the enzyme, as was proposed earlier on the basis of paramagnetic NMR and fluoride inhibition studies (43). There it was shown that the pH dependence of chloride binding to  $\text{Ty}_{\text{met}}$  shows analogous behaviour to that of fluoride binding. It is therefore unlikely that the observed pH dependence of the apparent  $k_{\text{on}}$  for fluoride originates from the exclusive binding of HF ( $\text{p}K_{\text{a}} 3.14$ ), since HCl ( $\text{p}K_{\text{a}} -7$ ) occurs fully dissociated in the pH range of the experiment.



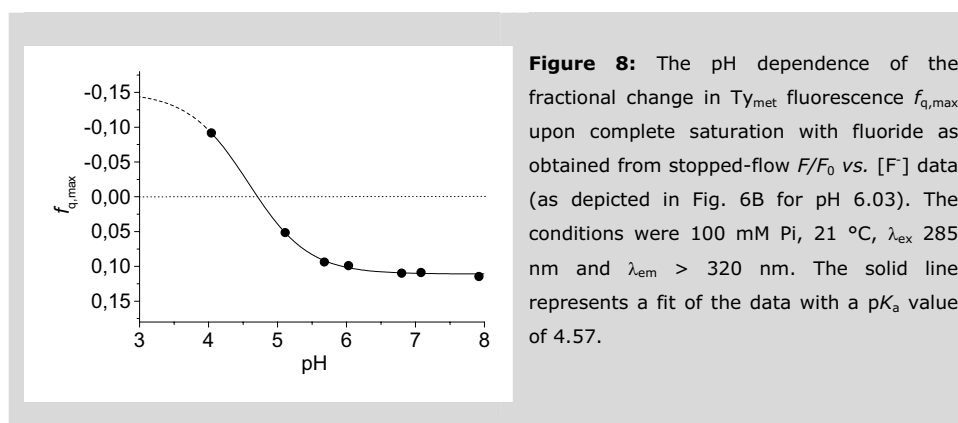
The finding that the fluoride binding traces follow mono-exponential behaviour, as well as linear dependence of  $k_{obs}$  on  $[F^-]$  at all pH values, show that the pH dependent step is fast in comparison with the fluoride binding step. In that case, the measured  $k_{on}^{app}$  values are proportional to the fraction of  $Ty_{met}$  that is in the low pH form (45) according to:

$$k_{on}^{app} = k_{on} \frac{[H^+]}{[H^+] + K_a} \quad (\text{Equation 8})$$

Fitting the data in Fig. 7A to this function yielded a  $pK_a$  of  $4.57 \pm 0.11$ , which is within error of the  $pK_a$  found for the pH dependence of native  $Ty_{met}$  fluorescence as depicted in Fig. 4. The fit also yielded an estimate for the  $k_{on}$  of fluoride binding to the low pH form of the enzyme, amounting to  $(3.3 \pm 0.7) \cdot 10^5 \text{ M}^{-1}\text{s}^{-1}$ . The determined values for  $k_{off}$  are much less dependent on the pH, in agreement with the mechanism in Scheme 1 (45), and varied between  $8 \text{ s}^{-1}$  and  $16 \text{ s}^{-1}$  without showing a clear correlation with the pH (not shown). From the  $k_{on}$  value and the value of  $k_{off}$  determined at the lowest pH used (pH 4.04;  $12.3 \pm 0.8 \text{ s}^{-1}$ ), the  $K_d$  for fluoride for binding to the low pH enzyme can be estimated from the relation  $K_d = k_{off}/k_{on}$ , amounting to  $37 \pm 8 \text{ }\mu\text{M}$ .

The values for the apparent dissociation constants  $K_d^{\text{app}}$  as determined from signal amplitudes and Eq. 5 follow similar behaviour as the  $k_{\text{on}}^{\text{app}}$  values, as expected from the relative insensitivity of  $k_{\text{off}}$  to the pH, as shown in Fig. 7B. Here, the data could be fitted to an equation of the type of Eq. 8 with a  $\text{p}K_a$  value of  $4.68 \pm 0.23$  while the dissociation constant for the  $\text{Ty}_{\text{met}}\text{F}$  complex was estimated at  $54 \pm 22 \mu\text{M}$  by extrapolation to low pH. As depicted in Fig. 7B, there is good agreement between the  $K_d^{\text{app}}$  values determined from amplitude data and those calculated from  $K_d^{\text{app}} = k_{\text{off}}/k_{\text{on}}^{\text{app}}$ . From the latter data, values of  $4.69 \pm 0.18$  for the  $\text{p}K_a$  and  $48 \pm 10 \mu\text{M}$  for the  $K_d$  for the  $\text{Ty}_{\text{met}}\text{F}$  complex were obtained.

The pH dependence of the determined  $f_q$  values, i.e. the fractional changes in fluorescence upon complete saturation of  $\text{Ty}_{\text{met}}$  with fluoride, is shown in Fig. 8. The obtained values are in good agreement with the data obtained for the pH dependence of the  $\text{Ty}_{\text{met}}$  and  $\text{Ty}_{\text{met}}\text{F}$  fluorescence intensities as described above (Fig. 4). The data could be fit assuming that  $f_q$  is dependent on a single acid/base equilibrium, yielding an estimate for the  $\text{p}K_a$  value of  $4.57 \pm 0.12$ .



#### Stopped-flow fluorescence studies of organic inhibitor binding.

The fluorescence changes observed upon ligand binding to  $\text{Ty}_{\text{met}}$  appeared not to be limited to fluoride. Large changes in protein emission also occur when organic inhibitors bind to Ty. A steady-state titration of resting Ty with *p*-toluic acid in 100 mM Pi and at 21 °C followed by recording fluorescence emission spectra at each  $[\text{L}]$  showed that the emission intensity significantly decreased with increasing ligand concentration, while both the position of the emission maximum and the bandshape remained unaffected (not shown).

We evaluated the transient-state kinetics of the binding of several organic inhibitors (benzoic acid, *p*-toluic acid, *p*-chlorobenzoic acid, Kojic acid and mimosin) to resting Ty under pseudo-first order conditions at pH 6.80 and 21 °C by stopped-flow fluorimetry. In all cases, significant fluorescence decreases were observed upon mixing the ligand solution with a solution containing 2  $\mu\text{M}$  of resting Ty (both in a buffer containing 100 mM Pi). No change in fluorescence on the time-scale of the binding to the resting-form was observed when either of the ligands were mixed with Ty<sub>oxy</sub> or Ty<sub>red</sub>, showing that the observed kinetics were solely due to the interaction with the Ty<sub>met</sub> protein. This was also corroborated by the finding that, on the time-scale of the stopped-flow experiments, the addition of the ligands to a solution containing Ty<sub>oxy</sub> did not influence the intensity and the position of the UV/Vis LMCT transition of Ty<sub>oxy</sub> (not shown). All obtained traces could be accurately fit to a mono-exponential decay function yielding  $k_{\text{obs}}$  and  $A$  values at each [L]. All inhibitors appeared to bind in an apparent two-state mechanism as was apparent from the linearity of the  $k_{\text{obs}}$  vs. [L] plots (not shown), allowing for estimation of  $k_{\text{on}}$  and  $k_{\text{off}}$  using Eq. 7. The obtained values are reported in Table 1. The signal amplitude data could be accurately fitted to Eq. 5 for all ligands, yielding values for the apparent  $K_{\text{d}}$  and  $f_{\text{q}}$  as reported in the same table. The reported values for  $f_{\text{q}}$  were corrected for the contribution of Ty<sub>oxy</sub> and Ty<sub>red</sub> to the total emission.

**Table 1:** Kinetic parameters of inhibitor binding to Ty<sub>met</sub> as determined from stopped-flow fluorimetry.

Compound	$k_{\text{on}}^{\text{a}}$ ( $\text{mM}^{-1}\text{s}^{-1}$ )	$k_{\text{off}}^{\text{a}}$ ( $\text{s}^{-1}$ )	$k_{\text{off}}/k_{\text{on}}$ (mM)	$K_{\text{d}}^{\text{b}}$ (mM)	$f_{\text{q}}^{\text{b}}$	$K_{\text{i}}$ (mM)
Benzoic acid	99.0	37	0.37	0.36	0.14	0.80 <sup>c</sup>
<i>p</i> -toluic acid	94.1	14.8	0.16	0.12	0.17	0.20 <sup>c</sup>
<i>p</i> -chlorobenzoic acid	40.0	6.8	0.18	0.16	0.15	0.23 <sup>f</sup>
Kojic acid <sup>d</sup>	311	5.6	0.017	0.016	0.40	0.004 <sup>c</sup>
Mimosin	246	9.2	0.037	0.030	0.27	0.030 <sup>c</sup>
Fluoride	1.84	13.7	7.4	6.0	0.14	11.8 <sup>e</sup>

The conditions were 100 mM Pi, pH 6.80, 21 °C,  $\lambda_{\text{ex}}$  290 nm and  $\lambda_{\text{em}} > 320$  nm. <sup>a</sup> determined from  $k_{\text{obs}}$  vs. [L]; <sup>b</sup> determined from  $A/F_0$  vs. [L]; <sup>c</sup> taken from ref (25). <sup>d</sup> studied at pH 7.0. <sup>e</sup> taken from ref (26). <sup>f</sup> this work. The inhibition constants were determined using L-DOPA as the substrate. Standard deviations are smaller than 10 % of the measured quantity in all cases.

**Discussion****Ty fluorescence properties and emission quenching**

We have investigated the fluorescence properties of Ty and used the changes in protein fluorescence that occur when ligands bind to the type-3 copper center as a probe in studying ligand binding kinetics. The Ty from *Streptomyces antibioticus* contains 12 Tryptophans and 6 Tyrosines on a total of 272 amino acids. Consistent with the Trp/Tyr ratio and the excitation wavelength employed, all Ty species ( $Ty_{met}$ ,  $Ty_{oxy}$ ,  $Ty_{red}$ ) display emission spectra dominated by Trp fluorescence. The positions of the emission maxima ( $343 \pm 2$  nm for all species) are the highest reported for a type-3 copper protein and indicate that a significant fraction of the Trp residues is exposed to the solvent.

As was found earlier for several hemocyanins (27-39) and *Neurospora crassa* tyrosinase (40), it appears that the Ty fluorescence emission intensities are remarkably sensitive to the oxidation state of the dinuclear copper centre; the emission quantum yield of  $Ty_{red}$  and  $Ty_{oxy}$  differ by more than a factor two. The shape and position of the emission spectrum is not significantly different for  $Ty_{red}$ ,  $Ty_{met}$  and  $Ty_{oxy}$ , indicating that the quenching is not specific for buried Trp residues or for those exposed to the solvent, since a selective quenching of either class of fluorophore would result in a clear shift in the emission spectrum as it is well known that the emission maxima of buried Trp generally occur at shorter wavelength compared to those of solvent exposed Trp.

The mechanism of quenching has not been unambiguously established for any Hc or Ty. For  $Ty_{oxy}$ , the fluorescence quenching possibly occurs through Förster energy-transfer since the Ty emission spectrum ( $\lambda_{max} = 343$  nm) overlaps with the strong LMCT transition absorption band characteristic of  $Ty_{oxy}$  ( $\epsilon_{345} = 18.5 \text{ mM}^{-1}\text{cm}^{-1}$ ). The energy-transfer mechanism may also contribute to the fluorescence quenching in the  $Ty_{met}$  species considering the weak LMCT between the Cu(II) and the ligand nitrogens in the emission region ( $\epsilon_{320} \sim 2 \text{ mM}^{-1}\text{cm}^{-1}$ ). A Förster quenching for  $Ty_{oxy}$  and  $Ty_{met}$  would be consistent with the relatively high quantum yield of the  $Ty_{red}$  species that is devoid of absorption bands in the emission region.

For *Neurospora crassa* tyrosinase it has been suggested that the quenching of  $Ty_{red}$  and  $Ty_{met}$  fluorescence occurs through the heavy atom effect of copper while a paramagnetic quenching mechanism for  $Ty_{met}$  was supposed less likely based on the diamagnetic nature of the  $S = 0$  ground-state of the antiferromagnetically coupled  $Cu_2$  center (40). From recent paramagnetic NMR studies (8;25;43), it appears, though, that the paramagnetic  $S = 1$  triplet of *Streptomyces antibioticus*  $Ty_{met}$  is populated at ambient temperatures. It was



further shown that the value of the exchange coupling constant  $-2J$ , i.e. the parameter determining the relative population of the  $S = 1$  state, and the electronic structure of the  $Ty_{met}$  active site are perturbed upon the binding of exogenous ligands such as the halides (8;43) and organic inhibitors (25). However, for the cases where the value of the exchange coupling constant  $-2J$  has been determined ( $Ty_{met}$ :  $71 \text{ cm}^{-1}$ ;  $Ty_{met}$ -Kojic acid:  $156 \text{ cm}^{-1}$ ;  $Ty_{met}$ -fluoride:  $260 \text{ cm}^{-1}$ ) no correlation could be discerned between the value of  $-2J$  and the fluorescence quantum yield. Considering that Ty harbours 12 Trp residues, the high degrees of fluorescence quenching cannot result solely from direct interaction with the bound ligand. To elucidate the mechanism of quenching, therefore, further study is needed. For the purpose of the present investigations, however, it is sufficient to note that the large differences between the emission intensities of the various Ty species can be used as a sensitive probe of ligand binding and interconversion between the Ty redox states.

#### The composition of resting Ty and oxygen binding

It appears that the resting form of the enzyme in our preparations is a mixture of oxidised ( $Ty_{met}$ ) and reduced ( $Ty_{red} + Ty_{oxy}$ ) Ty. From the fluorescence data in Fig. 2, it was possible to calculate that 71 % of the enzyme occurs in the oxidised form, while the remainder is a mixture of  $Ty_{oxy}$  and  $Ty_{red}$ , the ratio of the latter two species depending on the concentration of oxygen in the sample. In the literature, it is usually reported that more than 85 % of the enzyme occurs in the oxidised form in resting Ty (5). The ratio of oxidised and reduced Ty in resting preparations determines in part the length of the lag phase observed in the conversion of monophenolic compounds (5). The stable percentage of  $Ty_{met}$  in resting preparations may reflect a natural equilibrium between the three Ty species present in solution. Establishment of this equilibrium may be connected with the dissociation of peroxide from  $Ty_{oxy}$  resulting in the formation of  $Ty_{met}$ , as observed for *Neurospora crassa* Ty (46). This would be consistent with the observed slow decay of  $Ty_{oxy}$  to  $Ty_{met}$  in fresh preparations of *Streptomyces antibioticus*  $Ty_{red}$  (unpublished data).

The large difference between the  $Ty_{red}$  and  $Ty_{oxy}$  quantum yield has been used to study the binding of molecular oxygen to the reduced enzyme (Fig. 3). The obtained dissociation constant for the oxygenated Ty complex of  $16.5 \mu\text{M}$  is lower than that reported for mushroom Ty ( $47 \mu\text{M}$ ; (47)) and *Octopus vulgaris* hemocyanin ( $90 \mu\text{M}$ ; (48)). This higher affinity of  $Ty_{red}$  for oxygen may reflect adaptation to an oxygen-poor environment, as experienced by soil bacteria like *Streptomyces* in their natural environment. Possibly the enzyme is optimised for recruiting the co-substrate rather than for exchanging molecular oxygen with its environment.

**The kinetics of fluoride binding.**

Recently a structural and mechanistic study of the interaction of halide ions with *Streptomyces antibioticus* Ty was reported (43). The interaction of fluoride with Ty was the most extensively studied. In contrast to the other halides, fluoride solely interacts with the Ty<sub>met</sub> form of the protein and acts as a simple competitive inhibitor in the conversion of L-DOPA, while the other halides interact with both Ty<sub>met</sub> and Ty<sub>red</sub>. Since a suitable method for the preparation of a 100 % Ty<sub>met</sub> sample is not available, fractions of Ty<sub>red</sub> and Ty<sub>oxy</sub> (29 % of total [Ty] under the experimental conditions) are always present in preparations of Ty<sub>met</sub>, therefore complicating the transient-state kinetics of halide binding other than fluoride.

It appears that the Ty<sub>met</sub> and the Ty<sub>met</sub>F fluorescence emission levels differ significantly and that this difference is dependent on the pH as depicted in figs. 4 and 8. This feature has been exploited in studying the transient-state kinetics of fluoride binding to Ty<sub>met</sub> by stopped-flow fluorescence spectroscopy. All data are in agreement with the binding of a single fluoride ion and can be explained by adopting a simple binding mechanism. Likewise, titrations of Ty<sub>met</sub> with fluoride followed by <sup>1</sup>H paramagnetic NMR (43) could also be explained by assuming a binding mechanism where a single fluoride ion binds to Ty<sub>met</sub>. From that work, it was proposed that a single halide ion binds to Ty<sub>met</sub> at the Cu<sub>2</sub> bridging position. The findings presented here are consistent with this hypothesis. The presence of a single Cu<sub>2</sub> bridging ligand in Ty<sub>met</sub> is also corroborated by EXAFS studies on *Streptomyces antibioticus* Ty (L. Bubacco, personal communication) and oxidised CO (49), indicating 3N / 1O coordination for each copper ion, as well as with the crystal structure of oxidised sweet potatoe CO, where a single Cu<sub>2</sub> bridging ligand (possibly chloride) was identified in the electron-density map upon refinement (12;50).

At pH 6.80, the  $K_d^{app}$  value determined from amplitude data is 6.0 mM while the  $K_d^{app}$  amounts to 7.4 mM by using the relation  $k_{off}/k_{on}^{app} = K_d^{app}$ . These values, taking into account the notable pH sensitivity of the fluoride binding, compare reasonably well with the competitive inhibition constant for fluoride of 11.8 mM obtained at the same pH and temperature and the dissociation constant of 5.08 mM for the fluoride Ty<sub>met</sub> complex determined at pH 7.06 and 4 °C using paramagnetic NMR (43). The relatively low value of the fluoride dissociation rate,  $k_{off}$  ( $13.7 \pm 0.5 \text{ s}^{-1}$  at pH 6.80), is in agreement with the previous finding that fluoride is in slow-exchange on the NMR shift timescale (43). Remarkably, the  $k_{off}$  value for fluoride is similar to those determined for aromatic inhibitors and hydroxy-ketone transition-state analogues (see Table 1 and below). The observation that no changes in fluorescence are observed when Ty<sub>red</sub> or Ty<sub>oxy</sub> are mixed with 50 mM fluoride at pH 6.80 is in agreement with the previous finding that fluoride

solely interacts with the  $Ty_{met}$  protein.

#### The pH dependence of the kinetic parameters of fluoride binding to $Ty_{met}$ .

It appears that the fluoride binding to  $Ty_{met}$  is strongly dependent on the pH, as was observed earlier by paramagnetic NMR of  $Ty_{met}$  and its halide bound species and by kinetic studies of the inhibition of the conversion of L-DOPA by halide ion (43). The latter data could be explained by assuming that the halide binding to  $Ty_{met}$  is under control of a single acid/base equilibrium where the ion only binds to the acidic form of  $Ty_{met}$ . Due to the experimental limitations imposed by the instability of  $Ty_{met}$  at low pH and the relatively long experimental times required, it was only possible to determine an upper limit for the  $pK_a$  of this acid/base equilibrium ( $pK_a < 5.5$ ). By using the faster method of stopped-flow fluorimetry, the problem of protein instability could be circumvented in the present study.

The kinetic parameters of fluoride binding corroborate the earlier finding that fluoride ion only binds to the acidic form of the enzyme as witnessed by the pH dependence of  $k_{on}^{app}$  (Fig. 7A) and  $K_d^{app}$  (Fig. 7B) and the relative insensitivity of  $k_{off}$  to the pH. The data obtained for the pH dependence of  $k_{on}^{app}$  could be fitted using a  $pK_a$  value of 4.57, which is equal, within the experimental error, to the  $pK_a$  values obtained from the pH dependence of  $K_d^{app}$  and  $k_{off}/k_{on}$  (4.68 and 4.69, respectively). Similar  $pK_a$  values are obtained from the pH dependence of the  $Ty_{met}$  fluorescence (Fig. 4;  $pK_a$  4.50) and of  $f_q$ , i.e. the fractional changes in  $Ty_{met}$  emission upon complete saturation with fluoride (Fig. 8;  $pK_a$  4.57). This provides a total of 5  $pK_a$  values, the average amounting to 4.61.

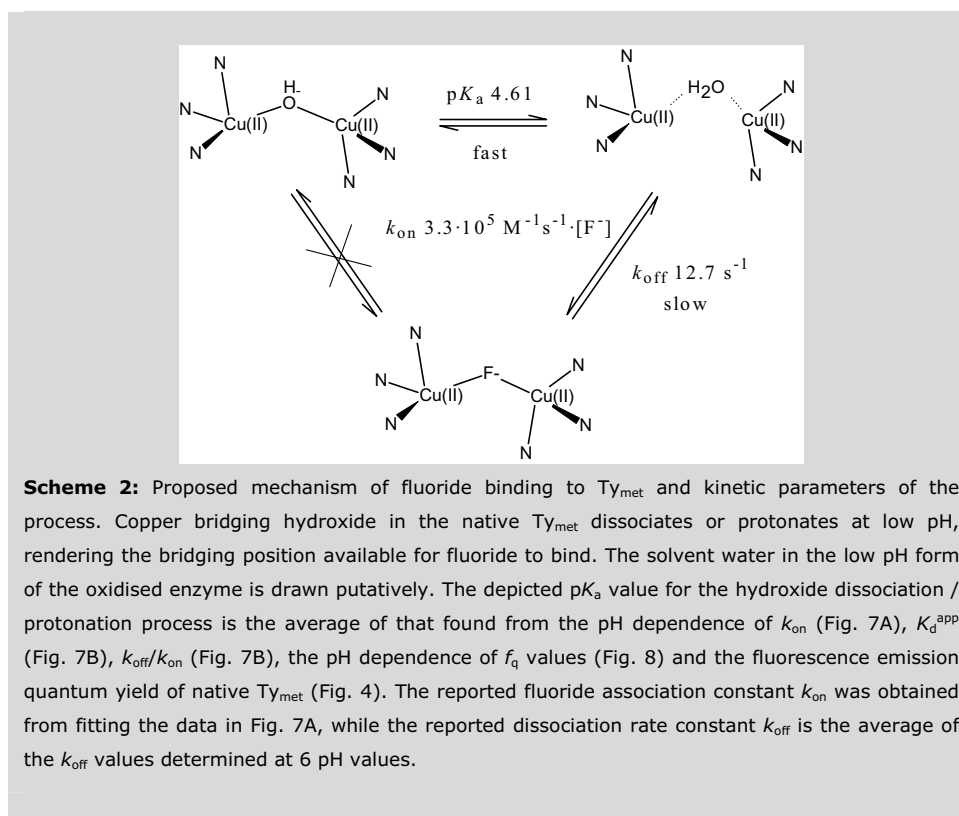
Extrapolation of the kinetic data to low pH provided estimates for the dissociation constant of the  $Ty_{met}$ -fluoride complex, the average amounting to  $43 \pm 13$  mM. Since chloride binding to  $Ty_{met}$  follows similar behaviour as the binding of fluoride (43), we can estimate the dissociation constant for chloride binding to the low pH form of the  $Ty_{met}$  enzyme using the chloride inhibition constant determined at pH 6.80 (0.16 M; (43)), a  $pK_a$  value of 4.61 and Eq. 8 ( $k_{on}$  replaced by the dissociation constant  $K_d$ ), giving a  $K_d$  value for chloride of 0.7 mM.

#### Fluoride replaces hydroxide as the bridging ligand in $Ty_{met}$ .

Fluoride is known to inhibit many metallo-enzymes (e.g. superoxide dismutase (51), urease (52), laccase (53), peroxidase (54), enolase (55)), often with apparent inhibition constants in the  $\mu$ M to mM range. In most cases, the fluoride binding is pH dependent and it is thought that fluoride replaces a metal-bound hydroxide ion or water ligand. The results presented here suggest that the same occurs with Ty. We propose that the pH

dependence of fluoride binding derives from the pH dependent dissociation of Cu<sub>2</sub> bridging hydroxide according to the mechanism outlined in Scheme 2. Direct dissociation of OH<sup>-</sup> or dissociation of water after protonation of the bound hydroxide are indistinguishable at present.

As established earlier on the basis of paramagnetic NMR of Ty<sub>met</sub> (43), it can be excluded that the pH dependence of fluoride binding results from a protonation and subsequent dissociation of a coordinating histidine residue at low pH. Such a mechanism was proposed earlier to explain the pH dependence of halide inhibition (22;56;57). A pH dependent dissociation of Cu<sub>2</sub> bridging hydroxide has been shown to occur for several small dinuclear copper model compounds (58-60). There, pK<sub>a</sub> values between 4.0 and 5.5 have been obtained for the dissociation process, comparing with the average pK<sub>a</sub> of 4.61 found in the present case. This low pK<sub>a</sub> value can be ascribed to the charge of the two copper ions and the relatively low basicity of the coordinating histidine ligands. The linear dependency of *k*<sub>obs</sub> on [F<sup>-</sup>] at all pH values implies that both the hydroxide dissociation and association processes are much faster than the corresponding steps for fluoride.



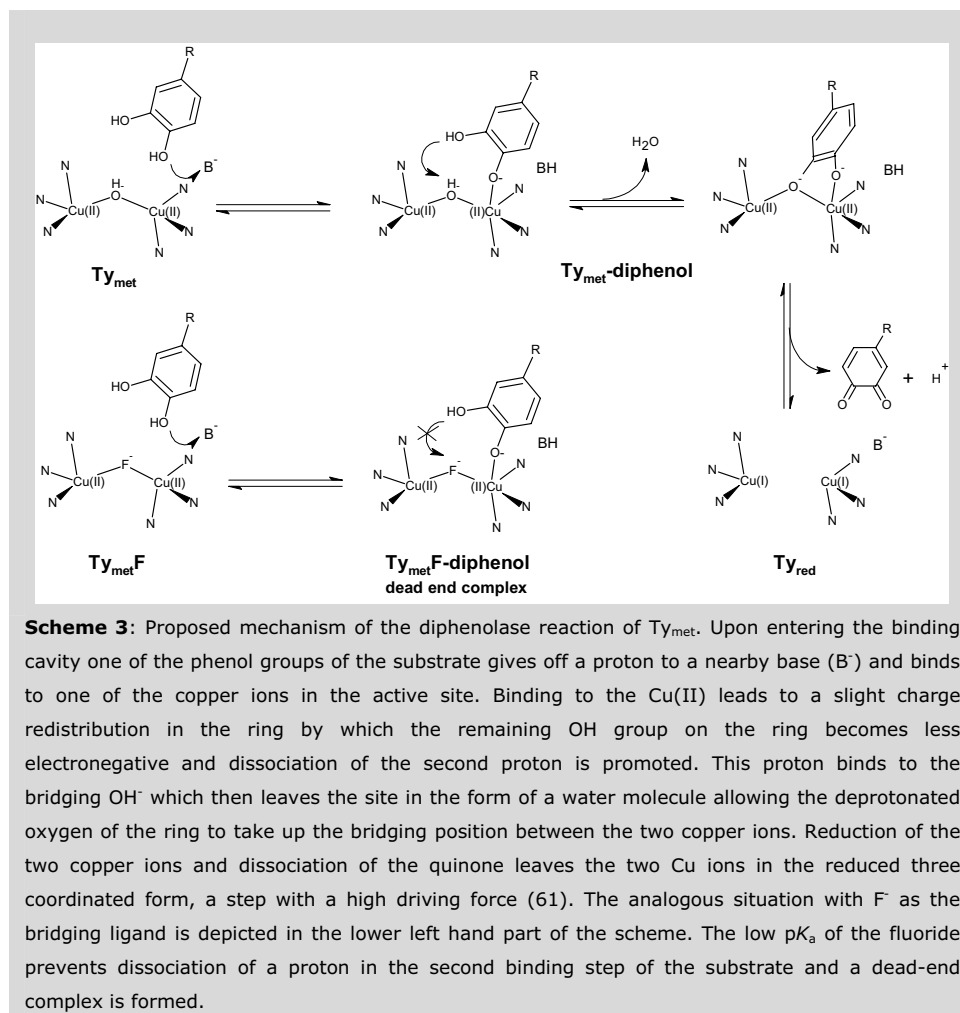
**The pH dependence of the  $Ty_{met}$  fluorescence emission.**

The pH dependence of the fluorescence emission intensity of Ty was studied under various conditions by pH-jump stopped-flow fluorimetry (Fig. 4). It appeared that the emission level of the  $Ty_{met}$  enzyme is dependent on an acid/base equilibrium with an apparent  $pK_a$  value of 4.50, which is identical to the experimental  $pK_a$  values found for fluoride binding. It was estimated that the low pH form of  $Ty_{met}$  has an emission intensity approximately 0.7 that of the high pH form. A pH dependence of the emission intensity is not observed for  $Ty_{red}$ ,  $Ty_{oxy}$  or  $Ty_{met}$  bound with fluoride. This strongly suggests that the pH dependence of  $Ty_{met}$  emission is associated with pH dependent changes occurring directly at the oxidised dinuclear copper centre, since a pH dependence of the emission would also be expected for the other species when it would reflect, for example, a protonation of a carboxylic acid residue in close vicinity to a fluorescent Trp or pH dependent changes in protein structure.

Thus, in view of the current proposal that bridging hydroxide dissociates at low pH, it is likely that this process is responsible for the decrease in quantum yield. We note that this process would lead to the loss of spin superexchange, and consequently the antiferromagnetic coupling, between both copper ions, as has been shown to occur for  $Cu_2$  model compounds. Therefore a marked change in paramagnetism is expected upon loss of the bridging ligand, which could be related to the lower quantum yield of the enzyme at low pH.

**The role of the bridging ligand in the diphenolase mechanism.**

The role of bridging hydroxide in the oxidation of diphenols has yet to be established. Previously it was shown that halide is displaced from  $Ty_{met}$  if inhibitors that mimic the transition state (e.g. mimosin, Kojic acid) are bound to the enzyme. On this basis we proposed a model for diphenol coordination where one of the phenolic oxygens bridges the two copper ions by displacing the bridging hydroxide that is present in native  $Ty_{met}$  (43). The displacement of an equatorial water ligand by bidentate ligands has also been shown for half oxidised Ty ( $Ty_{half-met}$ ) by means of pulsed EPR spectroscopies (61;62).



For oxidation of a diphenolic substrate to proceed, the diphenol must lose two protons in the process. Thus, the hydroxide could function as the proton acceptor for one of the phenolic protons in the conversion of diphenols as outlined in Scheme 3. The observation that catalysis does not proceed when fluoride bridges the copper ions, notwithstanding its size and charge being similar to hydroxide, would be in agreement with this hypothesis. Still, we cannot exclude that changes in the redox potential(s) of the system upon changing the bridging ligand, as demonstrated for  $Cu_2$  model complexes (63), might also be responsible for the absence of catalytic activity in halide bound  $Ty_{met}$ .

**Enzyme inactivation and the protective effect of halide ion.**

As depicted in Fig. 1, Ty is rapidly inactivated at low pH where the rate of inactivation is pH dependent. It is likely that this inactivation originates from the loss of the Cu<sub>2</sub> bridging hydroxide in Ty<sub>met</sub>, i.e. one negative charge, at low pH, which illustrates the importance of charge compensation in the stability of protein metal sites. Support for this is provided by the observation that protein inactivation proceeds much slower when fluoride or chloride ion, which are able to substitute for OH<sup>-</sup> and therefore conserve the native coordination number and charge, is present in solution. Furthermore, the stabilising effect of fluoride and the finding that this ion specifically interacts with Ty<sub>met</sub>, suggest that the inactivation is specifically due to the decay of the Ty<sub>met</sub> form. Ty<sub>oxy</sub> and Ty<sub>red</sub> do not seem to be susceptible to rapid protein inactivation, providing further support for the loss of bridging OH<sup>-</sup> as the cause for the inactivation of Ty<sub>met</sub>. The mechanism by which the inactivation proceeds after dissociation of OH<sup>-</sup> is unclear as yet but it may start, for example, with dissociation of coordinated copper, oxidation of one or more side chains in the vicinity of the copper ions or local unfolding of the active site.

**Physiological relevance of the halide inhibition.**

It has been proposed that the large variations in the extent of pigmentation in different human skin types originate from variations in the melanosomal pH (65;66). These pH variations would influence the Ty activity, a lower pH value being associated with a lower Ty activity and, thus, with a lower pigmentation level. For *Streptomyces antibioticus* Ty, we found that the apparent chloride inhibition constant (0.16 M at pH 6.80) is in the order of physiological chloride concentrations (5-200 mM). Similar values for the apparent chloride inhibition constant, as well as strong pH dependencies of halide inhibition, have been found for other Tys (22;56;57). Thus, depending on the [Cl<sup>-</sup>] to K<sub>i</sub> ratio, a significant fraction of the enzyme may exist as the inactive chloride bound form at low pH, which is, however, protected from protein degradation. This might provide an explanation of the sensitivity of Ty activity to the melanosomal pH.

**Stopped-flow studies of inhibitor binding other than fluoride.**

The quenching of Ty<sub>met</sub> fluorescence upon ligand binding appeared not to be limited to fluoride. For all organic inhibitors for which the binding kinetics were studied by stopped-flow fluorimetry, a significant decrease of the Ty<sub>met</sub> emission intensity is observed upon binding, the extent of quenching being dependent on the nature of the exogenous ligand (table 1). In all cases, the data were in agreement with the binding of a single inhibitor molecule to the Ty<sub>met</sub> enzyme and allowed for the determination of apparent  $k_{on}$ ,  $k_{off}$  and  $K_d$  values. Although the  $K_d$  values obtained from the  $k_{on}$  and  $k_{off}$  values are similar to those

obtained from amplitude data (table 1), the latter appear systematically lower. The reasons for this are unclear at present. However, given that  $Ty_{oxy}$  and  $Ty_{red}$  are always present in preparations of  $Ty_{met}$ , we note that the amplitude data is potentially subject to error introduced, for example, by slow changes in the ratio of oxidised and reduced enzyme in resting Ty preparations or partial protein degradation during the experiments. Since the  $k_{obs}$  values are not sensitive to the presence of  $Ty_{oxy}$  and  $Ty_{red}$  in the sample, we put more confidence in the  $K_d$  values calculated from the  $k_{on}$  and  $k_{off}$  values.

There is a reasonable correspondence between the  $K_i$  and  $K_d$  values except in the cases of benzoic acid and Kojic acid. For Kojic acid, the discrepancy may be explained by the different pH used in the inhibition and stopped-flow studies (pH 6.8 and 7.0 respectively). The reasonable agreement between  $K_d$  and  $K_i$  values, as well as the observation that no fluorescence changes or changes in the LMCT transition of  $Ty_{oxy}$  at 345 nm are observed on the time-scale of the stopped-flow experiments when the ligands are mixed with  $Ty_{oxy}$  and  $Ty_{red}$ , show that the  $Ty_{met}$  site is the site of interaction with inhibitors. The direct interaction of organic inhibitors and  $Ty_{met}$  has been shown earlier by means of paramagnetic NMR studies (8;25;43). The results strongly argue against an inhibition mechanism where inhibitors bind to  $Ty_{oxy}$  with concomitant transfer of an inhibitor proton to the bound peroxide (64).

As is apparent from both the  $K_i$  and  $K_d$  values, the compounds with a hydroxy-ketone moiety conjugated into the aromatic ring (i.e. Kojic acid and mimosin) bind much stronger to the enzyme than the aromatic carboxylic acids. The former compounds are transition-state analogues in the sense that they mimic the structure of diphenolic substrates, while they occur in an electronic configuration unsuitable for oxidation. It appears that L-mimosin binds less strong to the enzyme than Kojic acid under the experimental conditions, despite the presence of the amino-acid function in L-mimosin, as in the natural substrate L-DOPA. The kinetic data show that this is mainly due to a faster dissociation of L-mimosin, indicating that the amino-acid function does not critically contribute to the stability of the  $Ty_{met}$ -inhibitor complex.

The kinetic data show that the strong binding of L-mimosin and Kojic acid is due to higher association rates ( $k_{on}$ ) compared to those of the aromatic carboxylic acids; the values for the dissociation rates are similar for both types of inhibitor. From the X-ray structures of sweet potato catechol oxidase it has been shown that a precise coordination of diphenolic substrate in the active site is imposed by interactions of the substrate aromatic ring with protein residues in the substrate binding pocket. The higher  $k_{on}$  values for the transition-state analogues, as compared to the  $k_{on}$  values found for the aromatic carboxylic acids, may therefore be related to the fixed orientation of the coordinating



oxygens with respect to the aromatic ring in the former compounds. The aromatic carboxylic acids, instead, contain the freely rotateable carboxylic acid function that would require orientation with respect to the aromatic ring prior to binding, possibly resulting in a lower efficacy of association. Previously it was proposed that both the carboxylic acid and the hydroxy-ketone inhibitors coordinate in a bidentate fashion to the oxidised type-3 centre where one of the ligand oxygens bridges the two copper ions by displacing the bridging ligand (43). One may expect that the details of the coordination geometry depend on the distance between the two ligand oxygen atoms (mimosin: 2.79 Å; *p*-toluic acid: 2.23 Å), as well as their position with respect the aromatic ring. These variations in geometric details may have to do with the differences in the observed association rates. For mushroom Ty, it has been proposed that only aromatic carboxylic acids in their neutral form are capable of binding to the active site (64). Following this line of thought, an alternative explanation for the higher  $k_{\text{on}}$  values observed for Kojic acid and L-mimosin could be that these compounds predominantly occur in the protonated, neutral form while the carboxylic acids occur largely in the deprotonated, negatively charged form at the pH employed in the experiments.

Comparison of the  $k_{\text{off}}$  values for *p*-toluic acid, *p*-chlorobenzoic acid and benzoic acid shows that the presence of a substituent in the para position significantly stabilises the Ty<sub>met</sub>-inhibitor complex. However, since similar  $k_{\text{on}}$  values are observed for benzoic acid and *p*-toluic acid, this property does not appear to be directly correlated with the value of  $k_{\text{on}}$ . Similar results were obtained for *Neurospora crassa* Ty where the binding of inhibitors to Ty<sub>met</sub> was indirectly studied through displacement of peroxide from Ty<sub>oxy</sub> (46). The  $k_{\text{on}}$  for *p*-chlorobenzoic acid appears to be significantly lower than that for *p*-toluic acid and benzoic acid. This difference cannot be readily attributed to steric effects since the chloro substituent of *p*-chlorobenzoic acid has a similar size as the methyl group of *p*-toluic acid. The different  $k_{\text{on}}$  values obtained for the aromatic carboxylic acids may partly be related to the differences in the  $\text{p}K_{\text{a}}$  values of the carboxylic function (*p*-toluic acid 4.37; *p*-chlorobenzoic acid 4.00; benzoic acid 4.20 (42)). Only a small fraction of the inhibitors, depending on the  $\text{p}K_{\text{a}}$  of the carboxylic function, exists in the neutral form at neutral pH. If it is assumed that only the neutral form of the inhibitor can bind to Ty<sub>met</sub>, the apparent value of  $k_{\text{on}}$  would be proportional to the fraction of the inhibitor that is in its acid form and thus be dependent on the  $\text{p}K_{\text{a}}$  value of the inhibitor carboxylic moiety. Studying the pH dependence of inhibitor binding would provide more insight in this.

## Conclusion

In conclusion, the use of Ty fluorescence quenching as a probe in studying the kinetics of ligand binding to the type-3 copper centre yields results that are consistent with previously obtained kinetic and spectroscopic data. The method provides a direct spectroscopic probe of inhibitor binding to Ty<sub>met</sub>, which is the species that interacts with organic inhibitors. Stopped-flow fluorimetric experiments can be performed with high sensitivity and speed, thereby avoiding the need for large amounts of protein and the experimental difficulties arising from the intrinsic instability of the enzyme, the latter being important especially at the lower pH values. The quenching of the Ty<sub>met</sub> emission upon the binding of exogenous ligands may not be limited to the Ty from *Streptomyces antibioticus*; the establishment of a similar behaviour for other type-3 copper proteins would provide the means for a systematic comparison of the ligand binding properties of different tyrosinases, catechol oxidases and hemocyanins, potentially providing further insight into the mechanisms that underlie the variation in the functionality of these proteins. The notable sensitivity of the Ty emission quantum yield to the state of the type-3 copper centre holds promise for further studies. For example, the Ty fluorescence could be used to study the kinetics of the conversion of monophenolic and diphenolic substrates. The thermodynamics and pH dependence of inhibitor binding could be investigated by stopped-flow fluorescence kinetics.

## References

1. Oetting, W. S. and King, R. A. (1994) *J. Invest. Dermatol.* **103**, 131S-136S
2. Oetting, W. S. (2000) *Pigment Cell Res.* **13**, 320-325
3. van Gelder, C. W., Flurkey, W. H., and Wichers, H. J. (1997) *Phytochem.* **45**, 1309-1323
4. Solomon, E. I., Sundaram, U. M., and Machonkin, T. E. (1996) *Chem. Rev.* **96**, 2563-2605
5. Sanchez-Ferrer, A., Rodriguez-Lopez, J. N., Garcia-Canovas, F., and Garcia-Carmona, F. (1995) *Biochim. Biophys. Acta* **1247**, 1-11
6. Seo, S. Y., Sharma, V. K., and Sharma, N. (2003) *J. Agric. Food Chem.* **51**, 2837-2853
7. Decker, H., Dillinger, R., and Tuczec, F. (2000) *Angew. Chem. Int. Ed.* **39**, 1591-+
8. Bubacco, L., Salgado, J., Tepper, A. W., Vijgenboom, E., and Canters, G. W. (1999) *FEBS Lett.* **442**, 215-220

## Chapter 4

### Stopped-flow fluorescence studies of inhibitor binding

9. Cuff, M. E., Miller, K. I., van Holde, K. E., and Hendrickson, W. A. (1998) *J. Mol. Biol.* **278**, 855-870
10. Hazes, B., Magnus, K. A., Bonaventura, C., Bonaventure, J., Dauter, Z., Kalk, K. H., and Hol, W. G. J. (1993) *Prot. Sci.* **2**, 597-619
11. Magnus, K. A.; Hazes, B.; Ton-That, H.; Bonaventura, C.; Bonaventura, J.; Hol, W. G., W. G. (1994) *Proteins* **19**, 302-309
12. Klabunde, T., Eicken, C., Sacchettini, J. C., and Krebs, B. (1998) *Nat. Struct. Biol.* **5**, 1084-1090
13. Decker, H. and Tuczek, F. (2000) *Trends Biochem. Sci.* **25**, 392-397
14. Gerdemann, C., Eicken, C., and Krebs, B. (2002) *Acc. Chem. Res.* **35**, 183-191
15. Cabanes, J., Garcia-Carmona, F., Garcia-Canovas, F., Iborra, J. L., and Lozano, J. A. (1984) *Biochim. Biophys. Acta* **790**, 101-107
16. Espin, J. C. and Wichers, H. J. (1999) *J. Agric. Food Chem.* **47**, 2638-2644
17. Hashiguchi, H. and Takahashi, H. (1977) *Mol. Pharmacol.* **13**, 362-367
18. Healey, D. F. and Strothkamp, K. G. (1981) *Arch. Biochem. Biophys.* **211**, 86-91
19. Jimenez, M., Chazarra, S., Escribano, J., Cabanes, J., and Garcia-Carmona, F. (2001) *J. Agric. Food Chem.* **49**, 4060-4063
20. Kubo, I. and Kinst-Hori, I. (1999) *J. Agric. Food Chem.* **47**, 4121-4125
21. Maddaluno, J. F. and Faull, K. F. (1988) *Experientia* **44**, 885-887
22. Martinez, J. H., Solano, F., Penafiel, R., Galindo, J. D., Iborra, J. L., and Lozano, J. A. (1986) *Comp. Biochem. Physiol B* **83**, 633-636
23. Menon, S., Fleck, R. W., Yong, G., and Strothkamp, K. G. (1990) *Arch. Biochem. Biophys.* **280**, 27-32
24. No, J. K., Soung, D. Y., Kim, Y. J., Shim, K. H., Jun, Y. S., Rhee, S. H., Yokozawa, T., and Chung, H. Y. (1999) *Life Sci.* **65**, L241-L246
25. Bubacco, L., Vijgenboom, E., Gobin, C., Tepper, A. W. J. W., Salgado, J., and Canters, G. W. (2000) *J. Mol. Cat. B* **8**, 27-35
26. Tepper, A. W., Bubacco, L., and Canters, G. W. (2002) *J. Biol. Chem.* **277**, 30436-30444
27. Lippitz, M., Erker, W., Decker, H., van Holde, K. E., and Basche, T. (2002) *Proc. Nat. Acad. Sci. USA* **99**, 2772-2777
28. Schutz, J., Dolashka-Angelova, P., Abrashev, R., Nicolov, P., and Voelter, W.

## Chapter 4

### Stopped-flow fluorescence studies of inhibitor binding

- (2001) *Biochim. Biophys. Acta* **1546**, 325-336
29. Dolashka-Angelova, P., Hristova, R., Schuetz, J., Stoeva, S., Schwarz, H., and Voelter, W. (2000) *Spectrochim. Acta A* **56**, 1985-1999
  30. Dolashka-Angelova, P., Schick, M., Stoeva, S., and Voelter, W. (2000) *Int. J. Biochem. & Cell Biol.* **32**, 529-538
  31. Hristova, R., Dolashka-Angelova, P., Gigova, M., and Voelter, W. (2000) *Oxidation Comm.* **23**, 145-152
  32. Pervanova, K., Idakieva, K., Stoeva, S., Genov, N., and Voelter, W. (2000) *Spectrochim. Acta A* **56**, 615-622
  33. Dolashka-Angelova, P., Hristova, R., Stoeva, S., and Voelter, W. (1999) *Spectrochim. Acta A* **55**, 2927-2934
  34. Ali, S. A., Stoeva, S., Abbasi, A., Georgieva, D. N., Genov, N., and Voelter, W. (1999) *Comp. Biochem. Physiol. A* **122**, 65-74
  35. Hristova, R., Dolashka, P., Stoeva, S., Voelter, W., Salvato, B., and Genov, N. (1997) *Spectrochim. Acta. A* **53**, 471-478
  36. Dolashka, P., Genov, N., Parvanova, K., Voelter, W., Geiger, M., and Stoeva, S. (1996) *Biochem. J.* **315**, 139-144
  37. Idakieva, K., Stoeva, S., Voelter, W., and Genov, N. (1995) *Comparative Biochem. Physiol. B.* **112**, 599-606
  38. Stoeva, S., Dolashka, P., Bankov, B., Voelter, W., Salvato, B., and Genov, N. (1995) *Spectrochim. Acta. A* **51**, 1965-1974
  39. Shaklai, N., Gafni, A., and Daniel, E. (1978) *Biochemistry* **17**, 4438-4442
  40. Beltramini, M. and Lerch, K. (1982) *Biochem. J.* **205**, 173-180
  41. Jackman, M. P., Hajnal, A., and Lerch, K. (1991) *Biochem. J.* **274 ( Pt 3)**, 707-713
  42. Lide, D. R. (2000) *CRC Handbook of Chemistry and Physics*
  43. Tepper, A. W., Bubacco, L., and Canters, G. W. (2002) *J. Biol. Chem.* **277**, 30436-30444
  44. Lerch, K. and Ettlinger, L. (1972) *Eur. J. Biochem.* **31**, 427-437
  45. Fersht, A. (1999) *Enzyme Structure and Mechanism*,
  46. Wilcox, D. E., Porras, A. G., Lerch, K., Winkler, M. E., and Solomon, E. I. *J. Am. Chem. Soc.* 107(13), 4015-4027. 1985.
  47. Rodriguez-Lopez, J. N., Fenoll, L. G., Garcia-Ruiz, P. A., Varon, R., Tudela, J.,

## Chapter 4

### Stopped-flow fluorescence studies of inhibitor binding

- Thorneley, R. N. F., and Garcia-Canovas, F. (2000) *Biochemistry* **39**, 10497-10506
48. Salvato, B., Santamaria, M., Beltramini, M., Alzuet, G., and Casella, L. (1998) *Biochemistry* **37**, 14065-14077
49. Eicken, C., Zippel, F., Buldt-Karentzopoulos, K., and Krebs, B. (1998) *Febs Letters* **436**, 293-299
50. Eicken, C., Krebs, B., and Sacchettini, J. C. (1999) *Curr. Opin. Struct. Biol.* **9**, 677-683
51. Meier, B., Scherk, C., Schmidt, M., and Parak, F. (1998) *Biochem. J.* **331**, 403-407
52. Todd, M. J. and Hausinger, R. P. (2000) *Biochemistry* **39**, 5389-5396
53. Xu, F. (1997) *J. Biol. Chem.* **272**, 924-928
54. Neri, F., Kok, D., Miller, M. A., and Smulevich, G. (1997) *Biochemistry* **36**, 8947-8953
55. Leboadia, L., Zhang, E., Lewinski, K., and Brewer, J. M. (1993) *Proteins* **16**, 219-225
56. Martinez, J. H., Solano, F., Garcia-Borron, J. C., Iborra, J. L., and Lozano, J. A. (1985) *Biochem. Int.* **11**, 729-738
57. Penafiel, R., Galindo, J. D., Solano, F., Pedreno, E., Iborra, J. L., and Lozano, J. A. (1984) *Biochim. Biophys. Acta* **788**, 327-332
58. Belle, C., Beguin, C., Gautier-Luneau, I., Hamman, S., Philouze, C., Pierre, J. L., Thomas, F., and Torelli, S. (2002) *Inorg. Chem.* **41**, 479-491
59. Monzani, E., Quinti, L., Perotti, A., Casella, L., Gullotti, M., Randaccio, L., Geremia, S., Nardin, G., Faleschini, P., and Tabbi, G. (1998) *Inorg. Chem.* **37**, 553-562
60. Torelli, S., Belle, C., Gautier-Luneau, I., Pierre, J. L., Saint-Aman, E., Latour, J. M., Le Pape, L., and Luneau, D. (2000) *Inorg. Chem.* **39**, 3526-3536
61. Bubacco, L., van Gastel, M., Groenen, E. J., Vijgenboom, E., and Canters, G. W. (2002) *J. Biol. Chem.* **2003**, 278, 7381-7389
62. van Gastel, M., Bubacco, L., Groenen, E. J., Vijgenboom, E., and Canters, G. W. (2000) *FEBS Lett.* **474**, 228-232
63. Amudha, P., Akilan, P., and Kandaswamy, M. (1999) *Polyhedron* **18**, 1355-1362
64. Conrad, J. S., Dawso, S. R., Hubbard, E. R., Meyers, T. E., and Strothkamp, K. G. (1994) *Biochemistry* **33**, 5739-5744

## Chapter 4

### Stopped-flow fluorescence studies of inhibitor binding

65. Naeyaert, J. M., Eller, M., Gordon, P. R., Park, H. Y., and Gilchrest, B. A. (1991)  
*Brit. J. Dermat.* **125**, 297-303
66. Iozumi, K., Hoganson, G. E., Penella, R., Everett, M. A., and Fuller, B. B. (1993)  
*J. Invest. Dermat.* **100**, 806-811



# Chapter 5

## *Paramagnetic properties of the $Ty_{met}X$ species studied by $^1H$ NMR*

A.W.J.W. Tepper, G.W. Canters, to be submitted

### Summary

The  $^1H$  relaxation characteristics of the histidines in the oxidised type-3 copper site of tyrosinase ( $Ty_{met}$ ) from the bacterium *Streptomyces antibioticus* in the free and halide bound forms ( $Ty_{met}X$  with  $X = F^-, Cl^-, Br^-$ ) are evaluated. The  $^1H$  NMR spectra of the  $Ty_{met}X$  species display remarkably sharp well resolved paramagnetically shifted  $^1H$  signals, which originate from the protons of the six His residues coordinated to the two Cu(II) ions in the type-3 center. From the temperature dependence of the  $^1H$  paramagnetic shifts the following values for the exchange coupling parameter  $-2J$  were determined:  $260\text{ cm}^{-1}$  ( $Ty_{met}F$ );  $200\text{ cm}^{-1}$  ( $Ty_{met}Cl$ );  $162\text{ cm}^{-1}$  ( $Ty_{met}Br$ ) and  $71\text{ cm}^{-1}$  (free  $Ty_{met}$ ). The  $^1H$   $T_1$  relaxation is dipolar in origin and correlates with the Cu-H distances. Electronic relaxation times  $\tau_s$  derived from the  $^1H$   $T_1$  data are in the order of  $10^{-11}$  sec ( $Ty_{met}F > Ty_{met}Cl > Ty_{met}Br$ ). The results corroborate the purported  $Cu_2$  bridging coordination of the halide ions.



## Introduction

This chapter addresses the nuclear and electronic relaxation properties of the free and halide bound derivatives of oxidised tyrosinase (Ty). Ty catalyses the *ortho* hydroxylation of monophenols and the subsequent oxidation of the reaction product to the corresponding quinone under concomitant reduction of dioxygen to water. The quinones are precursors in the synthesis of melanin pigments. Ty occurs widely in nature and can be found in organisms ranging from bacteria to man. Although the enzyme has been known for over a century and despite its biological, industrial and biomedical importance, its structure and the details of its reaction mechanism remain to be solved<sup>1</sup>. The type-3 copper centre in the catalytic site of the enzyme is comprised of two closely spaced copper ions (Cu-Cu distance  $\sim 3\text{-}4$  Å) each coordinated by 3 protein derived His ligands<sup>2,3</sup>. The type-3 site can be further found in the catechol oxidases (COs) and the hemocyanins (Hcs). These proteins are responsible for the oxidation of diphenols in plants and oxygen storage and oxygen transport in arthropods and molluscs, respectively. Crystal structures are available for one CO<sup>4</sup> and several Hcs<sup>5-7</sup>. The type-3 centers of Tys, Hcs and COs appear remarkably similar as witnessed by their unique spectroscopic signatures and the conserved aa sequences of their  $Cu_2$  binding domains. The differences in their functionality are therefore believed to result from variations in the substrate binding pocket or the accessibility of substrates to the active site<sup>8,9</sup>.

Ty can exist in several forms, including (a) the reduced  $[Cu(I) Cu(I)]$  form ( $Ty_{red}$ ), (b) the oxygenated  $[Cu(II)-O_2^{2-}-Cu(II)]$  form ( $Ty_{oxy}$ ) and (c) the oxidised  $[Cu(II)-R-Cu(II)]$  form ( $Ty_{met}$ ). In  $Ty_{met}$ , the two  $S = \frac{1}{2}$  copper ions are antiferromagnetically coupled through spin superexchange mediated by a  $Cu_2$  bridging ligand, R<sup>1</sup>. This results in a diamagnetic singlet  $S = 0$  ground-state and a paramagnetic triplet  $S = 1$  excited-state with an energy splitting of  $-2J$ . At low temperature, only the diamagnetic  $S = 0$  ground state is populated, rendering the  $Ty_{met}$  site devoid of an EPR signal<sup>1</sup>.

Paramagnetic NMR is a powerful tool in the study of paramagnetic proteins. In general, paramagnetism induces large shifts and relaxation enhancements of nuclei in close vicinity to the paramagnetic centre, quantities that both contain information concerning the structure of and the spin-distribution over the active site<sup>10</sup>. The applicability of this technique depends on the electronic relaxation characteristics of the paramagnetic centre. When electron relaxation is fast (e.g. low-spin  $Fe^{3+}$ ,  $Ni^{2+}$  or high spin  $Co^{2+}$ ) good resolution is usually obtained. In systems where electron relaxation is slow (e.g.  $Cu^{2+}$ ), the signals of nuclei of coordinated ligands are often broadened beyond detection.

Yet, several *dinuclear* Cu(II) compounds complexes appear to give relatively sharp NMR signals (e.g. <sup>11-16</sup>). As in the case of Ty, these  $\text{Cu}_2$  compounds carry two closely spaced magnetically coupled copper atoms. If the magnetic exchange interaction  $-2J$  is of the order of  $k_{\text{B}}T$ , the paramagnetic  $S = 1$  level is only partially occupied, reducing both the nuclear shifts and the effect of paramagnetic relaxation. This partial occupation has been invoked to qualitatively explain why the signals in  $^1\text{H}$  NMR spectra of a number of biomimetic dinuclear copper compounds are relatively sharp <sup>17</sup>. In a number of cases, however, signals appeared much sharper than could be expected on the basis of a reduction in paramagnetism. In these cases the sharpening was connected to a shortening of the electron spin relaxation time,  $\tau_{\text{S}}$  <sup>17</sup>. Apparently, the coupling of the two  $\text{Cu}^{2+}$  ions provides for spin relaxation pathways that are unavailable to mononuclear Cu metal sites <sup>3;14;17-20</sup>.

The paramagnetically affected  $^1\text{H}$  NMR signals that are observed with  $\text{Ty}_{\text{met}}$  also appear remarkably sharp, especially in the presence of halides <sup>2</sup>. Paramagnetic  $^1\text{H}$  NMR studies demonstrated that  $\text{Ty}_{\text{met}}$  contains a classical type-3 copper center in the sense that the two copper ions in the active site are each coordinated by three histidine residues through the  $\text{N}^{\epsilon}$  atoms <sup>2;3</sup>. Furthermore, from paramagnetic NMR and kinetic studies <sup>3;21</sup>, it was concluded that halides bridge the two copper ions in the  $\text{Ty}_{\text{met}}$  active site, replacing the  $\text{Cu}_2$  bridging hydroxide that is present in native  $\text{Ty}_{\text{met}}$ .

Since the paramagnetically shifted signals in the  $\text{Ty}_{\text{met}}$   $^1\text{H}$  NMR spectrum provide a sensitive fingerprint of the active-site <sup>3;22</sup>, paramagnetic NMR can be used to follow ligand binding, for example, to obtain binding constants. Depending on the relaxation characteristics of the system,  $T_1$  and  $T_2$  relaxation data may also be used to estimate distances from the copper to the resonating nucleus to gain information on the coordination geometry of bound exogenous ligands. In order to pursue such an approach, the relaxation characteristics of the system should be known.

Here we report on a relaxation analysis of  $\text{Ty}_{\text{met}}$  in its free and halide bound forms. Values for the singlet-triplet spacing energy  $-2J$  were determined. Using the  $T_1$  relaxation data and HisH-Cu distances derived from crystal structures, estimates for the electronic relaxation times  $\tau_{\text{S}}$  were obtained. The results provide further evidence for the proposed bridging mode of halide ions.

## Experimental procedures

### Protein isolation and purification.

The enzyme was obtained from the growth medium of liquid cultures of *Streptomyces antibioticus* harbouring the pIJ703 Ty expression plasmid<sup>22;23</sup>. The protein was purified according to published procedures<sup>22</sup>. Purity was checked by SDS-PAGE and exceeded 95% in all preparations. Protein concentrations in pure samples were routinely determined optically using a value of 82 mM<sup>-1</sup>cm<sup>-1</sup> for the extinction coefficient at 280 nm<sup>24</sup>.

### Sample preparation and <sup>1</sup>H NMR measurements.

NMR Ty<sub>met</sub> samples (~0.6 mM in 100 mM NaPi at pH 6.80) were prepared as described before<sup>2</sup>. Samples recorded in H<sub>2</sub>O contained 5% D<sub>2</sub>O for the lock signal. <sup>1</sup>H spectra were recorded at 600 MHz or 300 Mhz <sup>1</sup>H resonance frequency and at 4 °C using a Bruker DMX-600 or DPX-300 spectrometer with the use of the 180°-τ-90°-t<sub>A</sub> super-WEFT pulse sequence<sup>25</sup>, using an interpulse delay time of typically 55 ms and a 8 s<sup>-1</sup> repetition rate. Depending on the required signal to noise ratio, 4,000 to 32,000 free induction decays were recorded, Fourier transformed using exponential apodization and a 60 Hz line-broadening function to increase the signal-to-noise ratio. The spectra were baseline corrected using the Bruker provided software. Chemical shifts were calibrated on the water signal. <sup>1</sup>H resonance T<sub>1</sub> values were measured by varying the interpulse delay time τ in the super-WEFT sequence using at least 16 values for τ, where the signal intensities were measured using peak-heights. The estimated errors in the T<sub>1</sub> values are ± 15%. Transversal relaxation rates R<sub>2</sub> (= T<sub>2</sub><sup>-1</sup>) of resolved signals were determined from the resonance line-widths by simulation of the signals using the line-fitting module implemented in the Mestre-C software (Cobas, J.C., Cruces, J. and Sardina, F.J., Universidad de Santiago de Compostela, Spain). The obtained line-widths were corrected for the contribution introduced by the LB function, after which the R<sub>2</sub> values (in Hz) were calculated from the relation R<sub>2</sub> = πΔν where Δν denotes the line-width at half-height.

*Calculations.* Values for -2J were determined from the temperature dependence of <sup>1</sup>H chemical shifts using the following equation<sup>18</sup>:

$$\delta_{con} = \frac{A}{T} \frac{g_e \mu_B}{\hbar \gamma_I k_B} \left( \frac{e^{(2J/k_B T)}}{1 + 3e^{(2J/k_B T)}} \right) \quad (\text{Equation 1})$$

where  $\delta_{con}$  represents the paramagnetic shift (equal to the observed shift  $\delta_{obs}$  minus an assumed 8 ppm for the diamagnetic contribution),  $A$  is the isotropic electron-nucleus interaction energy,  $g_e$  is the free electron g-value,  $\mu_B$  is the Bohr magneton,  $\hbar$  is Planck's constant divided by  $2\pi$ ,  $\gamma_1$  is the proton gyromagnetic ratio,  $k_B$  is the Boltzmann constant,  $2J$  is the singlet-triplet spacing energy and  $T$  is the absolute temperature. Dipolar, contact and Curie relaxation was interpreted using the following equations<sup>20</sup>:

$$T_{1dip}^{-1} = \frac{2}{15} \left( \frac{\mu_0}{4\pi} \right)^2 \left( \frac{\gamma_1^2 g_e^2 \mu_B^2}{r^6} \right) \left( \frac{7\tau_c}{1 + \omega_S^2 \tau_c^2} + \frac{3\tau_c}{1 + \omega_I^2 \tau_c^2} \right) P \quad (\text{Equation 2})$$

$$T_{2dip}^{-1} = \frac{1}{15} \left( \frac{\mu_0}{4\pi} \right)^2 \left( \frac{\gamma_1^2 g_e^2 \mu_B^2}{r^6} \right) \left( 4\tau_c + \frac{13\tau_c}{1 + \omega_S^2 \tau_c^2} + \frac{3\tau_c}{1 + \omega_I^2 \tau_c^2} \right) P \quad (\text{Equation 3})$$

$$T_{1cont}^{-1} = \frac{2}{3} A_c^2 \left( \frac{3\tau_c}{1 + \omega_S^2 \tau_c^2} \right) P \quad (\text{Equation 4})$$

$$T_{2cont}^{-1} = \frac{1}{3} A_c^2 \left( \frac{3\tau_c}{1 + \omega_S^2 \tau_c^2} + \tau_c \right) P \quad (\text{Equation 5})$$

$$T_{1Cur}^{-1} = \frac{2}{5} \left( \frac{\mu_0}{4\pi} \right)^2 \left( \frac{\omega_1^2 g_e^4 \mu_B^4}{r^6 (3k_B T)^2} \right) \left( \frac{3\tau_c}{1 + \omega_I^2 \tau_c^2} \right) 2P \quad (\text{Equation 6})$$

$$T_{2Cur}^{-1} = \frac{1}{5} \left( \frac{\mu_0}{4\pi} \right)^2 \left( \frac{\omega_1^2 g_e^4 \mu_B^4}{r^6 (3k_B T)^2} \right) \left( 4\tau_c + \frac{3\tau_c}{1 + \omega_I^2 \tau_c^2} \right) 2P \quad (\text{Equation 7})$$

with

$$\tau_c^{-1} = \tau_S^{-1} + \tau_R^{-1} \quad (\text{dipolar}) \quad (\text{Equation 8})$$

$$\tau_c^{-1} = \tau_S^{-1} \quad (\text{contact}) \quad (\text{Equation 9})$$

$$\tau_c^{-1} = \tau_R^{-1} \quad (\text{Curie}) \quad (\text{Equation 10})$$

and

$$P = \frac{1.5 \exp\left(\frac{2J}{k_B T}\right)}{1 + 3 \exp\left(\frac{2J}{k_B T}\right)} \quad (\text{Equation 11})$$

In Eqs. 2-7,  $T_1$  and  $T_2$  are the longitudinal and transversal dipolar induced nuclear relaxation times, respectively,  $r$  is the distance from the resonating nucleus to the paramagnetic center,  $\mu_0$  is the magnetic permeability of the vacuum,  $\gamma_1$  is the gyromagnetic

ratio of the nucleus of interest,  $g_e$  is the free-electron  $g$ -value,  $\mu_B$  is the Bohr magneton and  $\omega_S$  and  $\omega_I$  are the electronic and nuclear Larmor frequencies, respectively. In Eqs. 2-7,  $\tau_c$  denotes the correlation time as defined by Eqs. 8-10 where  $\tau_R$  is the rotational correlation time and  $\tau_S$  is the electronic relaxation time. Since we are investigating systems without chemical exchange, we have left out the  $\tau_M^{-1}$  contribution to  $\tau_c^{-1}$  in Eqs. 8-10<sup>20</sup>. The equations are based on the point dipole approximation for the electronic magnetic moment. Equations 2-7 are multiplied by a partition factor  $P$  (Eq. 11), accounting for the relative populations of the different spin levels of the system at a given temperature<sup>20</sup>.

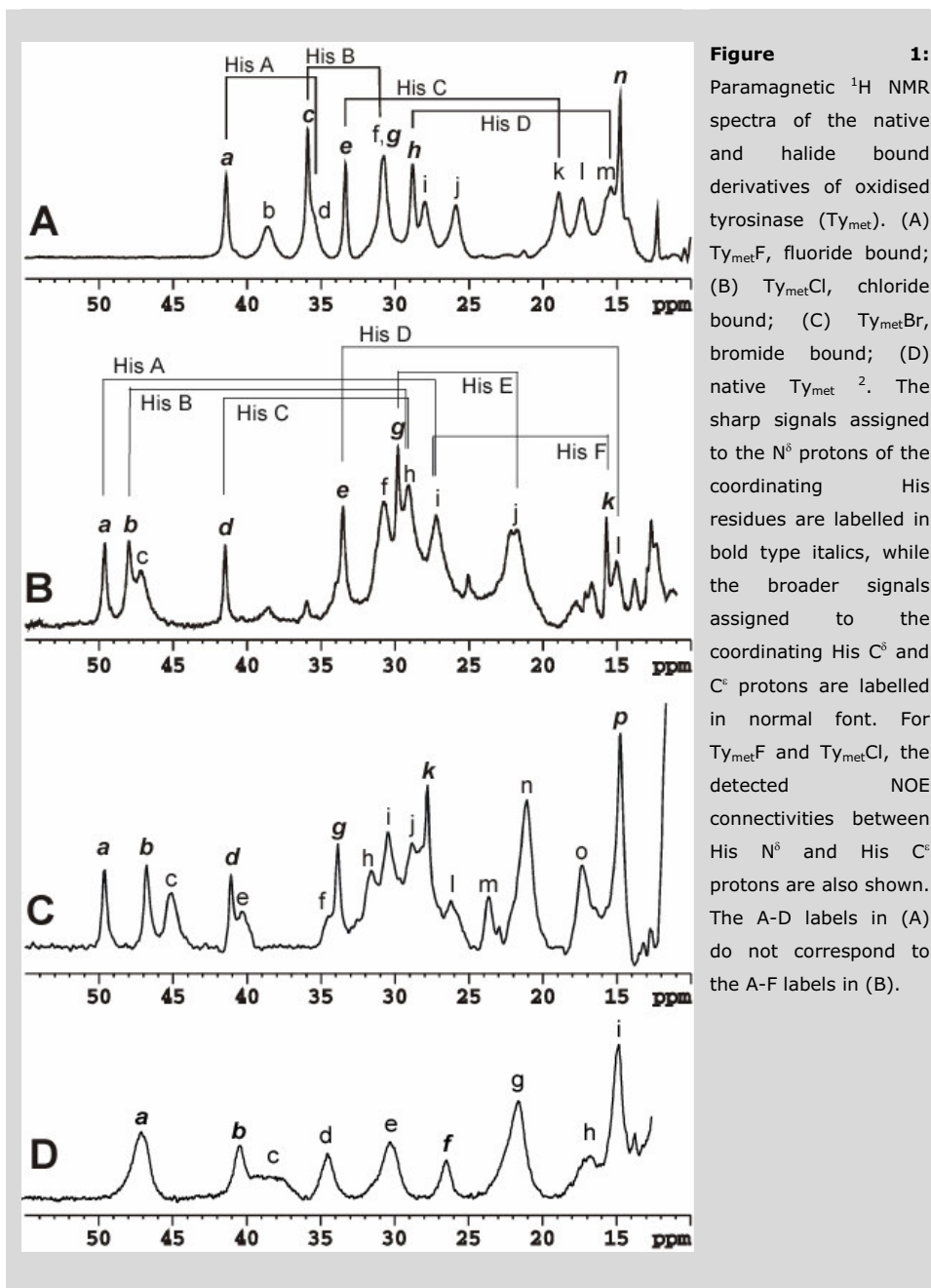
## Results

Figure 1 shows the 600 MHz  $^1\text{H}$  NMR spectra, recorded at pH 6.80 and 4 °C, of native  $\text{Ty}_{\text{met}}$  and the halide bound derivatives between 55 and 10 ppm<sup>2,3</sup>. For  $\text{Ty}_{\text{met}}\text{F}$  (Fig. 1A) and  $\text{Ty}_{\text{met}}\text{Cl}$  (Fig. 1B), the paramagnetically shifted resonances were assigned based on  $\text{H}_2\text{O}/\text{D}_2\text{O}$  exchange experiments, intra-residue NOE patterns and  $T_1$  relaxation data<sup>2,3</sup>. The sharp, solvent exchangeable, signals could be assigned to the  $\text{N}^\delta$  protons of the coordinating histidine residues, while the broader signals derive from the  $\text{C}^\epsilon$  and  $\text{C}^\delta$  protons of the histidines. Furthermore, the NOE patterns in the spectrum of  $\text{Ty}_{\text{met}}\text{Cl}$  were used to identify the coupling of each of the six sharp  $\text{N}^\delta$  proton signals with a  $\text{C}^\epsilon$  proton signal, thereby characterizing each histidine residue in the  $(\text{Cu-His}_3)_2$  coordination sphere as indicated in Fig. 1B<sup>2</sup>.

In the case of  $\text{Ty}_{\text{met}}\text{F}$  (Fig. 1A), the detection of NOE signals is complicated by signal overlap and by the fast  $T_1$  relaxation (see below). Four out of the six expected NOE connectivities in the  $\text{Ty}_{\text{met}}\text{F}$  species could be detected<sup>3</sup> as presented in Figure 1A.

## Chapter 5

### Paramagnetic properties of the $Ty_{met}X$ species



### Magnitude of the exchange coupling.

The magnitude of the exchange coupling ( $-2J$ ) between the two unpaired electrons of the Cu(II) ions can be estimated by investigating the temperature dependence of the chemical shifts (e.g. <sup>2;14;15;26;27</sup>). They were measured for all resolved paramagnetically shifted signals in the range 279-300 K. The Curie plots for the shift data for native  $\text{Ty}_{\text{met}}$  and the three  $\text{Ty}_{\text{met}}\text{X}$  derivatives are presented in Fig. 2. The data were analyzed by global fitting to Equation 1, resulting in a single value for  $-2J$  (table 2) and a value for the contact coupling constant  $A$  for each signal (table 1). In the cases of native  $\text{Ty}_{\text{met}}$ ,  $\text{Ty}_{\text{met}}\text{F}$  and  $\text{Ty}_{\text{met}}\text{Br}$ , one signal showed erroneous temperature dependence (marked with open symbols in Fig. 2) and we did not include the shift data of these signals in the fitting procedure.

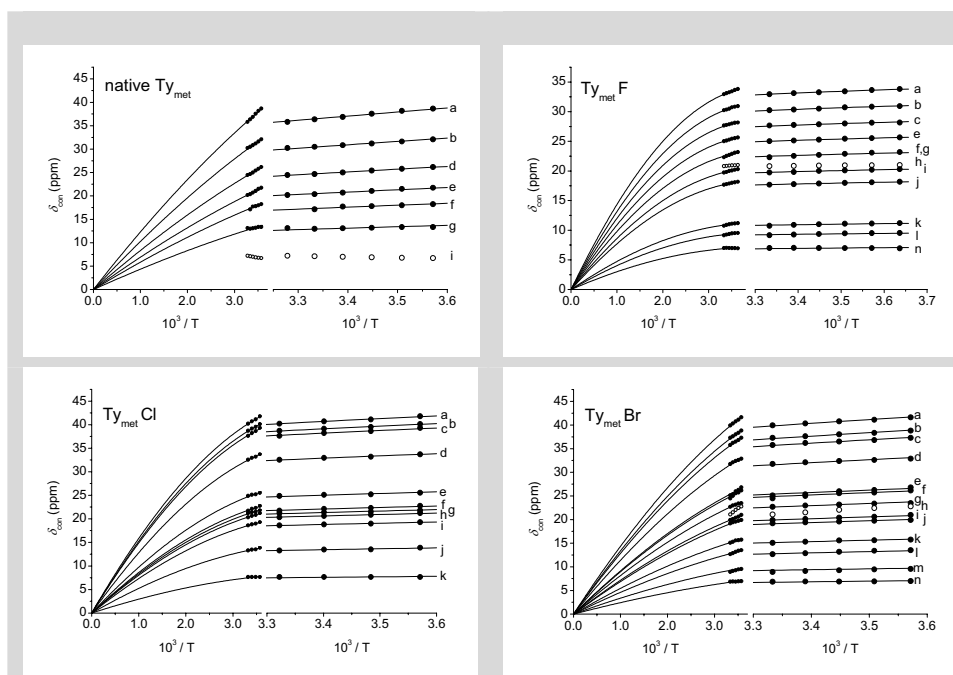


**Figure 2:** Curie plots for the paramagnetic shifts of native  $\text{Ty}_{\text{met}}$ ,  $\text{Ty}_{\text{met}}\text{F}$ ,  $\text{Ty}_{\text{met}}\text{Cl}$  and  $\text{Ty}_{\text{met}}\text{Br}$ . The solid lines represent fits to the data using Eq. 1 with  $-2J = 71 \text{ cm}^{-1}$  (native  $\text{Ty}_{\text{met}}$ ),  $260 \text{ cm}^{-1}$  ( $\text{Ty}_{\text{met}}\text{F}$ ),  $200 \text{ cm}^{-1}$  ( $\text{Ty}_{\text{met}}\text{Cl}$ ) and  $162 \text{ cm}^{-1}$  ( $\text{Ty}_{\text{met}}\text{Br}$ ). Signal shifts with open symbols were not included in the fitting procedure (see text).

**$T_1$  relaxation data.**

We have measured  $T_1$  values for native  $\text{Ty}_{\text{met}}$ ,  $\text{Ty}_{\text{met}}\text{F}$  and  $\text{Ty}_{\text{met}}\text{Br}$ . The data are presented in Table 1 together with previously derived data for the chloride bound species<sup>2</sup>. Mono-exponential relaxation behaviour is observed for all broad signals that consist of multiple overlapping resonances (as judged by signal integration), indicating that the resonances making up the total signal share similar  $T_1$  relaxation times. In the case of the  $\text{Ty}_{\text{met}}\text{X}$  species, the narrow widths and relatively long  $T_1$ s (see below) of the  $\text{N}^{\delta}\text{H}$  signals allowed for measurement of the  $T_1$  values of the latter despite the occasional overlap with broader  $\text{C}^{\delta,\varepsilon}\text{H}$  signals. The  $T_1$  could not be accurately estimated for signal *g* in  $\text{Ty}_{\text{met}}\text{F}$  and signal *p* in  $\text{Ty}_{\text{met}}\text{Br}$ , where a sharp  $\text{N}^{\delta}\text{H}$  signal is exactly superimposed with a broad His  $\text{C}^{\delta,\varepsilon}\text{H}$  signal. For  $\text{Ty}_{\text{met}}\text{F}$ , the  $T_1$  values of the broad signals (from the His  $\text{C}^{\delta}$  and  $\text{C}^{\varepsilon}$  protons), were measured in  $\text{D}_2\text{O}$ . Under these conditions the  $\text{N}^{\delta}\text{H}$  signals are not observed, which allows for a more accurate measurement of the  $T_1$  of the remaining signals. For the  $\text{Ty}_{\text{met}}\text{X}$  species, the longitudinal relaxation times divide in two distinct groups; the His  $\text{N}^{\delta}\text{H}$  signals all share similar  $T_1$  values (14-18, 17-27 and 26-32 ms for the  $\text{F}^-$ ,  $\text{Cl}^-$  and  $\text{Br}^-$  derivatives, respectively), as do the His-CH signals (2-4, 4-7 and 6-10 ms in similar order). There is no correlation between the determined coupling constants and  $T_1$  relaxation times, showing that contact relaxation is not dominant.

For native  $\text{Ty}_{\text{met}}$ , signals *a*, *b* and *f* (assigned to His  $\text{N}^{\delta}$  protons<sup>2</sup>) relax with  $T_1$  values of 13 - 15 ms. Tentative integration indicates that these signals together account for the signals of 5 or 6  $\text{N}^{\delta}$  protons. The spread in the  $T_1$  values of the remaining  $\text{C}^{\delta,\varepsilon}\text{H}$  signals (*c*, *d*, *e*, *g*, *i*;  $T_1$  2-10 ms) is much larger. It can not be excluded that one of the slower-relaxing signals (*d* or *i*) partially derives from a His  $\text{N}^{\delta}$  proton, therefore increasing the apparent  $T_1$ . Such a proton may have escaped detection in the H/D exchange experiments<sup>2</sup> in case it exchanges slowly with the solvent, as observed for a  $\text{N}^{\delta}$  proton in  $\text{Ty}_{\text{met}}\text{Cl}$  (signal *e*<sup>2</sup>).

**Mechanism of  $T_1$  relaxation.**

Maximum relaxation enhancements occur when  $\omega_S \tau_c^{\text{con}} \approx 1$  and  $\omega_I \tau_c^{\text{dip}} \approx 1$  for contact and dipolar  $T_1$  relaxation, respectively (see Eqs. 2 and 4). Since in the present case molecular tumbling is slow, the correlation time for dipolar relaxation is dominated by the electronic relaxation time and thus  $\tau_c^{\text{dip}} \approx \tau_c^{\text{con}} \approx \tau_S$ . Since  $\omega_I \tau_S \ll \omega_S \tau_S$ , contact relaxation will not significantly contribute to the  $T_1$ . This is also the case for Curie relaxation as the term  $\omega_I^2 \tau_R^2$  that occurs in the denominator of the dispersive term in the equation for longitudinal Curie relaxation (Eq. 6) is much larger than unity due to the long  $\tau_R$  of  $\text{Ty}_{\text{met}}$ . Thus, the paramagnetic  $T_1$ s are essentially dipolar in origin as already concluded at the end of the



previous paragraph on the basis of the experimental evidence.

### Correlation of $T_1$ s with Cu-H distances.

From the crystal structures of type-3 copper proteins it appears that the six His residues making up the highly conserved coordination sphere of the Cu site are nearly equivalent in terms of His proton-metal distances. This is illustrated by Fig. 3 in which a histogram is displayed of the distances between the His  $N^\delta$ ,  $C^\epsilon$  and  $C^\delta$  protons and the coordinated copper atom as observed in the crystal structures of *Limulus polyphemus* Hc (PDB entries 1OXY and 1LL1)<sup>6</sup>, *Octopus dofleini* Hc (PDB entry 1JS8)<sup>5</sup> and *Ipomoea batata* CO (PDB entries 1BT3 and 1BT1)<sup>4</sup> either in the oxidised or the oxygenated form. The distances of the  $N^\delta$  protons to Cu all amount to  $\sim 5.1$  Å ( $\pm 0.2$  Å), while the  $C^\epsilon$  and  $C^\delta$  protons occur at distances of  $\sim 3.4$  Å ( $\pm 0.3$  Å). There is no significant difference between the average distances obtained for the  $C^\epsilon$  and the  $C^\delta$  protons. Thus, since  $T_1$  is predominantly dipolar in origin, the overall relaxation characteristics should be similar for all equivalent His protons, as is indeed observed for the  $Ty_{met}X$  species ( $N^\delta H$   $T_1$ s in one class,  $C^{\delta,\epsilon} H$   $T_1$ s in another class).

When making the point-dipolar approximation, the ratio of the average  $T_1$  values obtained for the  $N^\delta$  protons and the  $C^\epsilon$  and  $C^\delta$  protons should equal the ratio of the corresponding sixth-power distances, i.e.  $(r_{Cu-NH})^6/(r_{Cu-CH})^6$ , which amounts to  $10.4 \pm 4.6$ . The experimental ratios for the  $N^\delta$  proton and the  $C^\epsilon$  and  $C^\delta$  proton  $T_1$  values reported in Table 2 disagree from this value. This is indicative of a breakdown of the point dipolar approximation<sup>28</sup>. Ideally, the dipolar interaction terms in Equations 2 and 3 should be replaced by the trace of the squared dipolar tensor. The latter is obtained by integrating the dipolar interaction over the wavefunction of the unpaired electron<sup>29,30</sup>.

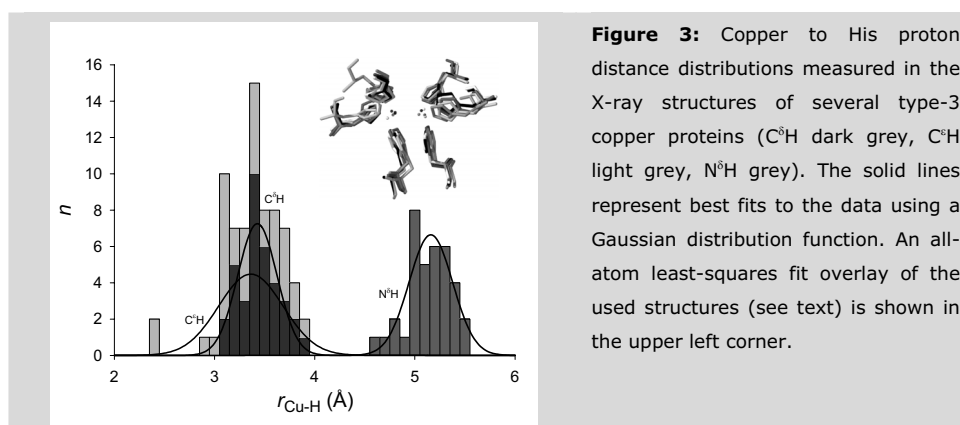


**Table 1:** Shifts, coupling constants and  $T_1$  values of the paramagnetically affected  $Ty_{met}X$   $^1H$  signals

Signal	$Ty_{met}F$			$Ty_{met}Cl$			$Ty_{met}Br$			Native $Ty_{met}$		
	$\delta$ (ppm)	$A/h$ ( $\times 10^5$ Hz)	$T_1$ (ms)	$\delta$ (ppm)	$A/h$ ( $\times 10^5$ Hz)	$T_1$ (ms)	$\delta$ (ppm)	$A/h$ ( $\times 10^5$ Hz)	$T_1$ (ms)	$\delta$ (ppm)	$A/h$ ( $\times 10^5$ Hz)	$T_1$ (ms)
<i>a</i>	<i>41.3</i>	<i>2.02</i>	<i>13.8</i>	<i>49.6</i>	<i>2.18</i>	<i>23.6</i>	<i>49.4</i>	<i>1.94</i>	<i>30.2</i>	<i>46.8</i>	<i>1.64</i>	<i>14.7</i>
<i>b</i>	<i>38.6</i>	<i>1.85</i>	<i>1.8<sup>a</sup></i>	<i>47.9</i>	<i>2.10</i>	<i>16.9</i>	<i>46.6</i>	<i>1.81</i>	<i>25.8</i>	<i>40.3</i>	<i>1.37</i>	<i>14.7</i>
<i>c</i>	<i>35.9</i>	<i>1.69</i>	<i>14.8</i>	<i>47.2</i>	<i>2.05</i>	<i>6.6<sup>a</sup></i>	<i>45.1</i>	<i>1.74</i>	<i>7.1</i>	<i>37.5</i>	nd	<i>1.7</i>
<i>d</i>	<i>35.6</i>	nd	<i>1.9<sup>a</sup></i>	<i>41.4</i>	<i>1.76</i>	<i>26.5</i>	<i>40.7</i>	<i>1.54</i>	<i>30.9</i>	<i>34.4</i>	<i>1.11</i>	<i>7.1</i>
<i>e</i>	<i>33.3</i>	<i>1.53</i>	<i>18.3</i>	<i>33.5</i>	<i>1.34</i>	<i>18.7</i>	<i>40.2</i>	nd	<i>10.1</i>	<i>29.9</i>	<i>0.92</i>	<i>2.2</i>
<i>f</i>	<i>30.7</i>	<i>1.38</i>	<i>3.2<sup>a</sup></i>	<i>30.7</i>	<i>1.19</i>	<i>5.5<sup>a</sup></i>	<i>35.0</i>	<i>1.34</i>	<i>7.9</i>	<i>26.4</i>	<i>0.78</i>	<i>13.8</i>
<i>g</i>	<i>30.7</i>	<i>1.38</i>	nd	<i>29.7</i>	<i>1.15</i>	<i>26.7</i>	<i>34.3</i>	<i>1.21</i>	<i>26.3</i>	<i>21.5</i>	<i>0.58</i>	<i>2.0</i>
<i>h</i>	<i>28.8</i>	<i>1.26</i>	<i>15.3</i>	<i>29.1</i>	<i>1.11</i>	<i>5.6<sup>a</sup></i>	<i>31.3</i>	<i>1.11</i>	<i>10.4</i>	<i>17.2</i>	nd	nd
<i>i</i>	<i>28.0</i>	<i>1.21</i>	<i>3.0<sup>a</sup></i>	<i>27.1</i>	<i>1.01</i>	<i>4.7<sup>a</sup></i>	<i>30.6</i>	<i>1.05</i>	<i>6.7</i>	<i>14.9</i>	<i>0.31</i>	<i>10.2</i>
<i>j</i>	<i>25.8</i>	<i>1.08</i>	<i>2.8<sup>a</sup></i>	<i>21.9</i>	<i>0.72</i>	<i>4.3<sup>a</sup></i>	<i>28.9</i>	<i>0.97</i>	<i>9.0</i>			
<i>k</i>	<i>19.0</i>	<i>0.67</i>	<i>3.8<sup>a</sup></i>	<i>15.6</i>	<i>0.41</i>	<i>24.5</i>	<i>27.7</i>	<i>0.93</i>	<i>32.2</i>			
<i>l</i>	<i>17.3</i>	<i>0.57</i>	<i>2.4<sup>a</sup></i>				<i>26.0</i>	nd	<i>7.3</i>			
<i>m</i>	<i>15.4</i>	nd	<i>2.1<sup>a</sup></i>				<i>23.8</i>	<i>0.74</i>	<i>9.2</i>			
<i>n</i>	<i>14.9</i>	<i>0.42</i>	<i>16.5</i>				<i>21.1</i>	<i>0.62</i>	<i>6.1</i>			
<i>o</i>							<i>17.2</i>	<i>0.44</i>	<i>6.3</i>			
<i>p</i>							<i>14.8</i>	<i>0.33</i>	<i>nd</i>			

See Fig. 1 for signal labelling. The data for the His  $N^{\delta}$  protons are presented in italic font; the data for the His  $C^{\delta}$  and  $C^{\epsilon}$  protons are presented in normal font. nd: values not determined. <sup>a</sup> Determined in  $D_2O$ . The shift and  $T_1$  data were measured at 4 °C, pH 6.80 and 600 MHz field strength.

When the wave function is unknown and the point dipole approximation breaks down, the next level of approximation assumes that the experimental  $T_1^{-1}$  is the sum of a metal-centred and a ligand-centred contribution<sup>28</sup>. The ligand-centred contribution may dominate the  $T_1$  for protons that are situated relatively far from the copper, even if the amount of spin on the ligand is small. This also means that the point-dipolar estimate (Eq. 2) is a better approximation for nuclei close to the paramagnetic center, as for the His C<sup>ε,δ</sup> protons in the present case<sup>28;31</sup>.

### Electronic relaxation times.

A value for the electronic relaxation time,  $\tau_S$ , can be obtained from the X-ray Cu-H distances (see above and Fig. 3), the experimental  $T_1$  and  $-2J$  values with the use of Eq. 2. The calculated values are presented in Table 2. The error margins reported for  $\tau_S$  mainly reflect the uncertainty in  $r$  and in the experimental  $T_1$  values. Although the point-dipolar description is an approximation as pointed out above, this will not destroy a possible trend in  $\tau_S$  values. With the Ty<sub>met</sub>X species, such a trend is indeed observed (Ty<sub>met</sub>Br < Ty<sub>met</sub>Cl < Ty<sub>met</sub>F).

**Table 2:** The exchange coupling parameter  $-2J$ , average  $T_1$  values and estimated electronic relaxation times,  $\tau_S$ , for the different Ty<sub>met</sub> species. nd: values not determined.

Species	$-2J^a$ (cm <sup>-1</sup> )	Average $T_1^b$ C <sup>δ,ε</sup> H (ms)	Average $T_1^b$ N <sup>δ</sup> H (ms)	$T_1$ N <sup>δ</sup> H/ $T_1$ C <sup>δ,ε</sup> H	$\tau_S$ calc C <sup>δ,ε</sup> H <sup>c</sup> (x 10 <sup>-11</sup> s)	$\tau_S$ calc N <sup>δ</sup> H <sup>c</sup> (x 10 <sup>-11</sup> s)
Ty <sub>met</sub> F	261±6	2.6±0.7	16±3	6.0±1.8	2.5±0.7	5.4±1.3
Ty <sub>met</sub> Cl	200±10	5.3±0.9	23±4	4.3±1.1	1.0±0.2	3.1±0.8
Ty <sub>met</sub> Br	162±11	8.0±1.5	29±3	3.7±0.8	0.6±0.1	2.2±0.7
Native	71±23	nd	14±1	nd	nd	3.7±1.0

<sup>a</sup> Values for  $-2J$  were estimated on the basis of the temperature dependence of signal paramagnetic shifts and Eq. 1 (see Fig. 2). <sup>b</sup> The average  $T_1$  values are based on the values listed in Table 1. <sup>c</sup> The values for  $\tau_S$  were estimated on the basis of Eq. 2 using the determined values for  $-2J$ , the average  $T_1$  values and the average Cu-H distances found in type-3 copper proteins (Fig. 3).

**Mechanism of  $T_2$  transversal relaxation.**

To analyze the mechanism of the transversal relaxation we selected the linewidths of the well resolved  $Ty_{met}F$  CH signals (*b, i, j, k, l* in Fig. 1A) at 600 MHz and 300 MHz as reported in Table 3. Based on the obtained  $\tau_S$  values (see above), the experimental  $-2J$  value and  $r = 3.4 \text{ \AA}$ , it is possible to estimate the dipolar contributions to the transversal relaxation of the  $C^\delta$  and  $C^\epsilon$  protons by using Equation 3.

**Table 3:**  $T_2^{-1}$  values for the resolved  $C^\delta, \epsilon$ H signals in  $Ty_{met}F$ .

Signal	$R_2$ at 600 MHz (kHz)	$R_2$ at 300 MHz (kHz)	$\Delta R_2$ (kHz)
<i>b</i>	1.54	0.93	0.61
<i>i</i>	1.05	0.74	0.31
<i>j</i>	0.92	0.58	0.34
<i>k</i>	1.05	0.57	0.48
<i>l</i>	1.11	0.66	0.45

For  $Ty_{met}F$ , a value of 0.5 kHz is calculated for the dipolar contribution to  $T_2^{-1}$ . Further, with a Cu-H distance of 3.4  $\text{\AA}$ , a  $\tau_R$  value of 15-20 ns and 600 MHz field strength, a Curie contribution between 0.6 kHz and 0.8 kHz to  $T_2^{-1}$  is calculated using Eq. 7. Thus, dipolar and Curie relaxation contribute about equally to the transverse relaxation rate. Since Curie relaxation scales with the square of the magnetic field, a sharpening of signals is expected at lower field strength if the Curie mechanism contributes to  $T_2^{-1}$ . This is indeed observed. The  $T_2^{-1}$  values of  $Ty_{met}F$  are significantly less at 300 MHz field-strength, where the average of the estimated  $T_2^{-1}$  values for the CH signals amounts to 0.7 kHz. The difference between the experimental linewidths at 600 and 300 MHz amounts to 0.4 kHz, corresponding well with a  $\Delta T_2^{-1}$  of 0.4 kHz - 0.6 kHz calculated by using Eq. 7 and the parameters given above.

**Discussion**

Based on paramagnetic NMR, enzyme kinetics and kinetics of fluoride binding<sup>3;21</sup> we previously showed that a single halide ion bridges the two copper ions in the active site of  $Ty_{met}$  and replaces the hydroxide molecule that is present in the native form<sup>3;21</sup>. The typical type-3 coordination geometry is maintained in all halide bound species<sup>3</sup>. This facilitated the interpretation of the relaxation data observed for  $Ty_{met}$  when changing the bridging ligand.

**Magnitude of the exchange coupling.**

It was found that the paramagnetic shifts are predominantly contact in origin. This agrees with the small magnetic anisotropy previously observed for Cu(II) systems, leading to negligible pseudocontact shifts<sup>18</sup>. In native  $Ty_{met}$ ,  $Ty_{met}F$  and  $Ty_{met}Br$ , the paramagnetic shift of one signal appeared not to follow the temperature dependence as predicted by Equation 1, possibly due to a structural rearrangement of the corresponding His residue with changing temperature.

Many attempts have been made to correlate the structural features of dinuclear copper complexes with the sign and magnitude of the magnetic exchange interaction, especially in relation with the nature and the coordination geometry of the bridging ligand (e.g.<sup>32-34</sup>). It appears that the Cu-X-Cu bridging angle is the most important parameter, larger Cu-X-Cu bond angles leading to stronger antiferromagnetic coupling<sup>32-34</sup>. The  $|-2J|$  value may vary over hundreds of wavenumbers in a group of related compounds with Cu-X-Cu bridging angles between about 100° and 125°. In the  $Ty_{met}$  species, we find a moderate to strong antiferromagnetic coupling with  $-2J$  values following the order of  $Ty_{met}F > Ty_{met}Cl > Ty_{met}Br$  (table 2). By considering the radius of  $X^-$  when going down the halide group, the Cu-X-Cu angles would follow the order  $F^- > Cl^- > Br^-$ , thereby paralleling the experimental trend in  $-2J$  values. The finding that  $-2J$  is dependent on the nature of the halide ligand, as well as the clear trend in their values, supports the proposed bridging mode of halide ions.

**Nuclear relaxation.**

The present data show that the paramagnetic longitudinal proton relaxation is dominated by the dipolar relaxation in all  $Ty_{met}X$  derivatives. This means that  $T_1$  data contain information on the distances from the copper to the resonating nucleus. The line-widths (i.e.  $T_2$ s), instead consist of contributions from dipolar and Curie relaxation of similar magnitude. Since both relaxation mechanisms depend on the distance between the paramagnetic centre and the resonating nucleus (Eqs. 3 and 7), the line-widths in the paramagnetic  $^1H$  NMR spectra of the  $Ty_{met}X$  species serve as a qualitative indicator for the Cu-H distance.

**Electronic relaxation.**

The paramagnetically shifted signals of proteins with a mono-nuclear Cu-site are often too broad to be detectable due to a long electronic relaxation time,  $\tau_S$ . In dinuclear Cu containing model compounds an appreciable sharpening of the NMR signals has been

observed, apparently because  $\tau_S$  has shortened<sup>17</sup>. Our experiments show that a shortening of  $\tau_S$  can also occur in macromolecular structures harbouring a type-3 center. The estimated  $\tau_S$  values of the three  $\text{Ty}_{\text{met}}$  derivatives are of the order of  $10^{-11}$  s and decrease according to  $\text{Ty}_{\text{met}}\text{F} > \text{Ty}_{\text{met}}\text{Cl} > \text{Ty}_{\text{met}}\text{Br}$ , as do the  $-2J$  values.

The mechanism responsible for the shortening of  $\tau_S$  has not been established, yet. Fast electronic relaxation in Cu(II) dimers may be due to the modulation of the zero-field splitting (ZFS) of the  $S = 1$  level<sup>17;20</sup>. The modulation of the ZFS could arise from fluctuations in coordination geometry, collisions with solvent molecules or molecular rotation. Still, even with fast relaxation between the sublevels of the  $S = 1$  state, an additional fast relaxation between the  $S = 0$  ground and the  $S = 1$  excited state is needed to obtain (averaged) sharp paramagnetically shifted signals in the NMR spectrum. Actually, fast relaxation between the two states is sufficient to get sharp paramagnetically shifted NMR lines. The density of phonon states in the protein framework is probably high enough in the  $100\text{-}300\text{ cm}^{-1}$  range to allow fast thermal relaxation between the triplet and singlet states. Relaxation may be promoted by the extreme sensitivity of the  $-2J$  splitting for the Cu-X-Cu angle. Thermal motion affecting this angle may provide an efficient time dependent perturbation mechanism to enhance relaxation. Also, the spin-orbit coupling along the series  $\text{F} < \text{Cl} < \text{Br}$  may help enhance relaxation. It would explain the observed decrease in  $\tau_S$  along this series.

A similar mechanism has been suggested to explain the enhanced relaxation observed for the mixed-valence  $[\text{Cu}(1.5)\text{ Cu}(1.5)]\text{ Cu}_A$  site of an engineered amicyanin<sup>35</sup> and cytochrome *c* oxidase<sup>36</sup> that also yield sharp NMR signals. In the  $\text{Cu}_A$  system, the energy difference between the electronic ground state MO ( $^2\text{B}_{3u}$ ) and the first excited state MO ( $^2\text{B}_{2u}$ ) is again of the order of a few  $100\text{ cm}^{-1}$ <sup>36</sup>, similar to the situation of  $\text{Ty}_{\text{met}}$ . The experimental  $\tau_S$  values of the three  $\text{Ty}_{\text{met}}\text{X}$  species are similar to the  $\tau_S$  value reported for the  $\text{Cu}_A$  center ( $\tau_S \sim 10^{-11}$  s<sup>35;36</sup>).

### The $^1\text{H}$ NMR properties of the native $\text{Ty}_{\text{met}}$ species.

In native  $\text{Ty}_{\text{met}}$ , the NMR signals are broader than in the halide bound species. Yet, the calculated electronic relaxation time (table 2) for the native species is similar to that of  $\text{Ty}_{\text{met}}\text{F}$  and  $\text{Ty}_{\text{met}}\text{Cl}$ , meaning that the dipolar contribution to the line-width should be similar in both species. Furthermore, since the rotational correlation times should be equal for all  $\text{Ty}_{\text{met}}$  species, the Curie contribution should be similar in all cases. This then raises the question why the signals in the native species are so much broader than in  $\text{Ty}_{\text{met}}\text{F}$ .

Through a study of the transient-state kinetics of fluoride binding to  $\text{Ty}_{\text{met}}$  and its pH

dependence, it was shown that the fluoride ion replaces the hydroxide ion that bridges the two copper ions in the native species<sup>3;21</sup>. The kinetic data further indicated that the hydroxide molecule is in fast exchange with the solvent ( $k_{off} > 600 \text{ s}^{-1}$  at 21 °C), while fluoride forms a stable complex with the  $Ty_{met}$  enzyme ( $k_{off} 12.3 \text{ s}^{-1}$  at 21 °C). The larger line-widths observed in the native species might therefore be related to an exchange process associated with the  $Cu_2$  bridging hydroxide ion.

In conclusion, in this study we have found that the properties of the  $Ty_{met}X$  derivatives depend on the nature of the exchangeable  $Cu_2$  bridging ligand. The  $Ty_{met}X$  species are moderately antiferromagnetically coupled, with the experimental  $-2J$  values following the same order as the expected Cu-X-Cu bridging angle in the  $Ty_{met}X$  complexes.

Longitudinal relaxation is dipolar in origin, while the transversal relaxation arises from both the dipolar and the Curie relaxation. This implies that both  $T_1$  and  $T_2$  relaxation contain information on the distance of the copper to the resonating nucleus, a feature that may be used to study  $Ty_{met}$ -inhibitor complexes. It was further established that the relative sharpness of the signals in the  $Ty_{met}X$  species is due to short electronic relaxation times that are different for each  $Ty_{met}X$  species; the  $\tau_s$  values follow the order of  $Ty_{met}F > Ty_{met}Cl > Ty_{met}Br$  and lie in the range of  $10^{-11}$  sec. The data show that  $^1H$  paramagnetic NMR is a valuable tool for structural and mechanistic studies on type-3 [Cu(II)-R-Cu(II)] copper proteins and provides a better understanding of the phenomena that determine nuclear and electronic relaxation in dimeric Cu(II) compounds.

## References

- (1) Solomon, E. I.; Sundaram, U. M.; Machonkin, T. E. *Chem. Rev.* **1996**, *96*, 2563-2605.
- (2) Bubacco, L.; Salgado, J.; Tepper, A. W. J. W.; Vijgenboom, E.; Canters, G. W. *FEBS Letters* **1999**, *442*, 215-220.
- (3) Tepper, A. W.; Bubacco, L.; Canters, G. W. *J. Biol. Chem.* **2002**, *277*, 30436-30444.
- (4) Klabunde, T.; Eicken, C.; Sacchettini, J. C.; Krebs, B. *Nat. Struct. Biol.* **1998**, *5*, 1084-1090.
- (5) Cuff, M. E.; Miller, K. I.; van Holde, K. E.; Hendrickson, W. A. *J. Mol. Biol.* **1998**, *278*, 855-870.
- (6) Magnus, K. A.; Hazes, B.; Ton-That, H.; Bonaventura, C.; Bonaventura, J.; Hol, W. G. *Proteins* **1994**, *19*, 302-309.
- (7) Volbeda, A.; Hol, W. G. *J. Mol. Biol.* **1989**, *209*, 249-279.

- (8) Decker, H.; Tuzcek, F. *TIBS* **2000**, *25*, 392-397.
- (9) Gerdemann, C.; Eicken, C.; Krebs, B. *Acc. Chem. Res.* **2002**, *35*, 183-191.
- (10) La Mar, G. N.; Horrocks, W., Jr.; Holm, R. H. *NMR of Paramagnetic Molecules*; 1973; pp 53-83.
- (11) Holz, R. C.; Alvarez, M. L.; Zumft, W. G.; Dooley, D. M. *Biochemistry* **1999**, *38*, 11164-11171.
- (12) Asokan, A.; Manoharan, P. T. *Inorg. Chem.* **1999**, *38*, 5642-6554.
- (13) Brink, J. M.; Rose, R. A.; Holz, R. C. *Inorg. Chem.* **1996**, *35*, 2878-2885.
- (14) Byers, W. and Williams, R. J. P. *J. Chem. Soc. Dalton* **1973**, 555-560.
- (15) Maekawa, M.; Kitagawa, S.; Munakata, M.; Masuda, H. *Inorg. Chem.* **1989**, *28*, 1904-1909.
- (16) Zelonka, R. A.; Baird, M. C. *Inorg. Chem.* **1972**, *11*, 134.
- (17) Murthy, N. N.; Karlin, K. D.; Bertini, I.; Luchinat, C. *J. Am. Chem. Soc.* **1997**, *119*, 2156-2162.
- (18) Bertini, I.; Luchinat, C. *Coord. Chem. Rev.* **1996**, *150*.
- (19) Bertini, I.; Galas, O.; Luchinat, C.; Parigi, G.; Spina, G. *J. Magn. Reson.* **1998**, *130*, 33-44.
- (20) Clementi, V.; Luchinat, C. *Acc. Chem. Res.* **1997**, *31*, 351-361.
- (21) Tepper, A. W.; Bubacco, L.; Canters, G. W. *J. Biol. Chem.* **2003**, *279*, 13425-13435.
- (22) Bubacco, L.; Vijgenboom, E.; Gobin, C.; Tepper, A. W. J. W.; Salgado, J.; Canters, G. W. *J. Mol. Cat. B* **2000**, *8*, 27-35.
- (23) Katz, E.; Thompson, C. J.; Hopwood, D. A. *J. Gen. Microbiol.* **1983**, *129* (Pt 9), 2703-2714.
- (24) Jackman, M. P.; Hajnal, A.; Lerch, K. *Biochem. J.* **1991**, *274* ( Pt 3), 707-713.
- (25) Inubushi, T.; Becker, E. D. *J. Magn. Reson.* **1983**, *51*, 128-133.
- (26) Asokan, A.; Varghese, B.; Manoharan, P. T. *Inorg. Chem.* **1999**, *38*, 4393-4399.
- (27) Mandal, P. K.; Manoharan, P. T. *Inorg. Chem.* **1995**, *34*, 270-277.
- (28) Doddrell, D. M.; Healy, P. C.; Bendall, M. R. *J. Magn. Reson.* **1978**, *29*, 163-166.



## Chapter 5

### Paramagnetic properties of the $Ty_{met}X$ species

- (29) Canters, G. W.; de Boer, E. *Mol. Phys.* **1974**, *27*, 665-687.
- (30) Canters, G. W.; Hill, H. A. O.; Kitchen, N. A. *J. Magn. Reson.* **1984**, *57*, 1-23.
- (31) Banci, L.; Bertini, I.; Luchinat, C.; Scozzafava, A. *J. Am. Chem. Soc.* **1987**, *109*, 2328-2334.
- (32) Rodriguez, M.; Llobet, A.; Corbella, M.; Martell, A. E.; Reibenspies, J. *Inorg. Chem.* **1999**, *38*, 2328-2334.
- (33) Tandon, S. S.; Thompson, L. K.; Manuel, M. E.; Bridson, J. N. *Inorg. Chem.* **1994**, *33*, 5555-5570.
- (34) Thompson, L. K.; Mandal, S. K.; Tandon, S. S.; Bridson, J. N.; Park, M. K. *Inorg. Chem.* **1996**, *35*, 3117-3125.
- (35) Dennison, C.; Berg, A.; Canters, G. W. *Biochemistry* **1997**, *36*, 3262-3269.
- (36) Salgado, J.; Warmerdam, G.; Bubacco, L.; Canters, G. W. *Biochemistry* **1998**, *37*, 7378-7389.

# Chapter 6

## *Paramagnetic NMR studies of p-nitrophenol binding to tyrosinase*

Published as: A.W.J.W. Tepper, L. Bubacco, G.W. Canters, *J. Am. Chem. Soc.* (2005), 127, 567-575

### Summary

The interaction of the monooxygenating type-3 copper enzyme Tyrosinase (Ty) from *Streptomyces antibioticus* with its inhibitor *p*-nitrophenol (pnp) was studied by paramagnetic NMR methods. The pnp binds to oxidised Ty (Ty<sub>met</sub>) and its halide (F<sup>-</sup>, Cl<sup>-</sup>) bound derivatives with a dissociation constant in the mM range. The Cu<sub>2</sub> bridging halide ion is not displaced upon the binding of pnp showing that the pnp does not occupy the Cu<sub>2</sub> bridging position. The binding of pnp to Ty<sub>met</sub> or Ty<sub>met</sub>Cl leads to localised changes in the type-3 (Cu-His<sub>3</sub>)<sub>2</sub> coordination geometry reflecting a change in the coordination of a single His residue that, still, remains coordinated to Cu. The binding of pnp to Ty<sub>met</sub>Cl causes a decrease in the Cu<sub>2</sub> magnetic exchange parameter  $-2J$  from 200 cm<sup>-1</sup> in the absence to 150±10 cm<sup>-1</sup> in the presence of pnp. From the <sup>1</sup>H and <sup>2</sup>D NMR relaxation parameters of pnp bound to Ty<sub>met</sub>, a structural model of pnp coordination to the Ty type-3 center could be derived. The model explains the absence of monophenolase activity in the closely related type-3 copper protein catechol oxidase. The relevance of the experimental findings towards the Ty catalytic mechanism is discussed.

## Introduction

Tyrosinase (Ty) catalyses the *ortho* hydroxylation of monophenolic substrates (monophenolase activity) and the subsequent oxidation of the diphenolic products to the quinone analogues (diphenolase activity). The reactions are rate limiting in the biosynthesis of melanin pigments, that fulfil various roles in different organisms<sup>1</sup>. The enzyme is widely distributed throughout the phylogenetic scale and occurs in organisms ranging from bacteria to man. In mammals, Ty is responsible for skin and hair pigmentation and defects in the enzyme are related to a range of medical conditions like type I human oculocutaneous albinism<sup>2</sup>. In fruits and mushrooms, the enzyme is responsible for the economically undesirable browning that occurs upon bruising or long-term storage, while in plant products such as cocoa, raisins and green tea, the action of Ty gives rise to distinct organoleptic properties<sup>3</sup>. The enzyme has further been reported to catalyse the dehalogenation of xenobiotic fluorophenols<sup>4</sup>, a reaction potentially applicable in bioremediation. Consequently, the enzyme poses considerable interest from medical, agricultural and industrial points-of-view.

Ty is a member of the type-3 copper protein family, that further includes the hemocyanins (Hcs) and the catechol oxidases (COs). The type-3 copper proteins are thought to have developed from an ancient ancestor that was possibly involved in scavenging of (toxic) oxygen in a predominantly anaerobic atmosphere<sup>5</sup>. The type-3 proteins contain a dinuclear copper active site that is comprised of two closely spaced copper atoms each coordinated by 3 histidine residues. Although the dinuclear site is highly conserved as witnessed by its characteristic spectroscopic signatures, by sequence homologies and by the available crystal structures for several Hcs<sup>6-9</sup> and CO<sup>10</sup>, the functionality of the Tys, Hcs and COs is different. While Hcs function as oxygen carriers and oxygen storage proteins in arthropods and molluscs, the COs oxidise diphenols to the corresponding quinones but lack the Ty hydroxylation activity.

The Ty type-3 site can exist in three forms. The (a) reduced [Cu(I) Cu(I)] species ( $Ty_{red}$ ) binds molecular oxygen to render the (b) oxygenated [Cu(II)-O<sub>2</sub><sup>2-</sup>-Cu(II)] species ( $Ty_{oxy}$ ), in which molecular oxygen is bound to the Cu<sub>2</sub> centre as peroxide in a  $\mu-\eta^2:\eta^2$  side-on bridging mode<sup>11</sup>. The  $Ty_{oxy}$  form is competent to react with monophenols and diphenols and is characterised by a strong Ligand to Metal Charge Transfer (LMCT) band centred around 345 nm. Upon reaction of  $Ty_{oxy}$  with mono- or diphenolic substrates, the (c) oxidised [Cu(II)-OH<sup>-</sup>-Cu(II)] met species ( $Ty_{met}$ ) is formed, which is competent to react with diphenols only. The  $Ty_{met}$  form is the predominant species in the absence of substrate and can bind a range of organic and inorganic ligands that yield complexes in which the enzymatic activity is inhibited<sup>12-15</sup>. The Cu(II) ions in native  $Ty_{met}$  are bridged by a hydroxide ion that can be replaced by a halide ion ( $X^- = F^-, Cl^-, Br^-$ )<sup>13;14</sup>, and they are antiferromagnetically coupled to yield a diamagnetic ground-state. Finally, (d) a half-oxidised [Cu(I) OH<sup>-</sup>-Cu(II)] species ( $Ty_{half-met}$ ) can be prepared in which only one of the two coppers occurs in the oxidised form, which is, thus, EPR active.

The interaction of  $Ty_{met}$  with exogenous ligands is difficult to probe due to the scarcity of suitable spectroscopic methods. The  $Ty_{met}$  enzyme is devoid of strong transitions in the UV/Vis and cannot be studied by EPR methods. However, it has been shown that the  $Ty_{met}$  paramagnetic triplet state is partially populated at room temperature, rendering the site amenable to paramagnetic NMR study<sup>16</sup>. Although paramagnetic NMR is usually not feasible for copper systems due to the inherently large widths of the NMR signals,  $Ty_{met}$ , a Cu-substituted aminopeptidase<sup>17</sup> and some antiferromagnetically coupled dinuclear Cu(II) complexes (e.g. <sup>18-20</sup>) appear to give remarkably sharp paramagnetically shifted NMR signals due to fast electronic relaxation<sup>16,21</sup>.

Since the paramagnetism is only sensed by the protons close to the metallic center, paramagnetic NMR provides a powerful and selective probe of the coordination geometry of the active site and the changes that occur upon ligand binding<sup>22</sup>. The method has previously been used to study inhibitor binding to  $Ty_{met}$ <sup>12,13</sup>. It was also demonstrated that *S. antibioticus* Ty contains a classical type-3 site in which the two copper ions are coordinated by six histidine residues through their  $N^{\epsilon}$  atoms<sup>16</sup>, as in the Hcs and COs.

Although the mechanism of the enzyme has been addressed by a wide variety of (bio)chemical, spectroscopic and theoretical methods, its structural details remain obscure to date. The crucial and rate limiting step in the rather complex kinetic mechanism<sup>23</sup> is the  $Ty_{oxy}$  catalyzed hydroxylation reaction that comprises fissure of the peroxide O-O bond and oxygen transfer to the bound phenolic substrate and for which various mechanisms have been proposed (reviewed in, e.g., <sup>24-26</sup>).

A critical event is the binding of phenolic substrate to  $Ty_{oxy}$ . It is generally assumed that phenolate coordinates axially to one of the copper atoms in the Ty active site but experimental evidence for this is scarce. The binding of the phenol is further thought to activate the bound peroxide<sup>11</sup>. Due to their transient nature, the complexes of Ty with monophenols are difficult to study. However, with *p*-nitrophenol (pnp), the presence of the strongly electron withdrawing nitro group sufficiently deactivates the phenolic ring to prevent its hydroxylation. In fact, pnp acts as a simple competitive inhibitor in the conversion of L-DOPA with an inhibition constant in the mM range<sup>27</sup>.

Here we report on a paramagnetic NMR study of the interaction of pnp with  $Ty_{met}$  and its fluoride and chloride bound derivatives, which is aimed at providing insight into the binding mode of monophenols to the Ty active site. The results have a direct bearing on the understanding of the substrate inhibition in the monophenolase reaction and they provide further insight into the hydroxylation mechanism in the monophenolase reaction.

## Materials and methods

### Protein isolation and purification.

The enzyme was obtained from the growth medium of liquid cultures of *Streptomyces antibioticus* harbouring the pIJ703 Ty expression plasmid<sup>12</sup>. The protein was purified according to published procedures<sup>12</sup>. Purity was checked by SDS-PAGE and exceeded 95% in all preparations. Protein concentrations in pure samples were determined optically using a value of 82 mM<sup>-1</sup>cm<sup>-1</sup> for the extinction coefficient at 280 nm<sup>28</sup>. The protein was stored at -80 °C at a concentration of 1 mg/ml in 100 mM Pi buffer at pH 6.8 containing 20 % glycerol as a cryoprotectant. Prior to further experiments, glycerol was removed from the storage buffer by repetitive dilution and concentration by using Amicon ultra-filtration over a 10 kDa cut-off membrane.

### Paramagnetic <sup>1</sup>H NMR measurements.

NMR Ty<sub>met</sub> samples (~0.6 mM in 100 mM NaPi at pH 6.80) were prepared as described before<sup>16</sup> and contained 5% D<sub>2</sub>O for the lock signal. In standard titration experiments, the [pnp] was varied by step-wise addition of μl amounts of a 20 mM pnp stock solution made up in the NMR buffer. <sup>1</sup>H spectra were recorded at 600 MHz and 300 MHz and at 4 °C using a Bruker DMX-600 or DPX-300 spectrometer with the application of a 180°-τ-90°-t<sub>A</sub> super-WEFT pulse sequence<sup>29</sup>, an interpulse delay time of typically 55 ms and a 8 s<sup>-1</sup> repetition rate. Depending on the required signal-to-noise ratio, 4,000 to 64,000 free induction decays were recorded and Fourier transformed using exponential apodization and a 40-60 Hz line-broadening function to increase the signal-to-noise ratio. The spectra were baseline corrected in the program Mestre-C (Cobas, J.C., Cruces, J. and Sardina, F.J., Universidad de Santiago de Compostela, Spain) using its spline based semi-automatic fitting procedure. All spectra were calibrated on the water signal.

### NMR measurements of the bulk pnp signals.

T<sub>1</sub> values of pnp were measured by standard inversion recovery using at least 16 values for the interpulse delay time. After baseline correction, signal intensities were measured using peak areas. The R<sub>2</sub> values of the pnp <sup>1</sup>H or <sup>2</sup>D signals were determined from the resonance line-widths by line-shape simulation. The obtained line-widths were corrected for the contribution introduced by the LB function, after which the R<sub>2</sub> values were calculated from the relation  $R_2 = \pi\Delta\nu$  where Δν denotes the line-width at half-height. The T<sub>1</sub>, R<sub>2</sub> and signal shifts of the bulk pnp signals were corrected for the diamagnetic contribution, the latter being obtained by measuring the T<sub>1</sub>, R<sub>2</sub> and shift of the pnp bulk signals after reducing paramagnetic Ty<sub>met</sub> to diamagnetic Ty<sub>red</sub> with excess hydroxylamine<sup>13</sup> at the end of the titration experiment.

## Results

### Titration of native $Ty_{met}$ , $Ty_{met}F$ and $Ty_{met}Cl$ with p-nitrophenol followed by paramagnetic $^1H$ NMR.

*Titration of native  $Ty_{met}$ .* The paramagnetic  $^1H$  NMR spectrum of native  $Ty_{met}$  is characterized by several broad and partially overlapping signals between 50 and 13 ppm, which integrate to a signal intensity of  $18 \pm 2$  protons accounting for six coordinating His residues, each contributing three protons. Figure 1A shows  $^1H$  paramagnetic NMR spectra of a sample of 0.7 mM of the native  $Ty_{met}$  enzyme in the presence of increasing amounts of pnp from 0 to 1.77 mM at 4 °C and pH 6.8. As the [pnp] is increased, signals *a* and *c* appear to shift towards signal *b* at ~30 ppm, which is accompanied by severe line-broadening, while the remainder of the spectrum is much less sensitive to the presence of pnp. Signal *c* was previously assigned to a solvent exchangeable His  $N^\delta$  proton while signal *b* was attributed to two overlapping His  $C^\delta/C^\epsilon$  proton signals. The similarity in the behavior of these signals indicates that they correspond to the same His residue. Establishment of NOE connectivity between these signals was prevented by signal overlap, large signal linewidths and fast  $T_1$  relaxation of the native  $Ty_{met}$   $^1H$  signals. That signal *c* shifts downfield shows that the corresponding His residue is not detached upon pnp binding. In that case, an upfield shift towards the diamagnetic region of the spectrum would have been observed.

*Titration of fluoride bound  $Ty_{met}$ .* In the absence of pnp, the spectrum of the fluoride bound form of  $Ty_{met}$  ( $Ty_{met}F$ ) is much better resolved than the spectrum of native  $Ty_{met}$ . Six sharp solvent exchangeable signals have been identified before<sup>13</sup> and assigned to the coordinating His- $N^\delta$  protons (labelled *a-f* in Figure 1B), while the remaining broader signals were assigned to the His- $C^\epsilon$  and His- $C^\delta$  protons of the coordinating histidines. Under the experimental conditions (200 mM  $F^-$ , 4 °C, pH 6.8),  $Ty_{met}$  is fully saturated with fluoride ( $K_d$  3 mM<sup>13</sup>), while fluoride itself is in slow exchange on the NMR timescale ( $k_{off} < 12 \text{ s}^{-1}$ <sup>14</sup>).

Upon addition of pnp large changes in the paramagnetic  $^1H$  NMR spectrum of  $Ty_{met}F$  are observed, demonstrating the binding of pnp to the  $Ty_{met}F$  form. Throughout the spectrum, an increase in [pnp] induces signal shifts and severe line broadening. Since these changes occur gradually with increasing [pnp], the pnp exchange must be intermediate to fast on the NMR timescale. The large line-broadening observed upon pnp binding and the presence of signal overlap precluded a quantitative analysis of the linewidths as a function of [pnp].

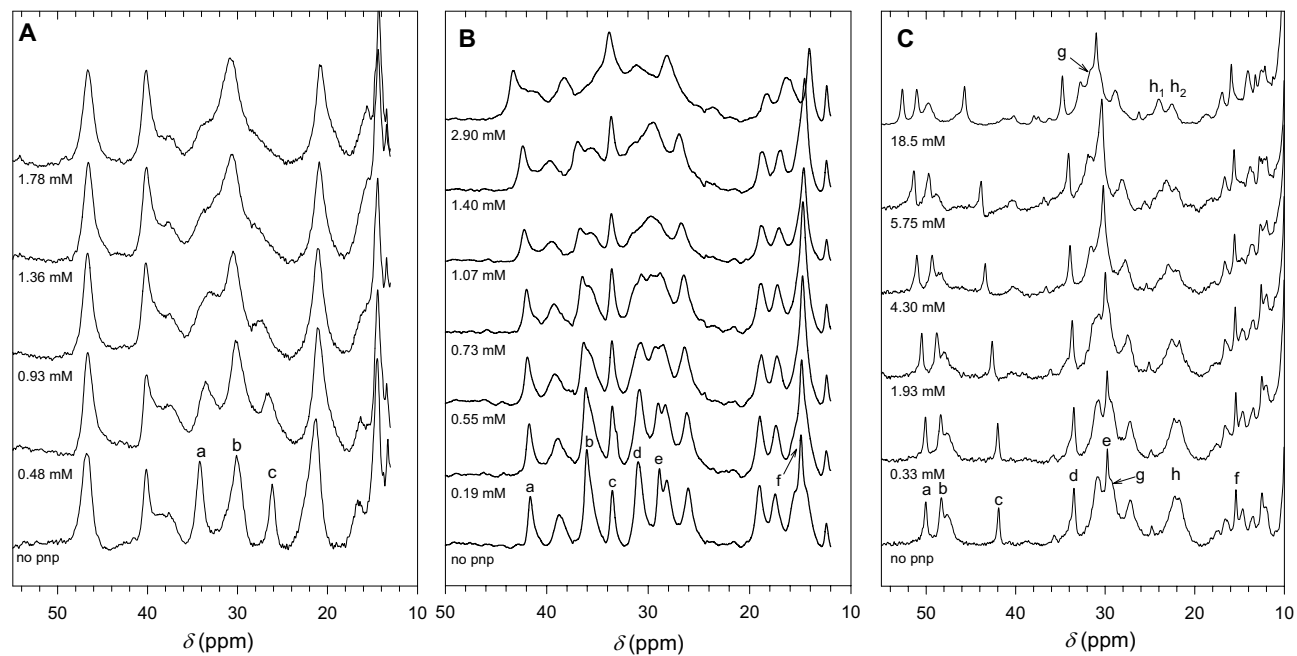


**Figure 1:** Titrations of (A) native  $\text{Ty}_{\text{met}}$ , (B) fluoride bound  $\text{Ty}_{\text{met}}\text{F}$  and (C) chloride bound  $\text{Ty}_{\text{met}}\text{Cl}$  followed by paramagnetic  $^1\text{H}$  NMR. Spectra in panels A and C were recorded at 600 MHz resonance frequency while the spectra in panel B were recorded at 300 MHz. In all cases,  $[\text{Ty}]$  was  $\sim 0.7$  mM in 100 mM Pi at pH 6.80 at 4  $^\circ\text{C}$ . The various  $[\text{pnp}]$  are indicated under each trace. See text for details and signal labelings.

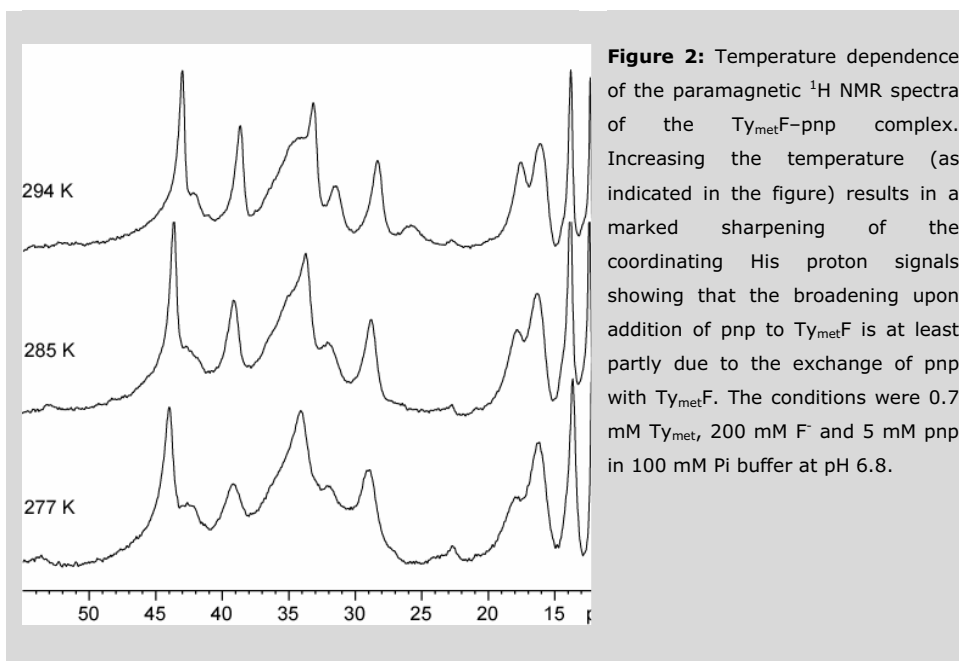
## Chapter 6

### Paramagnetic NMR studies of p-nitrophenol binding

For the majority of signals the amount of signal broadening appears related to the observed shift. For example, signals *c* and *f* shift by a relatively small amount and are still clearly observed at the highest [pnp] used in the titration, while signal *e* already shifts by a substantial amount at low [pnp] and seems to vanish completely upon further increase of [pnp]. This observation is compatible with exchange being the cause for the observed line-broadening. For signal *d* in Fig. 1B, no clear shift is observed while its intensity decreases with increasing [pnp]. This can be explained by assuming that this signal shifts by a relatively large amount in comparison to the other signals, causing it to be in slow exchange on the NMR timescale. An exchange contribution to the line-width is confirmed by a marked sharpening of the majority of the signals upon a relatively small increase in temperature (see Fig. 2).

For the majority of signals the amount of signal broadening appears related to the observed shift. For example, signals *c* and *f* shift by a relatively small amount and are still clearly observed at the highest [pnp] used in the titration, while signal *e* already shifts by a substantial amount at low [pnp] and seems to vanish completely upon further increase of [pnp]. This observation is compatible with exchange being the cause for the observed line-broadening. For signal *d* in Fig. 1B, no clear shift is observed while its intensity decreases with increasing [pnp]. This can be explained by assuming that this signal shifts by a relatively large amount in comparison to the other signals, causing it to be in slow exchange on the NMR timescale. An exchange contribution to the line-width is confirmed by a marked sharpening of the majority of the signals upon a relatively small increase in temperature (see Fig. 2).





*Titration of chloride bound  $\text{Ty}_{\text{met}}$ .* Figure 1C shows selected spectra of  $\text{Ty}_{\text{met}}\text{Cl}$  in the absence and in the presence of various amounts of pnp at 4 °C and pH 6.80. The spectra of 0 to 9.0 mM pnp were recorded during a standard titration experiment, while the spectrum containing 18.5 mM pnp was recorded on a different sample where  $\text{Ty}_{\text{met}}$  was concentrated in a buffer containing 18.5 mM pnp. In contrast with the pnp titrations of native  $\text{Ty}_{\text{met}}$  and  $\text{Ty}_{\text{met}}\text{F}$ , changes in the paramagnetic  $^1\text{H}$  spectrum of  $\text{Ty}_{\text{met}}\text{Cl}$  appear less drastic, while much higher concentrations of pnp are needed to produce significant changes. Little broadening is detected upon addition of pnp while all signals appear to gradually shift downfield with increasing [pnp], consistent with the pnp ligand being in fast exchange on the NMR timescale.

The absence of large broadening effects allowed us to accurately determine the signal positions of the 6 sharp  $\text{N}^{\text{e}}\text{H}$  signals as a function of [pnp]. The resulting  $\Delta\delta$  vs. [pnp] are presented in Fig. 3. Modest saturation is detected in the data even up to 18.5 mM pnp (close to the pnp solubility limit), indicating that the  $K_{\text{d}}$  for the  $\text{Ty}_{\text{met}}\text{Cl}$ -pnp complex is much higher than the  $\text{Ty}_{\text{met}}\text{Cl}$  concentration employed and justifying the use of the simple two-state ligand binding relation given by Equation 1:

$$\Delta\delta = \Delta\delta_{\text{max}} \cdot [\text{pnp}] / ([\text{pnp}] + K_{\text{d}}) \quad (\text{Equation 1})$$

where  $\Delta\delta_{\text{max}}$  represents the shift for the fully bound  $\text{Ty}_{\text{met}}\text{Cl}$ -pnp complex. Equation 1 was

## Chapter 6

### Paramagnetic NMR studies of p-nitrophenol binding

used to simultaneously fit all shift data in Fig. 3 where a value for  $\Delta\delta_{\max}$  was determined for each signal using a single value for the  $K_d$ . Setting the  $K_d$  as a shared parameter between all data sets during the fitting procedure allowed for accurate values to be determined, which are presented in Table 1.

From the  $\Delta\delta_{\max}$  values and the corresponding paramagnetic shifts of  $\text{Ty}_{\text{met}}\text{Cl}$  in the absence of pnp (assuming a diamagnetic shift of 8 ppm for all signals), we also calculated the fractional differences between the  $\text{Ty}_{\text{met}}\text{Cl}$  and the estimated  $\text{Ty}_{\text{met}}\text{Cl}$ -pnp shifts (see Table 1). Examination of these values shows that all signals (with the exception of signal *c*, see below) shift downfield by a relatively constant factor of 0.11-0.14 of the original shift upon the binding of pnp. This indicates that the singlet-triplet spacing parameter  $-2J$  decreases upon the binding of pnp, causing the fractional population of the paramagnetic  $S = 1$  level to increase and, as a consequence, causing the signals to shift farther downfield. The  $-2J$  value for  $\text{Ty}_{\text{met}}\text{Cl}$  of  $200 \text{ cm}^{-1}$ <sup>16</sup> corresponds to 17 % of spin in the triplet state at 4 °C.

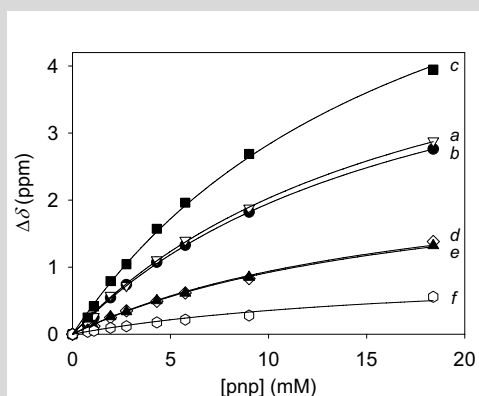


**Figure 3:** Paramagnetic shift differences  $\Delta\delta$  vs. [pnp] for the 6 sharp  $\text{Ty}_{\text{met}}\text{Cl}$   $\text{N}^{\text{H}}$  signals measured during a titration of  $\text{Ty}_{\text{met}}\text{Cl}$  with pnp. The trace labeling *a-f* corresponds to that in Fig. 1C. All data were simultaneously fit to Eq. 1 resulting in a single  $K_d$  value for the  $\text{Ty}_{\text{met}}\text{-pnp}$  complex ( $18 \pm 1 \text{ mM}$ ) and the  $\Delta\delta_{\max}$  values presented in Table 1.

Signal	$\delta_0$ (ppm)	$\Delta\delta_{\max}$ (ppm)	$\Delta\delta_{\max}/\delta_{0,p}$
<i>a</i>	50.04	5.5	0.13
<i>b</i>	48.32	5.7	0.14
<i>c</i>	41.89	7.9	0.23
<i>d</i>	33.48	2.7	0.11
<i>e</i>	29.76	2.6	0.12
<i>f</i>	15.39	1.0	0.13

**Table 1:** Shift differences ( $\Delta\delta_{\max}$ ) of the  $^1\text{H}$   $\text{N}^{\text{H}}$  signals between  $\text{Ty}_{\text{met}}\text{Cl}$  and the  $\text{Ty}_{\text{met}}\text{Cl}$ -pnp ternary complex. Values for  $\Delta\delta_{\max}$  were estimated on the basis of the data in Fig. 1C and Eq. 1 with a  $K_d$  value of 18.0 mM. The  $\delta_0$  values are the signal positions measured in the absence of pnp, while  $\delta_{0,p}$  represents the  $\delta_0$  value minus 8 ppm for the diamagnetic contribution to the observed shift.

To produce an average increase of 12 % in shift, the population of the paramagnetic  $S = 1$  level has to increase to 19 %, corresponding to a  $-2J$  value of  $150 \pm 10 \text{ cm}^{-1}$  for the  $\text{Ty}_{\text{met}}\text{Cl-pnp}$  ternary complex. A direct measurement of  $-2J$  for the ternary  $\text{Ty}_{\text{met}}\text{Cl-pnp}$  complex from the temperature dependence of paramagnetic  $^1\text{H}$  shifts is precluded by the temperature dependent equilibrium between free and pnp bound  $\text{Ty}_{\text{met}}\text{Cl}$  (affecting shifts) and the difficulty that  $\text{Ty}_{\text{met}}\text{Cl}$  cannot be saturated with pnp due to the high  $K_d$  and limited solubility of pnp. Since both the shifts and the linewidths are proportional to the fractional population of the paramagnetic  $S = 1$  level, a change in  $-2J$  should also be reflected in the linewidths. Indeed, for the signal *a*, for which the linewidth could be determined with reasonable accuracy, a broadening of around 10% is found for the fully bound form.

An exception to the observed trends is signal *c*, which shifts much more (by a fraction of 0.23) upon pnp binding. Since the shift is primarily contact in origin, a substantial change in the contact coupling parameter  $A$  must occur upon pnp binding. From previous work<sup>16</sup> it was established that the  $\text{N}^\delta\text{H}$  signal *c* shows NOE connectivity to signal *g*, which, therefore, belongs to the same His residue. Due to signal overlap, the position of signal *g* could not be determined precisely as a function of [pnp], but its position could be measured in the absence of pnp (29.26 ppm, see Fig. 1C) and in the presence of 18.5 mM pnp (31.72 ppm). By using the experimental  $K_d$  value of 18.0 mM and Eq. 1, it is estimated that  $\Delta\delta_{\text{max}}$  amounts to 4.85 ppm for signal *g*. Using this value to calculate the fractional increase in shift yields a value of 0.23, i.e. the same value as was found for the corresponding  $\text{N}^\delta\text{H}$  signal. Furthermore, signal *h* at 22.27 ppm in the absence of pnp consists of overlapping  $\text{C}^\delta\text{H}$  and  $\text{C}^\epsilon\text{H}$  signals. Upon addition of pnp, this signal becomes resolved and component  $h_1$  shifts to 24.05 ppm in the presence of 18.5 mM pnp. This difference in shift yields a fractional increase of 0.24, similar to signals *c* and *g*, suggesting that signal  $h_1$  originates from the same His residue. For signal  $h_2$  (assigned to a  $\text{C}^\epsilon\text{H}$  signal coupled to  $\text{N}^\epsilon\text{H}$  signal *e*<sup>16</sup>), a fractional increase in shift of 0.12 is calculated, which puts it in the same class as all the other signals.

Thus, similar to the situation of native  $\text{Ty}_{\text{met}}$ , the binding of pnp to  $\text{Ty}_{\text{met}}\text{Cl}$  apparently causes a change in coordination of one His residue while the remainder of the His residues seem to be less sensitive to the binding of pnp. Using the highest  $\Delta\delta_{\text{max}}$  value found (signal *c*, 7.9 ppm), and given that pnp is in fast exchange at 600 MHz on the NMR timescale, an upper limit of the exchange time  $\tau_M$  can be estimated as  $\tau_M < 7 \cdot 10^{-5} \text{ s}$ .

**NMR of the pnp signals in the bulk solution.**

*Protonated pnp.* The observation that the pnp ligand appears to be in fast exchange with native Ty<sub>met</sub> on the NMR time-scale, as well as the absence of signals originating from the bound nitrophenol in the paramagnetic <sup>1</sup>H Ty<sub>met</sub> spectra (not shown), prompted us to investigate the <sup>1</sup>H NMR signals of the pnp in the bulk. In general, the shift and relaxation parameters of a free ligand in the bulk solution are a function of the molar fraction of ligand bound at the paramagnetic center ( $f_M$ ), the lifetime of the ligand in the metal-bound state ( $\tau_M$ ), as well as of the paramagnetic shift ( $\Delta\omega_M$  in rad·s<sup>-1</sup>) and the paramagnetic  $R_{1M}$  and  $R_{2M}$  relaxation rates of the metal-bound ligand resonances<sup>30</sup>. Thus, providing that exchange is sufficiently fast, the NMR signals of the ligand in the bulk solution contain information on the ligand bound to the protein.

The equations for the observed paramagnetic contributions to the chemical shift and the transversal and longitudinal relaxation rates (for all exchange conditions) are given by<sup>22</sup>:

$$\Delta\omega_p = \frac{f_M}{\tau_M} \cdot \frac{\Delta\omega_M}{(R_{2M} + \tau_M^{-1})^2 + \Delta\omega_M^2} = f_M \Delta\omega_M^{\text{app}} \quad (\text{Equation 2})$$

$$R_{2p} = \frac{f_M}{\tau_M} \cdot \frac{R_{2M}^2 + R_{2M}\tau_M^{-1} + \Delta\omega_M^2}{(R_{2M} + \tau_M^{-1})^2 + \Delta\omega_M^2} = f_M R_{2M}^{\text{app}} \quad (\text{Equation 3})$$

$$R_{1p} = f_M (T_{1M} + \tau_M)^{-1} = f_M R_{1M}^{\text{app}} \quad (\text{Equation 4})$$

where  $\Delta\omega_p$ ,  $R_{2p}$  ( $= T_{2p}^{-1}$ ) and  $R_{1p}$  ( $= T_{1p}^{-1}$ ) are the paramagnetic contributions to the shift (in rad·s<sup>-1</sup>), the  $R_2$  (in Hz) and the  $R_1$  (in Hz) of the bulk ligand, respectively. When a solution of Ty is titrated with a solution of pnp, both the pnp and Ty concentrations change during the experiment. To facilitate interpretation of the data it is convenient to express  $f_M$  in terms of  $R$ , defined as the ratio between the total pnp and Ty concentrations, as given by Equation 5.

$$f_M^{-1} = R + \frac{K_d R}{\text{pnp}_0} + \frac{K_d}{\text{Ty}_0} \quad (\text{Equation 5})$$

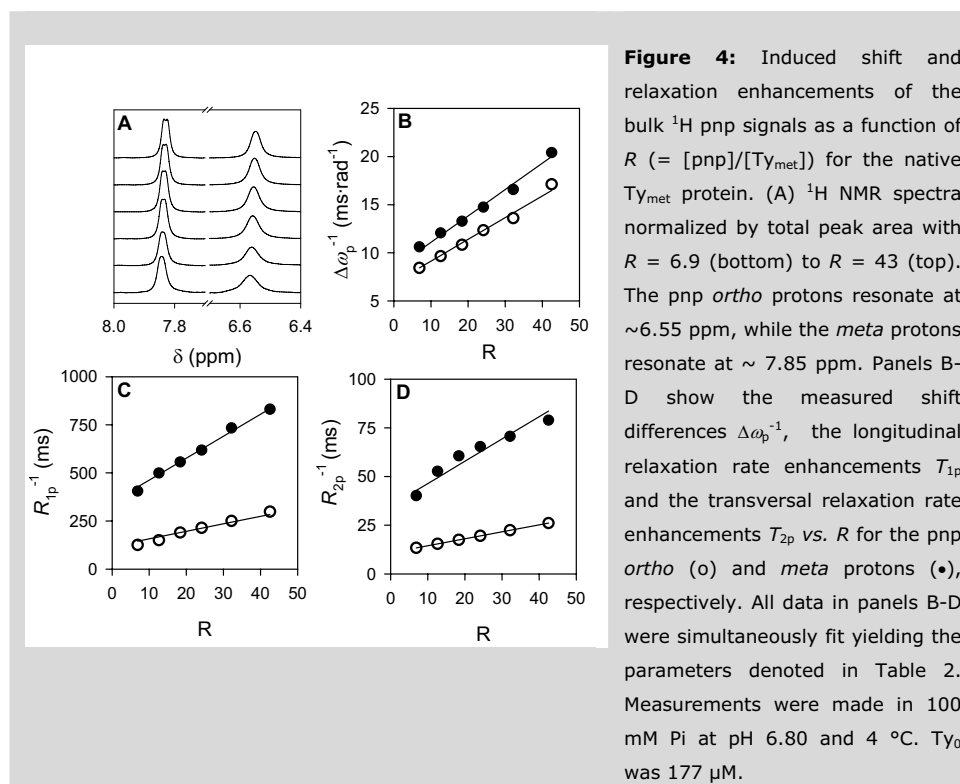
The latter equation is valid provided that  $R \gg 1$ .  $\text{Ty}_0$  represents the Ty<sub>met</sub> at the start of the experiment and  $\text{pnp}_0$  represents the [pnp] in the added stock solution. The values for the  $R_{2p}^{-1}$ ,  $R_{1p}^{-1}$  and  $\Delta\omega_p^{-1}$  of the pnp *ortho* and *meta* proton signals have been determined as a function of  $R$  in 100 mM Pi buffer at pH 6.80 and 279 K by <sup>1</sup>H NMR titration experiments. Selected spectra recorded in an experiment where a 174 μM solution of Ty<sub>met</sub> was titrated with a 18 mM solution of pnp are shown in Fig. 4A. In absence of Ty<sub>met</sub>,

## Chapter 6

### Paramagnetic NMR studies of p-nitrophenol binding

the two equivalent *ortho* protons resonate at 6.53 ppm, while the two equivalent *meta* protons give rise to the signal at 7.82 ppm. Apart from the pnp resonances, no other signals become detectable even after prolonged incubation of pnp with large amounts of enzyme, showing that pnp does not react with Ty under the experimental conditions. The presence of Ty<sub>met</sub> induces broadening of the *ortho* and *meta* pnp protons, the broadening of the former being the largest. The experimental values of  $R_{1p}^{-1}$ ,  $R_{2p}^{-1}$  and  $\Delta\omega_p^{-1}$  as a function of  $R$  are presented in fig 4B-4D.

According to Eqs. 2-4,  $R_{2p}^{-1}$ ,  $R_{1p}^{-1}$  and  $\Delta\omega_p^{-1}$  are directly proportional to  $f_M^{-1}$ , meaning that the dependence of  $R_{2p}^{-1}$ ,  $R_{1p}^{-1}$  and  $\Delta\omega_p^{-1}$  on  $R$  allows for estimation of the dissociation constant  $K_d$  and  $R_{2M}^{app}$ ,  $R_{1M}^{app}$  and  $\Delta\omega_M^{app}$ . Accordingly, the data in Fig. 4B-4D were simultaneously fitted to Equations 2-4 where  $K_d$  was set as a global parameter for all datasets. Equal weight was given to all data. Good fits were obtained, in accordance with the binding of a single pnp per Ty<sub>met</sub> molecule and confirming that the observed changes in  $R_{2p}$ ,  $R_{1p}$  and  $\Delta\omega_p$  relate to one and the same exchange process. The determined parameters are listed in Table 2 (with  $\Delta\omega_M^{app}$  presented as  $\Delta\delta_M^{app}$  in ppm).



The titration was repeated for fluoride bound  $Ty_{met}$  where 200 mM  $F^-$  was present in both the  $Ty_{met}$  and pnp stock solutions. The overall behaviour was found to be remarkably similar to that observed for native  $Ty_{met}$  (not shown). The determined parameters for the  $Ty_{met}F$  pnp binding are presented in Table 2 and do not differ significantly from the parameters determined for native  $Ty_{met}$ .

**Table 2:** pnp dissociation constants  $K_d$  and values for  $T_{1M}^{app}$ ,  $R_{2M}^{app}$  and  $\Delta\omega_p^{app}$  (expressed as  $\delta_M^{app}$  in ppm units) determined from the data presented in Fig. 4. Standard errors are less than 20% for all parameters.

Species	$K_d$ pnp (mM)	pnp protons	$T_{1M}^{app}$ (ms)	$R_{2M}^{app}$ (kHz)	$\delta_M^{app}$ (ppm)
Native $Ty_{met}$	7.2	<i>meta</i>	8.4	1.2	1.3
		<i>ortho</i>	2.8	3.8	1.6
$Ty_{met}F$	6.2	<i>meta</i>	8.0	1.5	1.5
		<i>ortho</i>	3.6	4.5	2.0

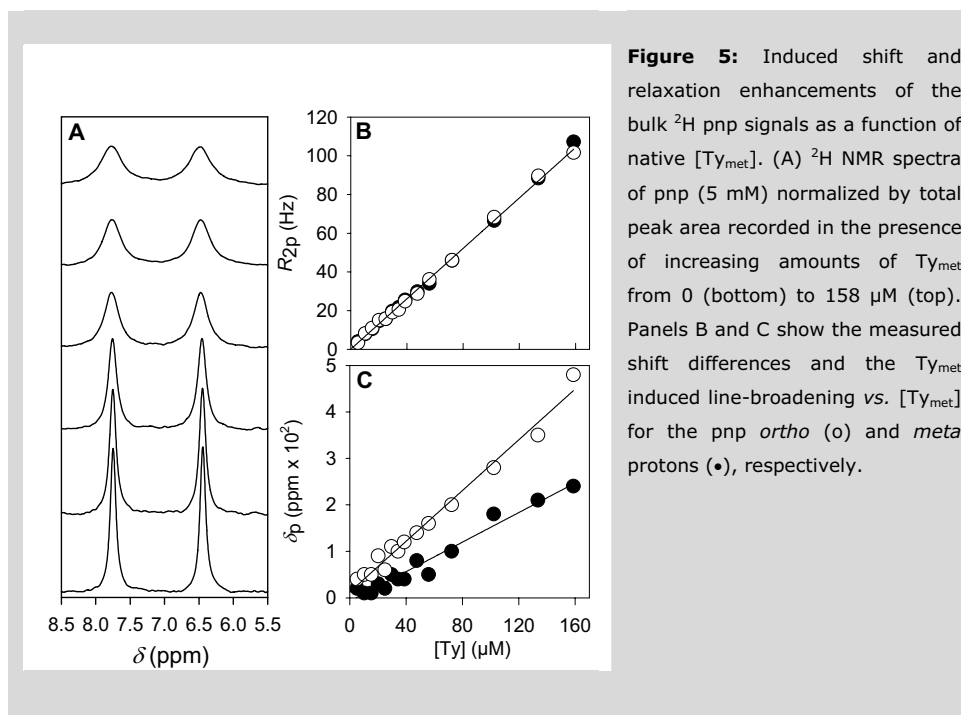
Since the  $T_{1M}^{app}$  is a simple function of  $\tau_M$  and  $T_{1M}$  (Eq. 4), the different  $T_{1M}^{app}$  values determined for the pnp *ortho* and *meta* proton signals immediately demonstrate that the exchange contribution to  $T_{1p}$  is dominated by the  $T_{1M}$  term in Eq. 4. Thus, the experimental  $T_{1M}^{app}$  values closely correspond to the paramagnetic  $T_{1M}$  relaxation times of the pnp protons when bound to  $Ty_{met}$  and  $\tau_M$  must be smaller than the shortest  $T_{1M}^{app}$  determined, i.e.  $\tau_M < 3 \cdot 10^{-3}$  s, for both native  $Ty_{met}$  and  $Ty_{met}F$ . According to Eqs. 2 and 3, the  $T_{2M}^{app}$  and  $\Delta\omega_M^{app}$  are complex functions of  $R_{2M}$ ,  $\Delta\omega_M$  and  $\tau_M$ , each of which is not known explicitly and cannot be solved from the data presented in Fig. 4B-4D. It is therefore impossible to state whether the calculated values for  $R_{2M}^{app}$  and  $\delta_M^{app}$  in Table 2 correspond to  $R_{2M}$  and  $\delta_M$  (i.e.  $\Delta\omega_M$ ) values in Eqs. 2-4 without further knowledge of the exchange conditions.

*Deuterated pnp.* To obtain insight in the exchange conditions, the shift and broadening parameters of the  $^2D$  signals of completely deuterated pnp were determined as a function of  $[Ty_{met}]$ . While the absolute shifts (in ppm) of the two pnp signals in the fully  $Ty_{met}$  bound form are the same for  $^1H$  and  $^2D$  pnp, the  $\Delta\omega_M$  in Eqs. 2 and 3 is proportional to the gyromagnetic ratio of the nucleus under investigation and, as a consequence, the  $^2D$   $\Delta\omega_M$  amounts to 0.152 the  $^1H$   $\Delta\omega_M$ . When  $R_{2M} < \Delta\omega_M$  and  $\tau_M^{-1} \ll \Delta\omega_M$  (slow exchange), Eq. 2 simplifies to  $\Delta\omega_p \approx f_M / \tau_M^2 \Delta\omega_M$ . This means that the shifts of the bulk pnp signals for the protonated and deuterated pnp obey the relation  $\Delta\omega_M^H / \Delta\omega_M^D = \Delta\omega_p^D / \Delta\omega_p^H$ . Therefore, towards the slow exchange limit, the observed  $^2D$  shift measured in ppm amounts to 44 times the  $^1H$  shift. For fast exchange ( $\tau_M^{-1} \gg \Delta\omega_M$ ), on the other hand, equal shifts (in ppm) are expected for both  $^1H$  and  $^2D$ .

Figure 5A shows selected  $^2\text{D}$  spectra recorded during a titration of deuterated pnp with native  $\text{Ty}_{\text{met}}$  where [pnp] was kept constant at 5 mM throughout the experiment. All spectra were recorded at 4 °C in 100 mM Pi buffer at pH 6.80 at 92.124 MHz resonance frequency. As in the case of  $^1\text{H}$  pnp, small shifts are observed for both  $^2\text{D}$  signals (Fig. 5A). The measured shift is the largest for the pnp *ortho* protons next to the hydroxyl group. The measured shifts vs.  $[\text{Ty}_{\text{met}}]$  are plotted in Fig. 5C. The data were fit to a linear function and from the corresponding slopes and the  $K_{\text{d}}$  of 7.2 mM (table 2), it is estimated that the  $\delta_{\text{M}}^{\text{app}}$  in the fully  $\text{Ty}_{\text{met}}$  bound form amount to 3.3 and 1.9 ppm for the *ortho* and *meta* deuterons, respectively. For the *ortho* position, the  $^2\text{D}$   $\delta_{\text{M}}^{\text{app}}$  is about twice the  $^1\text{H}$   $\delta_{\text{M}}^{\text{app}}$ , while the  $^2\text{D}/^1\text{H}$   $\delta_{\text{M}}^{\text{app}}$  ratio is  $\pm 1.5$  for the *meta* position. These relatively small ratios, together with the observation that a larger ratio is measured for the protons with the larger  $\delta_{\text{M}}^{\text{app}}$ , indicate that the pnp is in the fast (for  $^2\text{D}$ ) to intermediate (for  $^1\text{H}$ ) exchange regime on the NMR time-scale. Thus, the estimated pnp  $^2\text{D}$   $\delta_{\text{M}}^{\text{app}}$  should equal the paramagnetic shifts,  $\delta_{\text{M}}$ , in the fully bound  $\text{Ty}_{\text{met}}$  form.

As for the relaxation rates, the paramagnetic  $R_{2\text{M}}$  scales with the square of the nuclear gyromagnetic ratio, meaning that the  $^2\text{D}$   $T_{2\text{M}}$  should be 44 times that of the  $^1\text{H}$   $T_{2\text{M}}$ . An evaluation of the  $^2\text{D}$   $T_{2\text{M}}^{\text{app}}$  values, however, should also include the quadrupolar relaxation contribution that depends on the rotational correlation time  $\tau_{\text{R}}$  and may dominate the  $T_2$  when the ligand is bound to a protein with slow molecular tumbling.

With increasing  $[\text{Ty}_{\text{met}}]$ , severe broadening of the  $^2\text{D}$  signals is observed where the broadening is equal, within the experimental error, for both the pnp *ortho* and *meta* deuterons. Linewidths were measured by lineshape fitting and the resulting  $R_{2\text{p}}$  values vs.  $[\text{Ty}_{\text{met}}]$  are presented in Fig. 5B. From the slope of a linear fit to the data and the experimental  $K_{\text{d}}$  of 7.2 mM, the  $R_{2\text{M}}^{\text{app}}$  values for the  $^2\text{D}$  signals are estimated at 7.9 kHz for both the *ortho* and *meta* deuterons. Comparison of this value with the values measured for  $^1\text{H}$  (table 2) shows that the broadening is larger in the case of  $^2\text{D}$ , meaning that the quadrupolar relaxation significantly contributes to the observed linewidth. The quadrupolar relaxation scales with the square of the quadrupolar coupling constant, which amounts to 193 kHz for the aromatic deuterons of toluene and benzene<sup>31</sup>. Furthermore, the quadrupolar  $R_2$  depends on the rotational correlation time  $\tau_{\text{r}}$ , which amounts to 15 – 20 ns for a 31 kD protein at 4 °C<sup>32</sup>. With these values, a quadrupolar  $R_2$  between 5 and 7 kHz is calculated<sup>33</sup>, which accounts for most of the experimental  $^2\text{D}$   $R_{2\text{M}}^{\text{app}}$ . Factorising out the quadrupolar relaxation contribution from the observed linewidths would require knowledge of the exact value of  $\tau_{\text{r}}$  and the quadrupolar coupling constant. From the  $^2\text{D}$   $\delta_{\text{M}}$ , the  $^1\text{H}$   $R_{2\text{M}}^{\text{app}}$ , the  $^1\text{H}$   $\delta_{\text{M}}^{\text{app}}$  values (table 2) and Equations 2 and 3, it is now possible to estimate the lifetime of the pnp- $\text{Ty}_{\text{met}}$  complex  $\tau_{\text{M}}$  yielding a value of  $7 \cdot 10^{-5}$  sec.



## Discussion

### Nitrophenol does not occupy the Cu-X-Cu bridging position.

The experiments in which  $\text{Ty}_{\text{met}}\text{F}$  and  $\text{Ty}_{\text{met}}\text{Cl}$  were titrated with pnp demonstrate that a ternary  $\text{Ty}_{\text{met}}$ -halide-pnp complex is formed. It was previously demonstrated that halides bind at the bridging position between the two Cu(II) ions, replacing the bridging hydroxide in native  $\text{Ty}_{\text{met}}$ <sup>13;14</sup>. The pnp must therefore bind at a site other than the bridging position. Furthermore, the values for the dissociation constant  $K_d$ , as well as the values for the paramagnetic shift and relaxation times of the  $\text{Ty}_{\text{met}}$  bound pnp protons (see below) do not strongly differ between native and fluoride bound  $\text{Ty}_{\text{met}}$ . This shows that the presence of fluoride in the active site does not markedly influence the binding of pnp, compatible with different binding sites for fluoride and pnp.

The dissociation constant increases to 18 mM in the case of  $\text{Ty}_{\text{met}}\text{Cl}$ . Little broadening is detected for the paramagnetically affected signals of  $\text{Ty}_{\text{met}}\text{Cl}$  upon pnp binding, demonstrating that pnp is in fast exchange on the NMR timescale ( $\tau_M < 7 \cdot 10^{-5}$  s), contrary to the case of  $\text{Ty}_{\text{met}}\text{F}$  where pnp exchange is slower. Thus, the higher  $K_d$  measured for the  $\text{Ty}_{\text{met}}\text{Cl}$ -pnp complex is at least partly due to a larger pnp off rate, possibly related to steric



hindrance by the larger chloride ion.

In previous studies on  $Ty_{\text{half-met}}$ , it was found that a signal assigned to an equatorial hydroxide or water molecule is lost upon pnp binding, while the Cu(II) remains 4-coordinate (3N/1O). It was concluded that the phenolic hydroxyl displaces the hydroxide or water ligand from the paramagnetic Cu(II) ion. The reasons for the different behaviour observed in  $Ty_{\text{met}}$  and  $Ty_{\text{half-met}}$  are unclear but may reflect, for example, a more spacious active site or a weaker binding of the equatorial OH/H<sub>2</sub>O ligand in  $Ty_{\text{half-met}}$ , rendering this ligand more prone to dissociation.

#### The binding of pnp weakens antiferromagnetic coupling in $Ty_{\text{met}}\text{Cl}$ .

In  $Ty_{\text{met}}\text{Cl}$ , pnp binding causes a decrease in the antiferromagnetic exchange coupling parameter  $-2J$  from 200 to 150  $\text{cm}^{-1}$ , meaning that the two Cu(II) ions become less strongly coupled. Variations in  $-2J$  in bridged dinuclear Cu systems have been explained in terms of changes in the Cu-X-Cu bridging angle, smaller angles inducing stronger couplings (e.g. <sup>34,35</sup>). A correlation between the  $-2J$  value and the size of the bridging ion has been observed for the halide complexes of  $Ty_{\text{met}}$  ( $Ty_{\text{met}}\text{F}$  ( $-2J$  260  $\text{cm}^{-1}$ ) >  $Ty_{\text{met}}\text{Cl}$  ( $-2J$  200  $\text{cm}^{-1}$ ) >  $Ty_{\text{met}}\text{Br}$  ( $-2J$  160  $\text{cm}^{-1}$ ); Chapter 5). The lower  $-2J$  value for the  $Ty_{\text{met}}\text{Cl}$ -pnp complex may therefore reflect a decrease in the Cu-Cl-Cu bridging angle connected with an decrease in Cu-Cu distance.

For native  $Ty_{\text{met}}$ , there are no systematic upfield or downfield shifts of the paramagnetically shifted signals observed upon pnp binding and no change in  $-2J$  had to be invoked to explain the changes in the paramagnetic <sup>1</sup>H NMR spectra. However, the  $-2J$  value of 77  $\text{cm}^{-1}$  estimated for the native species <sup>16</sup> is much lower than  $k_{\text{B}}T$  ( $\sim 200 \text{ cm}^{-1}$ ), meaning that the paramagnetic triplet state is close to full population at ambient temperatures. So, a further decrease in  $-2J$  will not significantly alter the fractional population of the triplet state and, consequently, the magnitude of the hyperfine shifts.

#### The binding of p-nitrophenol affects only one His residue.

In the absence of a structural model of Ty, it is customary to use CO <sup>10</sup> and Hc <sup>6-9</sup> structures as models for Ty. An all-atom rmsd minimised superposition of the active sites of CO<sub>met</sub> (pdb 1BT3) and phenylthiourea (PTU) bound CO<sub>met</sub> (pdb 1BUG) is depicted in Fig. 6. Apart from a larger Cu-Cu distance found in the PTU bound CO<sub>met</sub>, the structures superimpose well and the positions of 5 of the 6 coordinating His residues remain nearly unchanged upon PTU binding. The interaction with CuB however induces a displacement of His244, while the PTU aromatic ring acquires a  $\pi$ - $\pi$  interaction with the same His residue. The CuB goes from distorted tetrahedral in the native met form to almost

perfectly trigonal bipyramidal in the PTU bound form<sup>10</sup> with His240, His244 and the PTU sulfur atom in the equatorial plane and His274 and the PTU nitrogen atom in the two axial positions. In our case, it appears that one His residue is particularly sensitive to the binding of pnp in native  $Ty_{met}$  and  $Ty_{met}Cl$ . Thus, signals *b* and *c* for native  $Ty_{met}$  (Fig. 1A) and signals *c*, *g* and *h*<sub>1</sub> for  $Ty_{met}Cl$  (Fig. 1C) may well correspond to a His similar to His244 in  $CO_{met}$ .

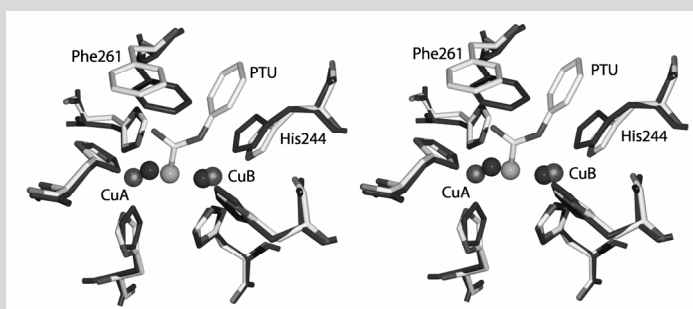


**Figure 6:** Stereo view of a superposition of the type-3 center of sweet potato catechol oxidase in the native oxidized form (dark grey; PDB entry 1BT1) and with PTU bound (CPK color coding; PDB entry 1BUG). Upon binding of PTU, His244 and Phe261 are displaced while CuB adopts a trigonal bipyramidal coordination geometry. The position of the PTU aromatic ring is fixed by Phe261. The copper ions and the Cu<sub>2</sub> bridging sulfur atom of PTU are shown as spheres (with arbitrary radii). The overlay was generated using the all-atom least square superimposition fitting algorithm implemented in the Swiss-PBD Viewer program. Hydrogen atoms of coordinating His residues are omitted for clarity.

### The p-nitrophenol is coordinated to the type-3 copper.

From the <sup>1</sup>H/<sup>2</sup>D titration experiments, it was found that the pnp is in fast exchange on the <sup>2</sup>D NMR timescale. The shift differences  $\delta_M$  between free pnp and pnp in the  $Ty_{met}$  bound form amount to 3.3 ppm (*ortho*) and 1.9 ppm (*meta*). Since the paramagnetic shifts are dominated by the contact contribution in  $Ty_{met}$ <sup>16</sup>, the non-zero  $\delta_M$  values are consistent with direct coordination of pnp to the metal centre.

A comparison of the experimental  $\delta_M$  values with the paramagnetic shifts of the coordinating histidines indicates that the contact couplings of the pnp ring protons are weak. This is because the pnp protons are one bond further away from Cu than their His imidazole counterparts. A similar observation has been reported for several small dinuclear Cu<sub>2</sub> complexes where the signal shifts of the Cu<sub>2</sub> bridging phenolate ring protons are smaller than the shifts of the signals from the coordinating imidazole or pyridyl protons<sup>18;19;36</sup>.

**Structural model of pnp binding.**

The longitudinal relaxation times ( $T_{1M}$ ) for the *ortho* and *meta* ring protons of pnp bound to native Ty<sub>met</sub> and Ty<sub>met</sub>F (table 2) do not differ much and will be discussed together. They are dominated by the dipolar contribution<sup>16</sup>, which is proportional to the inverse sixth-power of the distance  $r$  between the resonating nucleus and the paramagnetic centre. This, in principle, allows for the calculation of H-Cu distances. However, since the paramagnetism is spread over the whole unpaired spin wavefunction, a quantitative evaluation of dipolar  $T_1$ s requires the integration of the dipolar interaction over the total wavefunction. The latter is not available. Therefore, a simplified model for the spin distribution allowing for a semi-quantitative analysis will be used.

First it should be noted that the  $T_1$  values found for the pnp *ortho* protons are smaller than for the *meta* protons, in line with the hydroxylic moiety being oriented towards the active site Cu and the *ortho* protons being closer to Cu than the *meta* protons. Furthermore, the experimental  $T_{1M}$  values for the pnp *ortho* protons (table 2) are similar to those of the His-C<sup>δ</sup>H and His-C<sup>ε</sup>H protons, which are located at ~3.4 Å from Cu ( $T_1 \sim 3 \text{ ms}^{16}$ ) in native Ty<sub>met</sub> and Ty<sub>met</sub>F. This is compatible with a Cu-H distance of 3-4 Å for the pnp *ortho* protons, again consistent with pnp coordination to Cu through the phenolic hydroxyl group.

For a semi-quantitative analysis, a model is used in which single magnetic point dipoles are placed on the two Cu atoms. Keeping in mind that there are two *ortho* and two *meta* protons and that the measured  $T_1$ s are the averages both for the *meta* ( $T_{1m}$ ) and for the *ortho* ( $T_{1o}$ ) protons, the  $T_{1m}/T_{1o}$  ratio is given by:

$$\frac{T_{1m}}{T_{1o}} = \frac{\sum_{i,j} r_{m_i-Cu_j}^{-6}}{\sum_{i,j} r_{o_i-Cu_j}^{-6}} \quad (\text{Equation 9})$$

with  $i,j = 1$  and  $2$ . The experimental  $T_{1m}/T_{1o}$  ratios are ~3 and ~2 for pnp bound to native Ty<sub>met</sub> and Ty<sub>met</sub>F, respectively.

As a starting configuration for the semi-quantitative analysis, the CO<sub>met</sub> with bound PTU was taken, in which the PTU was replaced with phenol without adjusting the position of the aromatic ring. Subsequently, the phenol was moved along its long axis until the CuB-O distance amounted to 1.9 Å<sup>37</sup>. The Cu-Cu distance was set at 2.9 Å as in CO<sub>met</sub>. This configuration yields a  $T_{1m}/T_{1o}$  ratio of 13 (Eq. 9), which corresponds badly to the experimental ratio of 2-3. The situation could not be improved by allowing the aromatic ring to move in its original plane and/or to rotate around the Ar-O bond. A lower  $T_{1m}/T_{1o}$

ratio could only be achieved by allowing the aromatic ring to tilt towards CuA (see Fig. 7). The particular structure drawn in Fig. 7 does not result in steric clashes with any of the coordinating His residues and has a calculated  $T_{1m}/T_{1o}$  ratio of 3.5, which brings it within the bandwidth of the experiment considering the simplicity of the model used for the calculation. For the drawn configuration, the Cu-O-Ar angle is  $114^\circ$ , which is similar to the Cu-O-Ar angle of  $127^\circ$  for the tyrosine coordinated to Cu in galactose oxidase<sup>37</sup>. We note that this ensures maximum overlap between the oxygen lone pair of the phenolic hydroxyl group and the copper  $d_z^2$  orbitals (the Cu  $d_{x^2-y^2}$  orbitals being oriented in the Cu-X-Cu equatorial plane<sup>25</sup>). Furthermore, the coordination geometry of the phenol in Fig. 7 would be compatible with the proposed binding mode of diphenolic substrates in  $Ty_{met}$  13:47;49

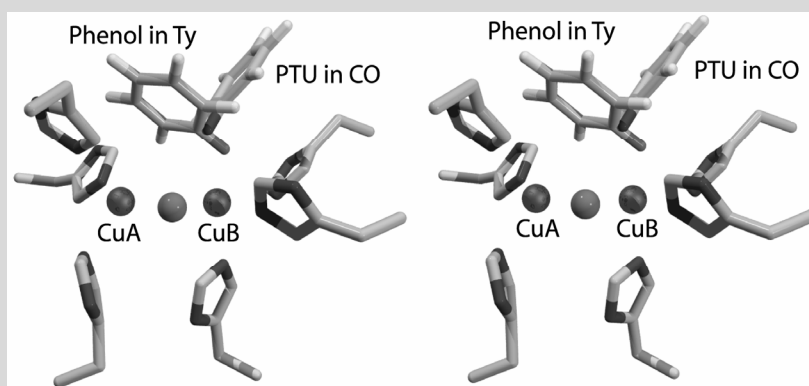


**Figure 7:** Model of phenol coordination to the oxidized tyrosinase type-3 center. The drawn structure is based on the X-ray structures of oxidised sweet potato catechol oxidase (1BT1 and 1PTU) and explains the presented NMR data of pnp binding to  $Ty_{met}$  (see text for details). The position of PTU in catechol oxidase is fixed in place by Phe261 (as shown in Fig. 6). In Ty, instead, the *ortho* protons of the bound phenol can approach the  $Cu_2$  bridging peroxide present in oxygenated Ty because there is no aromatic residue at the equivalent position in Ty. Both the copper ions and the bridging atom (= OH<sup>-</sup>, F<sup>-</sup>, Cl<sup>-</sup>) are presented by spheres (with arbitrary radii). Only the aromatic ring and coordinating O or N atom are shown for the bound pnp and PTU, respectively. The hydrogen atoms of coordinating His residues are omitted for clarity.

### Mechanistic implications.

While the present study has addressed the binding of monophenols to  $Ty_{met}$ , the mechanistically relevant complex is that between monophenols and  $Ty_{oxy}$ . Monophenol binding to  $Ty_{met}$  results in a dead-end complex. Still, the present results may be relevant for a better understanding of the interaction of  $Ty_{oxy}$  with phenols. It has been observed that the active site His residues in oxidised and oxygenated *Limulus* Hc nearly exactly

superimpose (rmsd 0.20 Å). This supports the idea that the positions of the His ligands need not be largely different for the oxy and the met forms of a type-3 Cu centre. The recognition of exogenous substrates, therefore, need not differ either between the oxy and met forms.

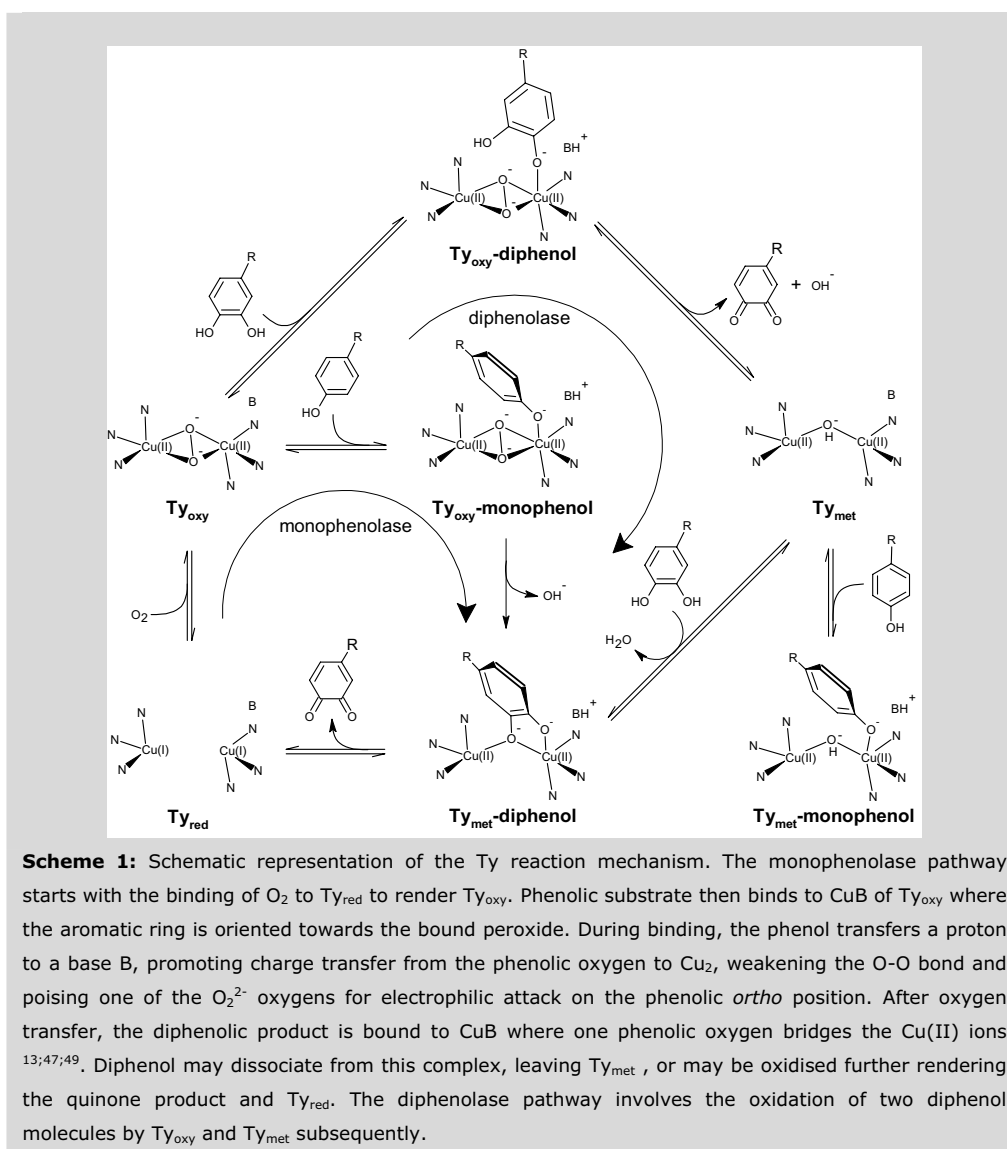
From spectroscopic evidence it has been concluded that there is a 3 His coordination around each Cu in Ty<sub>oxy</sub><sup>38</sup>. The current results demonstrate that all six His ligands remain bound to the Cu<sub>2</sub> site upon pnp binding to Ty<sub>met</sub>. These results are at variance with suggestions that the Ty active site only contains five His ligands or that a sixth His ligand, if present, detaches from Cu upon phenol binding<sup>39</sup>.

There has been considerable debate regarding the origins of the different activities of Hcs, COs and Tys. It is generally believed that these originate from variations in protein structure that modulate the accessibility of substrates to the type-3 center. For example, in octopus Hc, a capping domain is present that shields the type-3 site from the access of potential substrates. A homologous domain is found in a latent form of CO, which inhibits CO activity<sup>40</sup>. Indeed, proteolytic removal of the capping domain from octopus Hc<sup>41</sup> induces weak phenolase activity, while several Hcs show diphenolase activity upon mild denaturation<sup>42-44</sup>. To explain the absence of monophenolase activity in COs, it is been suggested that in Ty phenolic substrates interact with CuA<sup>11;42;45;46</sup>, while diphenolic substrates would interact with CuB. Access to CuA in CO would be blocked by Phe261, leaving CO with diphenolase activity only<sup>42;46</sup>. For *S. antibioticus* Ty, however, experimental data suggest that pnp and bidentate inhibitors both interact with CuB<sup>47</sup>.

The present and previous<sup>47</sup> results are consistent with pnp binding to CuB, where the pnp aromatic ring is tilted towards the non-coordinating CuA as depicted in Fig. 7. In this orientation, one of the *ortho* protons of the phenolic ring would be oriented towards the bound peroxide in Ty<sub>oxy</sub>, a prerequisite for efficient oxygen atom transfer. In contrast, the PTU aromatic ring is tightly held in place by Phe261 in CO<sub>met</sub>, preventing a similar orientation of the aromatic ring and precluding a direct approach of the aromatic *ortho* protons towards the bound peroxide. An aa sequence alignment of various Hcs, Tys and COs<sup>1;5;48</sup> shows that a Phe analogous to Phe261 in CO is absent in Tys. We, therefore, suggest that the difference in the monophenolase activity between Ty and CO is due the blocking activity of Phe261 in CO, preventing a direct approach of the substrate to the bound peroxide.

The presented and previous results allow for the proposal of a reaction mechanism as outlined in Scheme 1 (see scheme legend for details), which includes some extensions of previous proposals (e.g.<sup>11;23;45</sup>). The modifications include: 1) phenol coordinates to CuB

in an orientation allowing for oxygen transfer to the phenolic *ortho* position; 2) the diphenol coordinates to CuB in  $Ty_{met}$  where one of the phenolic oxygens bridges the two Cu ions<sup>13;47;49</sup>; 3) Proton transfer from a phenolic hydroxyl to the  $Cu_2$  bridging  $OH^-$  ion assists in diphenol binding to  $Ty_{met}$ <sup>14</sup>. 4) A second base assists in the deprotonation of both monophenolic and diphenolic substrates.



In the proposed reaction scheme, the total charge of the complex cycles between +3 and +2 during all stages of the mechanism, which limits both destabilising fluctuations in net

charge and in the flux of protons from and to the Cu<sub>2</sub> center. From the structure of CO and from sequence homology, a role for proton uptake has been suggested for a conserved Glu residue that is present in the CuB site of most COs and Tys<sup>50</sup>. In this regard, we add that in all Tys and COs a conserved non-coordinating His residue is present that is sequentially positioned directly adjacent to a His residue coordinating equatorially to CuB (His274 in sweet potato CO) making this residue another possible candidate as the proton acceptor. The imidazole ring of this (buried) His residue is in direct contact with the imidazole group of His244 that interacts with the bound substrate in CO.

## Conclusion

We have presented a paramagnetic NMR study of the interaction between the monophenolic inhibitor *p*-nitrophenol (pnp) and the oxidised form of *Streptomyces antibioticus* tyrosinase (Ty) in its native and halide bound forms. The study was aimed at providing insight into the binding mode of monophenolic substrates and has implications towards the understanding of the Ty monophenolase mechanism and the structural principles underlying the different activities observed for Hcs, COs and Tys.

We find that the pnp forms a ternary complex with halide (F<sup>-</sup>, Cl<sup>-</sup>) bound Ty<sub>met</sub>, showing that the pnp phenolic oxygen does not take up the Cu<sub>2</sub> bridging position. Furthermore, the experimental pnp *K*<sub>d</sub> values as well as the shifts and the relaxation parameters of the pnp protons bound to native do not significantly differ between Ty<sub>met</sub> and Ty<sub>met</sub>F (table 2). Thus, the presence of Cu<sub>2</sub> bridging fluoride does not notably influence the binding of pnp. Additionally, the pnp is shown to directly coordinate to Cu, while the typical (Cu-His<sub>3</sub>)<sub>2</sub> coordination is maintained upon pnp binding. The pnp, therefore, must be bound to an open coordination position of one of the Cu ions. This is in agreement with earlier proposals for the Ty hydroxylation chemistry (e.g.<sup>11</sup>) and the binding mode of phenylthiourea in the X-ray structure of CO<sup>10</sup>.

The pnp is in fast exchange with Ty<sub>met</sub>Cl on the NMR timescale. The titration data of pnp binding to Ty<sub>met</sub>Cl (Fig. 1C) are explained by a decrease in the antiferromagnetic coupling parameter  $-2J$  upon pnp binding, indicating an decrease in the Cu-Cl-Cu bridging angle and the Cu-Cu distance. If a similar situation applies to the binding of monophenol to Ty<sub>oxy</sub>, it may influence the reactivity of the bound peroxide. Furthermore, the binding of pnp to native Ty<sub>met</sub> and Ty<sub>met</sub>Cl affects one His residue in the (Cu-His<sub>3</sub>)<sub>2</sub> coordination sphere, which is tentatively assigned to an Ty analogue of His244 that interacts with the PTU inhibitor in CO<sub>met</sub>.

The exchange of pnp between the free and the Ty<sub>met</sub> bound forms allowed for the

measurement of the  $T_1$  values of the pnp ring protons bound to  $Ty_{met}$  and  $Ty_{met}F$  (table 2). From this we were able to deduce a structural model for phenol coordination to  $Ty_{met}$  (Fig. 7). In this model, the phenol is axially coordinated to CuB with its aromatic ring tilted towards CuA. In the delineated orientation, the *ortho* protons of the bound phenol are oriented towards the bound peroxide in  $Ty_{oxy}$ , allowing for the hydroxylation of the phenol. In CO, instead, a similar orientation of phenol is prevented by Phe261 that shields the active site and locks the bound substrate in its place (Fig. 6), thereby explaining the absence of monophenolase activity in CO.

## References

- (1) van Gelder, C. W.; Flurkey, W. H.; Wichers, H. J. *Phytochem.* **1997**, *45*, 1309-1323.
- (2) Oetting, W. S. *Pigment Cell Res.* **2000**, *13*, 320-325.
- (3) Seo, S. Y.; Sharma, V. K.; Sharma, N. J. *Agric. Food Chem.* **2003**, *51*, 2837-2853.
- (4) Battaini, G.; Monzani, E.; Casella, L.; Lonardi, E.; Tepper, A. W.; Canters, G. W.; Bubacco, L. *J. Biol. Chem.* **2002**, *277*, 44606-44612.
- (5) van Holde, K. E.; Miller, K. I.; Decker, H. J. *J. Biol. Chem.* **2001**, *276*, 15563-15566.
- (6) Cuff, M. E.; Miller, K. I.; van Holde, K. E.; Hendrickson, W. A. *J. Mol. Biol.* **1998**, *278*, 855-870.
- (7) Magnus, K. A.; Hazes, B.; Ton-That, H.; Bonaventura, C.; Bonaventura, J.; Hol, W. G. *Proteins* **1994**, *19*, 302-309.
- (8) Perbandt, M.; Guthohrlein, E. W.; Rypniewski, W.; Idakieva, K.; Stoeva, S.; Voelter, W.; Genov, N.; Betzel, C. *Biochemistry* **2003**, *42*, 6341-6346.
- (9) Volbeda, A.; Hol, W. G. *J. Mol. Biol.* **1989**, *209*, 249-279.
- (10) Klabunde, T.; Eicken, C.; Sacchettini, J. C.; Krebs, B. *Nat. Struct. Biol.* **1998**, *5*, 1084-1090.
- (11) Solomon, E. I.; Sundaram, U. M.; Machonkin, T. E. *Chem. Rev.* **1996**, *96*, 2563-2605.
- (12) Bubacco, L.; Vijgenboom, E.; Gobin, C.; Tepper, A. W. J. W.; Salgado, J.; Canters, G. W. J. *J. Mol. Catal. B: Enzym.* **2000**, *8*, 27-35.
- (13) Tepper, A. W.; Bubacco, L.; Canters, G. W. J. *J. Biol. Chem.* **2002**, *277*, 30436-30444.
- (14) Tepper, A. W.; Bubacco, L.; Canters, G. W. J. *J. Biol. Chem.* **2003**, *279*, 13425-



## Chapter 6

### Paramagnetic NMR studies of p-nitrophenol binding

13435.

- (15) Wilcox, D. E.; Porras, A. G.; Hwang, Y. T.; Lerch, K.; Winkler, M. E.; Solomon, E. I. *J. Am. Chem. Soc.* **1985**, *107*, 4015.
- (16) Bubacco, L.; Salgado, J.; Tepper, A. W.; Vijgenboom, E.; Canters, G. W. *FEBS Lett.* **1999**, *442*, 215-220.
- (17) Holz, R. C.; Bennett, B.; Chen, G. C.; Ming, L.-J. *J. Am. Chem. Soc.* **1998**, *120*, 6329-6335.
- (18) Asokan, A.; Manoharan, P. T. *Inorg. Chem.* **1999**, *38*, 5642-6554.
- (19) Brink, J. M.; Rose, R. A.; Holz, R. C. *Inorg. Chem.* **1996**, *35*, 2878-2885.
- (20) Murthy, N. N.; Karlin, K. D.; Bertini, I.; Luchinat, C. *J. Am. Chem. Soc.* **1997**, *119*, 2156-2162.
- (21) Clementi, V.; Luchinat, C. *Acc. Chem. Res.* **1997**, *31*, 351-361.
- (22) Bertini, I.; Luchinat, C. *Coord. Chem. Rev.* **1996**, *150*.
- (23) Sanchez-Ferrer, A.; Rodriguez-Lopez, J. N.; Garcia-Canovas, F.; Garcia-Carmona, F. *Biochim. Biophys. Acta* **1995**, *1247*, 1-11.
- (24) Karlin, K. D.; Tyeklár, Z. *Bioinorganic Chemistry of Copper*; **1993**.
- (25) Solomon, E. I.; Chen, P.; Metz, M.; Lee, S.-K.; Palmer, A. E. *Angew. Chem. Int. Ed.* **2001**, *40*, 4570-4590.
- (26) Lewis, E. A.; Tolman, W. B. *Chem. Rev.* **2004**, *104*, 1047-1076.
- (27) Conrad, J. S.; Dawso, S. R.; Hubbard, E. R.; Meyers, T. E.; Strothkamp, K. G. *Biochemistry* **1994**, *33*, 5739-5744.
- (28) Jackman, M. P.; Hajnal, A.; Lerch, K. *Biochem. J.* **1991**, *274 ( Pt 3)*, 707-713.
- (29) Inubushi, T.; Becker, E. D. *J. Magn. Reson.* **1983**, *51*, 128-133.
- (30) Swift, T. J. in *NMR of Paramagnetic Molecules*; La Mar, G. N., Horrocks, W., Jr., Holm, R. H., eds. **1973**; pp 53-83.
- (31) Ando, M. E.; Gerig, J. T.; Weigand, E. F. *J. Am. Chem. Soc.* **1982**, *104*, 3172-3178.
- (32) Cantor, C. R.; Schimmel, P. R. in *Biophysical Chemistry, part. II, Techniques for the Study of Biological structure and Function*; Freeman, W.H.: **1980**; pp 539-590.
- (33) Sudmeier, J. L.; Anderson, S. E.; Frye, J. S. *Conc. Magn. Reson.* **1990**, *2*, 197-212.

## Chapter 6

### Paramagnetic NMR studies of p-nitrophenol binding

- (34) Komaei, S. A.; van Albada, G. A.; Haasnoot, J. G.; Kooijman, H.; Spek, A. L.; Reedijk, J. *Inorg. Chim. Acta* **1999**, *286*, 24-29.
- (35) Rodriguez-Forteza, A.; Alemany, P.; Alvarez, S.; Ruiz, E. *Inorg. Chem.* **2002**, *41*, 3769-3778.
- (36) Maekawa, M.; Kitagawa, S.; Munakata, M.; Masuda, H. *Inorg. Chem.* **1989**, *28*, 1904-1909.
- (37) Ito, N.; Phillips, S. E.; Stevens, C.; Ogel, Z. B.; McPherson, M. J.; Keen, J. N.; Yadav, K. D.; Knowles, P. F. *Nature* **1991**, *350*, 87-90.
- (38) Longa, S. D.; Ascone, I.; Bianconi, A.; Bonfigli, A.; Castellano, A. C.; Zarivi, O.; Miranda, M. *J. Biol. Chem.* **1996**, *271*, 21025-21030.
- (39) Siegbahn, P. E. *J. Biol. Inorg. Chem.* **2003**, *8*, 567-576.
- (40) Gerdemann, C.; Eicken, C.; Galla, H. J.; Krebs, B. *J. Inorg. Biochem.* **2002**, *89*, 155-158.
- (41) Salvato, B.; Santamaria, M.; Beltramini, M.; Alzuet, G.; Casella, L. *Biochemistry* **1998**, *37*, 14065-14077.
- (42) Decker, H.; Tucek, F. *Trends Biochem. Sci.* **2000**, *25*, 392-397.
- (43) Decker, H.; Ryan, M.; Jaenicke, E.; Terwilliger, N. *J. Biol. Chem.* **2001**, *276*, 17796-17799.
- (44) Decker, H.; Rimke, T. *J. Biol. Chem.* **1998**, *273*, 25889-25892.
- (45) Olivares, C.; Garcia-Borrón, J. C.; Solano, F. *Biochemistry* **2002**, *41*, 679-686.
- (46) Decker, H.; Dillinger, R.; Tucek, F. *Angew. Chem. Int. Ed.* **2000**, *39*, 1591-1595.
- (47) Bubacco, L.; Van Gastel, M.; Groenen, E. J.; Vijgenboom, E.; Canters, G. W. *J. Biol. Chem.* **2003**, *278*, 7381-7389.
- (48) Gerdemann, C.; Eicken, C.; Krebs, B. *Acc. Chem. Res.* **2002**, *35*, 183-191.
- (49) Van Gastel, M.; Bubacco, L.; Groenen, E. J.; Vijgenboom, E.; Canters, G. W. *FEBS Lett.* **2000**, *474*, 228-232.
- (50) Eicken, C.; Krebs, B.; Sacchettini, J. C. *Curr. Opin. Struct. Biol.* **1999**, *9*, 677-683.



# Chapter 7

*Summary, conclusion and future work*

## Summary

The work described in this thesis concerns spectroscopic and mechanistic studies on the type-3 Cu protein tyrosinase (Ty). Ty contains a dinuclear Cu site that is also found in the oxygen transport protein hemocyanin (Hc) and the diphenol oxidising enzyme catechol oxidase (CO). Ty is responsible for the hydroxylation of L-tyrosine and the subsequent oxidation of the diphenolic product L-DOPA to DOPAquinone. The formed product is a precursor in the biosynthesis of melanin pigments that serve various roles in different organisms. Although the enzyme has been studied for over a century, its structure and detailed mechanism remain to be solved.

The main aim of the thesis work was to learn about how small molecules (inhibitors as well as diphenolic and monophenolic substrates) interact with the type-3 copper centre. Knowledge of these interactions is essential for the understanding of the Ty reaction mechanism. The presence of the two copper ions gives the enzyme unique spectroscopic features, which make it amenable to techniques like paramagnetic Nuclear Magnetic Resonance (pNMR). The pNMR, in conjunction with kinetic methods, was extensively used throughout the thesis work to selectively study the active site and the structural changes therein that occur upon ligand binding. Such studies are highly valuable, also because a Ty crystal structure has not been reported to date.

In **Chapter 1**, a brief overview of the role of copper in biological systems is presented including a basic introduction into the properties of Ty. The chapter also contains the objectives and outline of the thesis research. The current knowledge regarding Ty, primarily from structural and mechanistic viewpoints, is reviewed in **Chapter 2**.

The investigation of the structural and mechanistic aspects of the inhibition of Ty by halides is the subject of **Chapter 3**. The work was motivated by the ubiquitous presence of chloride in living cells, whereas the halide inhibition of Ty was never investigated in great detail. It was shown that all halides ( $F^-$ ,  $Cl^-$ ,  $Br^-$ ,  $I^-$ ) are inhibitors in the conversion of L-DOPA. The inhibition is competitive for  $F^-$  and  $Cl^-$ , while  $Br^-$  and  $I^-$  inhibit L-DOPA conversion through a noncompetitive mechanism. The order in inhibition strength is  $I^- < F^- \ll Cl^- < Br^-$  at pH 6.80 with apparent inhibition constants ( $K_i^{app}$ ) in the mM range. The latter means that the inhibition by chloride ion is physiologically important as  $[Cl^-]$  varies from about 5 to 200 mM in biological systems. The pH dependence of the inhibition was studied for fluoride and chloride ion, revealing that the value of  $-\log(K_i^{app})$  is linearly proportional to the pH down to pH 5.5, meaning that the inhibition becomes 10 times stronger with the decrease of 1 pH unit. This is due to an acid/base equilibrium of a single protein derived group, with halide only inhibiting the low pH form (see below).

The structural basis for the halide inhibition was studied through  $^1\text{H}$  paramagnetic NMR (pNMR) and optical spectroscopy. The pNMR is selective for  $\text{Ty}_{\text{met}}$  and allows the characterisation of the interaction between inhibitors and this enzyme form on a structural level. It was shown that  $\text{F}^-$ ,  $\text{Cl}^-$  and  $\text{Br}^-$  induce large changes in the  $\text{Ty}^1\text{H}$  pNMR spectra, consistent with halide binding to the oxidised type-3 centre. In all cases, the observed pNMR signals could be assigned to the ring protons of six  $\text{Cu}_2$  coordinated His residues, showing that the type-3 ( $\text{Cu-His}_3$ )<sub>2</sub> coordination system is maintained in all halide bound species. The findings lead to the conclusion that halides bridge the two copper ions, in contrast to earlier suggestions that halides bind to Ty at an axial coordination position on one of the Cu ions after displacement of a coordinated His residue.

The pH dependence of fluoride binding to  $\text{Ty}_{\text{met}}$  was investigated through pNMR, showing that the fluoride binding to  $\text{Ty}_{\text{met}}$  follows a similar pH dependence to that of the fluoride inhibition. Additionally, the fluoride inhibition constant and the apparent dissociation constant  $K_d^{\text{app}}$  for the fluoride- $\text{Ty}_{\text{met}}$  complex were shown to be similar, leading to the conclusion that the inhibition of fluoride ion is primarily due to the interaction of  $\text{F}^-$  with the  $\text{Ty}_{\text{met}}$  form.

In contrast, iodide did not seem to bind to  $\text{Ty}_{\text{met}}$  as the presence of this ion did not induce changes in the  $\text{Ty}_{\text{met}}$  pNMR spectrum. Yet, it is the strongest halide inhibitor meaning that iodide interacts with a Ty species other than  $\text{Ty}_{\text{met}}$ . Indeed, iodide titrations of  $\text{Ty}_{\text{oxy}}$  followed by optical spectroscopy showed that iodide efficiently displaces oxygen from  $\text{Ty}_{\text{oxy}}$  by binding to the  $\text{Ty}_{\text{red}}$  form. Also bromide was found to bind to  $\text{Ty}_{\text{red}}$ , albeit with lower affinity than iodide, while fluoride and chloride ion did not bind to  $\text{Ty}_{\text{red}}$  with high affinity. The obtained apparent iodide- $\text{Ty}_{\text{red}}$  dissociation constant was found to be close to the apparent inhibition constant under the experimental conditions, showing that the iodide inhibition is due to its interaction with  $\text{Ty}_{\text{red}}$  and thereby explaining the noncompetitive inhibition observed for this ion. Thus,  $\text{F}^-$  and  $\text{Cl}^-$  inhibit Ty through binding to  $\text{Ty}_{\text{met}}$ , while the inhibition by  $\text{I}^-$  and  $\text{Br}^-$  is primarily due to binding to  $\text{Ty}_{\text{red}}$ . The latter provides the explanation for the complex halide inhibition patterns observed for Tys and possibly for other enzymes such as the laccases as well that contain a type-3 copper site as part of a trinuclear Cu cluster (see Chapter 1).

The affinity of halide binding to  $\text{Ty}_{\text{met}}$  follows the order  $\text{F}^- > \text{Cl}^- > \text{Br}^- \gg \text{I}^-$ , while the affinity of halide binding to  $\text{Ty}_{\text{red}}$  is the exact reverse. This can be explained by the simple rules of hard/soft ligand binding, softer ligands favouring the binding to the lower metal oxidation states. Alternatively, the different halide binding affinities could be related to the Cu-Cu distance, this distance being larger in  $\text{Ty}_{\text{red}}$  than in  $\text{Ty}_{\text{met}}$ , and  $\text{Ty}_{\text{red}}$  therefore being able to stabilise the binding of the larger halide ions.

## Chapter 7

Summary, conclusion and future work

The binding modes of monodentate (*p*-nitrophenol) and bidentate (Kojic acid and *p*-toluic acid) inhibitors to the Ty<sub>met</sub> form were assessed through their capability to displace halide from the Cu<sub>2</sub> bridging position as monitored by pNMR. It was shown that the bidentate inhibitors displace halide from the active site, whereas the monodentate *p*-nitrophenol forms a ternary complex with fluoride bound Ty<sub>met</sub>. From this, a structural model of diphenolic substrate binding to Ty<sub>met</sub> could be derived. In the model, one phenolic oxygen coordinates at an open axial position of CuB while the second phenolic hydroxyl bridges the two Cu ions. The model differs from previous models that assumed that diphenol coordinates bidentate over both copper ions.

The work described in **chapter 4** focusses at characterising the endogenous Ty fluorescence as a function of oxidation state and ligand binding. The motivation for this work was twofold, namely 1) to explore the possibility of using the highly sensitive method of protein fluorescence as a probe in studying ligand binding and 2) to characterise the kinetics of the binding of various inhibitors to provide insight into the structural features that determine the inhibition efficiency.

The fluorescence emission spectrum of Ty was shown to be dominated by Trp fluorescence and shows a maximum at 343 nm, indicating that a significant fraction of the 12 Trp residues in Ty is exposed to the solvent. The quantum yield of the fluorescence was shown to be highly dependent on the oxidation state of the protein; the fluorescence intensity of Ty<sub>red</sub> was found to be over twice that of Ty<sub>oxy</sub>. From the fluorescence intensities measured for various preparations of Ty, it could be determined that about 70 % of the enzyme occurs in the Ty<sub>met</sub> form in Ty resting preparations, while the remainder is a mixture of Ty<sub>red</sub> and Ty<sub>oxy</sub>, the molar ratio of the latter depending on the [O<sub>2</sub>] in the sample. Through a steady-state titration of Ty<sub>red</sub> with oxygen as monitored by the Ty fluorescence, an O<sub>2</sub> dissociation constant of 16.5 μM could be determined.

The stability of Ty was evaluated as a function of pH by activity measurements using sequential stopped-flow spectroscopy. It was shown that Ty is rapidly inactivated at low pH values ( $t_{1/2} = 17$  sec at pH 3.6) and that the presence of F<sup>-</sup> or Cl<sup>-</sup> protects the enzyme from this inactivation. It was further established that the quantum yield of the Ty<sub>met</sub> enzyme is dependent on a protein derived acid/base equilibrium with a pKa value of 4.5 where the fluorescence level of the low pH form of Ty is 0.7 that of the high pH form. A similar pH dependence of the emission intensity was not observed for fluoride bound Ty<sub>met</sub>, Ty<sub>oxy</sub> and Ty<sub>red</sub>, suggesting that the pH dependence of the native Ty<sub>met</sub> fluorescence is specifically due to changes occurring at the type-3 centre of Ty<sub>met</sub>.

## Chapter 7

Summary, conclusion and future work

The difference between the quantum yield of  $Ty_{met}$  and fluoride bound  $Ty_{met}$  was exploited in studying the transient-state kinetics of fluoride binding to  $Ty_{met}$ , as well as its pH dependence, by stopped-flow fluorescence spectroscopy. The obtained data could be explained by assuming a simple two-state binding mechanism where a single fluoride ion binds to  $Ty_{met}$ . It was established that the kinetic parameters of  $F^-$  binding ( $K_d^{app}$ ,  $k_{on}^{app}$ ,  $f_q$ ) are dependent on an acid/base equilibrium with an average  $pK_a$  value of 4.6, similar to the  $pK_a$  value of 4.5 determined for the pH dependence of the  $Ty_{met}$  fluorescence.

The kinetic data are consistent with the fluoride inhibition and the results obtained for fluoride binding to  $Ty_{met}$  monitored by pNMR (Chapter 3). All results are in accordance with a mechanism where  $Ty_{met}$   $Cu_2$  bridging hydroxide protonates and dissociates at low pH, rendering the bridging position available for fluoride to bind. The low pH form of  $Ty_{met}$  decays leading to rapid protein inactivation unless halides ( $F^-$ ,  $Cl^-$ ,  $Br^-$ ), which substitute for the missing  $OH^-$  bridging ligand, are present in solution. It is further proposed that the bridging  $OH^-$  is a proton acceptor for one of the phenolic hydroxyl protons in the binding of diphenolic substrates to  $Ty_{met}$ .

The binding of organic inhibitors was also shown to lead to changes in the  $Ty_{met}$  fluorescence intensity, which was utilized in elucidating the binding kinetics of several inhibitors by stopped-flow fluorescence spectroscopy. In all cases, the obtained dissociation constants were similar to the corresponding inhibition constants in the conversion of L-DOPA. This shows that the inhibition is mainly due to the interaction of the inhibitors with the  $Ty_{met}$  enzyme, at variance with earlier suggestions that inhibitors bind to  $Ty_{oxy}$ , displacing  $O_2$ . It was further shown that the high efficiency of inhibition of compounds that contain a hydroxyl-ketone moiety conjugated in the aromatic ring (e.g. Kojic acid and mimosin) is due to high association rates compared to those of carboxylic acid inhibitors (e.g. *p*-toluic acid, benzoic acid); the dissociation  $k_{off}$  rates are similar for both classes of inhibitors. Comparison of the dissociation rates for a set of carboxylic acid inhibitors showed that the presence of a substituent in the *para* position stabilises the  $Ty_{met}$ -inhibitor complex.

All results presented in this Chapter are consistent with those obtained using other techniques, validating the use of Ty Trp fluorescence as a highly sensitive and versatile probe in the study of Ty ligand binding and catalysis.

**Chapter 5** describes an investigation of the  $Ty_{met}$  physical properties that determine the applicability of pNMR. A primary goal of this work was to establish the reasons for the remarkable sharpness of the paramagnetically affected  $^1H$  signals observed for the halide bound  $Ty_{met}$  species. The work was further motivated by the prospect of using relaxation



data in determining the coordination geometry of  $\text{Ty}_{\text{met}}$  bound ligands, requiring knowledge of the relaxation mechanism(s).

The magnitude of the antiferromagnetic coupling constant  $-2J$  for the three halide bound  $\text{Ty}_{\text{met}}$  forms was determined from the temperature dependence of  $^1\text{H}$  signal hyperfine shifts, revealing moderate antiferromagnetic couplings that follow the order  $\text{Ty}_{\text{met}}\text{F} > \text{Ty}_{\text{met}}\text{Cl} > \text{Ty}_{\text{met}}\text{Br}$ . The latter order is explained in terms of the expected Cu-X-Cu bridging angles, larger angles inducing stronger couplings.

The longitudinal  $T_1$  relaxation times of the His  $^1\text{H}$  signals were measured for the  $\text{Ty}_{\text{met}}\text{X}$  species. The  $T_1$  relaxation is dominated by the dipolar contribution, which is related to the distance  $r$  from Cu to the resonating nucleus. A quantitative evaluation of  $T_1$  relaxation times in calculating Cu-H distances was shown to be complicated by the presence of ligand-centred contributions leading to the breakdown of the  $r^{-6}$  dependence of dipolar relaxation.

The experimental  $T_1$  and  $-2J$  data were used to estimate electronic relaxation times of the  $\text{Ty}_{\text{met}}\text{X}$  derivatives. The obtained values confirmed that the sharpness of the  $^1\text{H}$  signals is due to fast electronic relaxation; while mononuclear Cu systems are typically characterised by  $\tau_S$  values in the order of  $10^{-8}$ - $10^{-9}$  sec, the  $\tau_S$  values in the  $\text{Ty}_{\text{met}}\text{X}$  species ( $\sim 10^{-11}$  sec) are two to three orders of magnitude shorter. The value of  $\tau_S$  is significantly different for all  $\text{Ty}_{\text{met}}\text{X}$  species and follow the order  $\text{Ty}_{\text{met}}\text{F} > \text{Ty}_{\text{met}}\text{Cl} > \text{Ty}_{\text{met}}\text{Br}$ . The fast electronic relaxation in the type-3 centre and other  $\text{Cu}_2$  systems may be due to the modulation of the ZFS splitting of the  $S = 1$  level or a relaxation process related to the  $S = 0 \leftrightarrow S = 1$  transition. The  $^1\text{H}$  signal linewidth (i.e. the  $T_2$  relaxation times) was found to be determined by dipolar and Curie contributions that are both related to Cu-H distances.

The characterisation of interaction of the monophenolic substrate analogue *p*-nitrophenol (pnp) with native  $\text{Ty}_{\text{met}}$  and its halide bound derivatives is the subject of **Chapter 6**. This work was aimed at providing insight into the coordination mode of monophenolic substrates, relevant for the understanding of the mechanism of the Ty monophenolase reaction.

Titration of native  $\text{Ty}_{\text{met}}$ ,  $\text{Ty}_{\text{met}}\text{F}$  and  $\text{Ty}_{\text{met}}\text{Cl}$  with pnp monitored by pNMR showed that pnp binds to all three enzyme forms, with pnp being in fast to intermediate exchange on the NMR timescale. The pnp forms a ternary complex with halide bound  $\text{Ty}_{\text{met}}$  showing that the pnp does not occupy the  $\text{Cu}_2$  bridging position. Both in the cases of native  $\text{Ty}_{\text{met}}$  and  $\text{Ty}_{\text{met}}\text{Cl}$ , one coordinated residue was shown to be particularly affected by pnp binding, which is tentatively assigned to a Ty analogue of His244 of catechol oxidase that

interacts with the aromatic ring of the inhibitor phenylthiourea.

All His proton signals of  $Ty_{met}Cl$  were found to shift downfield upon pnp binding, which is explained by a decrease of the magnetic exchange parameter  $-2J$  from  $200\text{ cm}^{-1}$  in the absence to about  $150\text{ cm}^{-1}$  in the presence of pnp. This decrease was tentatively attributed to a decrease in Cu-X-Cu bridging angle suggesting that the Cu ions are pulled together upon pnp binding. The latter might be important in the oxygen activation upon monophenol binding to  $Ty_{oxy}$ .

The absence of  $^1H$  pNMR signals from pnp in the  $^1H$  pNMR spectra of the pnp bound  $Ty_{met}$  forms prompted the investigation of the pnp NMR signals in the solution bulk as a function of the pnp and  $Ty_{met}$  concentrations. This allowed for the determination of the pnp dissociation constants and the apparent values for the paramagnetic  $T_{1M}$ ,  $T_{2M}$  and shift  $\delta_M$  values of the pnp protons bound to native  $Ty_{met}$  and  $Ty_{met}F$ . The obtained values were not significantly different for the latter two enzyme forms, showing that the presence of  $Cu_2$  bridging fluoride does not markedly influence the pnp binding.

Since the apparent  $T_{1M}$ ,  $T_{2M}$  and  $\delta_M$  values are a complex function of their respective values in the  $Ty_{met}$  bound forms and of the pnp exchange rate, fully deuterated pnp and  $^2D$  NMR were used to establish the exchange conditions. This allowed for the confirmation of fast exchange conditions for the  $^1H$   $T_{1M}$ , as well as for estimates of the lifetime of the  $Ty_{met}$ -pnp complex  $\tau_M$  and the paramagnetic shift values of the  $Ty_{met}$  bound pnp signals. The results are consistent with a direct coordination of pnp to type-3 Cu.

The experimental  $T_{1M}$  values of the  $Ty_{met}$  bound pnp protons were used to generate a structural model of monophenol coordination. In the model, the phenol is axially coordinated to CuB with its aromatic ring tilted towards CuA. In the delineated orientation, the *ortho* protons of the bound phenol are oriented towards the bound peroxide in  $Ty_{oxy}$ , allowing for the hydroxylation of the phenol. In catechol oxidase, instead, a similar orientation of phenol is prevented by Phe261 that shields the active site and locks the CuB bound substrate in its place, thereby explaining the absence of monophenolase activity in CO.

## Conclusion

The work described in this thesis concerns a spectroscopic examination of the structural and mechanistic features that determine the activity of the type-3 copper protein tyrosinase (Ty), which provided important insights into the mechanisms of inhibitor action and catalytic conversion. The main aim of the thesis work was to obtain insight into how inhibitors as well as monophenolic and diphenolic substrates interact with the type-3 centre. The latter is essential for predicting the enzyme's behaviour, for the development of novel Ty inhibiting compounds and for the development of Cu<sub>2</sub> model compounds that mimic the Ty reaction chemistry.

The focus has been on the interaction of inhibitors with Ty in its oxidized form of (Ty<sub>met</sub>). Historically, Ty<sub>met</sub> has been studied little by spectroscopic methods due to its diamagnetism and the absence of strong optical transitions. The thesis work was initiated soon after it was found that Ty<sub>met</sub> is amenable to paramagnetic NMR (pNMR) that provides a detailed and selective probe of the electronic structure of the active-site. The first pNMR studies by Bubacco *et al.* provided the conclusive proof that the coordination sphere of the type-3 centre in Ty<sub>met</sub> consists of two Cu ions that are each coordinated by three His residues through their N<sup>ε</sup> atoms, as in the hemocyanins and catechol oxidases. Throughout the present work, the pNMR method was extensively applied in studying ligand binding to the Ty<sub>met</sub> type-3 centre.

Copper systems are not attractive for pNMR studies as they often yield very broad signals, leading to spectra with poor resolution. In the case of Ty<sub>met</sub> and other Cu<sub>2</sub> systems, however, the paramagnetism is reduced due to the only partial occupation of the paramagnetic  $S = 1$  spin level, reducing the paramagnetic shifts and the line-broadening. This, however, is not sufficient to explain the remarkably sharp <sup>1</sup>H signals observed in the pNMR spectra of Ty<sub>met</sub>. The sharpness of the signals appears to be connected with a drastic decrease in the electronic relaxation time  $\tau_S$  with respect to mononuclear Cu systems (**Chapter 5**), as was previously shown for some small Cu<sub>2</sub> complexes, as well as for the mixed valent [Cu(1.5) Cu(1.5)] Cu<sub>A</sub> site of an engineered amicyanin and cytochrome *c* oxidase. The relaxation and magnetic properties of these dinuclear Cu systems suggest that electronic relaxation may occur through an Orbach type process, but this remains to be established.

The structural and mechanistic features of the inhibition of Ty by halide ions were comprehensively studied (**Chapters 3 and 4**). The results showed that the inhibition by fluoride and chloride is due to the binding of halide ions at the Cu<sub>2</sub> bridging position, replacing the hydroxide present in native Ty<sub>met</sub> and thereby preventing the binding of

## Chapter 7

Summary, conclusion and future work

diphenolic substrates (see below). The inhibition becomes much more effective with decreasing pH, which could be traced to the protonation of the bridging OH<sup>-</sup> in native Ty<sub>met</sub> and the concomitant facilitation of the binding of halide ion. As chloride is universally present in living systems, the inhibition is physiologically important. Chloride inhibition should be taken into account in applications of Ty for industrial catalysis, bioremediation or biosensing. Care should be taken with the study of Ty in chloride containing buffers (e.g. Tris.HCl) and in diagnostic applications where Ty activity is used as a reporter for secondary events in complex (biological) solutions.

Since halides bridge the two Cu ions in the type-3 site, similar to the OH<sup>-</sup> in the native Ty<sub>met</sub> form, complexes of halide with Ty can be used to study the binding mode of organic inhibitors (**Chapters 3 and 6**). Furthermore, the systematic study of the magnetic and electronic properties of Ty<sub>met</sub> species containing various bridging ligands allows the establishment of correlations between various spectroscopic properties (**Chapter 5**).

The interaction between Ty<sub>met</sub> and organic inhibitors was studied using pNMR (**Chapters 3 and 6**) and stopped-flow fluorescence spectroscopy (**Chapter 4**). The investigations allowed for the proposal of a binding mode for diphenolic substrates in the Ty<sub>met</sub> site where one of the diphenol hydroxyl groups is axially coordinated to Cu<sub>B</sub>, while the other hydroxyl bridges both Cu ions. The model is in agreement with ESEEM and HYSCORE studies on Ty<sub>half-met</sub> derivatives. The binding model differs from the generally adopted model that assumes that both hydroxyl groups coordinate in a bidentate fashion to both copper ions.

In previous literature, there has been little insight into the mechanisms of the rather intense traffic of protons from and to the active centre during catalysis. Based on the proposed diphenol binding mode and the finding that the Cu<sub>2</sub> bridging OH is protonated at low pH (pK<sub>a</sub> 4.6; **Chapter 4**), it was proposed that the bridging OH is the proton acceptor for one of the phenolic protons upon the binding of diphenolic substrates. The investigation of the pH dependence of inhibitor binding kinetics by stopped-flow fluorescence spectroscopy (see below), as well as of kinetic isotope effects on the binding, would provide a test of this hypothesis and would afford further insight into the role of proton transfer in substrate conversion and inhibition.

The establishment of the structural features of organic inhibitors that determine the efficiency of inhibition is highly relevant in the development of new Ty inhibiting compounds for applications in, for example, skin-treatment or in the prevention of the post-harvest browning of fruits and mushrooms. Such features can be revealed by a systematic comparison of the binding kinetics of a series of inhibitors (**Chapter 4**). The

binding kinetics can be efficiently measured by stopped-flow fluorescence spectroscopy. A comparison of the binding kinetics of a limited number of compounds already provided important clues regarding the structural factors that are important for the efficiency of inhibition. A more detailed study involving a large number of compounds would be highly valuable. It was also shown that all investigated compounds inhibit Ty through direct binding to the Ty<sub>met</sub> form, in contrast to earlier suggestions that inhibitors bind to Ty<sub>oxy</sub>, displacing the bound O<sub>2</sub>.

The monophenolic substrate analogue *p*-nitrophenol (pnp) does not react with Ty due to the presence of the electron withdrawing nitro group and therefore forms a stable complex with Ty. The investigations on the interaction between pnp and various Ty<sub>met</sub> derivatives by pNMR (**Chapter 6**) provided the first direct evidence that phenol coordinates to the Ty<sub>met</sub> type-3 Cu. The coordinating hydroxyl group does not occupy the Cu<sub>2</sub> bridging position. A model for the binding geometry of monophenolic substrates could be derived from <sup>1</sup>H NMR *T*<sub>1</sub> relaxation data. In this model, the phenol coordinates at an open axial coordination position on CuB, while the aromatic ring portion is tilted towards CuA. This tilting results in a central location of the aromatic ring in the active site, orienting one of the pnp *ortho* protons towards the bound O<sub>2</sub> in Ty<sub>oxy</sub>, allowing for hydroxylation.

In the closely related type-3 Cu enzyme catechol oxidase (CO), a central orientation of bound phenol in the active-site is prevented because the movement of the substrate is constrained by Phe260, precluding a direct approach of the aromatic *ortho* protons towards the bound O<sub>2</sub>. This provides an explanation for the absence of monophenolase activity in catechol oxidase, a long standing issue in the research on type-3 Cu proteins. The explanation is at variance with earlier explanations for the absence of monophenolase activity in CO that assume that the phenol coordinates to CuA in Ty, while this would not be possible in CO. Mutational studies of Ty and CO may provide further insight into this issue.

Previous literature data and the combined results presented in this thesis allowed for the proposal of a detailed mechanism for the Ty catalytic activity (**Chapter 6**). Still, fundamental questions remain, mainly regarding the rather limited insight into the mechanisms of oxygen activation and hydroxylation (**Chapter 2**). Insight into these mechanisms may be provided by the spectroscopic characterization of (trapped) reaction intermediates or by studies of the transient-state kinetics of substrate conversion. The high sensitivity of the Ty fluorescence emission intensity to the binding of ligands and the oxidation state might provide the means to study the kinetics of substrate conversion.

The pNMR method has been used throughout this work. A current limitation in pNMR

## Chapter 7

Summary, conclusion and future work

studies on Ty is the absence of a Ty structure and a sequence specific assignment of the paramagnetically affected  $^1\text{H}$  signals. Both are needed to exploit the full potential of pNMR. It is noted that the stability and size (~30 kD) of Ty are on the limit for determining the structure through conventional multidimensional NMR. In the absence of a Ty structure, a (partial) sequence specific assignment may be achieved through the comparison of  $^1\text{H}$  pNMR spectra of Ty with mutations of residues in the second coordination sphere that form hydrogen bonds with coordinating His residues, as currently pursued in the Leiden laboratory (E. Leonardi, personal communication).

Also in the absence of a Ty structure and a sequence specific assignment, the pNMR has proven to be a very powerful technique and, in fact, allowed for a first-time structural characterization of the active site of  $\text{Ty}_{\text{met}}$  and its complexes with exogenous ligands. The pNMR shows large potential for future studies. For example, the pNMR study of  $\text{Ty}_{\text{met}}$  with tightly bound ligands is still largely unexplored. Targets may be Ty inhibitors that are currently applied in agriculture and medical treatment. These studies might provide further insight into the structural reasons for the inhibition, with implications towards the understanding of the enzymatic mechanism and the development of new Ty inhibiting compounds.

## Nederlandse samenvatting

Het werk beschreven in dit proefschrift betreft spectroscopische en mechanistische studies aan het type-3 koper eiwit tyrosinase (Ty) afkomstig uit de groundbacterie *Streptomyces antibioticus*. Ty bevat een dinucleair kopercentrum dat ook voorkomt in het zuurstof-transporteiwit hemocyanine (Hc) en in het difenol oxiderend enzym catechol-oxidase (CO). Ty is verantwoordelijk voor de hydroxylering van L-tyrosine. Het product van deze reactie, L-DOPA, wordt vervolgens catalytisch geoxideerd tot L-DOPAquinon. Het gevormde product is een precursor in de biosynthese van melanines, een heterogene groep van pigmenten die verschillende rollen in diverse organismen vervullen. Melanine is bijvoorbeeld verantwoordelijk voor de bruiningkleuring van de menselijke huid en de kleur van haar bij mensen en zoogdieren. Hoewel Ty meer dan een eeuw is bestudeerd zijn de structuur en het gedetailleerd reactiemechanisme nog onbekend.

In **Hoofdstuk 1** wordt een beknopt overzicht gegeven van de rol van koper in biologische systemen alsook een beknopte introductie in Ty. De huidige kennis betreffende Ty wordt nader belicht in **Hoofdstuk 2**, vooral vanuit een structureel en mechanistisch perspectief.

Het onderzoek naar de structurele en mechanistische aspecten van de remming van Ty door de haliden is het onderwerp van **Hoofdstuk 3**. Dit werk werd gemotiveerd door aanwezigheid van chloride in alle levende cellen, terwijl de remming van Ty door halides nooit in detail is onderzocht. Aangetoond kon worden dat alle halides ( $F^-$ ,  $Cl^-$ ,  $Br^-$ ,  $I^-$ ) remmers in de conversie van L-DOPA zijn. De remming is competitief voor  $F^-$  en  $Cl^-$ , terwijl  $Br^-$  en  $I^-$  de L-DOPA conversie non-competatief remmen. Voor *Streptomyces* Ty is de volgorde in remmend effect  $I^- < F^- \ll Cl^- < Br^-$  bij pH 6.80 met schijnbare remmingsconstanten ( $K_i^{app}$ ) in het mM bereik. Het laatsgenoemde betekent dat de remming door chloride fysiologisch belangrijk is aangezien  $[Cl^-]$  in biologische systemen varieert van ongeveer 5 tot 200 mM. De pH afhankelijkheid van de remming werd bestudeerd voor fluoride en chloride ion, waaruit bleek dat de waarde van  $-\log(K_i^{app})$  lineair evenredig met de pH omlaag loopt tot aan pH 5.5. Dit betekent dat de remming 10 keer sterker wordt met elke afname van één pH eenheid. Dit kon teruggeleid worden naar een zuur/base evenwicht van een groep in het Ty waarbij halide alleen de lage pH vorm remt (zie beneden).

De structurele basis voor de halide remming werd door middel van paramagnetische  $^1H$  NMR (pNMR) en optische spectroscopie bestudeerd. De pNMR is selectief voor  $Ty_{met}$  en maakt de karakterisering van de interactie tussen remmers en deze enzymvorm op een structureel niveau mogelijk. Het bleek dat de aanwezigheid van  $F^-$ ,  $Cl^-$  en  $Br^-$  grote veranderingen in het Ty  $^1H$  pNMR spectrum veroorzaakt. Dit is in overeenstemming met

een directe binding van het halide aan het geoxideerde type-3 kopercentrum. In alle gevallen konden de pNMR signalen aan de ring-protonen van zes Cu<sub>2</sub> coördinerende residuen toegewezen worden, hetgeen aantoonde dat het type-3 (Cu-His<sub>3</sub>)<sub>2</sub> coördinatie gehandhaafd blijft wanneer halides zijn gebonden. De bevindingen leidden tot de conclusie dat halides de twee koperionen bruggen. Dit is in tegenspraak met vroegere suggesties waarbij werd aangenomen dat halides aan een axialecoördinatie positie op één van de Cu ionen binden na verdringing van een gecoördineerd His residu.

De pH afhankelijkheid van de fluoridebinding aan Ty<sub>met</sub> werd bestudeerd door middel van pNMR, waaruit bleek dat de binding aan Ty<sub>met</sub> een soortgelijke pH afhankelijkheid als de fluorideremming vertoont. Verder bleken de fluoride remmingsconstante en de schijnbare dissociatieconstante  $K_d^{app}$  voor het fluoride-Ty<sub>met</sub> complex gelijk te zijn. Dit leidde tot de conclusie dat de fluorideremming hoofdzakelijk veroorzaakt wordt door de binding van F<sup>-</sup> aan geoxideerd Ty.

In tegenstelling hiermee bleek jodide niet aan Ty<sub>met</sub> te binden aangezien de aanwezigheid van dit ion geen veranderingen in het Ty<sub>met</sub> pNMR spectrum veroorzaakte. Omdat jodide het sterkst remmende halide is betekent dit dat jodide via een ander mechanisme remt of bindt aan een andere Ty vorm. Inderdaad werd door middel van I<sup>-</sup> titraties aangetoond dat jodide de zuurstof van Ty<sub>oxy</sub> verdringt door te binden aan de Ty<sub>red</sub> vorm. Ook bromide bleek aan Ty<sub>red</sub> te binden, zij het met een lagere affiniteit dan jodide, terwijl fluoride en chloride niet met hoge affiniteit aan Ty<sub>red</sub> bleken te binden. Onder de experimentele condities bleek de schijnbare I-Ty<sub>red</sub> dissociatieconstante dichtbij de schijnbare remmingsconstante te liggen, hetgeen aantoonde dat de jodide remming voornamelijk veroorzaakt wordt door de wisselwerking met Ty<sub>red</sub>. Daarmee is ook het non-competatieve remmingsmechanisme voor dit ion verklaard. Dus, F<sup>-</sup> en Cl<sup>-</sup> remmen Ty door te binden aan Ty<sub>met</sub>, terwijl de remming door I<sup>-</sup> en Br<sup>-</sup> hoofdzakelijk veroorzaakt wordt door binding aan Ty<sub>red</sub>. Dit laatste verklaart de complexe halide remmingspatronen voor Tys en mogelijk ook die voor andere enzymen zoals de laccases die eveneens die een type-3 koper centrum bevatten als onderdeel van een trinuclear Cu groep (zie Hoofdstuk 1).

De affiniteit van halide voor Ty<sub>met</sub> neemt af in de volgorde F<sup>-</sup> > Cl<sup>-</sup> > Br<sup>-</sup> > I<sup>-</sup>, terwijl de affiniteit van halide binding aan Ty<sub>red</sub> een omgekeerde volgorde te zien geeft. Dit kan verklaard worden met de eenvoudige regels van harde/zachte ligand binding waarbij zachtere liganden bij voorkeur binden aan de lagere oxidatietoestanden van een metaal. Een alternatieve verklaring zou gerelateerd kunnen zijn aan de Cu-Cu afstand, die, afgaand op de structuren van Hcs en CO, groter is in Ty<sub>red</sub> dan in Ty<sub>met</sub>. Hierdoor zou Ty<sub>red</sub> de binding van de relatief grotere halide ionen beter stabiliseren dan Ty<sub>met</sub>.



Voor de remmers p-nitrophenol, Kojic acid en p-tolueenzuur werd de capaciteit om halide van het Cu<sub>2</sub> centrum te verdringen geëvalueerd met pNMR. Aangetoond werd dat de bidentate remmers (Kojic acid en p-tolueenzuur) het halide ion van het actieve centrum verdringen, terwijl het monodentate p-nitrophenol een ternair complex met fluoride gebonden Ty<sub>met</sub> vormt. Mede op basis hiervan werd een structureel model van diphenol binding aan Ty<sub>met</sub> afgeleid. In het model coördineert een hydroxylaat groep van het fenol aan een open axiale positie op CuB terwijl de tweede hydroxylaat groep de twee Cu ionen brugt. Het model verschilt van vorige modellen waarin wordt aangenomen dat difenolen in bidentate vorm over beide koperionen coördineren.

Het werk beschreven in **Hoofdstuk 4** was gericht zich op het karakteriseren van de endogene Ty fluorescentie als een functie van oxidatie toestand en ligandbinding. De motivatie voor dit werk was tweevoudig, namelijk 1) om de mogelijkheid te onderzoeken of de zeer gevoelige methode van eiwitfluorescentie als een detectiemethode in het bestuderen van ligandbinding kan worden gebruikt en 2) om de kinetiek van de binding van verschillende remmers te karakteriseren ten einde inzicht te verkrijgen in de structurele eigenschappen die belangrijk zijn voor de remmingsefficiëntie.

Aangetoond kon worden dat het Ty emissiespectrum door Trp fluorescentie wordt gedomineerd. Het emissiespectrum toont een maximum bij 343 nm, hetgeen er op duidt dat een aanzienlijke fractie van de 12 Trp residuen aan het oplosmiddel is blootgesteld. De quantumopbrengst van de fluorescentie bleek in hoge mate afhankelijk te zijn van de oxidatievorm van het eiwit; de fluorescentie-intensiteit van Ty<sub>red</sub> bedraagt meer dan tweemaal die van Ty<sub>oxy</sub>. Van de relatieve fluorescentie-intensiteiten die voor verschillende monsters van Ty gemeten werden kon worden vastgesteld dat ongeveer 70% van het enzym in de Ty<sub>met</sub> vorm voorkomt in de 'resting state'. De rest is een mengsel van Ty<sub>oxy</sub> en Ty<sub>red</sub>, waarbij de molaire verhouding bepaald wordt door de zuurstofconcentratie in het monster. Uit een steady-state titratie van Ty<sub>red</sub> met O<sub>2</sub> gevolg met fluorescentie kon een dissociatieconstante voor zuurstof van 16.5 μM worden bepaald.

De stabiliteit van Ty werd geëvalueerd als functie van de pH met behulp van aktiviteitsmetingen en sequential stopped-flow spectroscopie. Vastgesteld kon worden dat Ty snel geïnactiveerd wordt bij lage pH waarden ( $t_{1/2} = 17$  sec bij pH 3.6) en dat de aanwezigheid van F<sup>-</sup> of Cl<sup>-</sup> het eiwit tegen deze inactivering beschermt. Verder werd gevonden dat de quantumopbrengst van het Ty<sub>met</sub> enzym afhankelijk is van een zuur/base evenwicht met een pK<sub>a</sub> waarde van 4.5, waarbij de fluorescentie intensiteit van de lage pH vorm 0.7 keer de intensiteit van de hoge pH vorm bedraagt. Een soortgelijke pH afhankelijkheid werd niet vastgesteld voor fluoride gebonden Ty<sub>met</sub>, voor Ty<sub>oxy</sub> en voor Ty<sub>red</sub>, hetgeen suggereert dat de pH afhankelijkheid van de natieve Ty<sub>met</sub> fluorescentie

wordt veroorzaakt door veranderingen in het  $Ty_{met}$  type-3 kopercentrum.

Het verschil in kwantumopbrengst tussen natief en met fluoride verzadigd  $Ty_{met}$  werd gebruikt om de 'transient-state' kinetiek van fluoridebinding aan  $Ty_{met}$  te bestuderen, alsmede de pH afhankelijkheid, met stopped-flow fluorescentie spectroscopie. De experimentele gegevens werden verklaard door de aanname van een simpel bindingsmechanisme waarbij een enkel fluoride ion bindt aan  $Ty_{met}$ . De kinetische parameters van fluoride binding ( $K_d^{app}$ ,  $k_{on}^{app}$ ,  $f_q$ ) bleken afhankelijk te zijn van een zuur/base evenwicht met een gemiddelde  $pK_a$  waarde van 4.6, gelijk aan de  $pK_a$  waarde van 4.5 gevonden voor de pH afhankelijkheid van de  $Ty_{met}$  fluorescentie.

De kinetische gegevens zijn in overeenstemming met de resultaten verkregen voor de fluorideremming en voor de fluoridebinding aan  $Ty_{met}$  (hoofdstuk 3). Alle resultaten zijn in overeenstemming met een mechanisme waarbij de  $Cu_2$  bruggende hydroxide in  $Ty_{met}$  geprotoneerd wordt en dissocieert bij lage pH, waarna de brugpositie vrijkomt voor de binding van fluoride. De dissociatie van bruggend hydroxide leidt tot een snelle deactivering van het eiwit, tenzij halides ( $F^-$ ,  $Cl^-$ ,  $Br^-$ ) aanwezig zijn die de missende  $Cu_2$  brug kunnen substitueren. Verder werd voorgesteld dat de  $Cu_2$  bruggende hydroxide de protonacceptor is voor één van de fenolische hydroxylgroepen van difenole substraten tijdens de binding aan  $Ty_{met}$ .

Veranderingen in de  $Ty_{met}$  fluorescentie werden ook waargenomen bij de binding van organische remmers. Dit effect werd gebruikt om de bindingskinetiek van verschillende remmers te bestuderen. In alle gevallen liggen de verkregen dissociatieconstanten dichtbij de corresponderende remmingsconstanten. Dit toont aan dat de remming hoofdzakelijk wordt veroorzaakt door de binding van remmers aan de  $Ty_{met}$  vorm. Dit in tegenstelling tot eerdere suggesties waarbij aangenomen werd dat remmers aan  $Ty_{oxy}$  binden onder verdringing van de gebonden zuurstof. Vastgesteld kon worden dat de hoge remmingscapaciteit van verbindingen waarbij een hydroxy-keton groep is geconjugeerd in een aromatische ring (bijv. Kojic acid) vooral veroorzaakt wordt door een hoge associatiesnelheid ( $k_{on}$ ) die aanmerkelijk hoger ligt dan de associatiesnelheden gemeten voor carboxylaat bevattende remmers (bijv. p-tolueenzuur). De dissociatiesnelheden zijn vergelijkbaar voor beide groepen remmers. Uit een onderlinge vergelijking van de dissociatiesnelheden binnen een groep carbonzuur bevattende remmers kon worden geconcludeerd dat de aanwezigheid van een substituent in de para-positie het  $Ty_{met}$ -remmer complex aanzienlijk stabiliseert.

**Hoofdstuk 5** beschrijft een onderzoek naar de fysische eigenschappen van  $Ty_{met}$  die belangrijk zijn voor de toepasbaarheid van pNMR. Een belangrijk doel van dit werk was

het vaststellen van de oorzaken van de opmerkelijk scherpte van de  $^1\text{H}$  pNMR signalen voor halide gebonden  $\text{Ty}_{\text{met}}$ . Het werk werd verder gemotiveerd door het vooruitzicht om  $T_1$  relaxatiedata te gebruiken voor het bepalen van de coördinatiegeometrie van remmers gebonden aan  $\text{Ty}_{\text{met}}$ , waarvoor kennis van de relaxatiemechanismen vereist is.

De waarde van de antiferromagnetische interactieconstante  $-2J$  werd bepaald uit de temperatuursafhankelijkheid van de verschuivingen van de paramagnetische  $^1\text{H}$  signalen voor de drie halide-gebonden  $\text{Ty}_{\text{met}}$  vormen. De koppeling voor de drie  $\text{Ty}_{\text{met}}\text{X}$  vormen is matig antiferromagnetisch waarbij  $-2J$  afneemt volgens  $\text{Ty}_{\text{met}}\text{F} > \text{Ty}_{\text{met}}\text{Cl} > \text{Ty}_{\text{met}}\text{Br}$ . Het laatste kan verklaart worden in termen van de verwachte Cu-X-Cu bruggingshoek, waarbij grotere hoeken sterkere koppelingen veroorzaken.

De longitudinale  $T_1$  relaxatietijden van de His  $^1\text{H}$  signalen werden gemeten voor de  $\text{Ty}_{\text{met}}\text{X}$  vormen. De  $T_1$  relaxatie wordt gedomineerd door de dipolaire contributie, die gerelateerd is aan de afstand  $r$  van Cu tot de resonerende kern. Een kwantitatieve interpretatie van de  $T_1$  relaxatietijden wordt bemoeilijkt door de aanwezigheid van ligand-gecentreerde bijdragen waardoor de  $r^{-6}$  afhankelijkheid van de dipolaire relaxatie niet meer opgaat.

De experimentele  $T_1$  en  $-2J$  waarden werden gebruikt voor het schatten van elektronische relaxatietijden ( $\tau_S$ ). De gevonden waarden bevestigden dat de scherpte van de signalen veroorzaakt wordt door snelle elektronische relaxatie; terwijl mononucleaire Cu systemen worden gekarakteriseerd door relaxatietijden in de orde van  $10^{-8}$ - $10^{-9}$  sec, zijn de  $\tau_S$  waarden in de  $\text{Ty}_{\text{met}}\text{X}$  vormen ( $\sim 10^{-11}$  sec) twee tot drie ordes van grootte korter. De waarde van  $\tau_S$  is significant verschillend voor de verschillende  $\text{Ty}_{\text{met}}\text{X}$  vormen en neemt af volgens  $\text{Ty}_{\text{met}}\text{F} > \text{Ty}_{\text{met}}\text{Cl} > \text{Ty}_{\text{met}}\text{Br}$ . De snelle elektronische relaxatie in het type-3 centrum en andere  $\text{Cu}_2$  systemen wordt mogelijk veroorzaakt door een modulatie van de nulveldsplitsing (ZFS) van de  $S = 1$  spin toestand of door een relaxatieproces gerelateerd aan de  $S = 0 - S = 1$  overgang. De lijnbreedte van de  $^1\text{H}$  signalen (bepaald door de  $T_2$  relaxatietijden) bestaat uit dipolaire en Curie bijdragen die beide gerelateerd zijn aan Cu-H afstanden.

De karakterisering van de interactie tussen het substraat analoog p-nitrofenol (pnp) met natief  $\text{Ty}_{\text{met}}$  en de halide gebonden derivaten is het onderwerp van **Hoofdstuk 6**. Dit werk was gericht op het verkrijgen van inzicht in de coördinatiegeometrie van monofenol substraten. Dit kan bijdragen tot een beter begrip van de Ty monofenolase reactie.

Titraties van natief  $\text{Ty}_{\text{met}}$ ,  $\text{Ty}_{\text{met}}\text{F}$  and  $\text{Ty}_{\text{met}}\text{Cl}$  met pnp, zoals gevolgd met pNMR, toonden aan dat pnp aan alle drie de enzymvormen bindt. Het pnp vormt een ternair complex met

halide en  $Ty_{met}$ , wat aantoont dat pnp de  $Cu_2$  brugpositie niet bezet. Voor natief  $Ty_{met}$  en  $Ty_{met}Cl$  werd aangetoond dat met name één His residu gevoelig is voor de binding van pnp. Dit residu werd voorlopig toegewezen aan het Ty analoog van His244 in catechol oxidase dat in direct contact staat met de aromatische ring van de gebonden remmer p-fenylthioureum in de kristalstructuur.

Alle His proton signalen in  $Ty_{met}Cl$  verschuiven naar lager veld bij pnp binding, hetgeen werd verklaard door een afname in de antiferromagnetische koppelingsconstante  $-2J$  van  $200\text{ cm}^{-1}$  in de afwezigheid tot ongeveer  $150\text{ cm}^{-1}$  in de aanwezigheid van pnp. Dit werd toegeschreven aan een afname van de  $Cu-X-Cu$  bruggingshoek doordat de Cu atomen naar elkaar toe bewegen bij pnp binding. Het laatste kan belangrijk zijn in de aktivering van gebonden zuurstof bij fenol binding aan  $Ty_{oxy}$ .

De afwezigheid van signalen van gebonden pnp in de  $^1H$  pNMR spectra van de pnp  $Ty_{met}$  complexen leidde tot een studie van de NMR signalen van 'vrij' pnp in de oplossing als functie van de  $Ty_{met}$  and pnp concentraties. Hieruit konden de pnp dissociatieconstanten en de schijnbare waarden van de paramagnetische  $T_{1M}$ ,  $T_{2M}$  and  $\delta_M$  van de pnp protonen gebonden aan natief en fluoride gebonden  $Ty_{met}$  worden bepaald. Deze waarden bleken niet significant te verschillen voor natief  $Ty_{met}$  en  $Ty_{met}F$ , wat aantoont dat de aanwezigheid van  $Cu_2$  bruggend fluoride de pnp binding niet noemenswaardig beïnvloedt.

Omdat de schijnbare  $T_{1M}$ ,  $T_{2M}$  en  $\delta_M$  waarden een complexe functie zijn van de overeenkomstige waarden in de  $Ty_{met}$  gebonden vorm alsmede van de uitwisselingssnelheid, werd gedeutereerd pnp in combinatie met  $^2D$  NMR gebruikt om de uitwisselingsparameters vast te stellen. Hieruit bleek dat voor de  $^1H$   $T_{1M}$  'snelle uitwisseling' optreedt terwijl waarden voor de levensduur van het  $Ty_{met}$ -pnp complex en de paramagnetische verschuivingen van de  $Ty_{met}$  gebonden pnp signalen konden worden bepaald. De resultaten zijn in overeenstemming met een directe interactie van het pnp met Cu van het type-3 centrum.

De experimentele  $T_1$  waarden van de pnp protonen in het  $Ty_{met}/pnp$  complex werden gebruikt voor het afleiden van een structuur model van het  $Cu_2$  centrum waarbij monofenol gebonden is. In dit model is het fenol gecoördineerd aan CuB waarbij de aromatische ring naar CuA is gericht. In deze oriëntatie zijn de *ortho* protonen van het aan  $Ty_{oxy}$  gebonden fenol naar de zuurstof gericht, hetgeen hydroxylering van het fenol mogelijk maakt. In tegenstelling hiermee wordt in catechol oxidase een soortgelijke orientatie van het fenol verhinderd door Phe261 dat het actieve centrum afschermt en het gebonden substraat op zijn plaats houdt.

## List of publications

Krooshof, G.H., Ridder, I.S., Tepper, A.W.J.W., Vos, G.J., Rozeboom, H.J., Kalk, K.H., Dijkstra, B.W., Janssen, D.B., *Kinetic Analysis and X-ray Structure of Haloalkane Dehalogenase with a modified Halide-Binding Site*, *Biochemistry* 37, 15013-15023, **1998**

Krooshof, G.H., Floris, R., Tepper, A.W.J.W., Janssen, D.B., *Thermodynamic Analysis of Halide Binding to Haloalkane Dehalogenase Suggests the Occurrence of Large Conformational Changes*, *Protein Science* 8, 355-360, **1999**

Bubacco, L., Salgado, J., Tepper, A.W.J.W., Vijgenboom, E., Canters, G.W., *<sup>1</sup>H NMR spectroscopy of the dinuclear Cu(II) active site of Streptomyces antibioticus tyrosinase*, *FEBS Letters* 442, 215-220, **1999**

Bubacco, L., Vijgenboom, E., Gobin, C., Tepper, A.W.J.W., Salgado, J., Canters, G.W., *Kinetic and paramagnetic NMR investigations of the inhibition of Streptomyces antibioticus tyrosinase*, *J. Mol. Catalysis B*, 8, 27-35, **2000**

Streffer, K., Vijgenboom, E., Tepper, A.W.J.W., Makower, A., Scheller, F.W., Canters, G.W., Wollenberger, U., *Determination of phenolic compounds using recombinant tyrosinase from Streptomyces antibioticus*, *Analytica Chimica Acta* 427, 201-210, **2001**.

Tepper, A.W.J.W., Bubacco, L., Ubbink, M., Kolczak, U., Canters, G.W., *The interaction of the substrate analogue p-nitrophenol with the oxidised type-3 copper protein tyrosinase studied by paramagnetic NMR*, *J. Inorg. Biochem.* 86 (1), 452-452, **2001**

Bubacco, L., Mardegan, A., Giordano, G., van Gastel, M., Tepper, A.W.J.W., Canters, G.W., *Structure and reactivity of the dinuclear copper center in Streptomyces antibioticus Tyrosinase*, *J. Inorg. Biochem.* 86 (1), 28-28, **2001**

Battaini, G., Monzani, E., Casella, L., Lonardi, E., Tepper, A.W.J.W., Canters, G.W., Bubacco, L., *Tyrosinase-catalyzed oxidation of fluorophenols*. *J. Biol. Chem.* 277 (47), 44606-44612, **2002**

Tepper, A.W.J.W., Bubacco, L., Canters, G.W., *Structural basis and mechanism of the inhibition of the type-3 copper protein tyrosinase from Streptomyces antibioticus by halide ions*, *J. Biol. Chem.* 277 (34), 30436-30444, **2002**

Bubacco, L., Van Gastel, M., Benfatto, M., Tepper, A.W.J.W., Canters, G.W., *What are the structural features of the active site that define dinuclear copper proteins function?* *Micron.* 35, 143-145, **2004**

Tepper, A.W.J.W., Bubacco, L., Canters, G.W., *Stopped-flow fluorescence studies of inhibitor binding to tyrosinase from Streptomyces antibioticus*, *J. Biol. Chem.*, 279 (14), 13425-13435, **2004**

Tepper, A.W.J.W., Bubacco, L., Canters, G.W., *The interaction of the substrate analogue p-nitrophenol with the oxidised type-3 copper protein tyrosinase studied by NMR*, *J. Am. Chem. Soc.*, in press, **2004**

Tepper, A.W.J.W., Bubacco, L., Canters, G.W., *Electronic and nuclear relaxation in the halide bound derivatives of the oxidised type-3 copper centre of Streptomyces antibioticus tyrosinase*, to be submitted, **2005**

## Curriculum Vitae

Armand W.J.W. Tepper was born on the 17<sup>th</sup> of February 1971 in the town of Winschoten in the northeast of the Netherlands. After the secondary education (HAVO) at the Winschoter Scholengemeenschap, he commenced studying chemistry at the Rijkshogeschool Groningen. He specialized in biochemistry and completed a one-year research stage in the pharmacokinetics research group of the University of Groningen under supervision of Dr. P.J. Swart and Prof. D.K.F. Meijer. Here, protein conjugates showing anti-HIV activity were modified with polyethyleneglycols to decrease their immunogenicity and their plasma clearance rate. After graduating in 1992, he started studying biochemistry at the Rijksuniversiteit Groningen. The study was completed with a research project regarding mechanistic studies of a mutant of haloalkane dehalogenase in the 'Biotransformation of Synthetic Compounds' group under supervision of Dr. G. Krooshof and Prof. D.B. Janssen. The university study was completed with a literature research project entitled 'DNA Nanotechnology and Bioelectronics'. A degree (*cum laude*) was obtained in August 1997, after which Armand was appointed as a Ph.D. student at Leiden University in the Metallo Protein (Metprot) group under supervision of Prof. G.W. Canters. Here, he started to work on the type-3 copper enzyme tyrosinase, mainly using kinetic and spectroscopic techniques. As a side-activity, he generated artistic renderings of protein structures, which were displayed on the web and used as illustrations in several books, magazines and brochures. In 2002, he moved to Naples and started a Marie Curie Host Development Fellowship in the bioinorganic chemistry research lab of Prof. V. Pavone where he was occupied with studying structure/function relationships of *de novo* designed metal-containing 4-helix bundles as models for enzymes like methane monooxygenase. He is currently back in the Metprot lab in Leiden on a short-term post-doc position working on a small multicopper laccase isolated from *Streptomyces*.